INFORMATION TO USERS

This manuscript has been reproduced from the microfilm master. UMI films the text directly from the original or copy submitted. Thus, some thesis and dissertation copies are in typewriter face, while others may be from any type of computer printer.

The quality of this reproduction is dependent upon the quality of the copy submitted. Broken or indistinct print, colored or poor quality illustrations and photographs, print bleedthrough, substandard margins, and improper alignment can adversely affect reproduction.

In the unlikely event that the author did not send UMI a complete manuscript and there are missing pages, these will be noted. Also, if unauthorized copyright material had to be removed, a note will indicate the deletion.

Oversize materials (e.g., maps, drawings, charts) are reproduced by sectioning the original, beginning at the upper left-hand corner and continuing from left to right in equal sections with small overlaps. Each original is also photographed in one exposure and is included in reduced form at the back of the book.

Photographs included in the original manuscript have been reproduced xerographically in this copy. Higher quality 6" x 9" black and white photographic prints are available for any photographs or illustrations appearing in this copy for an additional charge. Contact UMI directly to order.

UMI

A Bell & Howell Information Company
300 North Zeeb Road, Ann Arbor MI 48106-1346 USA
313/761-4700 800/521-0600

Université d'Ottawa · University of Ottawa

National Library
of Canada

Acquisitions and
Bibliographic Services

395 Wellington Street
Ottawa ON K1A 0N4
Canada

Bibliothèque nationale
du Canada

Acquisitions et
services bibliographiques

395, rue Wellington
Ottawa ON K1A 0N4
Canada

Your file Votre référence

Our file Notre référence

0-612-32436-2

Canada

ACKNOWLEDGEMENTS

Many different factors effect the degree of pleasure and success one can have when doing scientific research. I have been quite fortunate that I had a supervisor during my Ph.D thesis work who intimately understands these factors and has made my stay at the University of Ottawa both educational and enjoyable. I would like to thank Dr. B.E. Conway for allowing me the freedom to pursue scientific research which was both stimulating and fulfilling. His encouragement and enthusiasm for this research inspired me to tackle many difficult problems. I would also like to thank Dr. Conway for sharing his extensive experience and knowledge of science with me, and for his precise editing of my work. I know this is a painstaking task.

Much love and thanks go to my wife, Mary Pat, whose contribution to my life during the course of this work is immeasurable. To my two sons, John Patrick and Grahame Harold, I thank you for being so wonderful. Your unconditional love inspires my positive outlook on my life and work.

I would like to show my appreciation to all my colleagues in the Conway group during my time here, for many useful discussions and for creating an atmosphere which was always exciting and friendly. A special thanks goes to Dr. S. Morin who educated me in the methods of preparation and usage of single-crystal electrodes.

Master glass-blowers Egon Kristoff and John Hopkins deserve special mention, their precise skills made possible many difficult experiments.

Finally, I would like to thank Dr. J.R. MacDonald whose excellent software, LEVM 6.1, enabled me to perform quantitative analyses which I feel added a major contribution to the following work.

TABLE OF CONTENTS

Chapter 4
The A.C. Impedance Method

Chapter 5
HER Studies at Pt(hkl) Single-crystal Electrodes in Acidic and Alkaline Solutions

Chapter 6
Competitive Effects of S-containing Catalyst Poisons on the UPD of H in Relation to H_2 Evolution Kinetics and OPD of H at Pt

Chapter 7
Electrochemical Permeation of H Through Metal Membranes

Chapter 8
Co-adsorption of Thiourea and H at Pd Cathodes in 0.5 mol dm^{-3} H_2SO_4 as it Affects H *Ad*sorption and *Ab*sorption

Chapter 9
Effects of Adsorption of Thiourea on the H_2 Evolution Reaction and H Absorption at Nickel in 0.5 mol dm^{-3} H_2SO_4

Appendix A

Introduction/Preamble

This thesis covers work done by John H. Barber during the time period of September 1992 to September 1997. The topics covered in this thesis and the order in which they are presented are:

1) The specificity of the hydrogen evolution reaction to the surface structure of Pt single-crystal electrodes in both acidic and alkaline media;

2) The effect of sulphur containing catalyst poisons on the processes of hydrogen adsorption and evolution at Pt polycrystalline electrodes;

and

3) Investigations into the H-sorption enhancement effect of thiourea at Pd and Ni electrodes.

Publications resulting from the work presented in this thesis are, at the time of writing are:

Publications

1) J.H. Barber and B.E. Conway "Structural Specificity of the Kinetics of the Hydrogen Evolution Reaction on the Low-index Surfaces of pt Single-crystal Electrodes in 0.5 mol dm^{-3} NaOH", **accepted for publication, J. Electroanal. Chem. (1998).**

2) J.H. Barber, S. Morin and B.E. Conway "Specificity of the Kinetics of H_2 Evolution to Structure of Single-Crystal Pt Surfaces, and the Relation Between OPD and UPD H", **accepted for publication, J. Electroanal. Chem. (1998).**

3) J.H. Barber, S. Morin and B.E. Conway "Dependence of Electrocatalysis in the H_2 Evolution Reaction on the Structure of Single-crystal Pt Surfaces", **Proceedings Volume of the 191st Meeting of the Electrochemical Society, May 1997, Montreal, P.Q., Canada, The Electrochemical Surface Science of Hydrogen Adsorption and Absorption into Metal, Alloys and Intermetallics Symposium.**

4) B.E. Conway, J.H. Barber, L. Gao and S. Qian "A study of the Promoting Effect of Catalytic Poisons on H Entry into Metal Cathodes", **J. Alloys and Comp., 253/254 (1997) 475.**

5) J.H. Barber and B.E. Conway "Competitive Effects of S-Containing Poisons on the UPD of H in Relations to H_2 Evolution kinetics and OPD of H at Pt", **Faraday Transactions, 92 (1996) 3709.**

Abstract

HER at Pt Single-crystal Electrodes

It is well known that transition metals exhibit a wide range of catalytic activities for various processes. One of the best examples is the dependence of H_2 evolution kinetics on the nature of the cathode metal. This leads to an expectation that a similar specific dependence would also be observed at various single-crystal surfaces of Pt. In the earlier literature, this had, however, not been found. In the present paper, it is shown that such conclusions arise from the actual surface-specific electrode kinetics being obscured by effects associated with diffusion of H_2 from a supersaturated region generated near the electrode.

By means of Tafel polarization and impedance measurements at several Pt single-crystal surfaces rotated at 3500 rpm, it is shown that *there are*, in fact, clear specific dependences of the H_2 evolution kinetic parameters on the Pt surface lattice geometry which are related to the underpotential deposition (UPD) of H kinetics and to the well known surface specificity of the H UPD behaviour at Pt as seen in cyclic voltammetry. The question of how the overpotential deposition (OPD) of H, additional to the UPD H, is accommodated at cathodic overpotentials, is addressed. The order of electrocatalytic activity for the HER at the low-index planes is found in 0.5 mol dm^{-3} H_2SO_4 to be (100) < (111) < (110).

An increase of the pH, decreases the kinetic facility of the hydrogen electrode reaction, i.e. abstraction of H to form H_2 is more difficult from H_2O than from H_3O^+; at such lowered rates, the H_2 diffusive effects can be totally eliminated by electrode rotation, unlike the situation in 0.5 mol dm^{-3} H_2SO_4 where rotation is found to only decrease the effect of diffusion. In § 5.5 we show that in 0.5 mol dm^{-3} NaOH the order of reactivity is identical with that found in acidic media, *viz.* (100) < (111) < (110). The slower rates arising in alkaline media allow a larger potential range to be probed and, unlike the situation in acid, quantitative rate information for each of the Volmer, Heyrovsky and Tafel steps of the HER is obtained by using electrochemical impedance spectroscopy (EIS) and steady-state dc methods. As well as rate information, the charge, q_1, corresponding to maximum fractional coverage by the overpotentially deposited H species (OPD H), can be obtained and will be discussed in terms of the results previously found in acid and related to the surface geometry and coverage by UPD H. The results of the present work will also be compared with those of other recent studies conducted in alkaline media.

Coadsorption of Sulphur Containing Compounds and H At Pt, and its Effect on the HER Rates

The competitive *ad*sorption of catalyst poisons and *ad*sorbed H is of interest in relation to their effects in promoting H *ab*sorption into transition metals. The capacity of three sulphur- containing compounds, thiourea, L-cysteine, and 2,2' diethanolsulphide (DES), to block H adsorption at Pt electrodes in both the underpotential deposition (UPD)

and overpotential deposition (OPD) regions was studied and is presented in chapter 6. Chapters 8 and 9 investigate the influence of poisons on the absorption of H into Pd and Ni electrodes. Differences in the rates of adsorption (cysteine and DES < thiourea) and the reactivity of these molecules (thiourea > cysteine and DES) are shown to play important roles in the extent to which the poison, P, can block the UPD of H and modify the Tafel relationship for the hydrogen evolution reaction (HER) at Pt. The relative H blocking, due to poison coverage, θ_P, is measured by means of cyclic voltammetry and potential-relaxation transient experiments. Measurements of rates of the HER as a function of overpotential are also made utilizing steady-state techniques. It is shown that for θ_P of cysteine and DES < 0.9, inclusion of a constant site blockage term is sufficient to account for the observed kinetic behaviour. In the presence of adsorbed thiourea, and virtually complete initial coverages of cysteine and DES, i.e. before any H_2 evolution takes place, θ_P varies with potential according to an isotherm determined by the kinetics of hydrogenation and/or desorption of the poison.

H Absorption Into Pd and Ni Cathodes and the Effect of Adsorbed Thiourea

Pd and Ni electrodes both *ad*sorb and *ab*sorb H electrochemically. Using these two materials as cathodes the effects of the adsorption of thiourea on the electrochemical reactions of H, adsorption, absorption and evolution were studied. For Pd and Ni the rate of H absorption is monitored using the H permeation technique, developed by Devanathan and Stachurski (1962). In clean 0.5 mol dm^{-3} H_2SO_4, the transport of hydrogen into Pd is found to be influenced by the reaction conditions at the surface, i.e. following the behaviour of the adsorbed intermediate (θ_H); whereas the rate of H transport into Ni is independent of the electrode potential (a limiting diffusion condition).

The adsorption of thiourea dramatically inhibits, by over one order of magnitude of current, the rate of H entry into Pd. The amount of H which enters the Pd electrode at equilibrium or steady-state conditions was only slightly effected by the coadsorption of thiourea. This is discussed in terms of the chemical potential, μ_H, of the adsorbed H in clean and poisoned electrolytes.

The adsorption of thiourea at a Ni surface on the other hand appears to have a relatively small effect on the rate of H entry, but it does have a significant influence on the rate of H_2 evolution, this manifests itself in a significant change in the chemical potential (μ_H) of adsorbed H. One other factor which is also dealt with in this study is: The instability of the Ni surface in the presence of thiourea in 0.5 mol dm^{-3} H_2SO_4 under HER condition, caused by a reduction product of thiourea, (possibly H_2S or adsorbed S).

List of Symbols

υ_i rate of an electrochemical step /mol s^{-1} cm^{-2}.

r_o rate of electron production /mol s^{-1} cm^{-2}.

r_1 rate of production of adsorbed H ,θ_H /mol s^{-1} cm^{-2}.

r_2 rate of production of H_2 at the electrode surface, for the case when H_2 diffusion is important /mol s^{-1} cm^{-2}.

Or the rate of production of adsorbed poisons, θ_p, for the case when poison adsorption and desorption is important /mol s^{-1} cm^{-2}.

k_{ads} rate constant for the generalized under potential deposition reaction /mol s^{-1} dm^{-3}.

k_i chemical heterogeneous rate constant /mol s^{-1} cm^{-2}.

i_o exchange current-density /A cm^{-2}.

i current-density /A cm^{-2}.

i_{lim} diffusion limited current-density /A cm^{-2}.

J_∞ , i_∞ the steady-state H permeation current-density /A cm^{-2}.

J_{diff} the steady-state diffusion current-density of a species towards or away from an electrode; not necessarily a limiting-diffusion current /A cm^{-2}.

i_1 the steady-state H permeation current-density prior to the application of a potential-step (see chapter 7) /A cm^{-2}.

β Electron transfer symmetry factor (usually given a value of 0.5).

α charge transfer coefficient.

b Tafel slope /V.

E,η electrode potential or overpotential referenced to the RHE throughout the thesis /V.

RHE Reversible Hydrogen Electrode.

F	Faraday Constant /96485 C mol^{-1}.
R	Ideal Gas Constant /8.314 J mol^{-1} K^{-1}.
T	Temperature /K
t	time /s.
f	F/RT /V^{-1}.
j	$\sqrt{-1}$ (imaginary number).
ω	ac voltage frequency /rad s^{-1}.
Y_f	Faradaic electrode admmitance, a complex quantity, $(Y' + j\omega Y'' = 1/Z_f)$ /Ω^{-1} cm^{-2}.
Z_t	Total electrode impedance $Z' + j\omega Z'' = (Y_f + j\omega C_{dl})^{-1}$ /Ω cm^2.
C_{dl}	Electrode double-layer cpacitance /Farads cm^{-2}.
A	$1/(R_{ct}) = F(\partial r_o/\partial E)$ /Ω^{-1} cm^{-2}.
B, C, D & E	variable parameters used in ac impedance modelling, for specific definitions see chapter 4.
s	L^2/D_i an ac impedance modelling parameter characterizing diffusion processes /s.
L/δ	Diffusion-layer length or membrane thickness /cm.
Ω	electrode rotation-rate /rad s^{-1}.
D_i	Diffusion coefficient for species (i) / cm^2 s^{-1}.
θ_H	fractional coverage of adsorbed H (UPD or OPD).
θ_H^*	equilibrium frational H coverage; at $\eta = 0$ for OPD H, and at any E in the UPD H region.
θ_P	fraction coverage of adsorbed poisons (thiourea, cysteine, S, or diethanolsulphide).
q_1	charge for full fractional coverage of an adsorbed species ($\theta = 1$) /C cm^{-2}.
c_i^s	surface concentration of a diffusing electroactive species (i) /mol cm^{-3}.

c_i^b bulk concentration of diffusing electroactive species (i) /mol cm^{-3}.

c_o concentration of H inside an electrode; at the electrode surface /mol cm^{-3}.

c_{sat} saturation concentration of H inside a given metal /mol cm^{-3}; for Ni or Pd this value is suggested to be 60% of the number of metal atoms, i.e. Ni c_{sat} = 0.09 mol cm^{-3}.

c(x,t) the transient H concentration inside a metal membrane /mol dm^{-3}.

X_H fractional site occupany of H absorbed into a metal lattice; $c_o/c_{sat.}$

ΔG^o_{ads} standard free energy of adsorption /kJ mol^{-1}.

μ_H chemical potential of adsorbed H /kJ mol^{-1}.

ΔG^*_{ads} Gibbs energy of activation for the adsorption process /kJ mol^{-1}.

ΔH_{ads} enthalpy of adsorption /kJ mol^{-1}.

Φ electronic work function of a metal / eV.

$\Re$ Real part of a number or expression.

List of Figures

Chapter 1

Chapter 3

Chapter 1

Introduction

1.1 Historical Aspects

Heterogeneous catalysis, in general, relies on catalytic materials which possess very large surface areas at which the given process takes place with a lower activation energy than that for the corresponding homogeneously conducted reaction. They usually have mixed/multi-component amorphous compositions e.g. as for the "CoMoS" catalyst used in hydrodesulphurisation of petroleum and Raney Ni materials used in electrolyzers and Pt-alloys which are used as fuel-cell catalysts, etc. These materials, although they possess good catalytic properties, are difficult to use when studying the essence of the catalytic reaction (i.e. its reaction mechanism, intermediate states, role of adsorption, and influence of the chemical nature of the catalytic substrate material). The researcher often looks for a "model" system when desiring to investigate the above properties. In heterogeneous catalysis, modern fundamental research on the kinetics and mechanism of a reaction is often carried out in ultra high vacuum (UHV) where the reactant of interest can interact at a well defined surface without interference from impurities. In electrocatalysis the electrochemist must replace the vacuum with a contaminant-free conducting electrolyte; in many cases this is a salt, acid or base dissolved in ultrapure water.

The reactions which have received the most attention and which have practical interest are the generation of H_2 [1,2,3] or O_2,[4,5] (in electrolyzers, or the reverse reaction in fuel-cells) and the production of Cl_2 [6,7] (chlor-alkali process).

The hydrogen evolution reaction has been one of the most extensively studied

electrochemical reactions over the past 92 years since Tafel's historical paper [8]. The first demonstration of water electrolysis to produce H_2 and O_2 was that of Nicholson and Carlisle in 1800 after learning of the recent development, at that time, of the Volta pile. Faraday's exploration of H_2 and O_2 generation in 1834 resulted in his two laws of electrolysis. The next historical milestone in the research into the hydrogen evolution reaction, abbreviated from this point on as HER, was in 1905 when Tafel [8] performed his pioneering work (originating from studies on the electrochemical hydrogenation of strychnine) which led to the development of the empirical relationship between the log of the electrochemical reaction rate (current-density, i) and the applied electrode voltage (η) measured relative to the potential for the same process proceeding reversibly at zero net i, the Tafel relation:

$$\eta = a + b \log(i) \qquad (1.1)$$

In the years which followed, investigations into the HER using a variety of metallic substrates and under many different conditions, e.g. at various pH's, use of a variety of electrolytes and solvents and H_2 pressures) were undertaken [9]. The ease with which aqueous electrolytes and electrode surfaces could be prepared and handled, (although in these early works the purity and cleanliness was not very good) in addition to the rudimentary equipment needed to make steady-state dc polarization measurements at most cathode materials, influenced greatly the amount of work carried out on the HER in those early years.

Even after Tafel's demonstration of the i(η) relationship, the predominant opinion of electrochemists was that reaction rates were controlled by chemical and diffusion

processes taking place away from the electrode surface and that electron transfer was virtually instantaneous. Studies examining the complexities of the HER mechanism and the elementary act of proton discharge were influenced by three factors (concepts) which were not discovered and generally accepted until the early 1930's. They are summarized below:

1) The recognition of the importance of the adsorbed H intermediate in the HER by Horiuti [10] in 1935 and its quantitative treatment by Butler [11] (1936), and the first experimental demonstration of what is now known as underpotential deposition of H (UPD of H) by Frumkin and Slygin [12].

2) The development of theories describing the rate of electron transfer at the electrode surface as a function of potential, including the introduction of the transition-state theory into electrode kinetics by Eyring and co-workers, based on earlier treatments by Erdey-Gruz and Volmer [13], Gurney [14] and by Butler [11].

3) The introduction by Gurney [14], for the first time, of the role of quantum-mechanical tunnelling of electrons in charge-transfer, predating the fuller development of this concept in later work by Weiss [15], Landau [16] and that of Marcus [17].

4) The introduction of the electrochemical double-layer concept, Stern (1924) [18], following Gouy [92], and the refinements made to the model through the meticulous experimental work of Grahame (1947) [19]. As well, the involvement of the double-layer in influencing charge-transfer rates, as proposed by Frumkin

(1933) [20], and later reviewed by Parsons in (1960) [21].

During the period between the 1940's and the 1970's, the introduction of more sophisticated measuring equipment (e.g. the potentiostat and on-line computers) and, from this, the advent of different measuring techniques, lead to renewed interest and new reinvestigations of the HER.

We see that various ideas concerning the HER mechanism were suggested during this time period. A specific example is the work of Horiuti *et al.* [22] who, based on their interpretation of radiotracer measurements and evaluations of stoichiometric numbers measured at both Pt and Hg substrates, advocated the participation of the H_2^+ intermediate. Others, e.g. Bockris [23] and Conway [24], being two of the major contributors at this time, contended that, for most metals, the HER mechanism follows the three-step process, shown below, involving adsorbed H as the intermediate. This scheme, steps I and II or III, is generally agreed upon at the present time. In acidic electrolyte these steps are written in the usual way as:

$$M + H_3O^+ + e^- \rightleftharpoons MH_{ads} + H_2O \qquad \textbf{(1.I)}$$

followed by either

$$MH_{ads} + H_3O^+ + e^- \rightleftharpoons H_2\uparrow + H_2O \qquad \textbf{(1.II)}$$

or

$$2MH_{ads} \rightleftharpoons H_2\uparrow + 2M \qquad \textbf{(1.III)}$$

Steps I, II and III are referred to, respectively, as the Volmer [13], Heyrovsky [25] and Tafel [8] reactions.

In more recent times, the availability of increasingly sophisticated electrochemical equipment and computers which can perform time consuming analyses have lead again to

an increased knowledge of the factors affecting the HER. Two important techniques which have seen extensive use in evaluation of the HER kinetics are potential relaxation and electrochemical impedance spectroscopy (EIS). Fundamental investigations by Bai and Conway [26] in the late '80's were published in which the chemical nature and surface properties of the substrate metal as they affect the HER rate were studies and, in turn, the extent of coverage by H deposited in the overpotential (η) region.

The overpotential deposited (OPD) H is that deposited in excess of the UPD H which arises at the Pt metals at potentials positive to the RHE. Recent major contributions to this area have also come from Lasia *et al.* [27] who have characterized the catalytic properties of a variety of high-area Ni alloys using steady-state dc measurements along with EIS and from Jerkiewicz and Conway [28] on the relation between OPD H coverage at various overvoltages and the tendency for the H to become sorbed into the electrode metal, as at Pd, Ni, Fe, etc.

1.2 Electrochemical Behaviour of Multistep Reactions

1.2.1 Tafel slopes and exchange current-densities

With the exception of one-electron ionic redox reactions, most electrochemical reactions, as is also the case for many chemical reactions, proceed through several consecutive reaction steps in forming the final product. As well, a particular type of reaction or reaction step may take place simultaneously, in parallel with some other step or process, at a given potential on a given substrate, e.g. simultaneous hydrogen evolution often occurs during metal deposition at catalytically active substrates (Ni, Fe and their

alloys). Taking the HER as our model reaction, we shall then treat its kinetics in detail in order to provide the basis for characterization and analysis of a multistep process, involving consecutive and parallel reactions, and thus provide a basis for the work to be described later.

Two types of consecutive reaction pathways are recognized in the scheme I, II and III above. i) Initial proton discharge, step (I), producing an adsorbed H intermediate on the metal surface, followed by a second proton discharge with simultaneous reaction with the adsorbed H to form an hydrogen molecule. ii) Step (I) occurring twice forming two adsorbed H intermediates which then combine on the surface, step (III), forming an hydrogen molecule which becomes desorbed into solution; this H_2 diffuses away from the electrode usually forming H_2 bubbles after local supersaturation of the solution near the electrode interface, a significant process that is treated in the present work. Both steps (II) and (III) are fed by step (I) resulting in two parallel reaction pathways for H_2 formation.

A useful way of examining the electrode kinetics is to plot the overpotential (η, the potential measured against the reversible potential of the reaction of interest) *vs.* the log of the current-density (i, the reaction rate in amperes per unit electrode area), the so-called "Tafel plot"; if this is done for each reaction step, the effect of consecutive and parallel reactions/reaction steps on the overall $i(\eta)$ relationship can be seen.

Figs. 1.1a and b show Tafel plots for consecutive and parallel reaction schemes, respectively. For consecutive reactions, the reaction rate is governed by the step with the *smallest* rate constant. In Fig. 1.1a it is shown how the overpotential can influence which

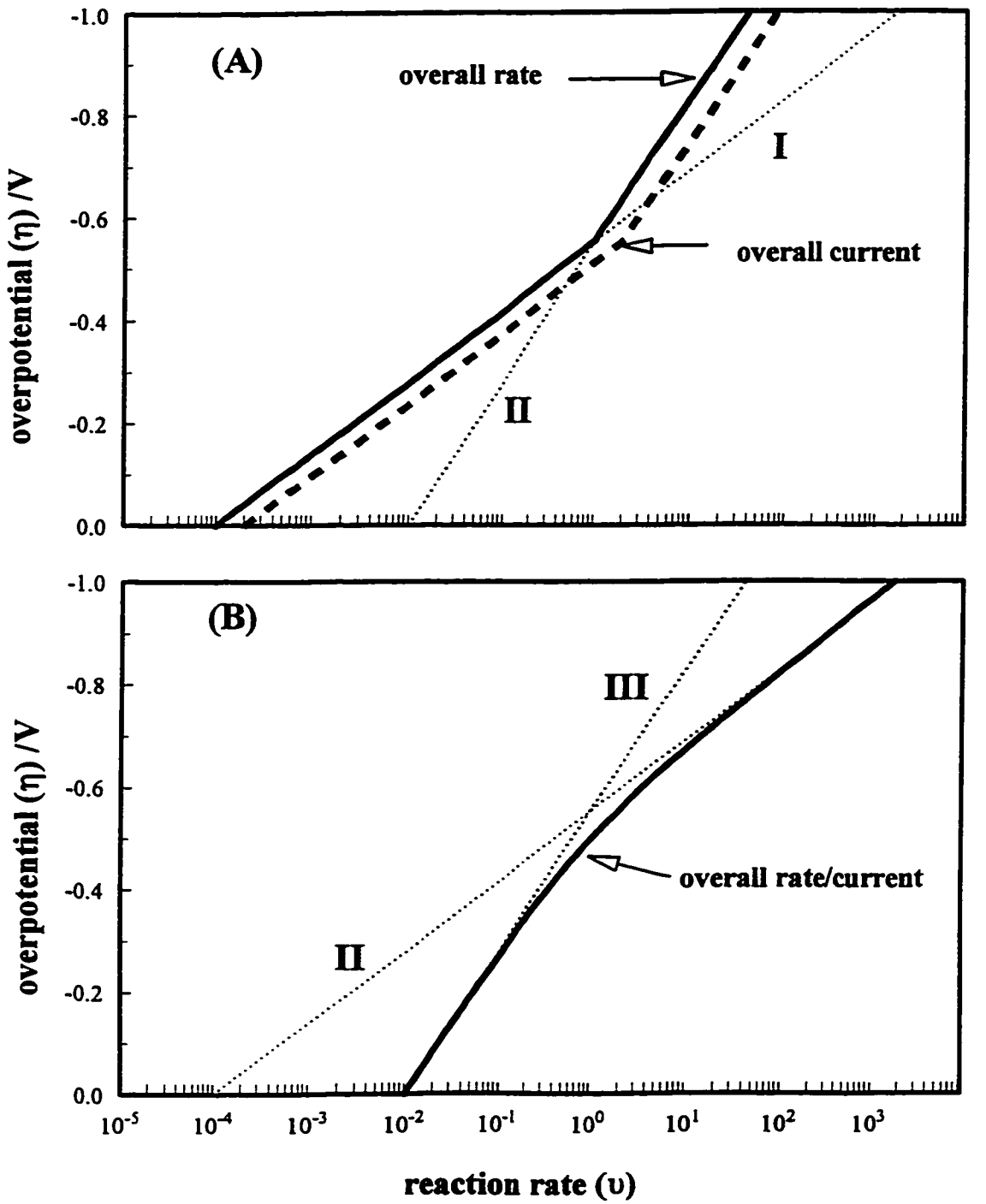

Fig. 1.1 A) A Tafel plot for a reaction with two consecutive reaction steps. Individual rates (dotted lines), overall rate (solid line) and the overall current (dashed line). **B)** A Tafel plot of two parallel reactions or reaction steps. Individual rates (dotted lines) and total rate and current (solid line).

step is rate-determining. This arises if the Tafel slope (b) and exchange current-density (i_o) for the two processes (I) and (II) have values: $b_I < b_{II}$ and $i_o(I) < i_o(II)$, as is the case for the example shown in Fig. 1.1a. For parallel reactions/reaction steps the measured rate corresponds to that of the *fastest* process/step. Again, as for consecutive reactions, the potential-dependence of the individual rates, through the parameters b and i_o, influences which step is rate-determining. In Fig. 1.1b at lower overpotentials, reaction (III) controls the rate due to its larger i_o value. As the overpotential increases, the rate of reaction (III) increases more rapidly than that of (II) and, after a critical overpotential, where the rates are identical, reaction (III) becomes rate-determining. In this example (Fig. 1.1b) the rate of step (I) is much larger than that of steps (II) or (III), and hence exerts no influence on the reaction rate and is not plotted.

It must be stated, because it is not clear from Fig. 1.1, that the rates for the consecutive reaction steps (although it is often said that one is the "slow step") *must* proceed at the *same* velocity in the steady-state. Note that the dotted lines are purely hypothetical in Fig. 1.1a. In contrast, the overall rate of the parallel reaction sequence is the *sum* of the rates of the parallel reaction steps. The rate of either parallel step is independent of the rate of the other although they can be coupled through the steady-state coverage of a reaction intermediate at a given value of η, e.g. steps II and III in the HER are coupled through the coverage by OPD H.

The governing factors determining the $i(\eta)$ relationship are varied, but are usually specific for a given type of reaction. For example, factors such as, the extent of formation of an intermediate, adsorbed or in solution, and its changes with overvoltage, or the

diffusion of products/reactants towards or away from the electrode surface, or a chemical change of the surface with overpotential (passivation, corrosion) can affect the rate of one step differently from that of another. The importance of comparing both i_o *and* b when evaluating the electrocatalytic activity of two materials, can also be seen from Fig. 1.1b. If lines II and III were associated with two different electrocatalysts, comparison of the i_o values alone would indicate that material giving line II is the better electrocatalyst, but if it happens that the operating voltage for an application is greater than the critical overpotential value, the material giving line III would be evaluated and chosen as the better catalyst.

1.2.2 Activation and Diffusion Processes

Heterogeneous catalytic processes, unlike most homogeneous chemical reactions, include a mass-transfer step, propelling the reactant and product species towards or away from the surface. In electrochemistry the most recognizable indication of a mass-transfer limited reaction rate is the observation of a limiting current-density, i.e. the current-density is, or becomes, independent of potential as the latter is raised. Otherwise, if mass-transfer is rapid compared to the electrode kinetics, the current-density is a function of overpotential following some form of the Tafel relation. Three categories of mass-transfer are generally recognized:

1) diffusion of a species along a concentration gradient, determined by Fick's laws of diffusion;

2) migration of a charged species in an electric field (e.g. that which is set

up when a build up of one of the charged species occurs at the interphase); and

3) convection which can be broken down into: natural convection - the flow of species caused by density differences near the interphase and forced convection - the flow of species induced by stirring or pumping of the electrolyte.

If a large excess of supporting electrolyte is present, significant electrolytic migration of the reactant ion species will not occur. The experimental arrangement used for the present work employed a rotating disk electrode (rde) [29]. This provides well defined forced convection, leading to a uniform concentration of species from the bulk to a distance close to the electrode surface. From there mass transport occurs via diffusion of the electroactive species through a thin layer, the so called "Nernst diffusion layer" symbolized, in thickness, as δ. The diffusion-layer length (thickness) is dependent on the hydrodynamic properties of the electrolyte. For example, the Nernst diffusion-layer length is inversely proportional to the rotation rate of a rotating disk electrode (rde), i.e. as the rotation rate increases, the diffusion-layer thickness decreases, resulting in an increase in the diffusion rate which is measured as an increase in the current-density.

Mass-transport effects on the reaction rate are taken into account theoretically by explicitly including the surface concentration of the reactant and product species in the overall rate equation. In order to illustrate the effects diffusion can have on the measured $i(\eta)$ relationship, a simple one-electron reduction reaction, written as follows, is used as the example:

$$Red^b \leftrightarrow Red^s \overset{ne^-}{\rightleftarrows} Ox^s \leftrightarrow Ox^b$$

The reactants (Red) diffuse to the surface and react to give the product (Ox) which then diffuses into the bulk. The superscripts b and s indicate bulk and surface species, respectively. The rate of the reaction assuming that the forward and backward electrochemical rate constants are equal at eqilibrium and equating them to i_o/F leads to the following rate equation with $f = F/RT$:

$$i = i_a - i_c = i_o\left(\exp((1-\alpha)\eta f)\left[\frac{c^s_{Ox}}{c^b_{Ox}}\right] - \exp(-\alpha\eta f)\left[\frac{c^s_{Red}}{c^b_{Red}}\right]\right) \qquad (1.2)$$

Experimentally, if the ratio of the surface and bulk concentrations is between 1.1 and 0.9 a quasi-quantitative measurement of the electrode kinetics can be made. If mass-transport is rapid then eq. 1.2 becomes the Butler-Volmer equation for activation-control. When the system has reached the steady-state it is thought that a linear concentration gradient is established through the Nernst diffusion-layer. Diffusion can be associated with either the reactants or the products.

1.2.2.1 Reactant diffusion

As current is passed through the cell the local concentration of the reactant at the electrode surface becomes smaller than its bulk concentration. When c^s, the surface concentration, becomes zero a limiting current is observed. To analyse this case, c^s_{Ox}/c^b_{Ox} is set equal to 1 for the above reaction; therefore any diffusive effects will be attributed to Red alone. Solving the general relation for the diffusion current, $i = nFD(\partial c^s/\partial x)_{x=0}$, under the condition of a linear concentration gradient gives:

$$i_{dif} = \frac{-nFD}{\delta} (c^{s}_{Red} - c^{b}_{Red}) \quad \textbf{(1.3)}$$

with D being the diffusion coefficient (mol sec^{-1} cm^{-2}) and δ the diffusion-layer thickness (cm). The limiting current-density (i_L) is calculated when c^{s}_{Red} equals zero in eq. 1.3. The ratio of the current-density to the limiting current-density is equivalent to the fraction $(c^{s}_{Red} - c^{b}_{Red})/c^{s}_{Red}$; after rearrangement, the ratio of the concentration at the surface to that of the species in the bulk solution can be expressed as:

Reactant Diffusion

$$\frac{c^{s}}{c^{b}} = 1 - \frac{i}{i_L} \quad \textbf{(1.4a)}$$

or

Product Diffusion

$$\frac{c^{s}}{c^{b}} = 1 + \frac{i}{i_L} \quad \textbf{(1.4b)}$$

Here the concentrations represent either that of the Red or the Ox species. Equation 1.4a applies to reactant diffusion while eq. 1.4b applies to product diffusion, i.e. depletion *vs.* accumulation. Substitution of eq. 1.4a into eq. 1.2, for the fraction $(c^{s}_{Red}/c^{s}_{Red})$ produces the following expression for the current-density as a function of overpotential:

$$i = \frac{-i_o \left[\exp(-\eta f) - \exp(\eta f)\right]}{1 + \frac{i_o}{i_L} \exp(\eta f)} \quad \textbf{(1.5)}$$

The $i(\eta)$ relationships in eq. 1.5, in addition to those for activation-control alone, for three different i_o values are shown in Fig. 1.2. The surface concentration of Red approaches zero ($i \rightarrow i_L$), when $(i_o/i_L)\exp(\eta f)$ is large compared with 1 in the denominator of eq. 1.5, and when η is sufficiently large that the back reaction does not influence the overall rate. All three curves in Fig. 1.2 exhibit a limiting current-density region. The overpotential at

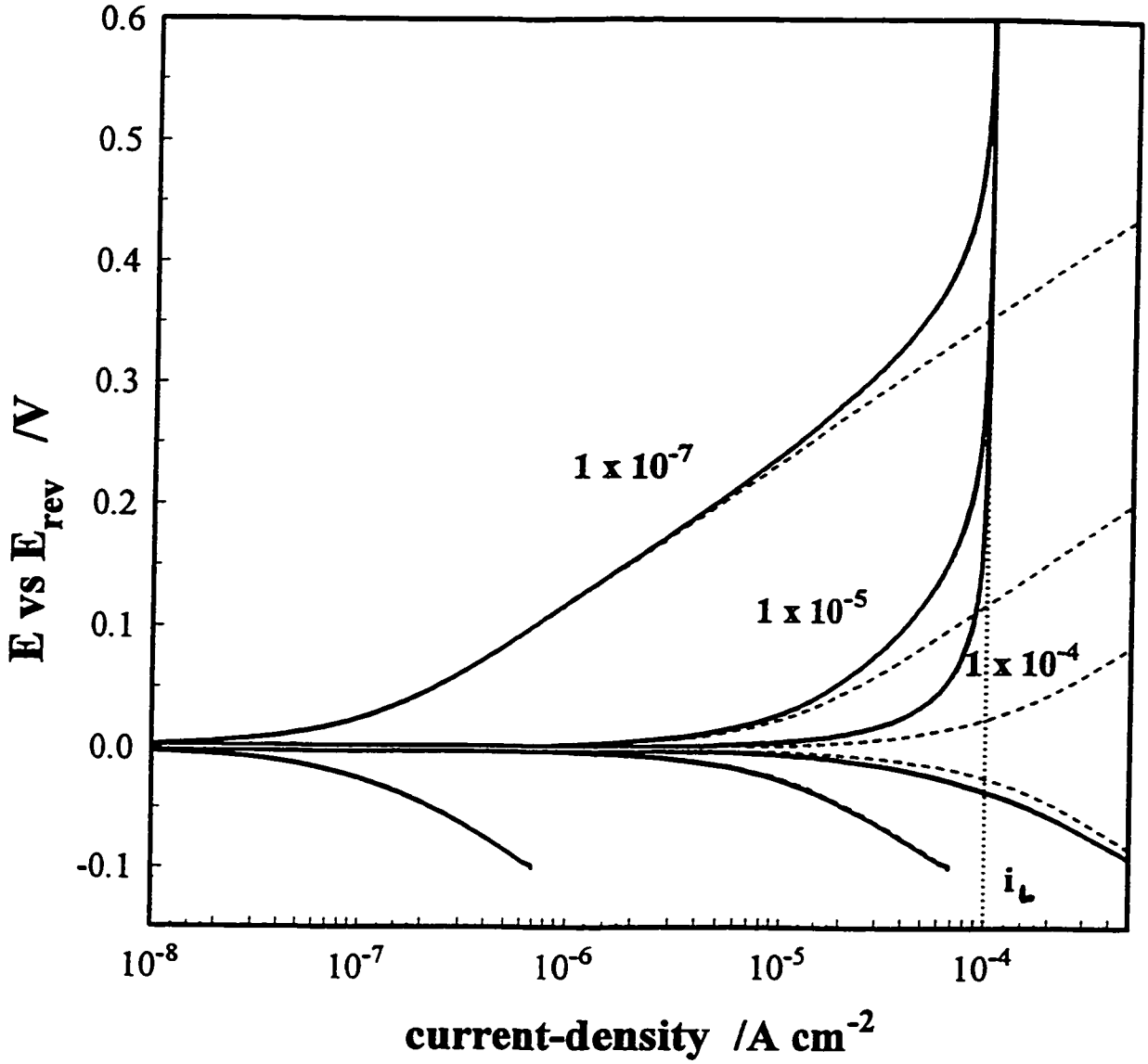

Fig. 1.2 Tafel plot showing the effect of reactant diffusion on a simple one electron charge-transfer reaction. Activation and diffusion - solid lines; activation alone - dashed lines; numbers represent the i_o values (A cm^{-2}) for the respective lines; $i_L = 1 \times 10^{-4}$ A cm^{-2}, $\alpha = 0.5$, throughout.

which this region is reached depends, however, on the i_o to i_L ratio. At smaller values of i_o, for the curve on Fig. 1.2 with an i_o to i_L ratio = $1 \times 10^{-7} / 1 \times 10^{-4} = 0.001$, a substantial activation-controlled region ($0 < \eta < 200$ mV) arises on the Tafel plot. For i_o values which are comparable to i_L, only a very small region of activation control is seen (see the curve for $i_o = 1 \times 10^{-5}$ A cm^{-2} in Fig. 1.2). Then, only with other techniques, e.g. EIS, electrode rotation-rate studies, potential-decay or potential-step transient methods, can quantitative information on the charge-transfer process be extracted.

In terms of the HER, this type of diffusion-controlled reaction is found to occur [30] at low concentrations of H_3O^+ (e.g., pH 2.0 - 6.0). At higher pH values the discharge step (Volmer) abstracts the H atom from H_2O instead of H_3O^+. In the case of proton abstraction from H_2O the reaction rates are usually several orders of magnitude lower (at a given η) than those for which the discharge occurs from H_3O^+ [26, 30]. This slower electrode reaction usually leads to a less pronounced diffusion effect.

1.2.2.2 Product Diffusion

As current passes, the surface concentration of the reaction product becomes greater than that in the bulk. Accumulation of the product then takes place until a process parallel to diffusion is favoured, e.g. crystallization, precipitation or gas evolution. No limiting current-density is observed for this case.

The mass-transport effects of Ox on the above anodic reaction are derived by following a similar procedure as that for reactant diffusion. The difference is that eq. 1.4(b) is substituted for c^s_{Ox}/c^b_{Ox} in eq. 1.2 and the ratio c^s_{Red}/c^b_{Red} is now set to one. This yeilds the the following i(η) relationship:

$$i = \frac{-i_o\,[\exp(\eta f) - \exp(-\eta f)]}{1 + (i_o/i_L)\exp(-\eta f)} \qquad (1.6)$$

Unlike eq. 1.5, when the term $(i_o/i_l)\exp(-\eta f)$ in the denominator is large compared to one, eq. 1.6 will become transformed into:

$$\eta_{dif} = \left(\frac{2.3RT}{nF}\right) \log\left[1 + \frac{i}{i_L}\right]$$

or

$$\eta_{dif} = \left(\frac{2.3RT}{nF}\right) \log\left[\frac{c_{Ox}^{s}}{c_{Ox}^{b}}\right] \qquad (1.7)$$

The electrochemical step is practically in equilibrium and the potential difference is determined solely by the ratio of the surface to bulk concentration of Ox, in a quasi-Nernstian equation. In Fig. 1.3 this behaviour is best illustrated when $i_o = 1 \times 10^{-1}$ A $cm^{-2} = 1000(i_L)$, showing a distinctive 60 mV $decade^{-1}$ Tafel region at lower overpotentials. At high overpotentials the current-density calculated from eq. 1.6 approaches that of the activation-controlled process alone, displaying an 120 mV $decade^{-1}$ Tafel slope.

The potential regions of product diffusion are in some ways the converse of that arising for reactant diffusion; in the sense that, the rate of the electrocatalytic surface-step is rate-determining at low overpotentials for reactant diffusion and at high overpotentials for product diffusion. Experimentally, Tafel behaviour for product diffusion may not exactly follow that in Fig. 1.3. Examples of this behaviour are seen for certain gas evolution reactions at extremely active electrocatalysts. These deviations from the theory arise when the parallel process of bubble formation occurs, consequently breaking up the

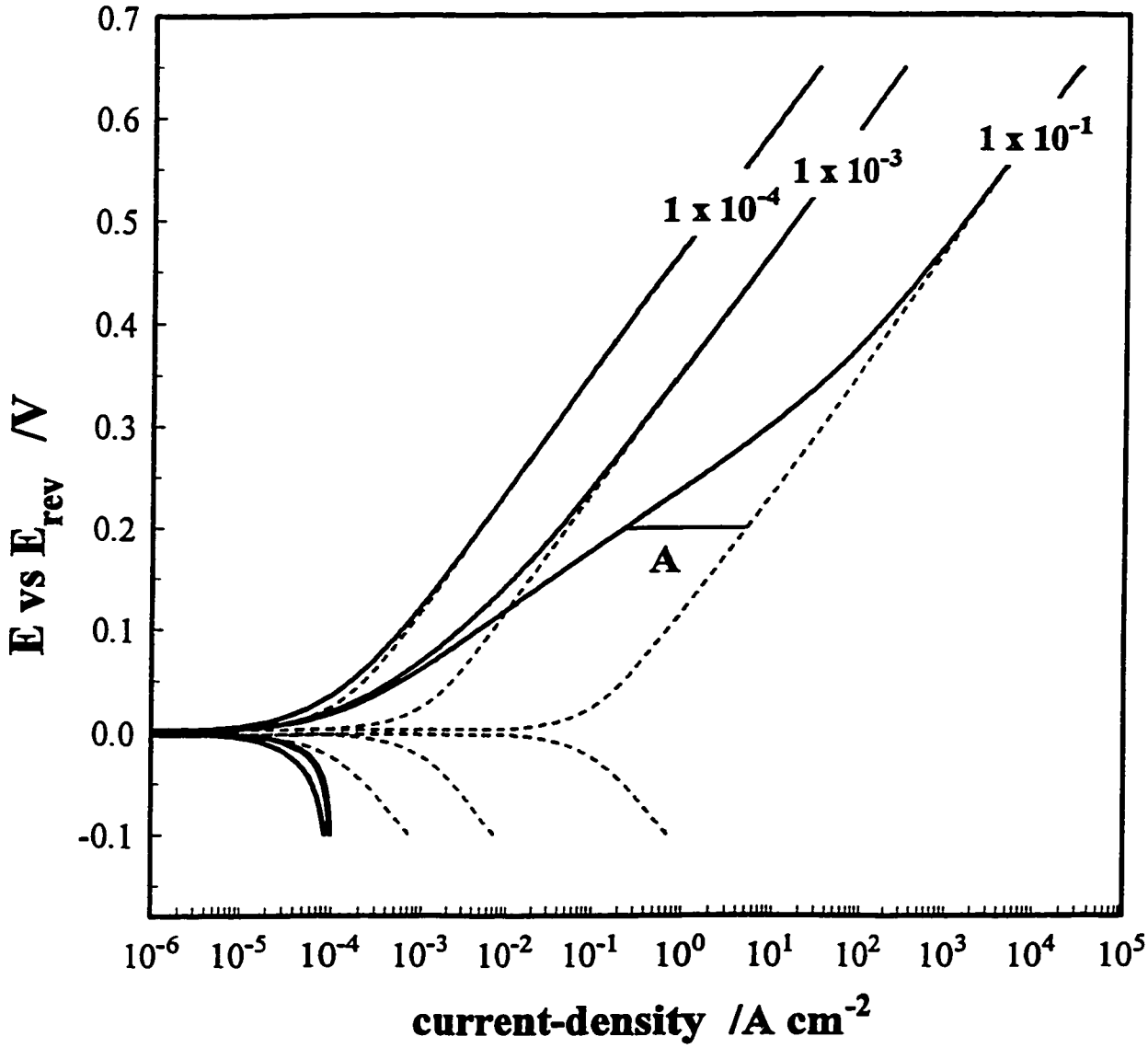

Fig. 1.3 Tafel plot showing the effect of product diffusion on the kinetics of a simple charge transfer reaction. Activation and diffusion steps - Solid lines; Activation alone - dashed lines; numbers refer to i_o values in A cm^{-2} of the respective curves; line A depicts a jump from diffusion to activation control which may occur upon bubble formation(see text); i_L= 1 x 10^{-4} A cm^{-2}, α = 0.5, throughout.

diffusion layer. This manifests itself in a zero mV decade^{-1} Tafel slope where the reaction *jumps* from diffusion to activation control. At 200 mV in Fig. 1.3, line **A** depicts the effect of bubble formation on the reaction rate. Several researchers have documented this type of behaviour, e.g. Losev *et al.* [31] for Cl_2 evolution on Pt and Schönfuss and Müller [32] for the HER at Pt in 5.0 M H_2SO_4. Other deviations may arise on account of products crystallizing onto the electrode surface, or precipitating out, changing the activity of the surface process. In the present context (HER), product (H_2) diffusion will be investigated as it is found to affect the reaction kinetics of the HER at single-crystal Pt(hkl) and Ir substrates.

1.2.3 Adsorbed Intermediates

Heterogeneous catalytic and electrocatalytic reactions, by definition, include the formation of an adsorbed intermediate surface complex. The reaction rate, energetics of adsorption, and the extent of coverage (θ_H) of the intermediate are all directly related (see § 1.3) and are the factors determining the electrocatalytic activity of a given substrate. Electrochemical techniques allow the evaluation of each of these three quantities. The potential dependence of θ_H will influence the Tafel slope, $(d\eta/d\log i) = b$, and in this way determine the reaction rate. For the HER a generalized relationship involving θ_H and η for the inverse Tafel slope is:

$$b^{-1} = \frac{d \ln \theta_H}{d \eta} + \frac{\beta F}{RT} \qquad (1.8)$$

where $d\log \theta_H / d\eta$ and $\beta F/RT$ are the electrochemical adsorption isotherm and the charge-transfer factors, respectively.

The rate equations for the three steps in § 1.1, i.e. Volmer, Heyrovsky and Tafel,

are expressed, with F/RT again denoted as f, as:

$$\upsilon_1 = k_1 (1-\theta_H) \exp(-\beta\eta f) - k_{-1}\, \theta_H \exp((1-\beta)\eta f) \quad (1.9)$$

$$\upsilon_2 = k_2\, \theta_H \exp(-\beta\eta f) - k_{-2} (1-\theta_H) \exp((1-\beta)\eta f) \quad (1.10)$$

and

$$\upsilon_3 = k_3\, \theta_H^2 - k_{-3} (1-\theta_H)^2 \quad (1.11)$$

When, at a constant potential, a steady-state current is passing, θ_H will be constant with time and can be expressed in terms of reaction velocites of the individual steps; thus

$$\frac{d\theta_H}{dt} = 0 = \upsilon_1 - \upsilon_2 - 2\upsilon_3 \quad (1.12)$$

Considering here only steps I and II as operative, and neglecting the reverse of the Heyrovsky step, θ_H is given by:

$$\theta_H = \frac{k_1 \exp(-\beta\eta f)}{k_1 \exp(-\beta\eta f) + k_{-1} \exp((1-\beta)\eta f) + k_2 \exp(-\beta\eta f)} \quad (1.13)$$

From eq. 1.13, the potential dependence of θ_H, in the form ($d \ln \theta_H / d\eta$) can be derived and its influence on the Tafel slope (b) found via eq. 1.8.

In order to illustrate this effect we shall consider two limiting cases where step II is rate-controlling: 1) When the terms $k_1 \exp(-\beta\eta f) \ll k_{-1} \exp((1-\beta)\eta f)$, a situation which is only possible when $k_{-1} \gg k_1$ and for small overpotentials, i.e. $\exp(-\beta\eta f)$ and $\exp((1-\beta)\eta f) \approx 1$; then eq. 1.13 can be approximated by:

$$\theta_H = K_1 \exp(-\eta F/RT) \quad (1.14)$$

which, after differentiation of $\log \theta_H$ with respect to η and substitution into eq. 1.8, a Tafel slope of: $b = -RT/(1+\beta)F$ or, with $\beta = ½$, as $b = -40$ mV decade^{-1} is found. At higher, (more negative) overpotentials, the relation between the terms in eq. 1.13 for θ_H,

will now be $k_1 \exp(-\beta\eta f) \gg k_{-1} \exp(-(1-\beta)\eta f)$ and $\gg k_2 \exp(-\beta\eta f)$, resulting in $\theta_H \approx 1$ and $d \log \theta_H / d\eta \approx 0$, yeilding a Tafel slope of RT/βF or -118 mV decade^{-1}. Taking the same approach as above but now allowing step III to be rate limiting, results in limiting Tafel slopes, with $\beta = 0.5$, of RT/2F (-30 mV decade^{-1}) and ∞ mV decade^{-1}. The latter case represents a current which is independent of potential, the reaction rate then being limited by the heterogeneous chemical reaction, step III.

The above analysis employs the assumption of Langmuir type adsorption of H. An arguably better model assuming Frumkin (ΔH_{ads} varying with coverage due to lateral or communal electronic interactions between adsorbates) or Temkin (ΔH_{ads} varying with coverage because of a energetic distribution among the adsorption sites) adsorption behaviour (both giving similar exponential mathematical relations between adsorption energy and coverage) can also be applied to the derivation of the HER kinetics, but leads to more complex analysis [24,33]. These types of adsorption isotherms, although more realistic, have had little application in terms of data analysis for the HER. The reasons for this are: i) an explicit equation of θ_H as $f(\eta)$ is not possible except by making several assumptions, some of which may not apply over the entire potential range[1], ii) for many metals θ_H does not change appreciably with overpotential (i.e. $\theta_H < 0.1$ or $\theta_H > 0.9$) at which point the Tafel slope becomes independent of the isotherm model, i.e. the Langmuir and Frumkin/Temkin approaches coincide and iii) metals where major changes in θ_H do occur with potential (i.e. Pt, Pd?, Ir, Rh and Ru), the interpretation of the results does not

---

[1]θ_H can be calculated numerically for Frumkin/Temkin adsorption conditions by solving eq. 1.8 using nonlinear-least squares methods.

usually necessitate use of the Frumkin/Temkin adsorption models since more than adequate representation of these results can be often found using the Langmuir model [34].

The approach used in the present work is based on the Langmuir model and no *a priori* decision is made concerning which step is rate-determining. Data analysis is achieved by fitting the data to the three-step HER reaction model using nonlinear least squares techniques, as will be discussed in detail later. Given a set of rate constants, the H coverage (θ_H) as f(η) is determined by solving the quadratic equation for θ_H which results from solving eq. 1.12, *viz*:

$$\theta_H = \frac{-b \pm \sqrt{b^2 - 4ac}}{2a} \qquad (1.15)$$

with a, b and c being:

$$a = -2(k_3 + k_{-3})$$

$$b = k_1 \exp(-\beta\eta f) + k_{-1} \exp((1-\beta)\eta f) + k_2 \exp(-\beta\eta f) + k_{-2} \exp((1-\beta)\eta f) + 2k_{-3}$$

$$c = -(k_1 \exp(-\beta\eta f) + k_{-2} \exp((1-\beta)\eta f) + 2k_{-3}$$

1.3 Specificity of H Adsorption to the Surface Structure of Pt Single-crystal Electrodes

1.3.1 The underpotential deposition reaction (UPD of H)

1.3.1.1 Thermodynamic rationalization

In the case of underpotential deposition processes, a clear thermodynamic condition for their observation can be specified as follows: the Gibbs energy of chemisorption to the surface lattice, ΔG_{ads}, must be less (more negative) than the Gibbs energy for formation of

the corresponding bulk material, e.g. as for H *vis à vis* ½H_2 or for metal adatoms *vis à vis* the bulk crystalline metal, on a molar basis. For H, this is represented as:

$$\Delta G_{ads,H} < \tfrac{1}{2}\Delta G_{H_2} \qquad (1.16)$$

i.e. for the formal chemisorption process ½H_2 + M → MH_{ads}, ΔG is negative at all coverages. This means that the binding energy of H to M, as ΔG, is stronger than that of H to another H atom in H_2, *vis* -215.5 kJ mol^{-1} per H_2/2. Such binding energies are strongly dependent on the electronic properties of the metal substrate, e.g. its work function. This situation arises for H at Pt, Rh, Ir, Ru and Pd, and also for a variety of base-metal atoms deposited at noble metals, e.g. Pb on Pt, Rh, Au, and Ag. In fact, some of the earliest studies on UPD were made with respect to base-metal adatoms [35], although the case of H at Pt was the first reported [12] but not at that time extensively studied.

Note that for the electrochemical half-cell reactions:

$$H_3O^+ + M + e^- \rightarrow MH_{ads} + H_2O \qquad \text{(UPD at M)}$$

or

$$H_3O^+ + e^- \rightarrow \tfrac{1}{2}H_2 + H_2O \quad \text{(OPD process at the equilibrium potential)}$$

one in relation to the other is simply equivalent to the dissociative chemisorption of H from gas-phase ½H_2, *viz.* ½H_2 + M → MH_{ads}.

When the condition (1.16) is fulfilled, the coverage by UPD species, e.g. H can be represented, in the limiting case, by a Langmuir isotherm (i.e. for random occupancy of a uniform substrate lattice and without external interactions between the adatoms):

$$\frac{\theta_H}{(1 - \theta_H)} = K_H \exp[-VF/RT] \qquad (1.17)$$

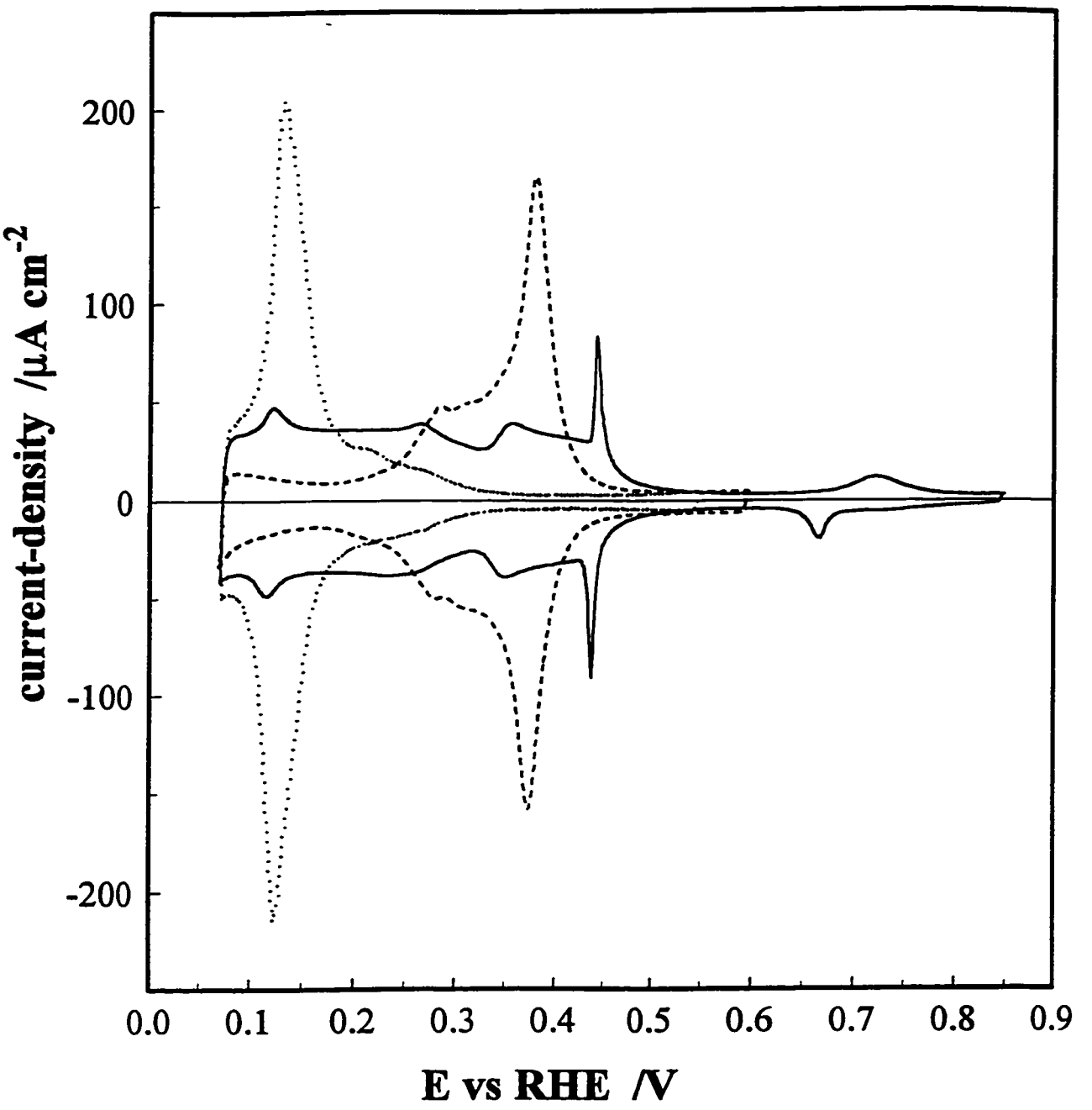

Fig. 1.4 Cyclic Voltammograms for the low-index single-crystal planes of Pt; (100)S_{II} ----, (111) —— and (110) ·····. Sweep rate 50 mV sec^{-1} 0.5 M H_2SO_4, T= 298 K.

where K_H contains the standard Gibbs energy of chemisorption, $\Delta G^\circ_{ads,H}$, i.e. $K_H = \exp[-\Delta G^\circ_{ads}/RT]$. From the form of eq. 1.17 it is seen that θ_H varies from a small value to near unity with increasing negative V, in fact, over about 120 mV to 95% coverage. Also, it is seen that the standard-state arises at $\theta_H = 1-\theta_H = 0.5$ for this case.

For more realistic conditions, where pair-wise lateral interactions are taken into account according to a Frumkin-type isotherm, the form of the relationship is:

$$\frac{\theta_H}{(1 - \theta_H)} = K_H \exp[-g\theta_H] \exp[-VF/RT] \qquad \textbf{(1.18)}$$

where g represents a lateral interaction energy parameter [36].

Since multiple-state chemisorption often arises in UPD processes, the course of increasing the coverage of the electrode surface lattice by electrosorbed ad-atoms cannot usually be represented by a *single* adsorption isotherm function such as eqs. 1.17 and 1.18 above.

One of the most significant aspects of the study of the UPD process, as revealed by cyclic voltammetry [37] and differentiated charging curves [12], has been the resolution of *multiple states* of chemisorption of the ad-species, *below a monolayer*, that are not due to the effects of polycrystallinity. Thus, one of the striking results in recent years has been that, at well ordered, single-crystal planes, multiple-state chemisorption of ad-atoms, e.g. H on Pt, Pb on Au, is still observed [37] and arises from progressive order/disorder 2-d lattice rearrangements in the ad-layer as coverage is increased, sometimes complicated by the co-adsorption of anions of the electrolyte, as with HSO_4^- at Pt(111) [38]. Such surface structures are now directly visible at atomic resolution under the Scanning Tunneling Microscope. As will be brought out later in this thesis, underpotentially

depositied H, e.g. at Pt, is the same chemical species as the adsorbed H intermediate in the HER but its binding to the surface is probably electronically and coordinationally different.

For base metals and also Au and Ag, UPD of H is undetectable but OPD chemisorption of the H intermediate in the HER must be involved in the mechanisms (e.g. I, II and III in § 1.1) of H^+ discharge and H_2 formation. In some cases, e.g. at Ni, the coverage of H as an OPD species at potentials negative to the H_2 reversible potential can be experimentally determined by means of transient methods [39].

1.3.1.2 Kinetic Interpretation

Underpotential deposition reactions, by their nature, are noncontinuous, reaching a finite equilibrium coverage of the deposited species rapidly at a given potential. Kinetic measurements of these reactions must then be based on time or frequency dependent techniques, e.g. potential-step [40], a.c. impedance [41,42], a.c. voltammetry [43] and fast-sweep cyclic voltammetry [44] methods. The noncontinuous nature of such UPD processes arises because, unlike H_2 evolution, the geometrical extent of coverage of an electrode surface, θ_H, by adsorbed H cannot exceed the available site-density, $\theta_{H,Max}$, for that adsorption.

As was noted previously the two adsorbed H species, OPD and UPD H, are chemically identical but differ in their bound state, including coordination, at the surface. This concept also applies to the species involved in the UPD of H alone where, as the coverage of H increases, the communal bonding configuration and energetics *must* change. With this in mind it is probably best to think of the UPD reaction as one in which, at each

potential (coverage), new communal arrangements of adsorbed H atoms arise [44,45] corresponding to communal changes of the electronic properties of the metal surface. In other words, at each potential (coverage) the UPD reaction is at equilibrium and each equilibrium state may have different reaction energetics, and kinetics, and sequential communal arrangements of the ad-species.

This approach is supported by the complex nature of the cyclic voltammograms for the UPD of H at the low-index Pt single-crystal surfaces as shown in Fig. 1.4, which cannot be interpreted by the use of either Langmuir or Frumkin type electrochemical isotherms. The voltammograms in Fig. 1.4 would indicate nonlinear dependences of the reaction energetics and coverage with potential and also major differences of adsorption energies with surface geometry (changes in Φ_e), which is to be expected [46]. The consequence of this type of interpretation in terms of the reaction kinetics is that the electrochemical rate constant, $k_{ads} = kT/h \exp(\Delta G^{\ddagger}_{ads}/RT)$ evaluated at one potential or coverage may be different from that evaluated at another potential, i.e. $\Delta G^{\ddagger}_{ads} \propto \Delta G^{\circ}_{ads}$ with its dependence on potential being a complicated function of several parameters as noted above. This situation is analogous to reaction kinetics based on Frumkin type adsorption where the role of the $\exp(-g\theta/RT)$ term can be thought of as a modifying function for the electrochemical rate constant, but unlike the observed UPD H behaviour the Frumkin modification is a simple exponential function of adsorbate converage.

Another important complexity entering into the interpretation and modelling of the H UPD process is the co-adsorption of specifically adsorbing anions (SO_4^{2-} or HSO_4^-) at potentials down to 0.150 V *vs.* RHE for the (110) face [38]. The amount adsorbed and

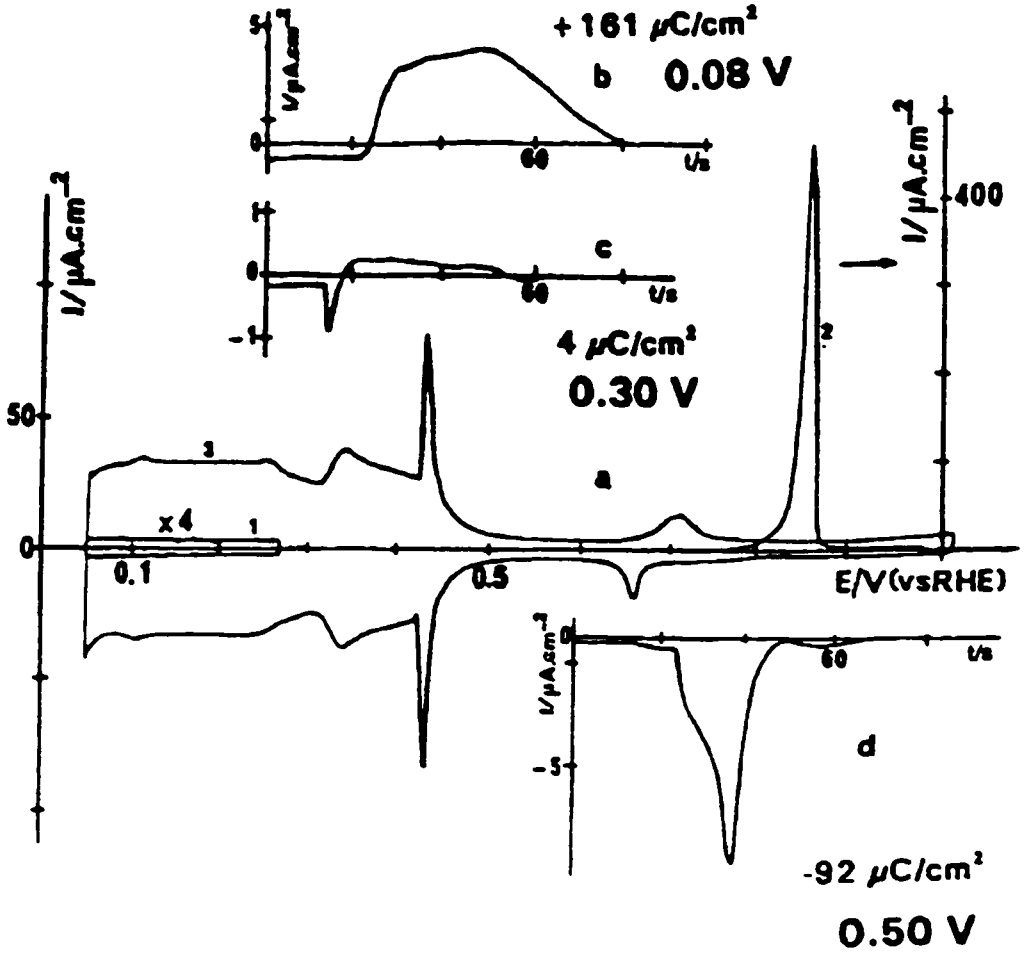

Fig. 1.5 Cyclic voltammogram and current transients from CO displacement measurements at Pt(111) [38]. 0.5 mol dm^{-3} H_2SO_4, 50 mV sec^{-1}, electrode potentials for the displacement measurements are given on the Figure. Anodic and cathodic current transients correspond to the desorption of H and HSO_4^- or $SO_4^=$ respectively.

the range of potential over which the anion is adsorbed, as well as the dependence of the adsorption on substrate surface structure, was characterized by Clavilier *et al.* [38] using the electrochemical displacement technique of MacDougall and Conway [47], employing CO as the displacing molecule. The method consists of holding the electrode potential at a constant value, where adsorption of H or the anion species is known to take place, and then passing CO gas into the solution and recording the desorption current transient. The sign of the current transient, anodic (+ve) or cathodic (-ve), during displacement is specific for H and anion desorption, with the displacement reactions being, for the anodic H desorption:

$$M-H_{ads} + CO \Rightarrow M-CO_{ads} + H^{+}_{aq} + e^{-} \qquad \textbf{(1.IV)}$$

and for the cathodic HSO_4^- desorption:

$$M-(HSO_4)_{ads} + CO + e^{-} \Rightarrow M-CO_{ads} + HSO_4^{-} \qquad \textbf{(1.V)}$$

The anodic H, low potential, and cathodic HSO_4^-, high potential, transients measured at the Pt(111) face are shown in Fig. 1.5, cf. Clavilier *et al.* [38]. The adsorption of anions and their coadsorption with UPD H was observed as well by Morin *et al.* [45] in this laboratory by EIS measurements at Pt(100), (110) and (311) single-crystal surfaces. The indicative feature in the EIS results associated with anion adsorption is an increase in the charge-transfer resistance which increases from an almost constant value of 0.4 Ω cm^{-2} between 0.075 to 0.375 V *vs.* RHE at Pt(100) to a maximum measured value of 2.5 Ω cm^{-2} at a voltage of 0.45 V *vs.* RHE where, from the voltammogram, Fig. 1.4, it can be seen that anion adsorption is complete. The measured potential range over which the anion adsorption takes place, measured by the two techniques corresponds well.

1.3.2 The hydrogen evolution reaction (HER)

The interaction of hydrogen, as H, with Pt has been extensively examined using surface science and electrochemical techniques which have shown that the H adsorption process is highly sensitive to the single-crystal surface structure. The bulk of the electrochemical studies of H adsorption at Pt have focussed on the behaviour of the easily evaluated, underpotentially deposited (UPD) H [37,45,48], as outlined above. The more weakly bonded, OPD H species is more difficult to characterize due to its participation, as an adsorbed intermediate, in the steps of the HER, see § 1.2.3. The electrochemical methods most commonly used for its evaluation are potential-relaxation [26,32], EIS [34,41,49] and potential-step coulometry [50,51,52], as well as classical dc Tafel steady-state polarization measurements.

These techniques have been successfully applied to the analysis of the HER kinetics and for evaluation of the OPD H coverages at Pt electrodes in basic solutions [26], as well as for relatively inactive Pt electrodes in acidic solution. However owing to the kinetic facility of the HER at clean polycrystalline Pt electrodes in acidic solutions the interpretation and analysis of the results obtained by these methods [26,50] has led to controversial conclusions [53], involving e.g. the possible formation of a near-surface hydride layer inside the Pt substrate. An alternate interpretation of the HER kinetic results at active Pt in acidic solution [32,41,53,54] is based on the formation of a supersaturation region of H_2 gas in solution at the electrode-electrolyte interphase, from which H_2 diffuses away. Application of the H_2 diffusion approach, as formulated by Losev [54], to the analysis of the steady-state current *vs.* voltage and potential-relaxation behaviour for a Pt

electrode in 0.5 M H_2SO_4, leads to results for which information about the kinetics of the actual reaction steps is obscured, at all potential studied, by the diffusion process and for which the diffusion process itself involving H_2 in the supersaturation region [32] is poorly characterized.

One of the clearest examples of electrocatalysis [46,55] is provided by the dependence of the kinetics of the HER, measured e.g. by its exchange current-density, i_o, on the cathode metal at which the process takes place. From Hg and Pb, to the Pt-metals, i_o varies over a range of ten decades, a result suggesting that a related dependence of HER kinetics on surface lattice structures of Pt would be expected.

The large variation of i_o appears empirically to be related to the work function, Φ, of the metal [56,57]. However, consideration of the energetics of electrode processes, as evaluated under conditions of experimentally controlled potentials, shows [24] that no direct involvement of Φ can arise. Experimental verifications using a variety of electrochemical couples have been given by several researchers, e.g. the $Fe^{2+/3+}$ couple by Bockris, Mannian and Danjanovic [58]; the $(Ru(NH_3)_6)^{2+/3+}$ couple by Wasita, Schmickler and Schultze [59]; the p-benzoquinone/ anion-radical couple in DMF with TEAP as the electrolyte by Parsons and Capon [60]. Rather, the apparent dependence of i_o or log i_o on Φ originates from a usually close relation between Φ and the heat of adsorption (ΔH_{ads}) of the H intermediate in the HER as was shown by Conway and Bockris [57]. The importance of the role of adsorption of H in the energetics of the HER was first discussed by Butler [11], related to the potential-energy curve representation of the activation process by Horiuti and Polanyi [61].

More detailed analysis [62] of kinetic and adsorption data for the HER shows that the relation of log i_o to metal properties follows a so-called volcano curve (cf. ref. 55) when plotted against metal(M)-to-H bond energy. This was recognized in important papers by Parsons [46] and Gerischer [63] in 1958 through the relationship of the product $(\theta_H^*)(1-\theta_H^*)$ to the standard Gibbs energy of chemisorption of H from $\frac{1}{2}H_2$, ΔG_H° where θ_H^* is the equilibrium fractional coverage of adsorbed H on the electrode surface. This relationship shows that a maximum in log i_o arises considering only Langmurian adsorption of H, when $\theta_H \simeq 0.5 \simeq 1-\theta_H$ and $\Delta G_H^\circ = 0$, for a value of the barrier symmetry factor $\beta = 0.5$. The maximum in log i_o at $\theta_H = 0.5$ holds regardless of which step in the HER mechanism is rate-controlling [46]. This is shown in Fig. 1.6 where log i_o is plotted *vs.* ΔG°_{ads} for each of the reaction steps I, II and III in the HER reaction mechanism. At

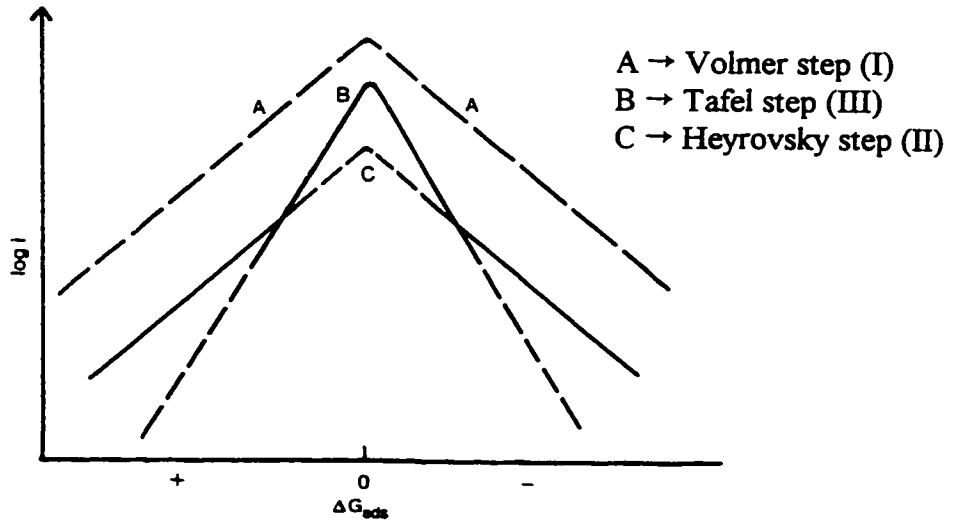

Fig. 1.6 Volcano plots showing theoretically derived curves representing the change of the log of the exchange current-density as a function of the standard Gibbs energy of adsorption for the three HER reaction steps [46].

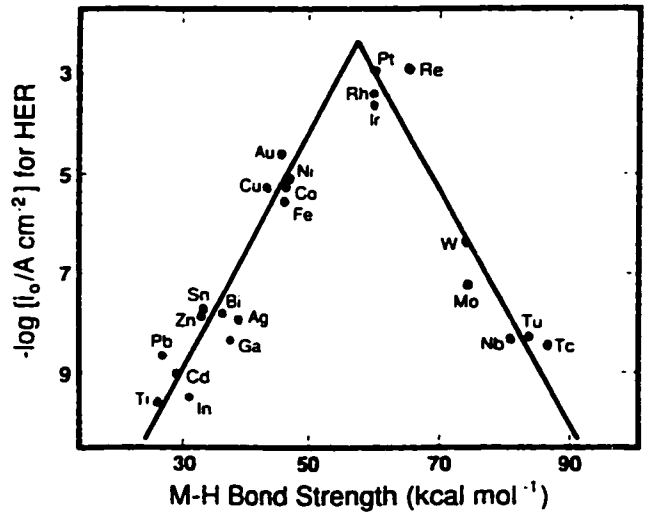

Fig. 1.7 Volcano plot of Trasatti [55] for log i_o values empirically plotted against M-H bond strength (which can be surface-structure dependent).

positive ΔG°_{ads} values, low equilibrium H coverages arise, and an exponential increase in i_o values is seen; conversely for negative ΔG°_{ads} values, where the H equilibrium coverage fraction approaches unity, an exponentially decreasing relation to i_o arises.

Although theoretically this relationship is independent of the rate-controlling process, practically the positive ΔG°_{ads} branch will usually correspond to the electrochemical adsorption, Volmer, step being rate-limiting while the negative ΔG°_{ads} branch would correspond to the electrochemical desorption, Heyrovsky, step being rate-limiting. Experimental values have been compiled by a number of workers and some of the best results, selected by Trasatti [55], are shown in Fig. 1.7.

It has been suggested [1] that the position of Pt at the top of the volcano curve of log i_o values *vs.* the standard Gibbs energy of adsorption of H (ΔG°_{ads}) is not so much because

$\Delta G^{\circ}_{ads} \sim 0$ (cf. ref. 46) for direct adsorption of H to the bare metal (in fact, the enthalpy of underpotentially electrosorbed H at a Pt electrode is a large negative value; see ref. 64) but because the relevant adsorption energy is that of the OPD H on, or amongst, a fully occupied lattice of UPD H, thus having smaller binding energy than that for the UPD of H at low θ_H. Therefore the ΔG°_{ads} for the OPD H could have a smaller value, around zero, on the "x-axis" of the volcano curve.

More recent work on the electrochemical surface science of Pt has demonstrated an high degree of specificity of the states and energies of UPD H to the 2-d lattice geometry (and related electronic properties) of Pt single-crystal surface planes [37]. Related to such observations are recent results from our own impedance studies which showed [45] that the *kinetics* of UPD of H are also clearly specific to surface lattice geometry. Of great interest, therefore, is the question whether the kinetics of OPD of H and the H_2 formation at finite overpotentials (η) are similarly dependent on surface geometry.

From the known major dependence of log i_o on cathode metal properties and the recently found [45] dependence of the kinetics of UPD of H on surface lattice structures of Pt, it is therefore surprising that what results have hitherto been obtained [51,65,66,67] on the influence of the surface structure of Pt on the H_2/OPD H kinetics indicate that there is *no* significant dependence. Contrarily, electrocatalysed reactions of small molecules at Pt are substantially sensitive to the crystal surface geometry, e.g. oxidation of HCOOH.

This unexpected result for the HER, and the contrary trends for the kinetics of the UPD of H [45], has led us to make a detailed study of the dependence of the kinetics of

the OPD H processes in the HER by means of ac impedance spectroscopy at several single-crystal surfaces of Pt having different geometries. Contrary to previous results [51,65,66,67], substantial specificity *is* found; the opposite conclusions reached in earlier work seem to be due to the real kinetic dependence on surface structure being obscured by effects associated with supersaturation by H_2 in the diffusion boundary-layer region [41] which arises at clean and hence active Pt cathode surfaces. By means of EIS measurements at rotated electrode surfaces, these complications due to H_2 diffusion can be factored out.

The resulting kinetic information is then found to be specific to the surface lattices examined and can be discussed in relation to the behaviour of the UPD of H on the same respective surfaces, as will be done later (see chapter 5). For most cases, with higher cathodic η, the H coverage will be expected [23] to increase beyond the UPD value at η = 0, so the important question arises how this extra H is accommodated in relation to occupancy of lattice sites on surfaces having various orientations. The state and chemical potential of this OPD H is also of major interest for the mechanism and rate of cathodic H sorption into certain transition metals [68].

A very limited amount of work on other single-crystal metals has been performed: for example, it was found by Piontelli *et al.* [69] that the kinetics of the HER at Ni, Cd, and V was structurally sensitive. In this work, *ca.* the 1960's, the single-crystal surfaces were not well characterized, by present standards.

The kinetics of the UPD of H from acidic solutions are greatly influenced by the Pt surface structure [45] as well as the HER kinetics in basic media, as found recently [70],

during the course of the present work. For the kinetics of the UPD of H [45] the rates of exchange are about two orders of magnitude lower on the (100) compared to the (111) face [45]. The use of single-crystal electrodes provides, in most cases, surfaces less active than Pt(poly) but which are still clean, and consequently allow for the opportunity to evaluate accurately the dependence of the reaction rates for the HER and the extent of OPD H formation on the surface geometries of different Pt single-crystal planes.

1.4 Relations Between H Adsorption, Absorption and H_2 Evolution, and the Effect of Competitively Adsorbed Poisons (e.g. S, Se, Te, As, Tl containing species)

The sorption of H into transition metals under cathodic polarization in aqueous solutions and in wet corrosion [71] is a topic of major interest in electrochemical surface science and in the materials science of metals. The process of H sorption into Fe and its alloys is well known to be promoted by catalyst poisons (P) such as As and S-containing compounds that are strongly chemisorbed at the metal. At other metals (in particular Pd), however, the effect of adsorbing these compounds leads to the opposite result, the inhibition of the rate of H sorption [72,73]. The mechanism(s) of the promotion effect is (are) poorly understood and quite controversial [68,74]. They must, however, be intimately connected with steps in the HER and the involvement of chemisorbed H in that process.

The study of poisoning of catalyst surfaces played an important and historical role in elucidation of the phenomenon of heterogeneous catalysis through the discovery that minuscule quantities of poisons could have a large effect on the rates of heterogeneous

reactions, a result that led to the concept of "active centres" [75,76,77]. Similar low-level effects of poisons were demonstrated in electrocatalysis of the HER [78,26]. It also appears that the mechanism of H absorption, in the absence of poisons (P) at a "clean" surface, is a contested issue [79], as recent articles have been indicating direct H absorption into the metal lattice by proton transfer whereas the bulk of the literature is centred around a mechanism involving an adsorbed H surface intermediate. The two mechanisms are written as follows:

direct H entry (Bagotskaya [80] and Frumkin [81]):

$$H^+ + M + e^- \rightleftharpoons M\text{-}H_{abs} \qquad \textbf{(1.VI)}$$

and with the adsorbed surface intermediate:

$$H^+ + M + e^- \underset{k_{-1}}{\overset{k_1}{\rightleftharpoons}} M\text{-}H_{ads} \qquad \textbf{(1.I)}$$

$$M\text{-}H_{ads} \underset{k_{-4}}{\overset{k_4}{\rightleftharpoons}} M\text{-}H_{abs} \qquad \textbf{(1.IV)}$$

with reaction 1.I being either that of the UPD of H or the Volmer step in the HER referred to earlier.

Most experimental evidence for either process is derived from H permeation experiments using the Devanathan-Stachurski [82] bielectrode technique. Briefly this method consists of electrochemically charging one side of a metal membrane with H while simultaneously anodically polarizing the other side of the membrane so that H which enters the cathodic side and diffuses through the membrane will be oxidized at the anodic side upon exiting the membrane. In this way the current and potential of H entry and exit

can be monitored at both sides of the membrane. Further experimental details, including a setup schematic, are described in § 3.6.

Considering the HER to proceed in parallel with the H *ab*sorption, the kinetic rate equations for the processes at the cathodic side of the membrane can be written as:

$$\upsilon_1 = k_1(1-\theta_H)\exp(-\beta\eta f) - k_{-1}\theta_H\exp((1-\beta)\eta f) \quad \textbf{(1.19)}$$

$$\upsilon_2 = k_2\theta_H\exp(-\beta\eta f) - k_{-2}(1-\theta_H)\exp((1-\beta)\eta f) \quad \textbf{(1.20)}$$

$$\upsilon_3 = k_3\theta_H^2 - k_{-3}(1-\theta_H)^2 \quad \textbf{(1.21)}$$

$$\upsilon_4 = k_4\theta_H(1-c_o/c_{sat}) - k_{-4}(1-\theta_H)c_o \quad \textbf{(1.22)}$$

with c_o representing the concentration of H inside the metal at x = 0, and c_{sat} being the value of c_o for saturation conditions. The current at the anodic side, assuming that a linear concentration gradient (see § 1.2.2, eq. 1.3) is set up throughout the membrane, is with D and L symbolizing the diffusion coefficient of H inside the membrane (mol sec^{-1} cm^{-2}) and the length of the membrane, respectively (cm) :

$$J_\infty = \frac{FDc_o}{L} = -F(\upsilon_4) \quad \textbf{(1.23)}$$

The surface coverage of H, and the subsurface concentration, c_o, are determined by applying the steady-state approximation, i.e.:

$$\frac{d\theta_H}{dt} = 0 = \upsilon_1 - \upsilon_2 - 2\upsilon_3 - \upsilon_4 \quad \textbf{(1.24)}$$

and for c_o:

$$\frac{dc_o}{dt} = 0 = \upsilon_4 - (J_\infty/F) \quad \textbf{(1.25)}$$

With θ_H and c_o explicitly in terms of the rate constants for steps 1 to 4, the cathodic and anodic currents are:

$$i_{cat} = -F(\upsilon_1 + \upsilon_2) \qquad J_\infty = -F(\upsilon_4) \quad \textbf{(1.26)}$$

From the above equations it is seen that J_∞ will increase with θ_H and reach a maximum value at $c_o = \frac{1}{2}c_{sat}$ for a given value of θ_H. For limiting cases, the i_{cat} (η) and $J_\infty(\eta)$ relationships (i.e. Tafel slopes) have been derived [74] and are indicative of the HER and H absorption reaction (HAR) mechanism and limiting conditions.

The direct relationship between θ_H and J_∞, as seen in Table 1.1, leads back to the curious situation of the promotion effect which adsorbed poisons exert on H sorption. Competitive adsorption of a poison, P, substantially diminishes θ_H in relation to its value in the absence of P at a given electrode potential [26,39], yet the current for H diffusing through the metal, J_∞ ,which is proportional to θ_H , increases. Several aspects of the mechanism of cathodic H sorption into metals were reviewed by Subramanyan [74]

Table 1.1

	$\frac{-\partial\eta}{\partial \log i}$			$\frac{-\partial\eta}{\partial \log J_\infty}$ or $\frac{-\partial\eta}{\partial \log \theta}$			$J_\infty = f(L)$; L= membrane thickness		
Mechanism of HER	Langmuir	Temkin Non-activated	Temkin Activated	Langmuir	Temkin Non-activated	Temkin Activated	Langmuir	Temkin Non-activated	Temkin Activated
Slow discharge-fast recombination	$\frac{2RT}{F}$	$\frac{2RT}{F}$	$\frac{2RT}{F}$	0	0	0	-	-	-
Slow discharge-fast electrochemical	$\frac{2RT}{F}$	$\frac{RT}{F}$	$\frac{RT}{F}$	$\frac{RT}{F}$	$\frac{RT}{F}$	$\frac{RT}{F}$	i^{-2}	i	i
Fast discharge-slow recombination	$\frac{RT}{2F}$	$\frac{RT}{2F}$	$\frac{RT}{F}$	$\frac{RT}{F}$	$\frac{RT}{F}$	$\frac{RT}{F}$	i	$i^{1/2}$	i
Fast discharge-slow electrochemical	$\frac{2RT}{3F}$	$\frac{2RT}{3F}$	$\frac{RT}{F}$	$\frac{RT}{F}$	$\frac{RT}{F}$	$\frac{RT}{F}$	$i^{2/3}$	$i^{2/3}$	i
Coupled discharge-recombination	$\frac{2RT}{F}$	$\frac{5RT}{2F}$	$\frac{3RT}{F}$	$\frac{4RT}{F}$	$\frac{5RT}{2F}$	$\frac{3RT}{2F}$	$i^{1/2}$	i	i^2
Coupled discharge-electrochemical	$\frac{2RT}{F}$	$\frac{2RT}{F}$	$\frac{2RT}{F}$	0	0	0	-	-	-

together with some discussion regarding suggestions that had been made previously [83-

86] as explanations of the promoting effect of chemisorbed catalyst poisons on H sorption at electrodes and also in wet corrosion (presumably through similar mechanisms to those at cathodes). The previous explanations took, however, no account of the *diminution* of the H coverage on cathode surfaces due to the competitive adsorption of the poisons. Some of the previous suggestions are, e.g. that M-H bond strengths were decreased due to the poison [91], that formation of gaseous hydrides (H_2S, AsH_3) or of "colloidal" particles were the origin of the effect or that poisons interfered with H atom recombination, leading supposedly to increasing probability of H entry, seem physically unrealistic [74] or are merely symptoms of the behaviour and not the physical process leading to the H absorption promotion effect.

In recent reports by Jerkeiwicz and Conway [68], and independently by Protopopoff and Marcus [87], the promotion effect was dealt with using a thermodynamic approach, looking at changes in the chemical potential of adsorbed H, μ_H, brought about by the co-adsorption of P. The basis behind this was that the presence of P led to changes of the configurational component of, μ_H, which in turn would increase the driving force for H entry into the metal lattice, assuming, as is usually done, that H enters via the adsorbed intermediate. It was later shown [28,68], however, that these changes of the H coverage, brought about by chemisorption of P, could not account for promotion of H sorption and only effects such as lateral surface-dipole interactions and/or communal electronic effects in the surface plasma could lead to a change (increase) in μ_H. The nature of the interactions between H and P that are needed to change μ_H in a way that the potential for H sorption is increased would have to be repulsive. In this way, however, the coverage of

θ_H would be decreased to a greater extent than for the case without interactions. These two effects thus tend to run counter to each other so that the overall increase in μ_H will be negligible in relation to the types of promoting effects seen experimentally [88].

The results presented here on the poisoning effects associated with competitive chemisorption of thiourea, cysteine and 2,2' diethanolsulphide (DES) on the UPD of H, i.e. below the H_2/H^+ reversible potential (Pt and Pd), and on the behaviour of the extra OPD H involved in the HER and hydrogen absorption reaction (HAR) at Pt, Pd and Ni, have been quantitatively evaluated by means of cyclic voltammetry, steady-state polarization measurements, potential relaxation transients, electrochemical impedance spectroscopy and H permeation measurements. These results provide the quantitative basis required for further understanding of effects of poisons on H coverage, thence H absorption. The interpretation of the results to be presented in later sections is based on four important aspects which, through the basis of their experimental acquisition, are important in understanding what role the poison plays in *ad*soprtion/*ab*sorption of H and the coupled evolution of H_2:

i) The poison's surface coverage, θ_P, can be potential dependent. This occurs either by reductive desorption of the poison or by simple electrostatic repulsion from the surface, involving preferred water-dipole polarization in the interphase [89,90].

ii) Upon the adsorption of poisons on the electrode surface, modifications to each separate HER/HAR rate constant takes place, i.e. k_1, k_{-1}, k_2, k_3 and k_4. This effects the overall HER and HAR rates (the H + H combination step is not the only step which is effected, as has been proposed in the literature [86]). This modifies the chemical potential

of the adsorbed H species (μ_H) which, through the θ_H terms in eqs. 1.24 and 1.25, exerts an influence on the *steady-state* or *equilibrium* concentration of H inside the metal.

These changes are associated with an interaction or chemical reaction between the poison (or the products of the poison's electrochemical degradation) and the metal surface. This interaction brings about local or communal changes in the M-H bond energy [91] (i.e. electron withdrawal or donation from the metal to the adsorbed poison, lateral surface interactions between the poison and H or actual chemical modification of the electrode surface with the formation of a metal-poison compound). As stated earlier in this section these changes in μ_H cannot be caused by the inclusion of a poison coverage term which only functions to block H adsorption.

iii) The coupling of the above mentioned changes in the HER/HAR reaction rates with active metal dissolution in a corrosion mechanism, e.g. as at Ni, can cause enhancement of the H sorption reaction although the poison (e.g. thiourea) may inhibit the metal dissolution process. It will be shown that although these two factors work in opposite directions in terms of enhancement of H sorption the modifications to the HER/HAR rates are so substantial that large increases in H-sorption are seen even though the dissolution reaction is severely impeded.

iv) A realization that both the kinetic and thermodynamic aspects of the H-sorption process need to be evaluated in order to fully appreciate the poison's involvement, i.e. a situation can be envisioned where the rate of hydrogen entry into the metal is decreased yet the equilibrium or steady-state H concentration inside the metal is increased. This will be explored further when the H-sorption results obtained by a variety of techniques at Pd

electrodes are discussed below.

References

1. B.E. Conway and B.V. Tilak, Adv. in Catalysis, 38 (1992) 1.

2. V. Plzak, B. Rohland and H. Wendt, Modern Aspects of Electrochemistry, Vol. 26, Eds. B.E. Conway, J.O'M. Bockris and R.E. White, Plenum Press, N.Y. (1994) pp. 105.

3. F. Gutmann and O.J. Murphy, Modern Aspects of Electrochemistry, Vol. 15, Eds. R.E. White, J. O'M. Bockris and B.E. Conway, Plenum Press, N.Y. (1983).

4. M.R. Tarasevich, A.Sadkowski and E. Yeager, Comp. Treatise of Electrochem., Vol. 7, Eds. B.E. Conway, J.O'M. Bockris, E.Yeager, S.U.M. Khan and R. White, Plenum, NewYork (1983) pp. 301.

5. J.P. Hoare, The Electrochemistry of Oxygen, Interscience Publ., N.Y., (1968).

6. F. Hine, B.V. Tilak, and K. Viswanathan, Modern Aspects of Electrochemistry, Vol. 18, Eds. R.E. White, J. O'M. Bockris and B.E. Conway, Plenum Press, New York, (1986) p. 253.

7. H.S. Burney, Modern Aspects of Electrochemistry, Vol 24, Eds. R.E. White, B.E. Conway and J. O'M. Bockris, Plenum, NewYork (1993) 393.

8. J. Tafel, Z. Phys. Chem. 50 (1905) 641.

9. K. Vetter, Electrochemical Kinetics, Academic Press, New York (1967).

10. J. Horiuti and M. Polanyi, Acta Physicochim. URSS, 2 (1935) 505.

11. J.A.V. Butler, Proc. Roy. Soc. London, Ser. A, 157 (1936) 423.

12. A. N. Frumkin and M. Slygin, Acta Physicochim., 64 (1960), 258.

13. T. Erdey-Gruz and M. Volmer, Zeit. Phys. Chem., A. 150 (1930) 203.

14. R.W. Gurney, Proc. Roy. Soc., London, A 134 (1931) 137.

15. J. Weiss, J. Chem. Phys., 19 (1951) 1066.

16. L. Landau, Phys. Zeit. Sowjetunion, 3 (1933) 664.

17. R.A. Marcus, J. Chem. Phys., 23 (1956) 966; R.A. Marcus, Can. J. Chem., 37 (1959) 138.

18. Stern, Zeit. Elektrochem., 30 (1924) 508.

19. D.C. Grahame, Chem. Rev., 41 (1947) 441.

20. A. Frumkin Zeit. Phys. Chem., A. 164 (1933) 121.

21. R. Parsons, Adv. in Electrochem. and Electrochem. Eng., Vol. 1, Eds. P. Delahay and C.W. Tobias, Wiley, NewYork, 1960.

22. G. Okamoto, J. Horiuti and Hirota, Sci. Papers Inst. Phys. Chem. Res., Tokyo, 29 (1936) 223; see also 28 (1936) 231; and J. Horiuti in E. Yeager (Ed.) Symposium on Electrode Processes, The Electrochemical Society, Wiley, NewYork (1961).

23. J. O'M Bockris and H. Mauser, Can. J. Chem., 37 (1959) 475.

24. B.E. Conway , "Theory and Principles of Electrode Processes", Ronald Press, New York (1964).

25. J. Heyrovsky, Rec. Trav. Chim. P.B., 44 (1925) 499.

26. L. Bai, J. Electroanal. Chem., 355 (1993) 37; L. Bai and B.E. Conway, Electrochim. Acta, 31 (1986) 1013.

27. A. Lasia and A. Rami, J. Electroanal. Chem., 294 (1990) 123; see also A. Lasia, in B.E. Conway and G. Jerkiewicz (Eds.), Proc. Symp. on Electrochemistry and Materials Science of the Cathodic Hydrogen Absorption and Adsorption, Vol. 94-21, The Electrochemical Society NJ., 261 (1994).

28. G. Jerkiewicz, J.J. Borodzinski, W. Chrzanowski, and B.E. Conway, J. Electrochem. Soc., 142 (1995) 3755; G. Jerkiewicz, J.J. Borodzinski, W. Chrzanowski, and B.E. Conway in, Proc. Symp. Electrochemistry and Materials Science of Cathodic Hydrogen Absorption and Adsorption, The Electrochemical Society, N.J., 94-21 (1995) 44.

29. B. G. Levich, Acta Physicochimica URSS, 17 (1942) 257; see also A.C. Riddiford, in Advances in Electrochemistry and Electrochemical Engineering, Eds. P. Delahay and C.W. Tobias, Vol. 4, Interscience Publishers, New York (1966), pp. 47-116.

30. D.R. Flinn and S. Schuldiner, Electrochim. Acta, 19 (1974) 421.

31. V.V. Losev, N.Y. Buné and L. Chuvaeva, Electrochim. Acta, 34 (1989) 929.

32. D. Schönfuss and L. Müller, Electrochim. Acta, 39 (1994) 2097.

33. J.G.N. Thomas, Trans. Faraday Soc., 57 (1961) 1603.

34. D.A. Harrington and B.E. Conway, Electrochim. Acta., 32 (1987) 1703; L. Bai, D.A. Harrington and B.E. Conway, Electrochim. Acta, 32 (1987) 1713.

36. Frumkin, Dolin and Ershler, Acta Physiochim., 13 (1940) 779.

37. J. Clavilier, A. Rodes, K. El Achi and M.A. Zamakhchari, J. Chim. Phys., 88 (1991) 1291.

38. J. Clavilier, J.M. Orts, R. Gómez, J.M. Feliu and A.Aldaz, Proc. Symp. on Electrochemisty and Materials Science of Cathodic Hydrogen Adsorption and Absorption, Eds. B.E. Conway and G. Jerkiewicz, The Electrochemical Society, NJ., 94-21 (1994) 167.

39. M. W. Brieter, J. Electrochem. Soc., 109 (1962) 42.

40. M. Rosen, D.R. Flin and S. Schuldiner, J. Electroanal. Chem., 95 (1979) 1.

41. M.W. Breiter in E. Yeager (Ed.), Symposium on Electrode Processes, The Electrochemical Society, Wiley, New York (1961), pp. 307-324.

42. V.I. Luk'yanycheva, E.M. Stochkova, V.S. Bagotskii and L.L. Knots, Elektrokhimiya, 7 (1971) 267.

43. D.A. Harrington, J. Electroanal. Chem., 355 (1993) 21.

44. H. Angerstein-Kozlowska and B.E. Conway, J. Electroanal. Chem. 95 (1979) 1.

45. S. Morin, H. Dumont and B.E. Conway, J. Electroanal.Chem., 412 (1996) 39, see also S. Morin, Ph. D. Thesis, University of Ottawa (1996).

46. R. Parsons, Trans. Faraday Soc., 54 (1958) 1053.

47. B. MacDougall, B.E. Conway and H. Angerstein-Kozlowska, J. Electroanal. Chem., 32 (1971) App.15.

48. S. Motoo and N. Furuya, J. Electroanal. Chem., 172 (1984) 339.

49. R. Durand, Electrochim. Acta, 24 (1979) 1095.

50. S. Schuldiner, J. Electrochem. Soc., 106 (1959) 891.

51. K. Seto, A. Iannelli, B. Love and J. Lipkowski, J. Electroanal. Chem., 226 (1987) 351.

52. Hanwei Lei, Bengliang Wu and Chuansin Cha, J. Electroanal. Chem., 332 (1992) 257.

53. M. W. Breiter, J. Electrochem. Soc., 109 (1962) 549.

54. V. V. Losev, Electrokhimiya, 17 (1981) 733.

55. S. Trasatti, J. Eletroanal. Chem., 39 (1977) 183.

56. P. Ruetschi and P. Delahay, J. Chem. Phys., 23, (1955), 105.

57. B.E. Conway and J. O'M. Bockris, J. Chem. Phys., 26, (1957), 532.

58. J. O'M. Bockris, R.J. Mannian, and A. Damjanovic, J. Chem. Phys., 48, (1968), 1898.

59. T. Iwasita, W. Schmickler and J.W. Schultze, Proc. Symp. on The Chemistry and Physics of Electrocatalysis, Eds. J.D. McIntyre, M.J. Weaver and E.B. Yeager, The Electrochemical Society, PV 84-12 (1984) pp. 591.

60. A. Capon and R. Parsons, J. Electroanal. Chem., 46 (1973) 215.

61. J. Horiuti and M. Polanyi, Acta Physicochim. URSS, 2 (1935) 505.

62. G.C. Bond, "Heterogeneous Catalysis", Clarendon Press, Oxford (1974).

63. H. Gerischer, Bull. Chim. Soc. Belg., 67 (1958) 506.

64. G. Jerkiewicz and A. Zolfaghari, J. Electrochem. Soc., 143 (1996) 1240.

65. I.I. Physhnogrva, A.M. Skumdin, Yu. B. Vasiliev and V.S. Bagotsky, Electrokhimiya, 6 (1970) 142.

66. S.Schuldiner, M. Rosen and D. Flin, J. Electrochem. Soc., 117 (1970) 1251.

67. H. Kita, S. Ye and Y. Gao, J. Electroanal. Chem., 334 (1992) 351.

68. B.E. Conway and G. Jerkiewicz, J. Electroanal. Chem., 357 (1993) 47.

69. R. Piontelli, G. Poli and G. Serravalle, Symposium on Electrode Processes, Ed. E. Yeager, The Electrochemical Society, John Wiley, New York, 1961, pp. 67-103; R. Piontelli, L. P. Bicelli and A. Vecchia, Lineci - Rend. Sc. fis. mat. e nat., 28 (1960) 139.

70. N.M.Marković, S.T. Sarraf, H.A. Gasteiger and P. Ross Jr., J. Chem. Soc., Faraday Trans., 92 (1996) 3719.

71. R.N. Iyer, I. Takeuchi, M. Zamanzadeh, and H.W. Pickering, Corrossion, 46 (1990) 360; see also O. Vosikovsky, M. Marecek, and D.J. Ross, Intl. J. Pressure Vessels and Piping, 13 (1983) 197.

72. J. H. Barber and B.E. Conway, J. Chem. Soc., Faraday Trans., 92 (1996) 3709.

73. M. Baldauf and D.M. Kolb, Electrochim. Acta, 38 (1993) 2145.

74. P.K. Subramanyan, in Comprehensive Treatise on Electrochemistry, Eds. J. O'M Bockris, B.E. Conway, E. Yeager and R. E. White, Plenum, New York, vol. 4 (1980), p. 11.

75. H.S. Taylor, J. Phys. Chem., 30 (1926) 145.

76. H.S. Taylor, Proc. Roy. Soc., London, A108 (1925) 105.

77. G.M. Schwab, Catalysis, Macmillan Co., London (1937) 280.

78. J. O'M. Bockris and B.E. Conway, Trans. Faraday Soc., 45 (1949) 989.

79. G. Zheng, B.P. Popov and R.E. White, J. Electrochem. Soc. 142 (1995) 154.

80. I. A. Bagotskaya, Zhurn. Fiz. Khim., 36 (1962) 2667.

81. A.N. Frumkin, Adv. in Electrochem. and Electrochem. Eng., Vol. 3 (1963) 287.

82. M.A.V. Devanathan and Z. Stachurski, Proc. Roy. Soc. London., A 270 (1962) 90.

83. K.E. Shuler and K.J. Laidler, J. Chem. Phys., 17 (1949) 212.

84. S.M. Belaglazov and M.I. Polukarov, Zh. Prikl. Chim. Mosk., 33 (1960) 389.

85. V.P. Alikin, Uchen. Zap. Perm. Gos. Univ., 19 (1961) 3.

86. U.R. Evans, The Corrosion and Oxidation of Metals, in Scientific Principles and Practical Appl., Arnold, London (1961) p. 397.

87. P. Marcus and E. Protopopoff, J. Chim. Phys., 88 (1991) 1423.

88. G. Jerkiewicz, J.J. Borodzinski, W. Chrzanowski and B.E. Conway, J. Electrochem. Soc., 142 (1995) 3755.

89. A.N. Frumkin, Zeit. Phys. Chem., 103 (1923) 55.

90. J.A.V. Butler, Proc. Roy. Soc., London, A 122 (1929) 399.

91. J. O'M Bockris, J. McBreen and L. Nanis, J. Electrochem. Soc. 112 (1965) 1025.

92. G. Gouy, J. Phys., 9 (1910) 457; Compt. Rend., 149 (1910) 654.

Chapter 2

Evolution and Aims of the Research

This research was initially undertaken to investigate the role and mechanism by which coadsorbed catalytic poisons promote H sorption into transition metal cathodes. In studying this phenomenon it was deemed necessary to examine how these poisons affect the adsorption of H in the absence of H sorption. This was accomplished by the examination of the underpotential and overpotential adsorption of H at Pt in alkaline and acidic electrolytes as it is affected by the coadsorption of sulphur-containing compounds.

The relation of poison adsorption to the coverage of overpotentially deposited H is manifested in the current-potential behaviour of HER at Pt. For a quantitative investigation of the poisoning influence it is imperative that the behaviour of the clean electrode surface be well characterized first. It was found that although much work had been done to study the rates of the HER at clean active Pt surfaces, substantial gaps in understanding, and debate on the actual mechanism and the rate-controlling process of the HER, still existed, see § 1.3.2.

These findings led to a reinvestigation of the HER and the OPD of H at clean Pt surfaces in 0.5 M H_2SO_4. Initially this part of the research was conducted using a polycrystalline Pt electrode, but in doing so we found that our results were inconclusive in respect of deriving information on the surface electrode process, as the reaction appeared to be diffusion controlled. At the same time that these studies were being undertaken it was found in our laboratory that the surface kinetics of the UPD of H at Pt were substantially sensitive to surface single-crystal geometry and, more importantly, that the

reaction rates at some single-crystal faces were much lower than at polycrystalline Pt. With this knowledge, an extensive study into the investigation of the HER at Pt(hkl) single-crystal electrodes was then pursued with the aim of characterizing quantitatively the kinetic behaviour of the HER and the extent coverage by OPD H at clean, well defined Pt surfaces.

The aims of this research project in order of their natural occurrence can then be stated as:

1) The evaluation of the H sorption promotion effect associated with coadsorbed catalytic poisons at transition-metal electrode substrates.

2) The effect that the adsorption of these poisons has on the underpotential and overpotential deposition of H as it relates to research aim (1) and the HER rates.

and

3) The study and characterization of the HER and the OPD of H at Pt single-crystal electrodes and examination of the relation of these processes to the surface lattice geometry and to the respective H UPD behaviour at such surfaces.

Additionally, another important aspect of the work evolved with regard to the application, and especially the interpretation, of ac impedance spectroscopy results applied to the HER at single-crystal Pt surfaces.

Chapter 3

Experimental

3.1 Choice of Experimental Procedures

The nature of the experimental work, and the aims of the research, necessitated complementary use of both steady-state polarization (Tafel relation) measurements and nonsteady state procedures such as electrochemical impedance spectroscopy (EIS), recording of potential-relaxation transients [13] from prior steady-state polarization and cyclic or single linear-sweep voltammetry. The use of these methods was coupled with studies employing rotating-disk electrodes in order to regulate diffusion processes at the interphases of the electrodes studied, especially the diffusion of H_2 *away* from cathodically polarized active single-crystal electrode surfaces. The results were also related to those obtained in the underpotential deposition (UPD) region for H electrosorption and desorption, previously studied in this laboratory by Morin [8]. In the EIS work, an important aspect was the use of computer simulation by non-linear least squares methods, in order to evaluate components of the EIS behaviour related to diffusion of H_2, electrosorption of H and double-layer capacitance, enabling the H_2 diffusion effects to be factored out from the overall electrode-kinetic behaviour of the HER at Pt cathode surfaces.

3.2 Electrochemical Cells and General Setup

The majority of the experiments, involving Pt single-crystal surfaces and Pt poisoning studies, were performed using a three-compartment rotating-disk electrode cell, shown in Fig. 3.1. The working electrode (rde) used in Fig. 3.1 could be interchanged to

any one of the following: a Ni rotating-disk and rotating-wire electrode (area = 0.002 cm^{-2}), a Pt polycrystalline rotating-disk electrode ($0.05 \leq$ area ≥ 0.5 cm^{-2}), Pt poly-oriented rotating-spheroid electrodes ($0.005 \leq$ area ≥ 0.01 cm^{-2}) and Pt(hkl) single-crystal rotating-disk electrodes (area ≈ 0.06 cm^{-2}).

The procedure for the preparation of the Pt polycrystalline surfaces consisted of: 1) for the disk electrodes, first polishing with SiC paper down to 4000 grit followed by polishing to a 0.25 μm finish with diamond paste. The polyspheroid electrodes were used, as formed, from melting of a Pt wire; 2) a thorough cleaning in concentrated sulphuric acid (Teflon-mounted electrodes were cleaned in sulphuric acid at room temperature and glassmounted electrodes in hot sulphuric acid); 3) extensive rinsing and soaking in Millipore water and finally 4) potential cycling between 0.07 and 1.5 V vs RHE until the characteristic H and O adsorption peaks were observed and remained stable.

Ni electrodes had either a disk or wire configuration. Both configurations were initially sealed in a bulb at the end of a soft glass tube under an H_2 environment, following the procedure of Conway [1]. The Ni wire electrode, after mounting was transferred under a cathodic potential into the electrochemical cell where the glass bulb was broken, exposing a clean oxide-free Ni surface. The Ni rotating disk electrode was made by cutting and polishing one of the used Ni wire electrodes prepared as described above, to a 1μm finish. This was followed by sonication and rinsing with Millipore water. It is expected that this manner of fabrication results in the presence of a thin NiO_x film on the electrode surface. It was found, though, that either method produced surfaces at which HER rates were similar (at a given potenial) in 0.5 M H_2SO_4 and in light of the procedure

A - Argon inlet.
B - Hydrogen inlet.
C - Connection tilted to eliminate O_2 entry into the W.E. compartment.
D- Wetted ground glass joints, opened slightly during impedance measurements.
E - Liquid seal (millipore H_2O) baffles in cup to maintain a good seal.
F - 0.5 mm Pt wire (in luggin) to reduce the high frequency impedance of the reference electrode.

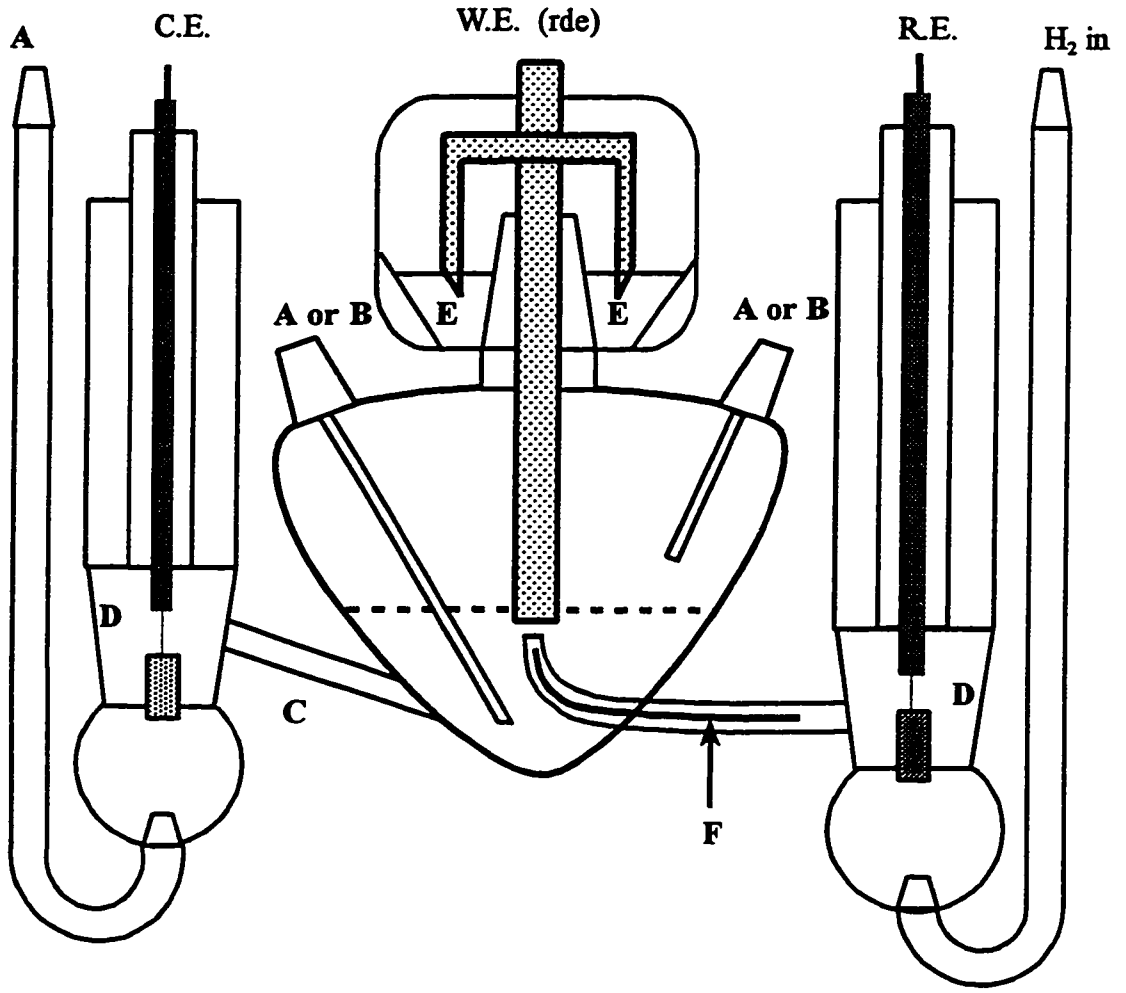

Fig. 3.1 Schematic of the electrochemical cell used for poisoning and single-crystal studies.

which was used to produce Ni foils for H permeation experiments, the rotating-disk electrode was used to gather most of the HER kinetic results.

Counter (C.E.) and reference (R.E.) electrodes consisted of high surface area, Pt wire mesh, which had been platinized in 2% chloroplatinic acid 2 N aqueous HCl solution at approximately 15 mA cm^{-2} for 10 min. When not in use, R.E.'s and C.E.'s were kept in concentrated sulphuric acid.

All electrochemical glassware was cleaned prior to experiments in hot, 200 to 250 °C, concentrated sulphuric acid with a small addition of HNO_3, and then washed at least three times in Millipore water. All gases, H_2, N_2 or Ar, were dried and deoxygenated [2], before they were passed through the electrochemical cell and the solution contained within it.

3.3 Poisoning Studies

3.3.1 Poisons

Three S-containing catalyst poisons, thiourea, cysteine, and 2,2' diethanolsulphide (DES) were chosen in order to examine the effect of different electronic and chemical environments of the sulphur atom which lead to different surface chemical reactivities and adsorptive affinities at Pt associated with poisoning of the electrolytic processes involved in the cathodic H_2 evolution reaction, HER. Each poison was either preadsorbed at a selected Pt electrode surface from a separate 0.1 mol dm^{-3} solution and then transferred to the electrochemical cell (*ex situ* adsorption) or added into the supporting electrolyte in the cell to give a known concentration (*in situ* adsorption).

3.3.2 Electrochemical measurements and data acquisition

Tafel type current *vs.* potential relations were recorded using either a Hokuto Denko HA 501 potentiostat/galvanostat controlled by an HP 9000 series computer, or a computer-controlled PAR Verostat or 273 potentiostat/galvanostat. All potentials were measured against a hydrogen reversible electrode in the same supporting electrolyte as that in the working electrode compartment but without the presence of poison, being separated from that compartment by a solution-sealed stopcock in the usual way. Experiments were conducted at 298 K. Corrections for the IR-drop between the Luggin capillary of the reference electrode, and the working electrode were made by means of ac impedance or current interruption methods. In all the following work, except for cyclic voltammograms, the electrode potential has been corrected for IR-drop.

The working electrodes used for the poisoning work were small Pt poly-oriented spheroids having known surface areas between 0.01 and 0.005 cm^2, enabling small currents to be used, thus avoiding significant build-up of any products of reaction of the poison in the working electrode compartment. The EIS measurements were made at a small rotating-disk electrode (rde, 0.05 cm^{-2}) (Pine Instrument Co.) to promote uniform mass-transport to the working electrode. Cyclic voltammograms were recorded on a digital oscilloscope (Nicolet 310). Potential-relaxation data obtained following interruption of previously adjusted constant currents were collected digitally using the oscilloscope and processed as described previously [3,4]. EIS results were collected using a Solartron 1286 potentiostat/galvanostat coupled with a Solartron 1255 frequency response analyzer (FRA) controlled by an IBM compatible computer running the ZPLOT

software (Scribner).

In order to relate the effects of adsorption of the poisons to the kinetics of the HER, the coverages, θ_P, by the respective poisons as a function of overpotential, η, are required. This information was provided by use of a new procedure in which, during evaluation of η as a function of current-density at Pt, the potential was switched in a fast transient to the H UPD range within which a fast cyclic voltammogram (CV) was immediately recorded giving θ_H. Argon was being continuously bubbled around the Pt electrode and, because small surface area electrodes were used, little H_2 was evolved, thus minimizing interference with the θ_P determinations by H_2 oxidation currents. This procedure enabled evaluation of θ_P, from $\Delta\theta_H$, when P had been initially preadsorbed, and was validated by separate experiments in which no poison had been adsorbed. In the *ex situ* type of experiment, no further poison adsorption could take place. This technique was also applicable to *in situ* experiments, when rates of adsorption of poisons were sufficiently slow that θ_P did not change during the evaluation of $\Delta\theta_H$ in the H UPD region.

3.3.3 Solutions and gases

All solutions were prepared using 18.2 MΩ Milli-Q water. Thiourea and cysteine were doubly recrystallized and 2,2'-diethanolsulphide (DES), 99+% purity, was used without further purification. For electrolytes, very high-purity sulphuric acid (Sea Star Chemicals) and BDH Aristar grade sodium hydroxide were used without further purification. Argon and hydrogen gases for bubbling in the cell compartments were purified, especially deoxygenated) as described previously [2].

3.4 Studies of the kinetics of the HER at Single-crystal Pt Surfaces

Pt single-crystal electrodes were made from 1 mm diameter 99.999% (metals basis) Pt wire (AESAR) which was melted at one end into a sphere approximately 3 mm in diameter. The resulting single-crystal sphere was oriented for cutting to the desired crystal face using the back-von Laue X-ray diffraction method [5] (see Appendix). Over half of the sphere was ground away with increasingly fine grit silicon carbide paper and then taken to a 1/4 micron finish with diamond paste. The resulting single-crystal electrode was spot welded to a Pt wire previously sealed in a Pyrex tube. The single-crystal surfaces examined were the (100) face, which was prepared by two different annealing techniques: cooling in H_2/Ar, denoted as (S_{II}), and cooling in air, denoted as (S_I). The Pt (19 11), (110) and (511) surfaces were exclusively cooled in H_2/Ar, while (111), for convenience, was cooled in air, since that procedure gives indistinguishable behaviour from that following cooling in H_2/Ar in the case of this surface. The electrodes were then mounted to an AFASR analytical rotator (Pine Instruments) via a Teflon adaptor. The electrode was then aligned, flame annealed, cooled under the above conditions [6] and placed in the electrochemical cell where a meniscus was formed with the electrolyte. After proper alignment of the electrode, rotation rates up to 4000 rpm could be satisfactorily achieved with the meniscus remaining intact. The procedure of flame annealing the electrode, and cooling in either air or an H_2/Ar mixture based on the method developed by Clavilier [7], as required, provided a clean surface having CV features virtually identical with those reported in other works [6,7,8]. This procedure was followed before every ac scan.

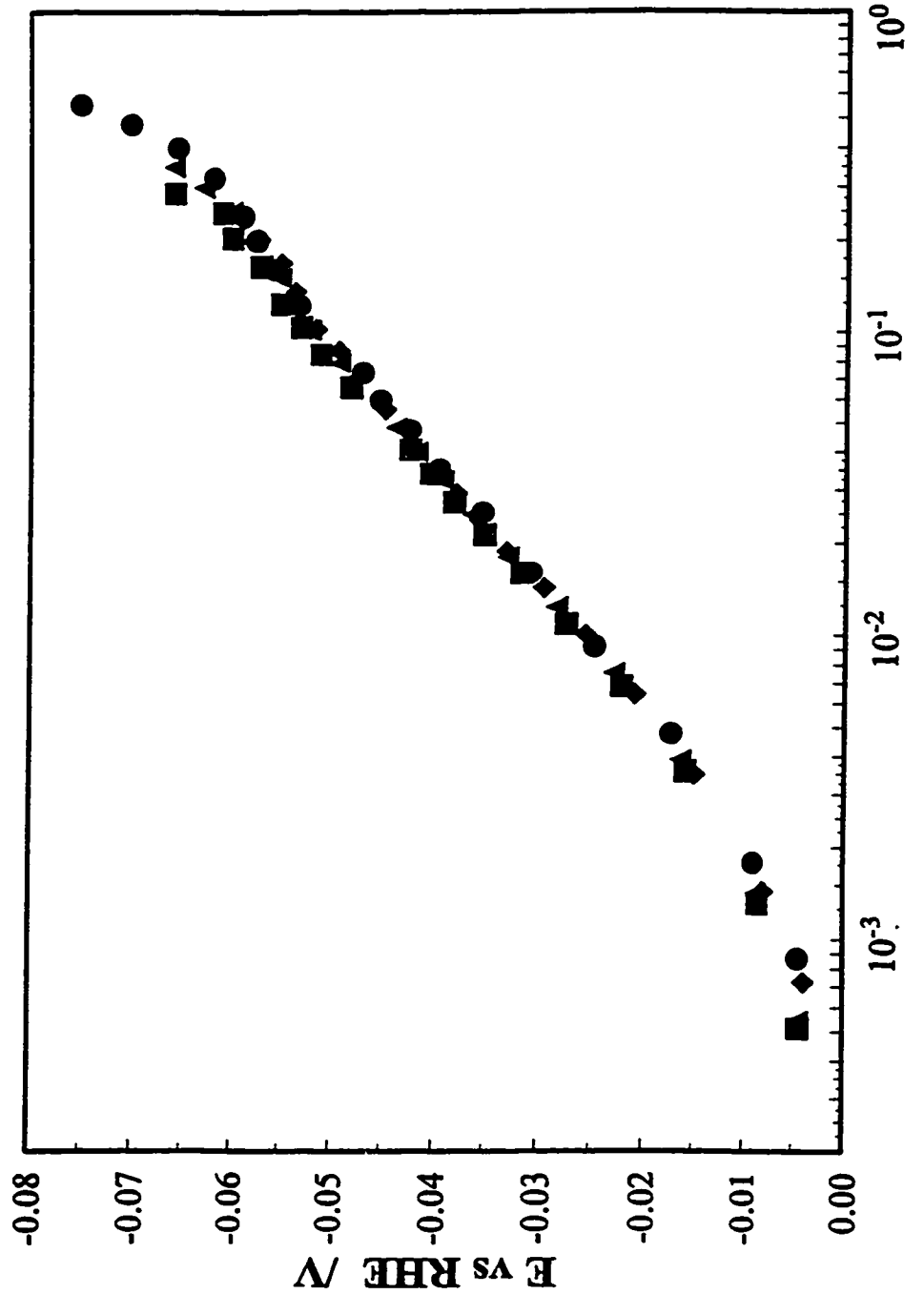

Fig. 3.2 Tafel plot for a Pt(poly) electrode showing the effect of its position relative to the Luggin capillary, and the effect of forming a meniscus on the measured current-density /overpotential relationship. ● - R_{sol} = 4.9 Ω electrode immersed, ▲ - R_{sol} = 8.03 Ω electrode immersed, ■ - R_{sol} = 9.8 Ω electrode at surface level, ◆ - R_{sol} = 12 Ω electrode in a meniscus configuration. Rotation rate - 3500 rpm, 0.5 M H_2SO_4, electrode sealed in soft glass.

The height of the meniscus is a factor which needs to be considered when making kinetic measurements with single-crystal electrodes [9]. In the present work the height of the meniscus varied slightly from experiment to experiment due to the fact that the electrode was removed from the cell and flame annealed before each ac measurement. This variable was monitored by observing the solution series resistance which was directly affected by the meniscus height. Reproducible results and those consistent with measurements taken at an immersed electrode, with only the disk surface exposed, were obtained when a meniscus height, corresponding to solution resistances in the range of 10.5 to 12 Ω, was established. In fact, Tafel type measurements were taken at a glass sealed Pt(poly) RDE at four different positions with respect to the Luggin capillary, ranging from a fully immersed state, $R_{sol} = 4.9\ \Omega$, to a meniscus configuration having $R_{sol} = 12\ \Omega$, similar to that arrising at the single- crystal electrodes. After IR correction it was found that the current-voltage relationship was independent of electrode position, Fig. 3.2. The difference between this conclusion and that of Herrero *et al.* [9] for H_2 oxidation could possibly be due to IR effects, difference in the direction of diffusion of H_2 from that in the HER, or that the meniscus factor is mitigated by rotation of the electrode. The factors which add scatter to the results are: i) the reproducibility of the annealing/cooling conditions; this was a factor since the electrode was annealed and cooled before *each* EIS measurement at a controlled η value, and ii) adventitious small contributions from the sides of the crystal. This point could be observed experimentally in some cases and it was concluded that this effect is dependent on the meniscus height and also on the cut of the crystal. In order to minimize the contributions from the sides, the crystals where cut so

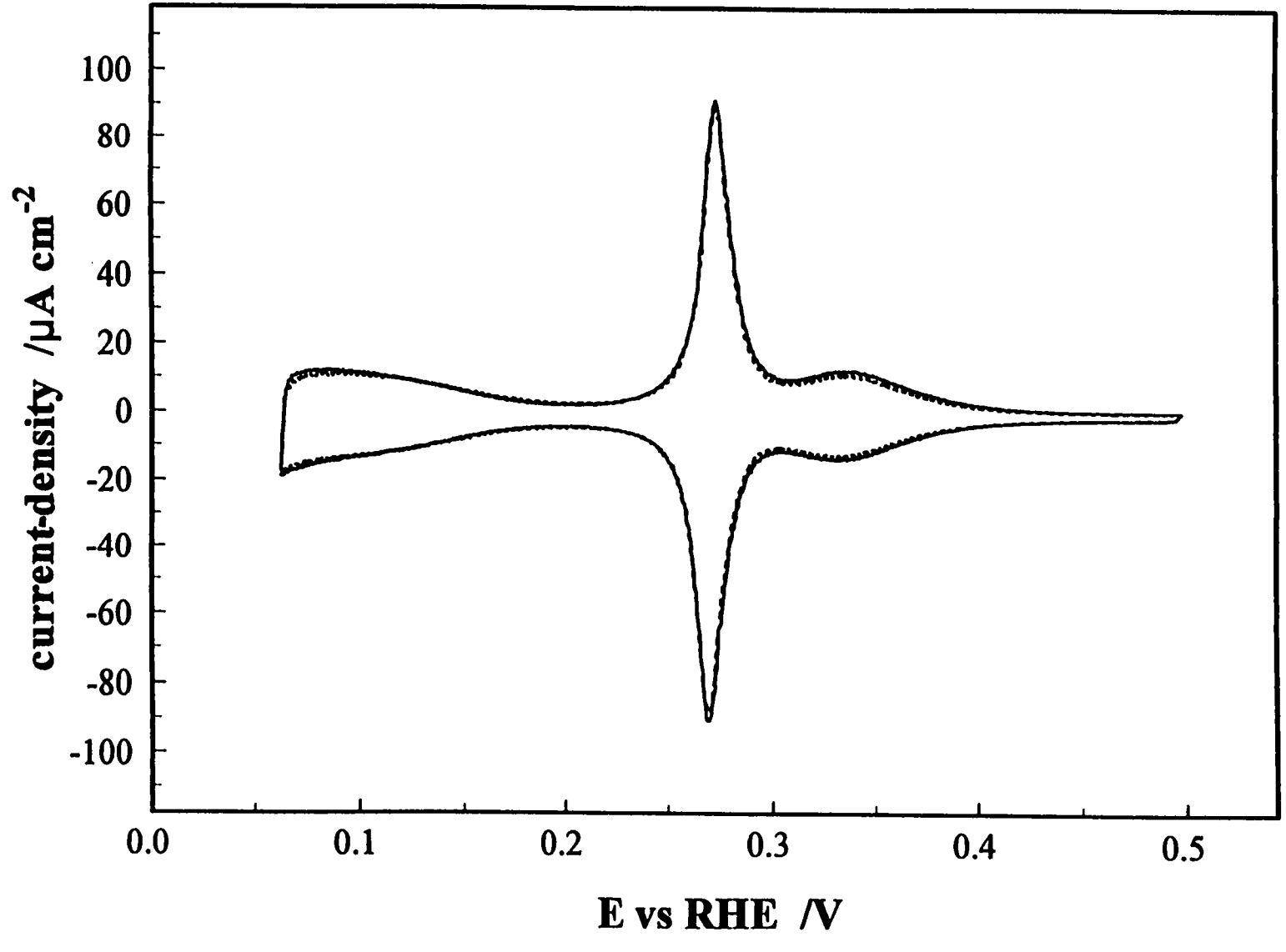

Fig. 3.3 Cyclic voltammogram of the (511) face; —— before and -------- after EIS measurements. Sweep rate 20 mV sec^{-1} 0.5 M H_2SO_4, T = 298 K.

that over 60 per cent of the poly-sphere was removed. By doing this it was then found that the effect became much less significant.

At the beginning of a set of experiments and periodically throughout the studies, cyclic voltammograms were recorded to check the cleanliness of the solution [2] and maintenance of the electrode surface structure [cf. ref. 6]. During the frequency scan in the impedance measurements, the steady-state dc current was monitored; it usually dropped slightly between the start and end of the scan due to adsorption of minimal amounts of unavoidable impurities from the solution. If, however, the decline of the dc current from the start to the end of the ac scan, (approx. 2 minutes), was greater than 10%, the results were rejected. The purity of the solution and the effectiveness of this procedure to characterize the HER at a clean single-crystal Pt substrate is demonstrated by the two voltammograms in Fig.3.3. The diminution of charge for H electrodeposition from the freshly annealed state to that after 2 ac scans and 5 minutes of Ar bubbling to remove H_2, is less than 5%.

Sulphuric acid solutions were prepared from 18.2 MΩ water (Millipore) and high purity sulphuric acid (Sea Star Chemicals). All solutions were initially deaerated with O_2-free argon. The electrolyte in the working and reference electrode compartments was then saturated with purified H_2 gas. Argon was continuously bubbled at the counter electrode.

Cyclic voltammograms were recorded using a HA-501 potentiostat/galvanostat controlled by a HB-104 function generator (Hokuto Denko). The current *vs* voltage response was recorded on a Nicolet 310 oscilloscope. Impedance spectra were recorded by scanning a frequency range from 200 kHz to 0.5 Hz using a Solartron 1286

Electrochemical Interface linked to a Solartron 1255 Frequency Response Analyser. The impedance spectral data were fitted to a given admittance model (see impedance derivation later) using LEVM 6.1 CNLS fitting software run on an IBM AIX UNIX system.

3.5 Details of Single-crystal HER Experiments in Aqueous NaOH

The Pt single-crystal electrodes were prepared by the procedure desribed above and previously [8]. The cyclic voltammograms for the UPD of H in 0.5 mol dm^{-3} NaOH for the three low index planes are shown in Fig. 3.4. The forms of these voltammograms are similar to those reported in the literature [10]. Electrolytic NaOH solutions were prepared from either BDH Aristar NaOH pellets, minimum assay 98.0 %, the main impurity being Na_2CO_3 or Alfa AESAR NaOH pellets, minimum assay 99.996 %, and Millipore 18.2 MΩ water. Either solution displayed identical results for CV's, steady-state d.c. measurements and EIS measurements. In NaOH, HER measurements were conducted at rotation rates of 3000 rpm. Higher rotation rates, up to 4000 rpm, produced unchanged EIS behaviour and steady-state dc results, and no diffusive processes were detected in the EIS spectrum at 3000 rpm in these alkaline solutions.

It was found, however, that the steady-state current-density was unstable after initial cathodic polarization and that a prepolarization time was needed before satisfactory EIS measurements could be taken. The change in current-density after cathodic polarization was dependent on both the polarization potential and the surface under study. At the Pt (111) and (100) surfaces, at low overpotentials, the current decreased slightly,

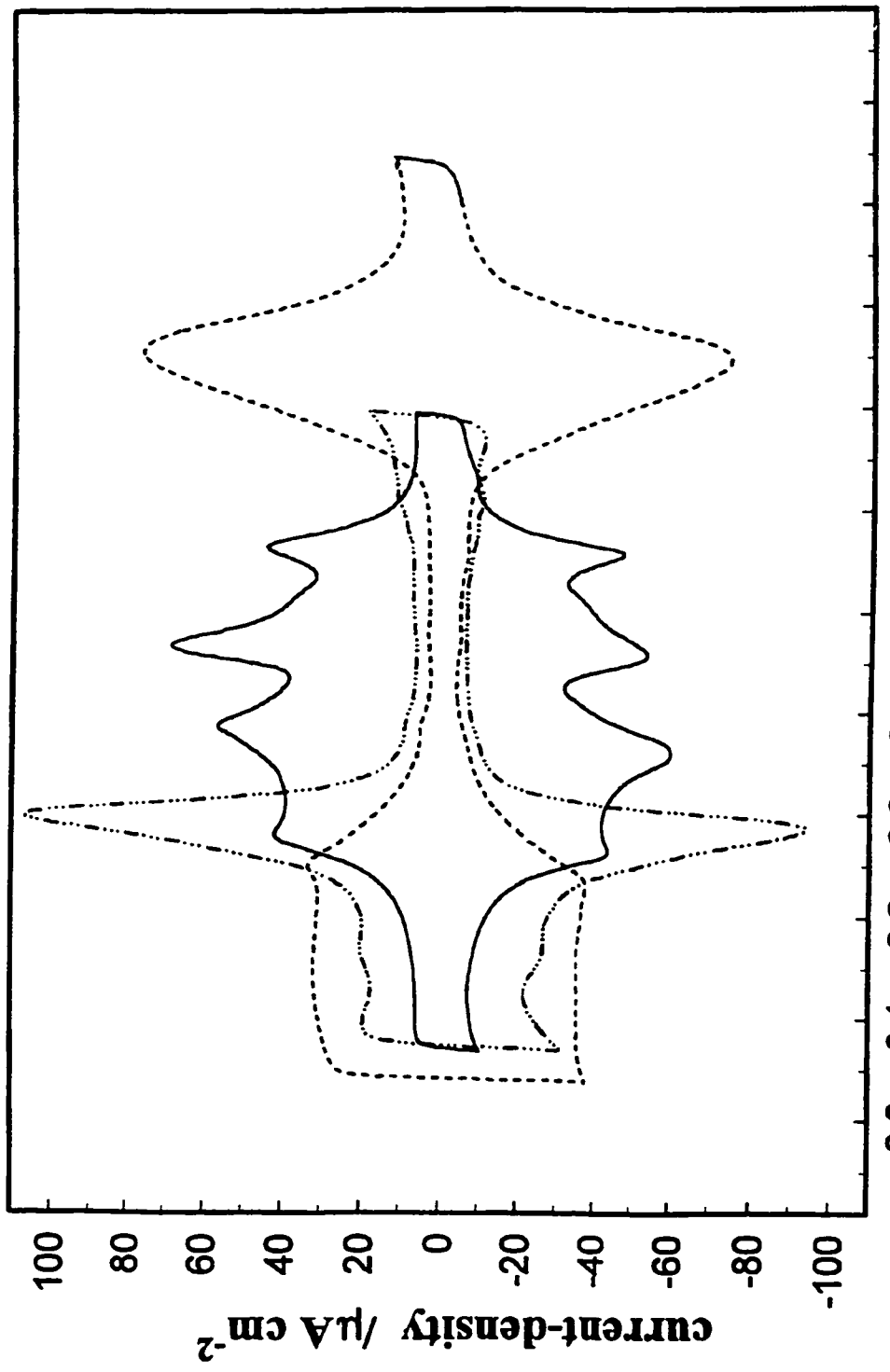

Fig 3.4 Cyclic Voltammograms of the low-index planes of Pt(hkl) electrodes; (100)S_{II} ——, (111) ---- and (110) - ··· -. The electrolyte was 0.5 mol dm^{-3} NaOH, at 298 K, scan rate - 50 mV sec^{-1}, (100) and (110) faces cooled in an H_2/Ar mixture.

i.e. <10%, and at the (100) face at higher overpotentials and at the (110) and poly-surfaces the current-density increased, 10%< $I_{init.} - I_{s.s}$<600% depending on potential and the surface. Details concerning this phenomenon will be discussed in chapter 5.

3.6 H Permeation Experiments and Poisoning

Hydrogen (as H or H^+) diffusion through a metal membrane is dependent on the state of the input and output surfaces. The principle of electrochemical permeation measurements is that control of each of these surfaces (potentiostatic or galvanostatic control) can be applied. The electrochemical permeation cell used here is illustrated in Fig. 3.5, following the design of Devanathan and Stachurski [11]. The cell in Fig. 3.5 consisted of two, three-compartment electrochemical cells with a common bielectrode as the working electrode. The potentiostat/galvanostats used in control of the two cells were required to have the same ground potential for the working electrode. The instruments of choice were two of the following Hokuto/Denko potentiostats: HA 501, 301, or 211A, controlled by an Hokuto/Denko HB 104 function generator. The data, cathodic potential or the H sorption + H_2 current and the anodic H desorption current, were recorded on a Nicolet 310 digital oscilloscope.

Both working electrode compartments were dearated by passing Ar or N_2 through the cell before and during experimentation. The H entry side for all experiments contained 0.5 mol dm^{-3} H_2SO_4 prepared from ultrapure concentrated H_2SO_4 (Seastar Chemicals) and Millipore 18.2 MΩ water. Poison (e.g. thiourea) was adsorbed on the H entry side of the membrane by metering the appropriate amount of a concentrated poison solution (0.1 to

A- Ar/N_2 **inlet**
B - H_2 **inlet**
R.E. - reference electrodes (R.H.E.)
C.E. - counter electrodes (Pt gauze)
W.E. - working electrode (Pd or Ni foil)

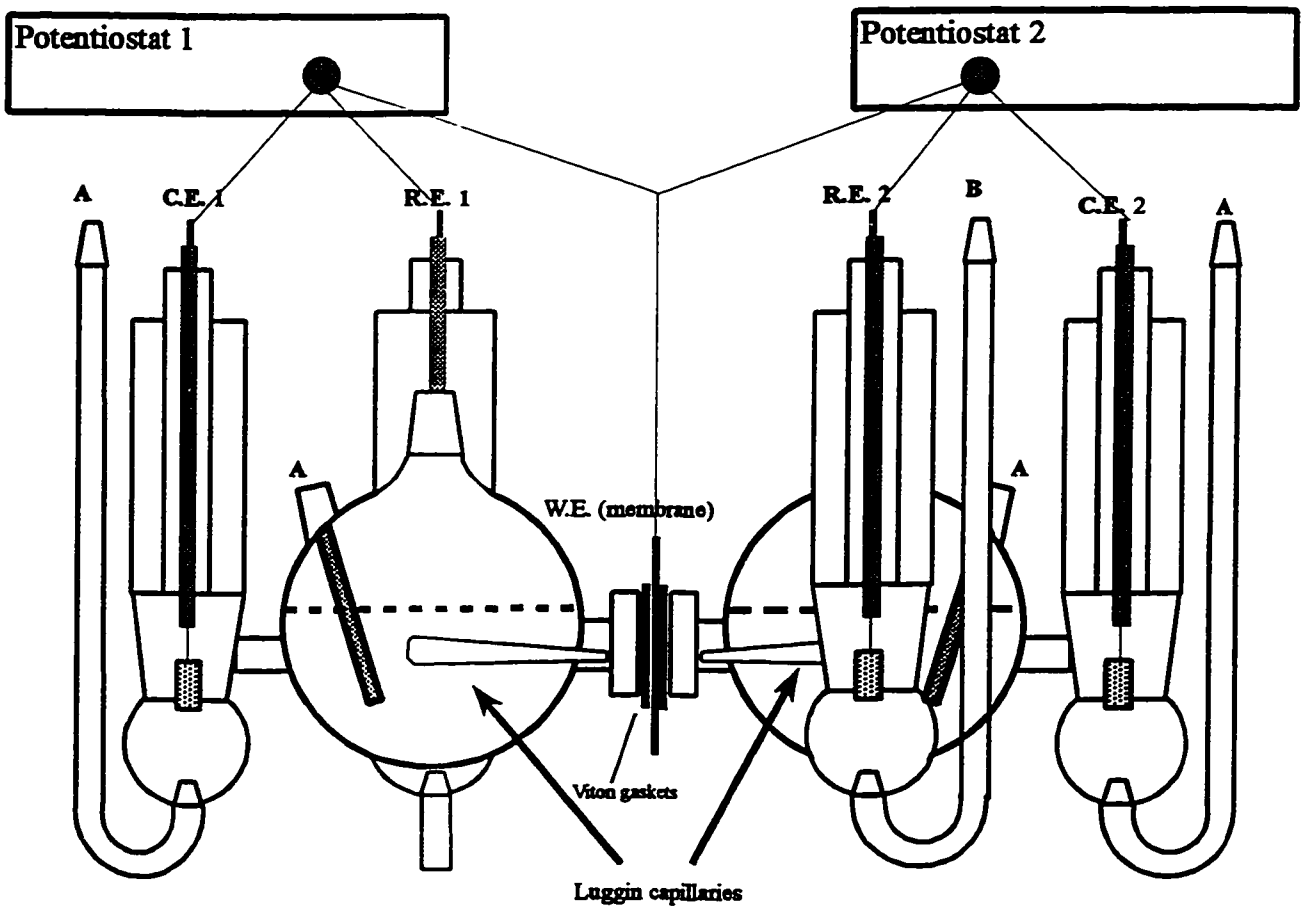

Fig. 3.5 Schematic of the bi-electrode cell used for hydrogen permeation measurements.

10 g l^{-1} solution) into that working electrode compartment. The H oxidation compartment contained either 0.5 mol dm^{-3} NaOH (BDH Aristar) used with the Ni membrane, to avoid dissolution of the metal or 0.5 mol dm^{-3} H_2SO_4 used with the Pd membrane. The cathodic side (H entry side) could be controlled either potentiostatically or galvanostatically. The anodic desorption side was held at a constant potential, e.g. for the Pd membrane at E = 0.8 V *vs.* RHE and for the Ni membrane at E = 0.5 V *vs.* RHE.

The Pd membrane, 0.1 mm thick, Aesar Puratronic 99.98% (metals basis), was annealed in vacuum at ≈ 700 ° C for 2 h, then polished to 1 micron finish, and sonicated before use. Reference and counter electrodes were identical to those mentioned earlier. Before H permeation experiments were conducted at Pd, the Pd H input and output surfaces were cycled between 0.3 and 1.4 V *vs.* RHE until sharp oxidation peaks and a flat double-layer charging region were observed. The surface area was determined by calculating the charge for monolayer oxidation, one O per Pd atom, using the Burshtein minimum method [12] and comparing that to the literature value of 4.2 μC cm^{-2} [2].

The Ni membrane

Aesar Puratronic grade 99.994% Ni (metals basis), 0.025mm in thickness, was annealed in an H_2 stream, at ≈ 600 ° C for 2 h, to avoid surface oxidation. It was then polished on both sides to a 1 micron finish, and sonicated in Millipore water.

The usual method for performing a permeation measurement is to apply a current or potential step to the cathodic side of the membrane and monitor the time-dependence and magnitude of the current response at the anodic side. The starting potential or current could either be in a region were no ingress of H occurred or a series of steps were applied,

with each one commencing after the previous H oxidation desorption current had reached a steady-state.

References

1. J. O'M Bockris and B.E. Conway, J. Sci. Instrum., 25 (1948) 205; J. O'M Bockris and B.E. Conway, J. Chem. Phys., 28 (1958) 707.

2. H. Angerstein-Kozlowska, Comprehensive Treatise of Electrochemistry, Eds. B.E. Conway, J.O'M. Bockris, S. Sarangapani and R.E. White, Plenum, New York, 9 (1984) 15.

3. B.E. Conway and L. Bai, Electrochim. Acta., 31(8) (1986) 1013.

4. L. Bai, D.A. Harrington and B.E. Conway, Electrochim. Acta, 32 (1987) 1713.

5. A. Hamelin, Modern Aspects of Electrochemistry, Eds. B.E. Conway, J.O'M. Bockris and R.E. White, Plenum, NewYork, 16 (1985) 1.

6. S. Motoo and N. Furuya, J. Electroanal. Chem., 172 (1984) 339.

7. J. Clavilier, A. Rodes, K. El Achi and M.A. Zamakhchari, J. Chim. Phys., 88 (1991) 1291.

8. S. Morin, H. Dumont and B.E. Conway, J. Electroanal.Chem., 412 (1996) 39, see also S. Morin, Ph. D. Thesis, Chemistry, University of Ottawa (1996).

9. E. Herrero, J. Clavilier, J. M. Feliu and A. Aldaz, J. Electroanal. Chem., 410 (1996) 125.

10. H. Kita, S. Ye, A. Aramata, N. Furuya, J. Electroanal. Chem., 295 (1990) 317.

11. M.A. Devanathan and Z. Stachurski, Proc. Roy. Soc. London. A., 270 (1962) 90.

12. A.A. Michri, A.G. Pshenichnikov and R.Kh. Burshtein, Elektrokhimiya, 8 (1972) 364.

13. B.E. Conway, L. Bai and D.F. Tessier, J. Electroanal. Chem., 161 (1984) 39.

Chapter 4

The A.C. Impedance Method

4.1 Introductory Remarks

The measurement of electrochemical kinetics involves the perturbation of a system from its equilibrium or steady-state condition either by "dc" polarization or by a voltage pulse or alternating voltage modulation. In the evaluation of chemical kinetics this is achieved by monitoring the rate at which the system returns to a new steady-state or equilibrium condition after the application of a perturbation of temperature, concentration, pressure, etc [1]. In electrochemistry, the reaction kinetics are controlled by electrical quantities (i.e. voltage or complementarily by current), additionally to temperature and pressure. Therefore the kinetics of a particular reaction can be deduced by monitoring either the conjugate current or the voltage as a function of time after a perturbation is applied to the other variable.

The use of large amplitude techniques, where $\Delta E > RT/nF$, is generally employed for the evaluation of diffusion-controlled reactions and forms the basis of many electroanalytical techniques [2]. The application of a large amplitude current or potential perturbation is generally *not* useful in the study of electron-transfer processes, except for the simplest of reaction mechanisms (which are rarely observed experimentally in electrode kinetics), due to the non-linear current-voltage relationship which makes the analysis of the relaxation response inextricable due, e.g. to generation of second-harmonic effects. Therefore the use of small-amplitude perturbation techniques is favoured in the measurement of electrode kinetics. The advantage of using a small-amplitude signal is that

the response can be analysed using *linearlized* reaction-kinetic equations. In this regard the treatment of results is made simpler when the response is recorded in the frequency-domain instead of the time-domain. In theory, all types of modulations (sine-wave, square-wave, triangular-wave, etc.) lead to equivalent results [3], though experimentally sine-wave techniques are favoured, giving conveniently analysable EIS behaviour. Cyclic voltammetry (large-amplitude triangular-wave potential modulation) provides an important basis for UPD studies and is an important technique complementary to EIS for the study of reaction kinetics, e.g. as in refs. [4] and [5].

When an alternating voltage (av) modulation, of frequency (ω), represented by a potential function

$$E = E_{ss} + E_{av}\sin(\omega t + \phi_E)$$

or, in complex-notation,

$$= E_{ss} + \Re[E_{av}\exp(j\phi_E + j\omega t)] \qquad \textbf{(4.1)}$$

is applied to a linear system in a steady-state or at equilibrium, the current response will be sinusoidal as well but may be shifted in phase from that of the voltage by the angle ϕ:

$$I = I_{ss} + I_{ac}\sin(\omega t + \phi_I)$$

or, as above, in complex-notation

$$= I_{ss} + \Re[I_{ac}\exp(j\phi_I + j\omega t)] \qquad \textbf{(4.2)}$$

The magnitude and sign of this phase shift is governed by the relaxation rates of the interfacial processes, rates of generation of electrons, and adsorbed and soluble intermediates or products. This behaviour is analogous to that seen in the response of solid-state circuitry where a +ve phase shift is induced by an inductive component and a

-ve phase shift is induced by a capacitance.

The relation between I and E is completely determined by the magnitude of the total impedance $|Z|$ which equals E_{av}/I_{ac}, and the phase angle ϕ. From eqs. 4.1 and 4.2 the impedance is written as:

$$Z = \frac{E_{av}\exp(j\omega t)}{I_{ac}\exp(j\phi_I + j\omega t)} \qquad \textbf{(4.3a)}$$

or

$$Z = |Z|\exp(j\phi_I) \qquad \textbf{(4.3b)}$$

with the voltage phase angle (ϕ_E) equal to zero. Noting Euler's Formula ($exp^{(jx)} = cos\ x + j\ sin\ x$) the impedance can be resolved into its real and imaginary components as: $Z = Z' - jZ''$ where,

$$Real\ Z' = |Z|\ \cos\ \phi$$

$$Imaginary\ Z'' = |Z|\ \sin\ \phi$$

with $\phi = \tan^{-1}(Z''/Z')$

The impedance can be equivalently defined as the quotient of the Laplace transforms (of course, any linear transform function could be used, e.g. a Fourier Transform [6]) of the voltage $\Delta V(s)$ and the current $\Delta I(s)$, with the imaginary Laplace transform variable s equalling $j\omega$, ω being the sinusoidal angular frequency. Thus,

$$Z' - jZ'' = \frac{\overline{\Delta V}(s)}{\overline{\Delta I}(s)} \qquad \textbf{(4.4)}$$

4.1.1 Data Representation and Conventions

As was discussed above, the total ac impedance response of an electrochemical system at a given electrode potential is described by three parameters: frequency (ω), real impedance (Z') and imaginary impedance (Z''). Three different permutations of the

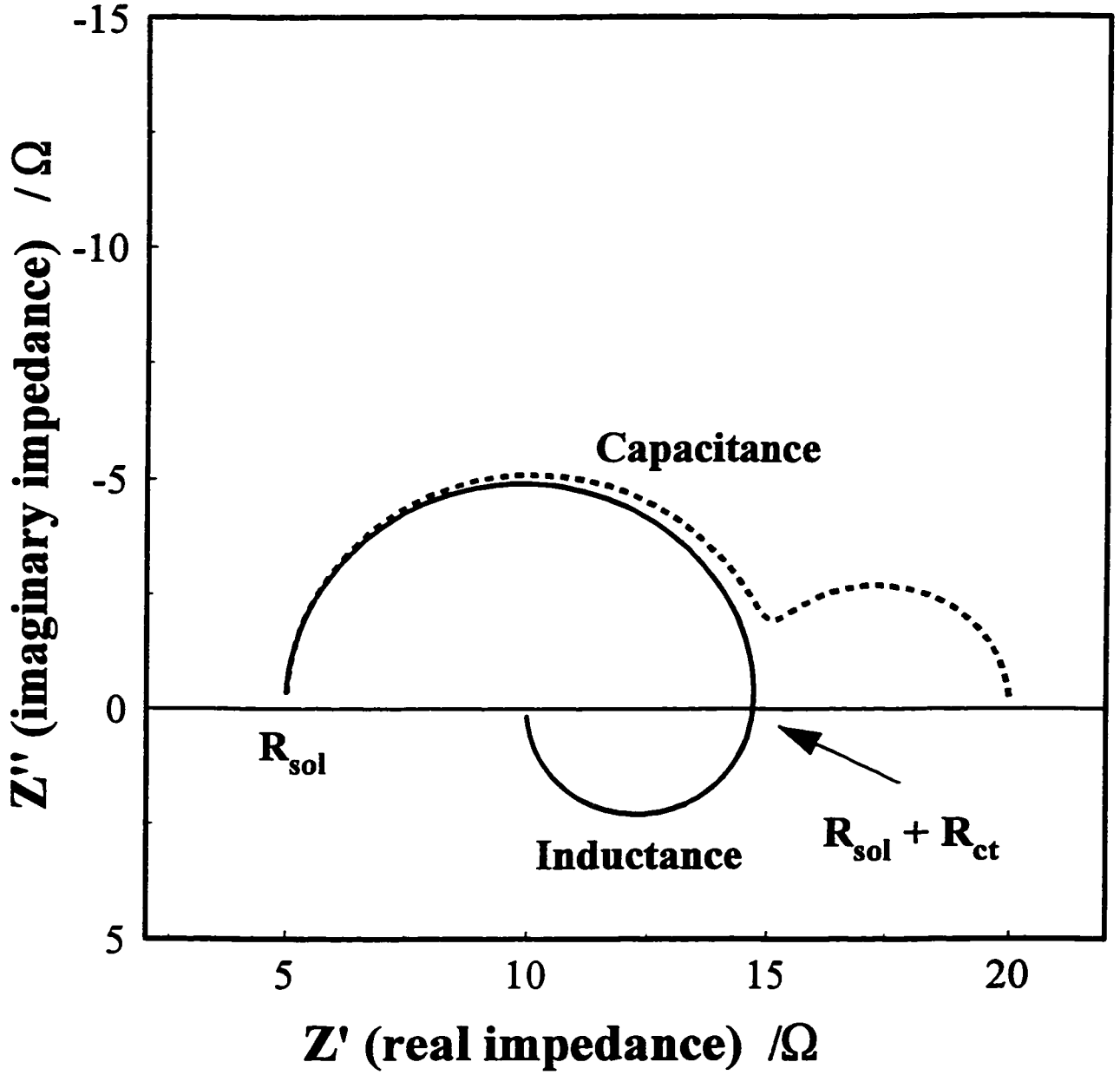

Fig 4.1A A complex-plane plot illustrating, capacitive (------) and inductive (——) EIS responses. These response are typical for a reaction scheme involving electron transfer and adsorption of an intermediate. (See chapter 5, § 5.5 and chapter 6, § 6.3)

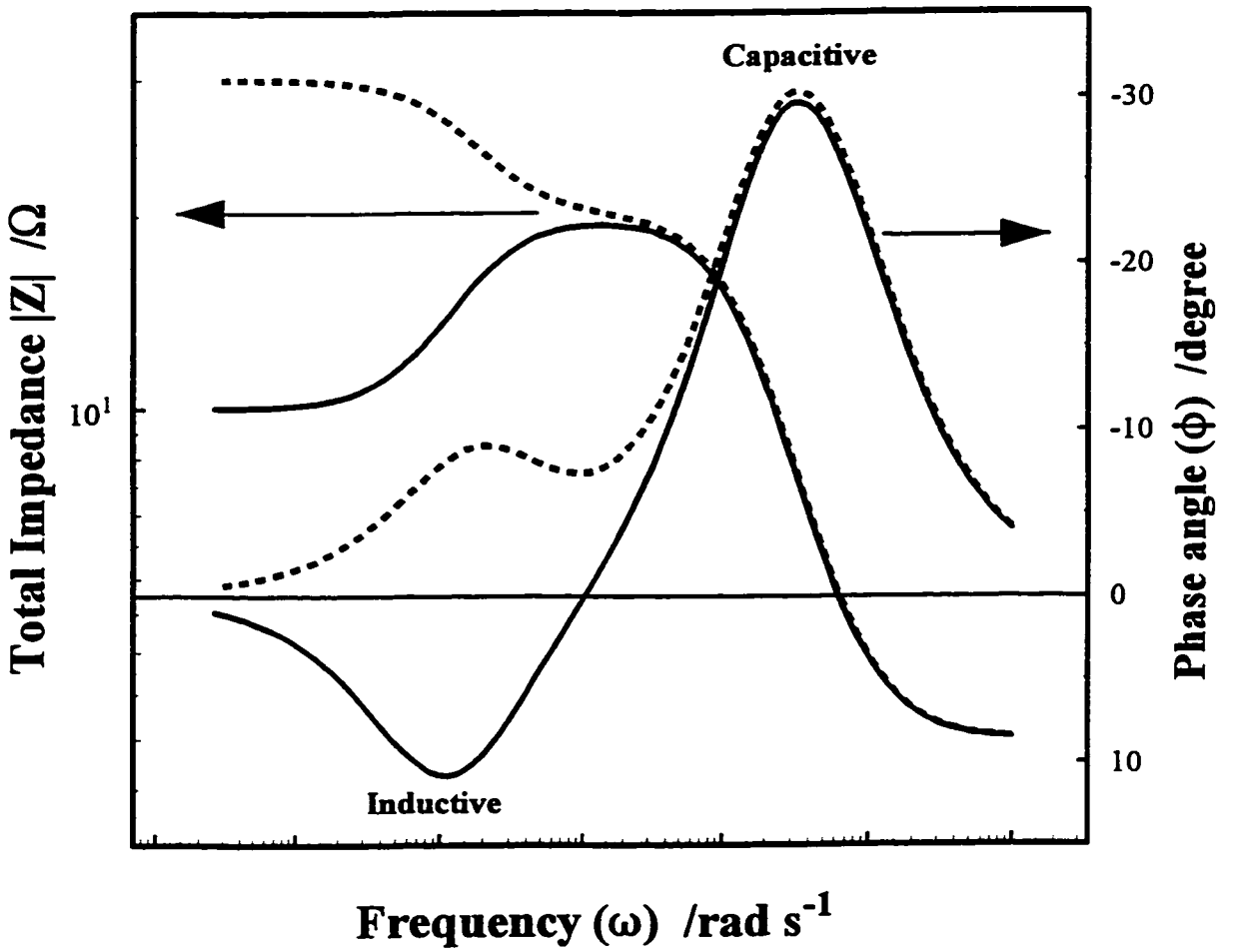

Fig. 4.1B A Bode magnitude and phase-angle plot corresponding to the curves shown in Fig. 4.1A.

impedance terms which are commonly used in the literature are: i) the complex-admittance ($Y = Z^{-1} = Y' - j\omega Y''$); ii) the complex dielectric-constant ($\epsilon = \epsilon' - j\epsilon'' = Y/j\omega C_o$); and iii) the complex-modulus ($M = \epsilon^{-1}$). These different notations are all emcompassed under the general designation of immitance [8,7]. The immitance function which is used to represent the results is immaterial but is usually dictated by the field of study under which the work falls. For electrochemical data, the most common representation is the complex impedance form.

The data are presented in two types of plots, 1) The complex-plane plot, where the real and imaginary parts of the immitance are plotted on the complex-plane and 2) Bode plots which are the phase angle ϕ and total impedance, $|Z|=(Z'^2 + Z''^2)^{1/2}$ plotted *vs.* the log of the frequency, log ω. Both forms of presentation are useful for qualitative data analysis. The faradaic impedance of simple electrochemical processes can be read directly off of the complex-plane plot as the diameter of the semicircle along the real axis. This value can be easily interpreted in terms of electrode kinetics since, in its simplest form, it is directly proportional to the rate of electron transfer at the electrode|electrolyte interphase, i.e. the current-density.

The Bode plots are useful when assessing the time constants of particular processes since, unlike the complex-plane plot representation, the frequency dependence is directly shown. Three-dimensional plots of Z' and Z''plotted *vs.* ω, which possess the virtues of both of the above representations, have been promoted by J.R. Macdonald [7]. These types of plots have not, however, been used widely to represent data in the electrochemical literature to the present date but these types of representations are found

to be very useful during data analysis.

Typical EIS results illustrating the complex-plane and Bode plots are shown in Figs. 4.1a, b respectively. The plots in Fig. 4.1 can be modelled by given arrangements of resistors, capacitors, inductors and Warburg type elements (for a description of Warburg type impedance elements, see following sections), e.g. [9,10,11,12]

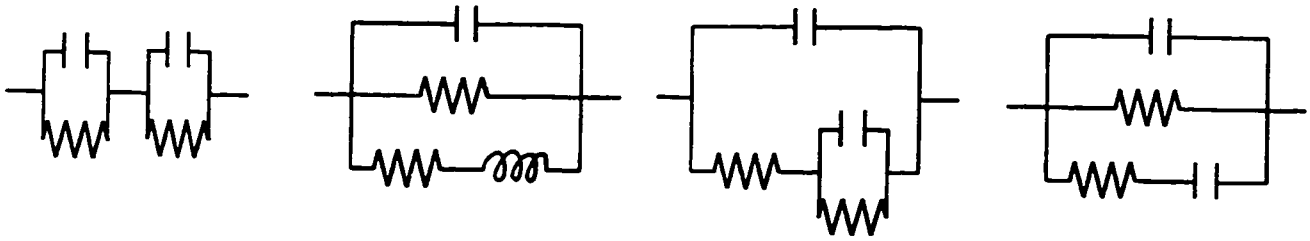

*Examples of equivalent circuits used in analysing electrochemical systems.

This type of anaylsis can lead to a simple picture of the electrochemical interphase and is extremely useful for diagnostic testing using ac impedance, e.g. for the evaluation of protective coatings or the state of charge in battery research. In order to examine quantitatively the kinetics of multi-step electrochemical processes, the "equivalent circuit" approach is undesirable[1]. The procedure followed in the present work is to derive expressions for the electrode impedance directly from the electrochemical rate equations. For a given electrochemical system an impedance equation can be found; which is then simplified into one involving adjustable parameters (A, B...etc.), whose relation to the reaction rates is known. Complex Nonlinear Least Squares (CNLS) fitting of the derived impedance expression to the EIS results then produces a set of data, i.e. η, i, A, B, ... etc.

---

[1]For simple systems the elements of an equivalent-circuit can be derived in terms of the electrochemical reaction-rates but the equivalent-circuit elements usually have a more complex nature than expressions derived directly from the rate equations themselves.

This set of data can then be examined using ordinary nonlinear least-squares (NLS) fitting routines in order to determine the "chemical" rate-constants for the reation steps, the coverage of reaction intermediates and any diffusion parameters that may be involved.

4.2 First-Order Charge Transfer Reaction Including Diffusion [18]

A general one-electron charge transfer reaction with non-adsorbing reactant and product species will be considered and is written as:

$$Ox + ne^- \underset{k_b}{\overset{k_f}{\rightleftharpoons}} Red \qquad (4.I)$$

The reaction rate, written in terms of the rates of electron transfer and the rates of diffusion for the Ox species to the electrode, and Red species away from the electrode, are:

1) Rate of electron transfer (r_o):

$$\frac{I}{F} = r_o = \upsilon_e = k_f \exp(-\alpha \eta f)\left[\frac{c_{Ox}^s}{c_{Ox}^b}\right] - k_b \exp((1-\alpha)\eta f)\left[\frac{c_{Red}^s}{c_{Red}^b}\right] \qquad (4.5)$$

2) Rate of mass transfer of Ox and Red (r_1):

$$r_1 = \upsilon_e = \varphi_{Ox} = \varphi_{Red} = D\left(\frac{\partial c_{Ox}}{\partial x}\right)_{x=0} = D\left(\frac{\partial c_{Red}}{\partial x}\right)_{x=0} \qquad (4.6)$$

where $f = nF/RT$, υ_e = the rate of electron transfer in mol sec^{-1} cm^{-2}, φ_i = flux of species i at the electrode surface, and c_{Ox} and c_{Red} are the concentrations of the reactants and products with superscripts s and b denoting surface and bulk concentrations, respectively.

The small signal ac impedance response can be obtained by linearlizing equations 4.5 and 4.6 by a Taylor series expansion limited to first-order terms. This expansion is performed about either the steady-state or the equilibrium potential to give:

$$\frac{\Delta I}{F} = \left(\frac{\partial r_o}{\partial E}\right)_{Ox,Red} \Delta E + \left(\frac{\partial r_o}{\partial c_{Ox}^s}\right)_{E,Red} \Delta c_{Ox}^s + \left(\frac{\partial r_o}{\partial c_{Red}^s}\right)_{E,Ox} \Delta c_{Red}^s \qquad \textbf{(4.7a)}$$

$$\Delta\varphi_{Ox} = \left(\frac{\partial r_1}{\partial E}\right)_{Ox,Red} \Delta E + \left(\frac{\partial r_1}{\partial c_{Ox}^s}\right)_{E,Red} \Delta c_{Ox}^s + \left(\frac{\partial r_1}{\partial c_{Red}^s}\right)_{E,Ox} \Delta c_{Red}^s \qquad \textbf{(4.7b)}$$

and

$$\Delta\varphi_{Red} = \left(\frac{\partial r_1}{\partial E}\right)_{Ox,Red} \Delta E + \left(\frac{\partial r_1}{\partial c_{Ox}^s}\right)_{E,Red} \Delta c_{Ox}^s + \left(\frac{\partial r_1}{\partial c_{Red}^s}\right)_{E,Ox} \Delta c_{Red}^s \qquad \textbf{(4.7c)}$$

where $\Delta E = E - E_{ss} = E_{ac} \exp(j\omega t)$ and $\Delta I = I - I_{ss} = I_{ac} \exp(j\phi_I + j\omega t)$; φ_{Ox}, $\Delta\varphi_{Red}$, Δc^s_{Ox} and Δc^s_{Red} will also vary sinusoidally but will differ from ΔI and ΔE in phase and amplitude. These relationships represent the time dependent components of the current-density, potential, diffusive flux of Ox and Red, and the surface concentrations of Ox and Red. Before eqs. 4.7a, b and c can be solved for the faradaic admittance, $Y_f = \Delta I/\Delta E$, the ac component of the diffusive flux, cf. eq. 6 (Fick's First law of diffusion), must be found in terms of the ac variation of the surface concentration of the diffusing species, Ox and Red.

Depending on the nature of the diffusion as well as diffusive constraints placed on the system by the cell configuration (e.g. thin-layer cells, spherical electrode geometry, rotated electrode, unstirred/stirred solutions, expanding electrodes, etc.), unique relationships will arise between the ac components of the surface concentration and the diffusive flux. In the following, the relationship between $\Delta\varphi$ and Δc^S will be derived for three cases:

i) semi-infinite linear diffusion to a planar electrode;

ii) bounded linear diffusion to a planar electrode with a *conductive* boundary; and

iii) bounded linear diffusion to a planar electrode with a *nonconductive* boundary.

These three cases will be examined as their solutions will be needed in the analysis and interpretation of the experimental results to be presented later for hydrogen (H_2) evolution.

In order to solve the diffusion problems we begin with Fick's second law of diffusion which, when defining Δc as the difference between the surface concentration and the bulk concentration ($c^s - c^b$), is written as:

$$D\frac{\partial^2 \Delta c}{\partial x^2} = \frac{\partial \Delta c}{\partial t} \tag{4.8}$$

This second-order partial differential equation is then transformed into a linear differential equation by means of a Laplace transform, giving:

$$D\frac{\partial^2 \overline{\Delta c}(x,s)}{\partial x^2} - s\overline{\Delta c}(x,s) = 0 \tag{4.9}$$

where $\overline{\Delta c}(x,s) = \mathcal{L}\{\Delta c(x,t)\}$ and s represents the imaginary Laplace parameter ($j\omega$), ω being again the angular frequency. The general solution of eq. 4.9 is:

$$\overline{\Delta c}(x,s) = M(s)\exp\left[-\sqrt{\frac{s}{D}}x\right] + N(s)\exp\left[\sqrt{\frac{s}{D}}x\right] \tag{4.10}$$

Variables M(s) and N(s) are determined by applying the boundary conditions which correspond to the particular diffusion conditions. The following will go through each specific case outlined above to derive the expression for $\Delta\varphi$ in terms of Δc, and then the appropriate admittance equations and their frequency dependent terms will be determined and compared.

4.2.1 Semi-Infinite Diffusion [2,13]

The boundary conditions written in Laplace space are:

$$\bar{c}(\infty,s) = s^{-1}c^{b} \quad or \quad \overline{\Delta c}(\infty,s) = 0 \qquad 1'$$

This states that the concentration is equal to that in the bulk at $x = \infty$

$$D\left(\frac{\partial\overline{\Delta c}(x,s)}{\partial x}\right)_{x=0} = \overline{\varphi(s)} \qquad 2'$$

which is a restatement of eq. 4.6 (Fick's first law of diffusion). Boundary condition **1'** states that equation 4.10 must apply in the limit of $x \to \infty$, therefore N(s) necessarily is equal to zero. Applying condition **2'** to equation 4.10 gives the expression for M(s) as:

$$D\left(\frac{\partial\overline{\Delta c}}{\partial x}\right)_{x=0} = \overline{\Delta\varphi}(s) = M(s)D\left(-\sqrt{\frac{s}{D}}\right)\left(\exp\sqrt{-\frac{s}{D}}(0)\right) \qquad \textbf{(4.11)}$$

or

$$M(s) = \frac{\overline{\Delta\varphi}(s)}{-\sqrt{sD}} \qquad \textbf{(4.12)}$$

Substitution of M(s) into equation 4.10 produces the relationship between $\Delta\varphi$ and Δc:

$$\overline{\Delta\varphi}(s) = \sqrt{sD}\,\overline{\Delta c}(0,s) = \sqrt{j\omega D}\,\overline{\Delta c_{Ox}^{s}} = -\sqrt{j\omega D}\,\overline{\Delta c_{Red}^{s}} \qquad \textbf{(4.13)}$$

4.2.2 Finite bounded linear diffusion with a conductive boundary [10,13,14,15]

In this situation we have a well defined diffusion layer of thickness L at the electrode surface. At x = L, the diffusion layer boundary, we have an infinitely rapid exchange between the species in the diffusion field and the species in the bulk. This situation corresponds to electrochemical systems where dc current is flowing and the ac penetration depth is comparable to the diffusion-layer length. Typical situations where this case arises are where rotating disk electrodes, thin surface films, or permeable membrane electrodes are employed.

These boundary conditions are expressed as:

$$x = L \qquad \overline{\Delta c}(L,s) = 0 \qquad 1''$$

$$x = 0 \qquad D\left(\frac{\partial \overline{\Delta c}(x,s)}{\partial x}\right)_{x=0} = \overline{\Delta \varphi}(s) \qquad 2''$$

As in the previous example, the boundary conditions **1″** and **2″** are applied to eq. 4.10 to obtain expressions for M(s) and N(s). Application of **2″** results in:

$$\frac{\overline{\Delta \varphi}(s)}{D} = -\sqrt{\frac{s}{D}}M(s) + \sqrt{\frac{s}{D}}N(s) \qquad \textbf{(4.15)}$$

and application of **1″** produces,

$$M(s) = -N(s)\ \exp\left(2\sqrt{\frac{s}{D}}L\right) \qquad \textbf{(4.14)}$$

Having two equations in two variables we can then solve for M(s) and N(s) giving:

$$M(s) = -\frac{\overline{\Delta \varphi}(s)\ \exp\left(\sqrt{\frac{s}{D}}L\right)}{\sqrt{sD}\ \exp\left(\sqrt{\frac{s}{D}}L\right) + \exp\left(-\sqrt{\frac{s}{D}}L\right)} \qquad \textbf{(4.16)}$$

and

$$N(s) = \frac{\overline{\Delta \varphi}(s)\ \exp\left(-\sqrt{\frac{s}{D}}L\right)}{\sqrt{sD}\ \exp\left(\sqrt{\frac{s}{D}}L\right) + \exp\left(-\sqrt{\frac{s}{D}}L\right)} \qquad \textbf{(4.17)}$$

and placing eq. 4.16 and 4.17 into eq. 4.10 yields the equation relating $\Delta\varphi$ to Δc:

$$\overline{\Delta \varphi}(j\omega) = \sqrt{j\omega D}\coth\sqrt{\frac{j\omega}{D}}L\ \overline{\Delta c}(0,j\omega) \qquad \textbf{(4.18)}$$

4.2.3 Finite bounded linear diffusion with a conductive boundary [10,16,17]

This case is similar to that for the conductive boundary except that at the limit of the diffusion layer (x = L) the exchange of the diffusing species with those in the bulk is effectively blocked. At a constant dc potential this translates to a zero current situation for the reaction involving the diffusing species. This situation arises for instance where the diffusing species are bound in a film on the electrode surface or if they are diffusing into a plate, sphere, or wire electrode. (e.g. diffusion of minority carriers in semiconductor type films, diffusion of H in hydride electrodes or diffusion of alkali metals into mercury electrodes).

The boundary conditions are as follows:

$$x = L \qquad \frac{\partial \overline{\Delta c}(x,s)}{\partial x} = 0 \qquad 1'''$$

and

$$x = 0 \qquad D\left(\frac{\partial \overline{\Delta c}(x,s)}{\partial x}\right)_{x=0} = \overline{\Delta \varphi}(s) \qquad 2'''$$

Applying these conditions to eq. 4.10, as was done in the previous cases, and solving for M(s) and N(s), we then find the following relationship between $\Delta\varphi$ and Δc:

$$\overline{\Delta \varphi}(j\omega) = \sqrt{j\omega D}\tanh\sqrt{\frac{j\omega}{D}}L\ \overline{\Delta c}(0,j\omega) \qquad (4.19)$$

With expressions 4.13, 4.18, and 4.19 defining the ac component of the diffusion flux, attention can be directed back to solving for the faradaic admittance using eqs. 4.7a, b and c. Substitution of either eq. 4.13, 4.18, or 4.19 for $\Delta\varphi$ in eqs.4.7 b and c,

followed by rearrangement, gives eqs. 4.7a, b and c in their respective forms, using 4.13 for $\Delta\varphi(j\omega)$, as:

$$\frac{\Delta I}{\Delta E} = F\left[\frac{\partial r_o}{\partial E}\right] + F\left[\frac{\partial r_o}{\partial c_{Ox}^s}\right]\left(\frac{\Delta c_{Ox}^s}{\Delta E}\right) + F\left[\frac{\partial r_o}{\partial c_{Red}^s}\right]\left(\frac{\Delta c_{Red}^s}{\Delta E}\right) \qquad \textbf{(4.20a)}$$

$$0 = F\left[\frac{\partial r_o}{\partial E}\right] + F\left[\left(\frac{\partial r_o}{\partial c_{Ox}^s}\right) - \sqrt{j\omega D}\right]\left(\frac{\Delta c_{Ox}^s}{\Delta E}\right) + F\left[\frac{\partial r_o}{\partial c_{Red}^s}\right]\left(\frac{\Delta c_{Red}^s}{\Delta E}\right) \qquad \textbf{(4.20b)}$$

and

$$0 = F\left[\frac{\partial r_o}{\partial E}\right] + F\left[\frac{\partial r_o}{\partial c_{Ox}^s}\right]\left(\frac{\Delta c_{Ox}^s}{\Delta E}\right) + F\left[\left(\frac{\partial r_o}{\partial c_{Red}^s}\right) - \sqrt{j\omega D}\right]\left(\frac{\Delta c_{Red}^s}{\Delta E}\right) \qquad \textbf{(4.20c)}$$

By applying Cramer's Rule to the above system of n equations in n variables, the faradaic admittance ($Y_f = \Delta I/\Delta E$) is found as the ratio of determinants $|\mathbf{T}|$ and $|\mathbf{B}|$:

$$Y_f = \frac{\det \boldsymbol{T}}{\det \boldsymbol{B}} = \frac{\begin{vmatrix} -\frac{\partial r_o}{\partial E} & \frac{\partial r_o}{\partial c_{Ox}^s} & \frac{\partial r_o}{\partial c_{Red}^s} \\ -\frac{\partial r_1}{\partial E} & \left(\frac{\partial r_1}{\partial c_{Ox}^s} - \sqrt{j\omega D}\right) & \frac{\partial r_1}{\partial c_{Red}^s} \\ -\frac{\partial r_2}{\partial E} & \frac{\partial r_2}{\partial c_{Ox}^s} & \left(\frac{\partial r_2}{\partial c_{Red}^s} - \sqrt{j\omega D}\right) \end{vmatrix}}{\begin{vmatrix} -\frac{1}{F} & \frac{\partial r_o}{\partial c_{Ox}^s} & \frac{\partial r_o}{\partial c_{Red}^s} \\ 0 & \left(\frac{\partial r_1}{\partial c_{Ox}^s} - \sqrt{j\omega D}\right) & \frac{\partial r_1}{\partial c_{Red}^s} \\ 0 & \frac{\partial r_2}{\partial c_{Ox}^s} & \left(\frac{\partial r_2}{\partial c_{Red}^s} - \sqrt{j\omega D}\right) \end{vmatrix}} \qquad \textbf{(4.21)}$$

where the subscripts have been dropped for reasons of clarity. Noting the relationships

between r_o, r_1 and r_2 row echelon reduction can be performed simultaneously on **T** and **B** to yeild a simplified form of Y_f.

The resulting admittance equation is then[2] [18]:

$$Y_f = \frac{-\sqrt{j\omega}\ nF\left(\frac{\partial r_o}{\partial E}\right)}{\sqrt{j\omega} - \left[\frac{1}{\sqrt{D_{Red}}}\left(\frac{\partial r_o}{\partial c^s_{Red}}\right) - \frac{1}{\sqrt{D_{Ox}}}\left(\frac{\partial r_o}{\partial c^s_{Ox}}\right)\right]} \qquad \textbf{(4.22)}$$

The impedance spectra shown in Fig.4.2 can be qualitatively evaluated by examining eq. 4.22 at some limiting frequencies. When ω reaches a value such that $(j\omega)^{1/2} \gg (1/D^{1/2}_{Red}\,(\partial r_o/\partial c^s_{Red}) - 1/D^{1/2}_{Ox}\,(\partial r_o/\partial c^s_{Ox}))$, Y_f reduces to $nF\,(\partial r_o/\partial E)$, which is equivalent to the reciprocal of the charge-transfer resistance (R_{ct}). This impedance, when in parallel with the double-layer capacitance (i.e. $Z_{tot} = (Y_f + j\omega C_{dl})^{-1}$), gives rise to the high-frequency semicircle in Fig 4.2B. The other limiting condition of eq. 4.22 is that for low frequencies where Y_f reduces to the form $(j\omega D)^{1/2}\,R_f$, with R_f being dependent on the behaviour of the electron transfer and diffusion process. The so-called Warburg impedance, the square-root dependence of Y_f on ω, is seen as the 45° slope region in the complex-plane plot, Fig. 4.2B. The other two mass-tranfer conditions, bounded diffusion with a conducting or nonconducting boundary, initially follow the 45°

---

[2]This equation can hold for all forms of the diffusion impedances if and only if the diffusion coefficients for all the species are equivalent, i.e. $D_{Ox} = D_{Red}$. Assuming this condition holds, the other cases are simply found by substitution for $(j\omega)^{1/2}$ of either $(j\omega)^{1/2}\coth(j\omega/D)^{1/2}L$ or $(j\omega)^{1/2}\tanh(j\omega/D)^{1/2}L$, in eq. 4.22, depending on which bounded diffusion conditions are appropriate, i.e. for the conducting or nonconducting boundary. If $D_{Ox} = D_{Red}$ is not valid, then some simplifications made in deriving eq. 4.22 from eq. 4.21 are also invalid, resulting in a more complicated expression for Y_f.

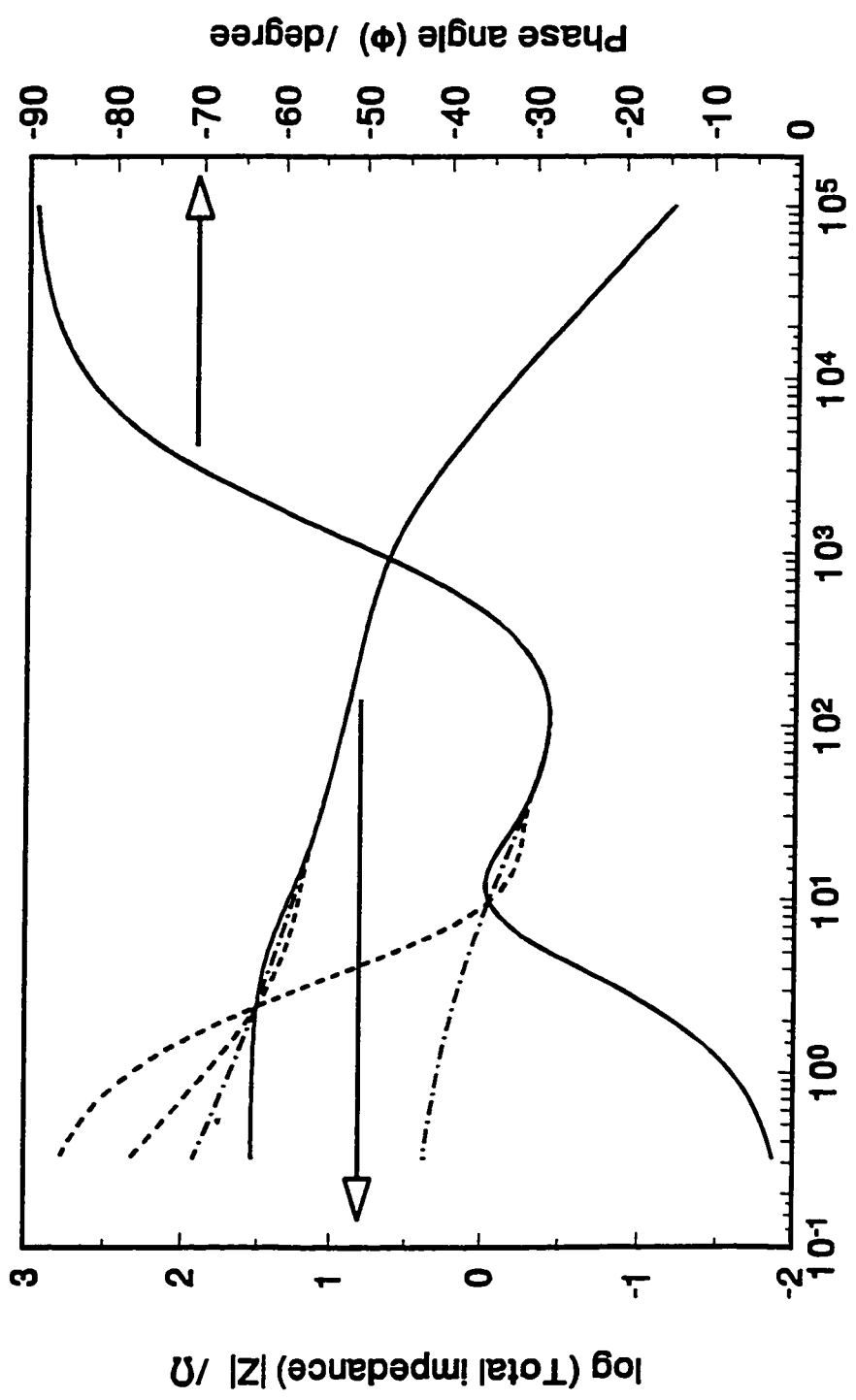

Fig. 4.2A A Bode impedance (log |Z|) and phase angle (Φ) plot showing the frequency response of the impedance given by eq. 4.22. This plot show the impedance response of the three different diffusion situations: case i (——), case ii (– – –) and case iii (-·-·-).

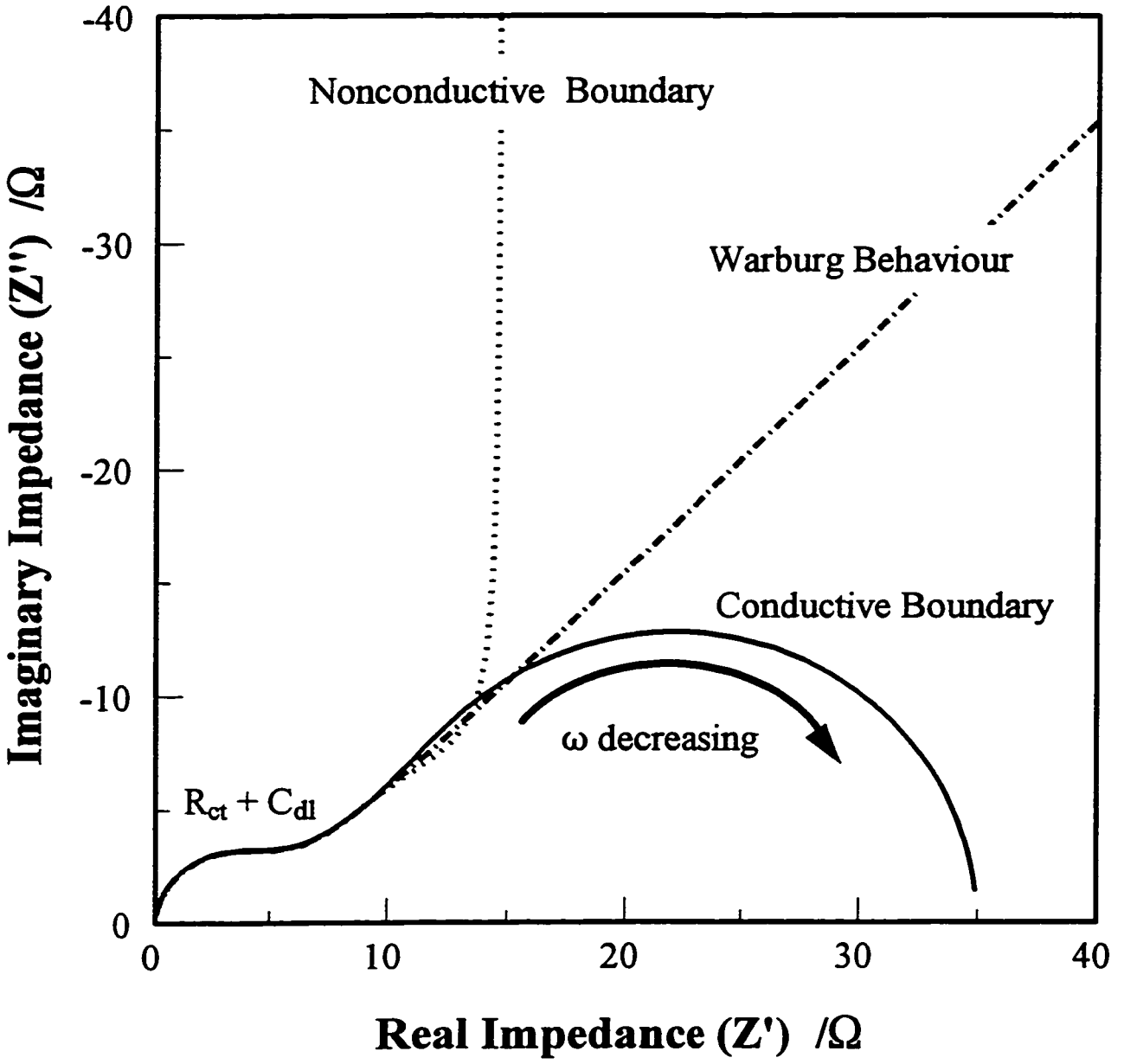

Fig. 4.2B The complex-plane plots, Z(imaginary) *vs.* Z(real), corresponding to the results shown in the Bode plot in Figs. 4.2A.

Warburg line (at intermediate frequencies), but deviate from this line when the ac frequency is made lower.

In the case where the boundary is conducting, the impedance intercepts the real axis as $\omega \rightarrow 0$, giving a finite diffusion resistance, whereas for the case where the boundary is nonconducting an infinite impedance, similar to capacitive behaviour, occurs as $\omega \rightarrow 0$. The frequency range over which this transition occurs (Warburg behaviour to either capacitive or resistive behaviour), is dependent on the magnitude of the diffusion coefficient and the diffusion-layer thickness. Armstrong [16] derived expressions, for certain situations, in which the transition frequency ω^* (the transition from Warburg to capacitive behaviour) could be used to estimate the diffusion coefficient for a species diffusing in a thin film with a nonconductive boundary.

4.3 Adsorption of the H Intermediate in the HER

4.3.1 HER with $[H^+]$ and $[H_2]$ constant [9,12]

Simple electrosorption of a species onto an electrode surface, where charge is passed during the adsorption process, is in many ways analogous to the charging or discharging of a capacitor. This analogy carries over to the EIS response of the adsorption reaction, which is commonly referred to as pseudo-capacitive behaviour. The surface concentration of adsorbed species is dealt with thoughout this thesis in terms of fractional coverages, θ. In the steady-state, which is a prerequisite condition for performing an EIS measurement [6,13], the change in coverage with time, $d\theta/dt$, is equal to zero. From this condition we are able to derive the steady-state adsorbate coverage, see § 1.2.3. For our model reaction, the one under study here, *viz* the HER,

θ_H in the steady-state is defined by:

$$\frac{q_1}{F}\frac{d\theta_H}{dt} = 0 = r_1 = \upsilon_1 - \upsilon_2 - 2\upsilon_3 \qquad \textbf{(4.23)}$$

where q_1 is the charge for maximum coverage, $\theta_H = 1$, of adsorbed H. With the application of a small amplitude potential signal, θ_H is then written as the sum of a dc part $\theta_{H,dc}$ and an ac part (see eqs. 4.1 and 4.2)

$\Delta\theta_H = |\Delta\theta_H| \exp(j\omega t + \phi_H) = |\Delta\theta_H| \exp(j\omega t) + \exp(j\phi_H)$, the amplitude of which is $|\Delta\theta_H|$ and whose phase relative to the input signal is ϕ_H. The time derivative $d\theta_H/dt$ is therefore $j\omega\Delta\theta_H$.

Separating the ac and dc parts of eq. 4.23 and expanding the right-hand-side in a truncated Taylor series about the dc potential, gives:

$$\frac{q_1}{F}\frac{d\theta_{H,dc}}{dt} + \frac{q_1 j\omega}{F}\Delta\theta_H = r_{1,dc} + \left(\frac{\partial r_1}{\partial E}\right)_\theta \Delta E + \left(\frac{\partial r_1}{\partial \theta_H}\right)_E \Delta\theta_H \qquad \textbf{(4.24)}$$

Cancelling the dc terms, dividing by ΔE and rearranging produces:

$$0 = F\left(\frac{\partial r_1}{\partial E}\right) + \left(\left(\frac{\partial r_1}{\partial \theta_H}\right) - \frac{q_1 j\omega}{F}\right)\frac{\Delta\theta_H}{\Delta E} \qquad \textbf{(4.25)}$$

Having already employed the linearlization of the electron flux equation, cf. eq. 4.7a, we can write, noting that, for the HER, $r_0 = -F(\upsilon_1 + \upsilon_2)$:

$$\frac{\Delta I}{\Delta E} = F\left(\frac{\partial r_o}{\partial E}\right) + F\left(\frac{\partial r_o}{\partial \theta_H}\right)\frac{\Delta\theta_H}{\Delta E} \qquad \textbf{(4.26)}$$

The faradaic admittance Y_f, $\Delta I/\Delta E$, is found, as before, by applying Cramer's rule, yielding two determinants with entries of partial derivatives:

$$Y_f\,(HER_1) = \frac{\begin{vmatrix} -\left(\frac{\partial r_o}{\partial E}\right) & \left(\frac{\partial r_o}{\partial \theta_H}\right) \\ -\left(\frac{\partial r_1}{\partial E}\right) & \left(\left(\frac{\partial r_1}{\partial \theta_H}\right) - \frac{q_1 j\omega}{F}\right) \end{vmatrix}}{\begin{vmatrix} -\frac{1}{F} & \left(\frac{\partial r_o}{\partial \theta_H}\right) \\ 0 & \left(\left(\frac{\partial r_1}{\partial \theta_H}\right) - \frac{q_1 j\omega}{F}\right) \end{vmatrix}} \qquad \textbf{(4.27)}$$

Solving this ratio of determinants and gathering terms yields:

$$Y_f\,(HER_1) = A + \frac{B}{j\omega + C} \qquad \textbf{(4.28)}$$

with $A = F(\partial r_o/\partial E)$, $B = (F^2/q_1)(\partial r_o/\partial \theta_H)(\partial r_1/\partial E)$ and $C = -(F/q_1)(\partial r_1/\partial \theta_H)$. Determining the potential dependence of each ac parameter, A, B and C, is of electrode-kinetic interest and aids in the determination of the electrochemical rate constants of the steps in the reaction mechanism. The parameters A, B and C in eq. 4.28 are the sums of the differentials for the respective individual reaction steps, following the relationships in the equation for r_o, see eq. 4.26 above, and in eq. 4.23 for r_1. We then have:

$$\left(\frac{\partial r_0}{\partial E}\right) = -F\left[\left(\frac{\partial \upsilon_1}{\partial E}\right) + \left(\frac{\partial \upsilon_2}{\partial E}\right)\right] \qquad \textbf{(4.29a)}$$

$$\left(\frac{\partial r_1}{\partial E}\right) = \left[\left(\frac{\partial \upsilon_1}{\partial E}\right) - \left(\frac{\partial \upsilon_2}{\partial E}\right) - 2\left(\frac{\partial \upsilon_3}{\partial E}\right)\right] \qquad \textbf{(4.29b)}$$

and

$$\left(\frac{\partial r_0}{\partial \theta_H}\right) = -F\left[\left(\frac{\partial \upsilon_1}{\partial \theta_H}\right) + \left(\frac{\partial \upsilon_2}{\partial \theta_H}\right)\right] \qquad \textbf{(4.29c)}$$

$$\left(\frac{\partial r_1}{\partial \theta_H}\right) = \left[\left(\frac{\partial \upsilon_1}{\partial \theta_H}\right) - \left(\frac{\partial \upsilon_2}{\partial \theta_H}\right) - 2\left(\frac{\partial \upsilon_3}{\partial \theta_H}\right)\right] \qquad \textbf{(4.29d)}$$

The above parital differentials in eqs. 4.29a to d for the individual rate of each of the steps, υ_1, υ_2 and υ_3, written as explicit functions in terms of η and θ_H, with β taken as 0.5 and $f = \beta F/RT = (1-\beta)F/RT$, are:

$$\left(\frac{\partial \upsilon_1}{\partial E}\right) = \frac{0.5F}{RT}\left(k_1(1-\theta_H)\exp(-\eta f) - k_{-1}\theta_H \exp(\eta f)\right) \qquad \textbf{(4.30a)}$$

$$\left(\frac{\partial \upsilon_2}{\partial E}\right) = \frac{0.5F}{RT}\left(k_2\theta_H \exp(-\eta f) - k_{-2}(1-\theta_H)\exp(\eta f)\right) \qquad \textbf{(4.30b)}$$

$$\left(\frac{\partial \upsilon_3}{\partial E}\right) = 0 \qquad \textbf{(4.30c)}$$

and

$$\left(\frac{\partial \upsilon_1}{\partial \theta_H}\right) = -k_1 \exp(-\eta f) - k_{-1}\exp(\eta f) \qquad \textbf{(4.31a)}$$

$$\left(\frac{\partial \upsilon_2}{\partial \theta_H}\right) = k_2 \exp(-\eta f) + k_{-2}\exp(\eta f) \qquad \textbf{(4.31b)}$$

$$\left(\frac{\partial \upsilon_3}{\partial \theta_H}\right) = 2k_3\theta_H + 2k_{-3}(1-\theta_H) \qquad \textbf{(4.31c)}$$

Again, the electrode impedance is $Z_{tot} = (Y_f(HER_1) + j\omega C_{dl})^{-1}$. Both A and C will always have positive values but B may take positive or negative values. The complex-plane plot will therefore have at the most two semicircles, the second of which,

being that corresponding to the fluctuation of coverage with frequency. The second semicircle will be of a capacitive ($B < 0$) or of an inductive ($B > 0$) nature. Fig. 4.1A shows two complex-plane plots coinsiding with different values of B. This example indicates that the upper limit of the number of inflections (N_B) in the log|Z| vs Log|ω| plot (Bode impedance plot) would be four, i.e. two inflections correspond to a semicircle in the complex-plane plot (compare the inflections in Fig. 4.1B to the number of semicircles in Fig. 4.1A). Seeing that one inflection must be attributed to the double-layer capacitance, Y_f will have three inflections. The formula, agreed upon in the literature, to predict N_B for a given mechanism which does not include diffusing species is $N_B = 2S_{ads} + 1$ with S_{ads} being the number of adsorbed species involved in the overall reaction and the 1 representing the fluctuation of electrons. This result also determines the number of linearly independent free parameters, which can be rationalized in the equation for Y_f, i.e. for Y_f(HER1) three parameters A, B and C. This point will be revisited when deriving the admittance equation for the HER + EHR (electrochemical hydrogenation reaction) where two adsorbed species are present and the number of parameters in Y_f is five. For a more in-depth discussion of the factors effecting N_B, see ref. 19.

The only exception to this rule arises for underpotential deposition reactions, where the maximum number of inflections in Y_f is two. The impedance function for the UPD of H for example, has only two parameters. This can easily be derived if it is noted that the impedance of the UPD of H is, mathematically speaking, just a limiting case of the HER impedance derived above. Considering that the process of UPD of H is

equivalent to the HER but with $\upsilon_2 = \upsilon_3 = 0$ and consequently $-r_o = r_1 = \upsilon_1$, the HER impedance equation , 4.28, can be reduced to:

$$Y_f(UPD) = A + \frac{AC}{j\omega + C} = \frac{j\omega A}{j\omega - C} \qquad (4.32)$$

This expression is found to be equivalent to the impedance of a resistor and capacitor in series, and is commonly represented by the following equivalent circuit: with $R_{ct} = 1/A$, and $C_\phi = A/B$. The total impedance of the circuit (i.e. including the double-layer capacitance) is

$Z_t = (Y_f(UPD) + j\omega C_{dl})^{-1}$ or in terms of R_{ct} and C_ϕ the total impedance is

$Z_t = ((R_{ct} + 1/j\omega C_\phi)^{-1} + j\omega C_{dl})^{-1}$. This circuit was used for Complex Nonlinear Least Squares (CNLS) fitting of the UPD of H results at Pt(hkl) surfaces in 0.5 mol dm^{-3} H_2SO_4 [4].

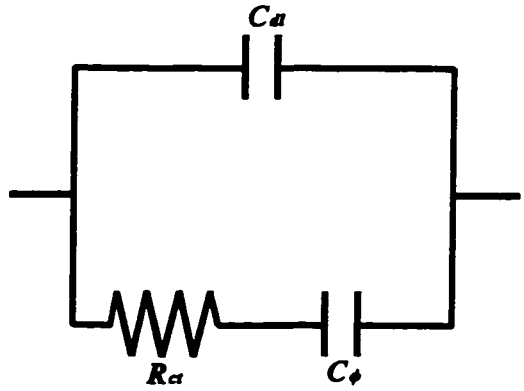

4.3.2 The HER and the Electrochemical Hydrogenation Reaction (EHR)

The derivation of the impedance for these processes will follow a similar procedure as that for the HER alone but, as was seen in § 6.3 when deriving the steady-state kinetics, we now are concerned not only with the variation of θ_H with potential but also θ_p (the coverage of co-adsorbed poison) which will decrease with increasing overpotential as the poison (P) becomes desorbed or is hydrogenated. Firstly, as was done before, the equations representing the flux of e^-, θ_H and θ_P , eqs. 6.8, 6.7 and 6.3 respectively, are linearlized yielding:

$$\frac{\Delta I}{\Delta E} = F\left(\frac{\partial r_o}{\partial E}\right) + F\left(\frac{\partial r_o}{\partial \theta_H}\right)\frac{\Delta \theta_H}{\Delta E} + F\left(\frac{\partial r_o}{\partial \theta_P}\right)\frac{\Delta \theta_P}{\Delta E} \qquad \textbf{(4.33a)}$$

$$0 = \left(\frac{\partial r_1}{\partial E}\right) + \left(\left(\frac{\partial r_1}{\partial \theta_H}\right) - \frac{j\omega q_1}{F}\right)\frac{\Delta \theta_H}{\Delta E} + \left(\frac{\partial r_1}{\partial \theta_P}\right)\frac{\Delta \theta_P}{\Delta E} \qquad \textbf{(4.33b)}$$

and

$$0 = \left(\frac{\partial r_2}{\partial E}\right) + \left(\frac{\partial r_2}{\partial \theta_H}\right)\frac{\Delta \theta_H}{\Delta E} + \left(\left(\frac{\partial r_1}{\partial \theta_P}\right) - \frac{j\omega q_2}{F}\right)\frac{\Delta \theta_P}{\Delta E} \qquad \textbf{(4.33c)}$$

Equations 4.33a to c are solved as above and, after rearrangements and gathering of common terms, we arrive at the following five-parameter equation for Y_f:

$$Y_f = A + \frac{j\omega B + C}{j\omega D - \omega^2 + G} \qquad \textbf{(4.34)}$$

where

$$A = F\left(\frac{\partial r_o}{\partial E}\right) \qquad \textbf{(4.35a)}$$

$$B = \frac{F^2}{q_1}\left(\frac{\partial r_o}{\partial \theta_H}\right)\left(\frac{\partial r_1}{\partial E}\right) + \frac{F^2}{q_2}\left(\frac{\partial r_o}{\partial \theta_P}\right)\left(\frac{\partial r_2}{\partial E}\right) \qquad \textbf{(4.35b)}$$

$$C = \frac{F^3}{q_1 q_2}\left[-\left(\frac{\partial r_o}{\partial \theta_H}\right)\left(\frac{\partial r_1}{\partial E}\right)\left(\frac{\partial r_2}{\partial \theta_P}\right) + \left(\frac{\partial r_o}{\partial \theta_H}\right)\left(\frac{\partial r_1}{\partial \theta_P}\right)\left(\frac{\partial r_2}{\partial E}\right) - \left(\frac{\partial r_o}{\partial \theta_P}\right)\left(\frac{\partial r_1}{\partial \theta_H}\right)\left(\frac{\partial r_2}{\partial E}\right) + \left(\frac{\partial r_o}{\partial \theta_P}\right)\left(\frac{\partial r_1}{\partial E}\right)\left(\frac{\partial r_2}{\partial \theta_H}\right)\right] \qquad \textbf{(4.35c)}$$

$$D = -\frac{F}{q_1}\left(\frac{\partial r_1}{\partial \theta_H}\right) - \frac{F}{q_2}\left(\frac{\partial r_2}{\partial \theta_P}\right) \tag{4.35d}$$

and

$$G = \frac{F^2}{q_1 q_2}\left[\left(\frac{\partial r_1}{\partial \theta_H}\right)\left(\frac{\partial r_2}{\partial \theta_P}\right) - \left(\frac{\partial r_1}{\partial \theta_P}\right)\left(\frac{\partial r_2}{\partial \theta_H}\right)\right] \tag{4.35g}$$

As was done for the HER with $[H^+]$ and $[H_2]$ constant, each differential in the relations for the parameters A to G can be evaluated from the rate equations derived in § 6.3 for the HER + EHR reaction. The two-intermediate (θ_1 and θ_2) impedance approach was used by Bai and Conway [20,21,22] to treat the kinetics of Al dissolution in acetonitrile. The relationship of the parameters in eq. 4.34 to the resistor, capacitor and/or inductor values in many different equivalent circuits was investigated by Cao [11].

4.4 Adsorption and Diffusion in a Multistep Reaction: HER impedance with considerations of H_2 Diffusion away from the electrode [23]

In deriving the electrochemical impedance for the above HER reaction mechanism, with $[H_2]$ as a diffusing species, § 5.1, we are concerned with the periodic flux of three species, electrons, adsorbed H and the surface-region concentration of H_2. The net rates of production of each of the species are defined as:

r_o, the net rate of electron production, given by

$$r_o = \frac{I}{F} = f_o\left[E,\ \theta,\ c^s_{H_2}\right] \tag{4.36}$$

r_1, the net rate of production of adsorbed H, where q_1 is the charge for maximum

coverage of OPD H, given by:

$$r_1 = \left(\frac{q_1}{F}\right)\left(\frac{d\theta}{dt}\right) = f_1\left[E,\ \theta,\ c^s_{H_2}\right] \tag{4.37}$$

and r_2, the net rate of production of $H_{2\,(aq)}$ at the electrode surface, given by

$$r_2 = \left(\sqrt{i\omega D}\coth\sqrt{\frac{i\omega}{D}}L\right)\left(\frac{dc^s_{H_2}}{dt}\right) = f_2\left[E,\ \theta,\ c^s_{H_2}\right] \tag{4.38}$$

When the electrode is rotated at the usually used rates, *ca.* 3000 ~ 4000 rpm, the diffusion-layer thickness is comparable to the ac penetration depth in the usual frequency range [14]. The diffusion problem must therefore be treated as in § 4.2.2, i.e. in terms of finite diffusion with a conductive boundary [10,14,15].

The appropriate periodic material flux equations are then obtained by expanding r_o, r_1, and r_2 in a Taylor series limited to the first-order terms:

$$\frac{\Delta I}{F} = \left(\frac{\partial r_o}{\partial E}\right)_{\theta,c^s}\Delta E + \left(\frac{\partial r_o}{\partial \theta_H}\right)_{E,c^s}\Delta\theta_H + \left(\frac{\partial r_o}{\partial c^s_{H_2}}\right)_{E,\theta}\Delta c^s_{H_2} \tag{4.39a}$$

$$j\omega q_1\frac{\Delta\theta}{F} = \left(\frac{\partial r_1}{\partial E}\right)_{\theta,c^s}\Delta E + \left(\frac{\partial r_1}{\partial \theta_H}\right)_{E,c^s}\Delta\theta_H + \left(\frac{\partial r_1}{\partial c^s_{H_2}}\right)_{E,\theta}\Delta c^s_{H_2} \tag{4.39b}$$

and

$$\sqrt{j\omega D}\ \coth\sqrt{\frac{j\omega}{D}}L\ \Delta c^s_{H_2} = \left(\frac{\partial r_2}{\partial E}\right)_{\theta,c^s}\Delta E + \left(\frac{\partial r_2}{\partial \theta_H}\right)_{E,c^s}\Delta\theta_H + \left(\frac{\partial r_2}{\partial c^s_{H_2}}\right)_{E,\theta}\Delta c^s_{H_2} \tag{4.39c}$$

Equations 4.39a, b and c are rearranged and solved to give the faradaic admittance, again using Cramer's Rule:

$$Y_f = \Delta I/\Delta E = \boldsymbol{T}/\boldsymbol{B} \tag{4.40}$$

The faradaic admittance is the quotient of the determinants **T** and **B**, which are written

as:

$$T = \begin{vmatrix} -\frac{\partial r_o}{\partial E} & \frac{\partial r_o}{\partial \theta} & \frac{\partial r_o}{\partial c^s_{H_2}} \\ -\frac{\partial r_1}{\partial E} & \left(\frac{\partial r_1}{\partial \theta} - \frac{q_1 j\omega}{F}\right) & \frac{\partial r_1}{\partial c^s_{H_2}} \\ -\frac{\partial r_2}{\partial E} & \frac{\partial r_2}{\partial \theta} & \left(\frac{\partial r_2}{\partial c^s_{H_2}} - \sqrt{j\omega D}\coth\sqrt{\frac{j\omega}{D}}L\right) \end{vmatrix} \qquad \textbf{(4.41a)}$$

and

$$B = \begin{vmatrix} -\frac{1}{F} & \frac{\partial r_o}{\partial \theta} & \frac{\partial r_o}{\partial c^s_{H_2}} \\ 0 & \left(\frac{\partial r_1}{\partial \theta} - \frac{q_1 j\omega}{F}\right) & \frac{\partial r_1}{\partial c^s_{H_2}} \\ 0 & \frac{\partial r_2}{\partial \theta} & \left(\frac{\partial r_2}{\partial c^s_{H_2}} - \sqrt{j\omega D}\coth\sqrt{\frac{j\omega}{D}}L\right) \end{vmatrix} \qquad \textbf{(4.41b)}$$

where the subscripts on the differential expressions have again been dropped for reasons of clarity.

Limiting the treatment to consideration of the Volmer-Tafel mechanism, as is suggested by the kinetic behaviour of the HER at Pt electrodes in alkaline media [24,25], and is implied by the value of the (H/T) separation factor [26] at Pt, the determinants **T** and **B** can then be simplified taking : $\partial r_o/\partial c^s = 0$, $\partial r_2/\partial E = 0$, $\partial r_o/\partial E = -\partial r_1/\partial E$, and $\partial r_2/\partial c^s = -2(\partial r_1/\partial c^s)$. The resulting equation can then be rearranged and terms collected to give the following expression for the faradaic admittance:

$$Y_f = A + \cfrac{AB}{j\omega C + \cfrac{1 - B}{1 - E\sqrt{j\omega s}\coth\sqrt{j\omega s}}} \qquad \textbf{(4.42)}$$

where $A = -F\,\partial r_o/\partial E$, $B = (-\partial r_o/\partial\theta)/(\partial r_1/\partial\theta)$, $C = q_1/(F\,\partial r_1/\partial\theta)$, $E = D/(L\,\partial r_2/\partial c^s)$, and $s = L^2/D$. The $j\omega s$ terms in Eq. 4.42 were raised to the power ϕ_w instead of 0.5 [8]. The parameter ϕ_w was allowed to vary to enhance the quality of the fit. The required value of ϕ_w ranged between 0.5 and 0.45. Values of ϕ_w lower than 0.5 can either be attributed to deactivation of the electrode which occurred mainly in the low frequency region of the frequency scan, or to non-uniform diffusion [8] of H_2.

The overall impedance, including the double-layer capacitance, is:

$$Z = (Y_f + j\omega C_{dl})^{-1} \qquad \textbf{(4.43)}$$

With the theoretical groundwork for the impedance analysis thus established, the discussion can now focus on the experimental results. Chapter 5 will treat the HER at Pt(hkl) single-crystal electrodes, hence eqs. 4.42, 4.28 and 4.22 will be used for data analysis where applicable in that chapter. Chapter 6 will use the impedance expression in eq. 4.34 to treat the results for the situation where thiourea reduction takes place during H_2 evolution. References will be made to this present chapter and the equations therein where it is appropriate in the text which follows.

References

1. K.J. Laidler, "Chemical Kinetics" 3rd. Edn., Harper and Row Inc., N.Y. (1987).
2. A.J. Bard and L. Faulkner, "Electrochemical Methods", Wiley, N.Y. (1980).
3. S.K. Rangarajan, J. Electroanal. Chem., 56 (1974) 1, Parts I, II, and III.
4. S. Morin, H. Dumont and B.E. Conway, J. Electroanal. Chem., 412 (1996) 39.
5. H. Angerstein-Kozlowska and B.E. Conway, J. Electroanal. Chem. 95 (1979) 1.

6. D.D. Macdonald and M.C.H. McKubre, in "Modern Aspects of Electrochemistry", Eds. J.O'M. Bockris, B.E. Conway and R.E. White, Plenum Press, N.Y.,Vol. 14 (1982) 61.

7. J.R. Macdonald, J. Electroanal. Chem., 233 (1987) 25.

8. J.R. Macdonald and D. Franceshetti, "Impedance Spectroscopy.", Ed. J.R. Macdonald, John Wiley and Sons, New York, (1987) p. 122.

9. D.A. Harrington and B.E. Conway, Electrochim. Acta., 32 (1987) 1703; L. Bai, D.A. Harrington and B.E. Conway, Electrochim. Acta, 32 (1987) 1713.

10. D. Franceschetti and J.R. Macdonald, J. Electroanal. Chem., 101 (1979) 307.

11. C. Cao, Electrochimica Acta, 35, (1990) 831.

12. R.D. Armstrong and M. Henderson, J. Electroanal. Chem., 39 (1972) 81.

13. M. Sluyters-Rehbach and J.H. Sluyters, in "Comp. Treat. of Electrochem." Eds. E. Yeager, J. O'M. Bockris, B.E. Conway and S. Sarangapani, Plenum Press, N.Y., Vol. 9 (1984) 177.

14. C. Delouis, I.Epelboin, M.Keddam and J.C. Lestrade, J. Electroanal. Chem., 28 (1970) 57.

15. D. Franceschetti, J.R. MacDonald and R.P. Buck, J. Electrochem. Soc., 138 (1991) 1368.

16. R. D. Armstrong, J. Electroanal. Chem., 198 (1986) 177.

17. O. Contamin, E. Levart, G.Magner, R.Parsons and M.Savy, J. Electroanal. Chem., 179 (1984) 41.

18. D.A. Harrington, J. Electroanal. Chem., 403 (1996) 11.

19. D.A. Harrington, J. Electroanal. Chem., in press (1997).

20. L. Bai and B.E. Conway, Electrochim. Acta, 38 (1993) 1803.

21. L. Bai and B.E. Conway, J. Electrochem. Soc., 137 (1990) 3737.

22. L. Bai and B.E. Conway, ibid. 138 (1991) 2897.

23. J.H. Barber, S. Morin and B.E. Conway, J. Electroanal. Chem., 1998 *in press*.

24. L. Bai, J. Electroanal. Chem., 355 (1993) 37; L. Bai and B.E. Conway, Electrochim. Acta, 31 (1986) 1013.

25. N.M.Marković, S.T. Sarraf, H.A. Gasteiger and P. Ross Jr., J. Chem. Soc., Faraday Trans., 92 (1996) 3719.

26. J. O'M. Bockris, S. Srinivasan and D.B. Matthews, Disc. Faraday Soc., 39 (1965) 239; J. O'M. Bockris and D.B. Matthews, J. Chem. Phys., 44 (1966) 198.

Chapter 5

HER Studies at Pt(hkl) Single-crystal Electrodes in Acidic and Alkaline Solutions

5.1 Kinetic Analysis of the HER Including Effects of H_2 Diffusion

The HER at Pt can be considered to follow the well known alternative, two-stage mechanisms consisting of the Volmer-Heyrovsky and Volmer-Tafel steps. The individual reaction steps, for acidic electrolyte, are written in the usual way as:

$$M + H_3O^+ + e^- \rightleftharpoons MH_{ads} + H_2O \qquad \textbf{(5.I)}$$

followed by either

$$MH_{ads} + H_3O^+ + e^- \rightleftharpoons H_2(g) + H_2O \qquad \textbf{(5.II)}$$

or

$$2MH_{ads} \rightleftharpoons H_2(g) + 2M \qquad \textbf{(5.III)}$$

Experimentally it will be shown that the rate of diffusion from the electrode surface ("x" = 0), of H_2 supersaturating the diffusion layer, also influences the overall electrode kinetics in an indirect way. We write this step as:

$$H_{2\,(x=0)} \overset{J_{diff}}{\Longrightarrow} H_{2\,(bulk)} \qquad \textbf{(5.IV)}$$

Note that, at Pt, where a "complete" monolayer of UPD H already exists at the H_2 reversible potential ($\eta = 0$), the species represented as MH_{ads} in the above equations really refers to the state of OPD H, i.e. the *extra* H coverage that must be accommodated on or amongst H atoms in the initial UPD layer. Defining $c^s(H_2)$ as the concentration of H_2 at the electrode surface and $c^b(H_2)$ as the concentration of H_2 in the bulk, the electrochemical rate equations for steps 1-3, with F/RT written as f, are:

$$\upsilon_1 = k_1 (1-\theta)\exp(-\beta \eta f) - k_{-1} \theta \exp((1-\beta) \eta f)) \qquad \textbf{(5.1)}$$

$$\upsilon_2 = k_2 \theta \exp(-\beta \eta f) - k_{-2} (c^s_{H_2}/c^b_{H_2}) (1-\theta) \exp((1-\beta)\eta f) \qquad \textbf{(5.2)}$$

and

$$\upsilon_3 = k_3(\theta)^2 - k_3(c^s_{H_2}/c^b_{H_2})(1-\theta)^2 \qquad (5.3)$$

The rate constants k_1 and k_2 are formal rate constants containing the H_3O^+ concentration in bulk together with a double-layer distribution factor in the usual way. Since a rotating disk electrode was used exclusively throughout this study, the rate equation describing H_2 diffusion[1] can be written directly from the Levich equation as:

$$J_{diff} = 0.620 D^{2/3} \nu^{-1/6} \Omega^{1/2} (c^s_{H_2} - c^b_{H_2}) \qquad (5.4)$$

where D is the diffusion coefficient of H_2 in the supersaturation region, ν the kinematic viscosity (taken to be 0.001 $cm^2\ s^{-1}$), and Ω is the rotation rate (rad s^{-1}).

In the steady-state the fractional coverage (θ) by adsorbed H and the surface concentration of H_2 gas [$c^s(H_2)$] are defined as:

$$\frac{d\theta}{dt} = 0 = \upsilon_1 - \upsilon_2 - 2\upsilon_3 \qquad (5.5)$$

and

$$\frac{dc^s_{H_2}}{dt} = 0 = \upsilon_2 + \upsilon_3 - J_{diff} \qquad (5.6)$$

Equations 5.5 and 5.6 were solved numerically using the modified Powell hybrid method in the Fortran algorithm named DNSQ [35]. Knowing θ and $c^s(H_2)$ the steady-state current could be calculated from :

$$i = -F(\upsilon_1 + \upsilon_2) \qquad (5.7)$$

---

[1]The alternative process of bubble formation for transport of H_2 away from the electrode is not taken into account in this treatment. Experimentally it is found that bubbles were formed only at the highest cathodic currents studied, i.e. the diffusion component in the impedance spectra was no longer detectable. This omission will only affect the value of $c^s(H_2)$ at the highest current-densities; however, the data will remain accurate for the bulk of the results which include H_2 diffusion.

When the rates of the electrochemical processes and the overall reaction are determined by the rate of diffusion of H_2 away from the electrode, a diffusion overvoltage is established resulting in a quasi-Nernstian Tafel slope of RT/2F, in a way similar to that formulated by Losev [13]. At higher overpotentials where the difference between $c^a(H_2)$ and $c^b(H_2)$ is large and the rate of diffusion is not the rate-controlling step, the usual Tafel slopes of 2RT/F, or for sufficiently low overpotentials, a value of 2RT/3F, for k_1 or k_2 rate-limiting, or a limiting current with k_3 rate-limiting, can arise.

5.2 Results and Discussion

5.2.1 Rotation rate studies

In order first to verify that the diffusing species is H_2 dissolved in a supersaturated region in the electrode|electrolyte interphase and not H absorbed and diffusing into the metal which, for Pd, produces a formally similar EIS response, the dependence of the diffusion response on electrode rotation was studied. Both the EIS and the steady-state current response to rotation rate were monitored. The linear dependence of the EIS parameter, denoted as **s**, on rotation rate for the (511) face, Fig. 5.1, indicated that the diffusing species were in solution, and therefore can be identified as H_2. The slope of this relation is 23.6 (± 0.2) rad which is equal to $(1.61)^2 \nu^{(2/6)} D^{-1/3}$ from which a diffusion coefficient of 1.5 (± 0.5) x 10^{-5} $cm^2 s^{-1}$ can be calculated. This value for H_2 diffusion through the supersaturated region is comparable to the known bulk diffusion coefficient for H_2 which is 5.2 x 10^{-5} $cm^2 s^{-1}$. The value of 1.5 x 10^{-5} $cm^2 s^{-1}$ will be used here to define

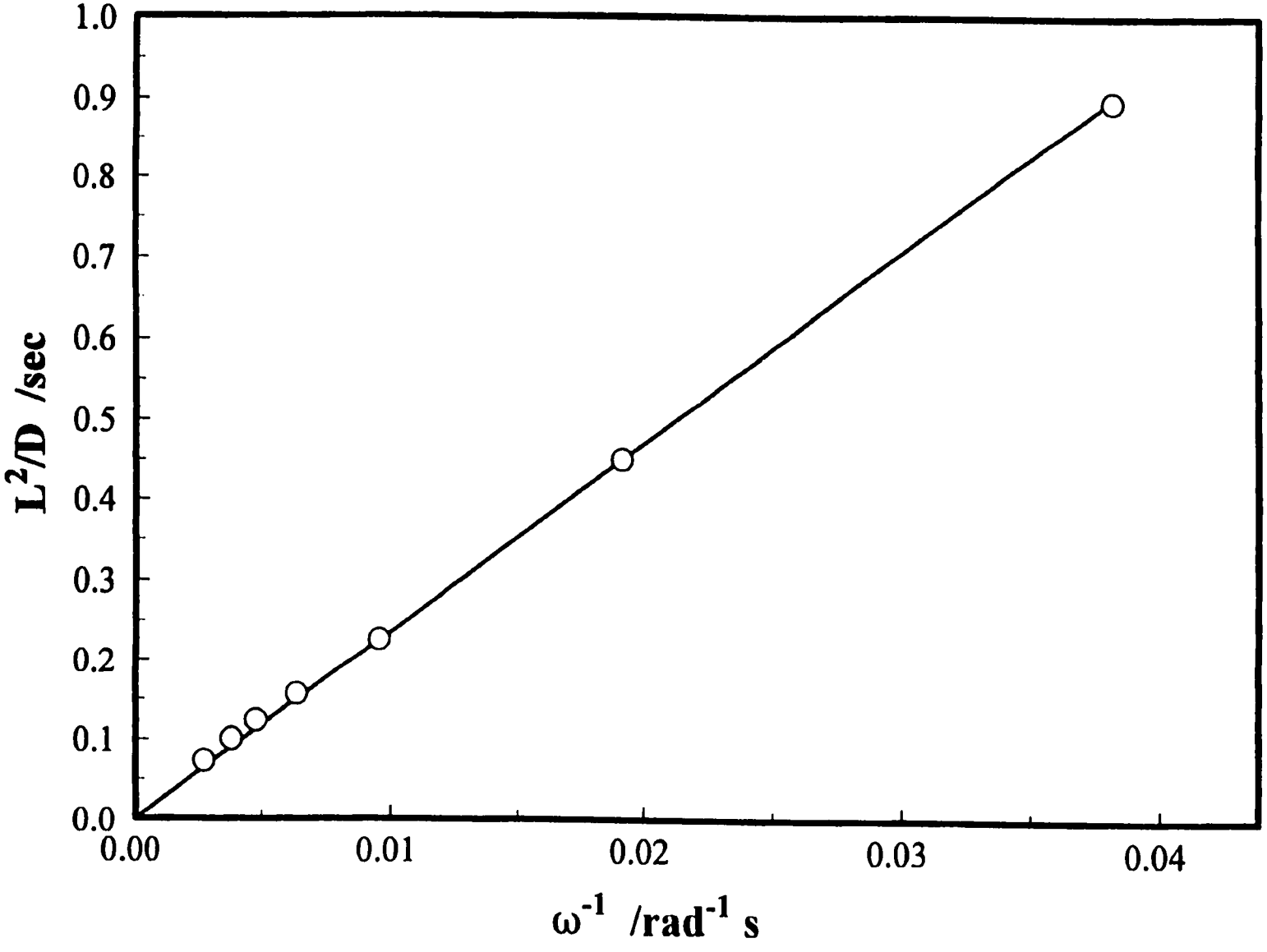

Fig. 5.1. Rotation rate, Ω, dependence of the ac parameter, $s = L^2/D$, for the HER in 0.5 mol dm^{-3} H_2SO_4. Slope = 23.6 ± 0.2 rad, (511) face E = -30 mV *vs.* RHE.

the rate of H_2 diffusion away from the electrode in the analysis of the overall reaction kinetics.

Using the dependence of H_2 diffusion on rotation rate we can also calculate the bulk H_2 concentration, which is the second value needed to define the hydrodynamic condition at the rotating electrodes. This value was determined by measuring the current for H_2 oxidation (HOR) as a function of rotation rate [41]. In this case the surface concentration of H_2 falls to zero allowing the Levich equation to be applied. Fig. 5.2 shows the Levich plot for H_2 oxidation at 400 mV *vs.* RHE (current maximum) at the (511) face; since the HOR is diffusion-controlled, the current will not depend on crystal face orientation, and therefore the derived bulk H_2 concentration will be valid for all crystal faces. The slope in Fig. 5.4 is 1.55 ($\pm$ 0.02) x 10^{-4} A cm^{-2} $rad^{-1/2}$ $s^{1/2}$, from which a bulk H_2 concentration of 1.38 ($\pm$ 0.05) x 10^{-3} mol dm^{-3}, is calculated. Introducing the values for D and $c^b(H_2)$ in Eqns. 5.5 and 5.6 it is possible to solve for $c^s(H_2)$ and θ.

5.2.2 Tafel relations (steady-state current *vs* voltage behaviour)

The steady-state current was measured at each dc voltage before and after application of the ac frequency scan. Tafel plots were also derived from data obtained by linear potential scans into the hydrogen evolution region. Both methods produced virtually identical results. Fig. 5.3 shows the Tafel plots for the three low-index planes, (100)S_{II}, (111) and (110). The order of reactivity as seen in Fig. 5.3 is (110) > (111) > (100)S_{II}. The (110) data give a Tafel slope of approximately 29 mV $decade^{-1}$; such a value, as was stated in the introduction, has been interpreted as either associated with recombination control at low coverages of adsorbed H or due to influence of a diffusion

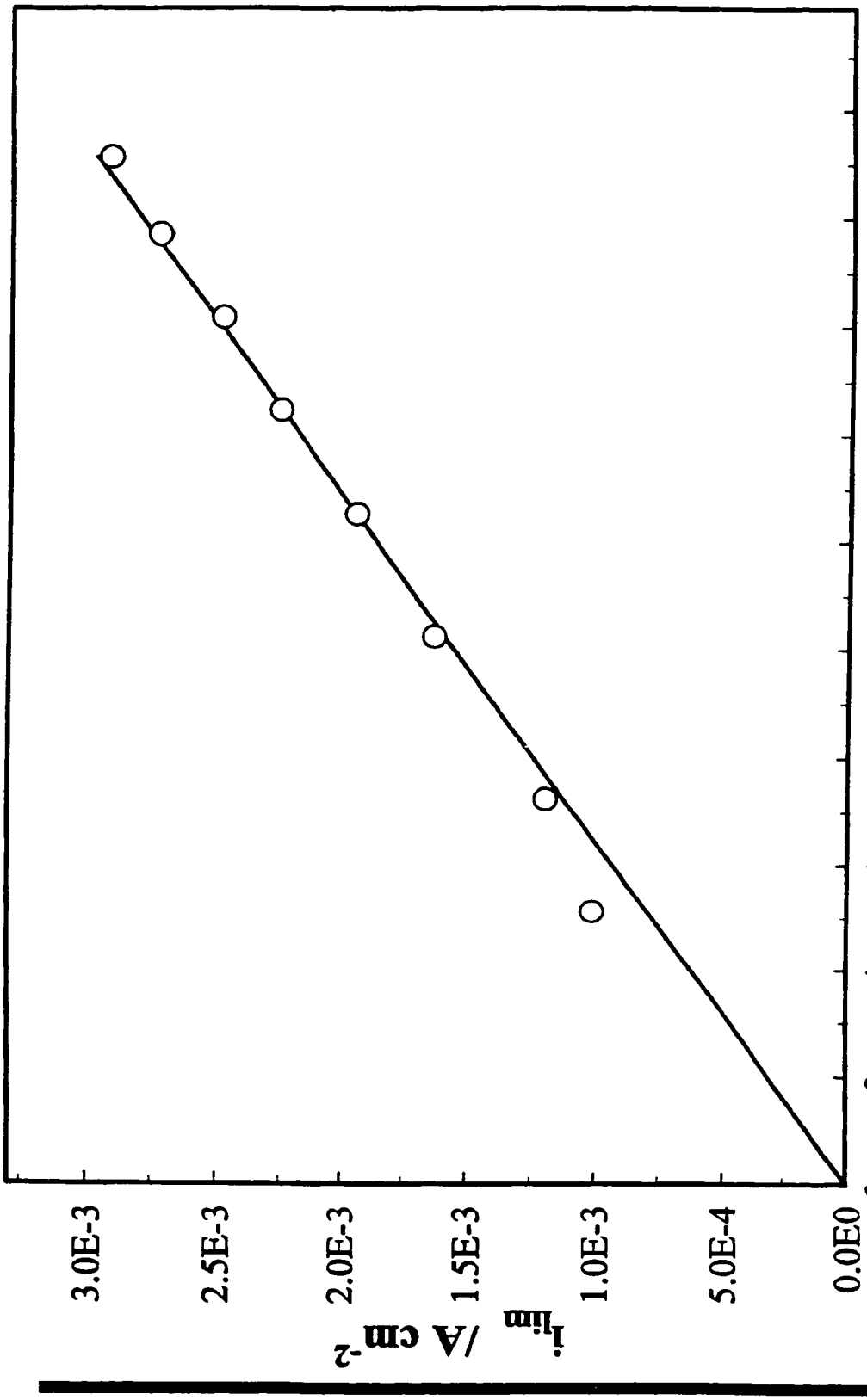

Fig. 5.2. Rotation rate, Ω, dependence of the limiting current-density for the hydrogen oxidation reaction at Pt(511) in 0.5 mol dm^{-3} H_2SO_4. Slope = 1.55 (± 0.02) x 10^{-4} A cm^{-2} rad$^{-1/2}$ s$^{1/2}$, E = 400 mV *vs.* RHE.

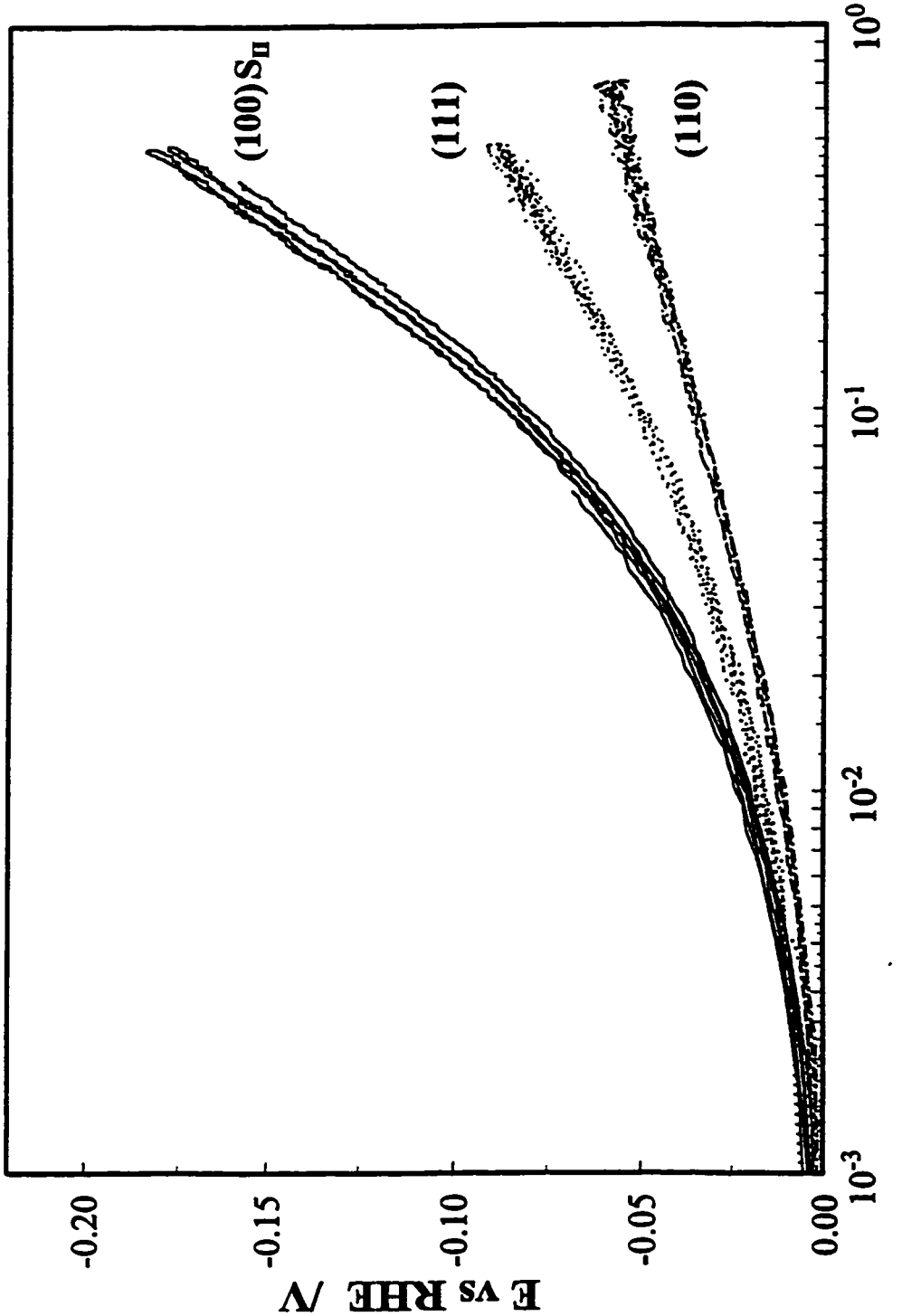

Fig. 5.3. Tafel plots for the (100)S_{II}, (111) and (110) faces. Rotation rate, Ω = 3500 rpm, 0.5 mol dm^{-3} H_2SO_4.

overvoltage.

From the steady-state current-voltage behaviour alone a distinction between these two interpretations cannot be made but introduction of the EIS data shows clearly that the 29 mV decade^{-1} Tafel slope is in fact due to the H_2 diffusion overvoltage. However, the Tafel plot for the (100)S_{II} face lies approximately 1 decade of current below that for the other surface geometries, and again at low overvoltages has a 29 mV decade^{-1} Tafel slope. The consequence of the (100)S_{II} face being less active is that the accessible potential range is 150 mV more negative than for the other faces. At such (relatively) higher overpotentials the reaction kinetics on Pt (100)S_{II} are now limited by the *electrode kinetics* alone, as is indicated by the EIS data. Also, for this face, the Tafel plot at overpotentials more negative than -100 mV shows an approach to a limiting current-density. This type of Tafel relation is indicative of a recombination-controlled reaction with the OPD $\theta_H \rightarrow 1$. From this qualitative analysis, plus information gained from the EIS measurements, we can state that at low overpotentials, 0 to -50 mV, the reaction rate is controlled by diffusion of H_2 from the surface but, at more negative overpotentials, -50 to -100 mV, by recombination between adsorbed H atoms on the electrode surface, while at the most negative overpotentials studied a contribution from the electrochemical desorption step arises.

5.2.3 EIS results

EIS data were collected at each of the experimentally measured overpotentials shown in Fig. 5.9. Each family of spectral data was then fitted to Eq. 4.42. Representative complex-plane plots are shown in Figs. 5.4, 5.5, 5.6 and 5.7 for the

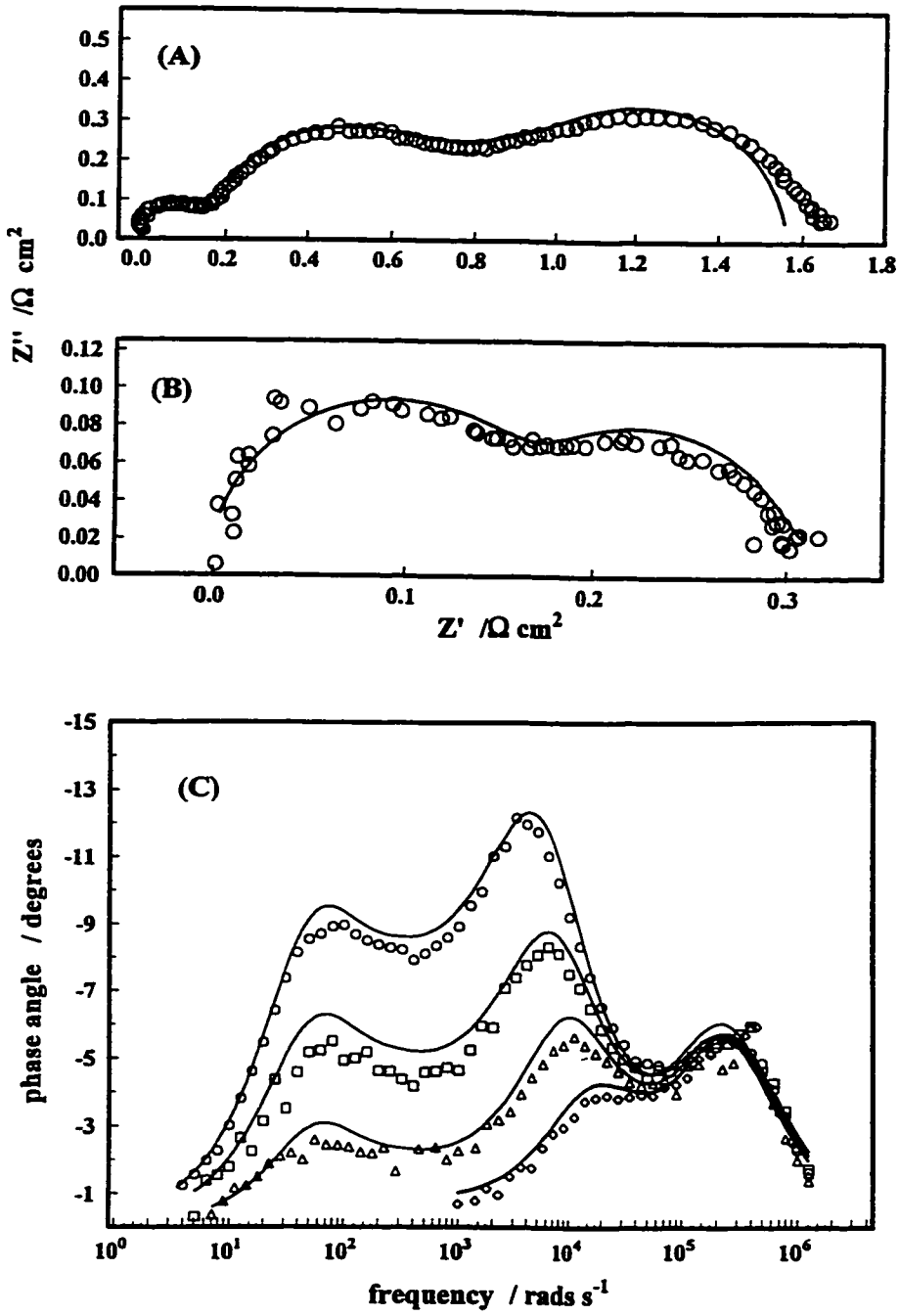

Fig. 5.4. Complex-plane plots for the HER at the (100)S_{II} face in 0.5 mol dm^{-3} H_2SO_4. **A)** E = -22 mV ; **B)** E = -91.5 mV; **C)** Bode phase-angle plot for overpotentials between -22 mV ○, -34 mV □, -51 mV Δ and -91.5 mV ◇ *vs.* RHE.

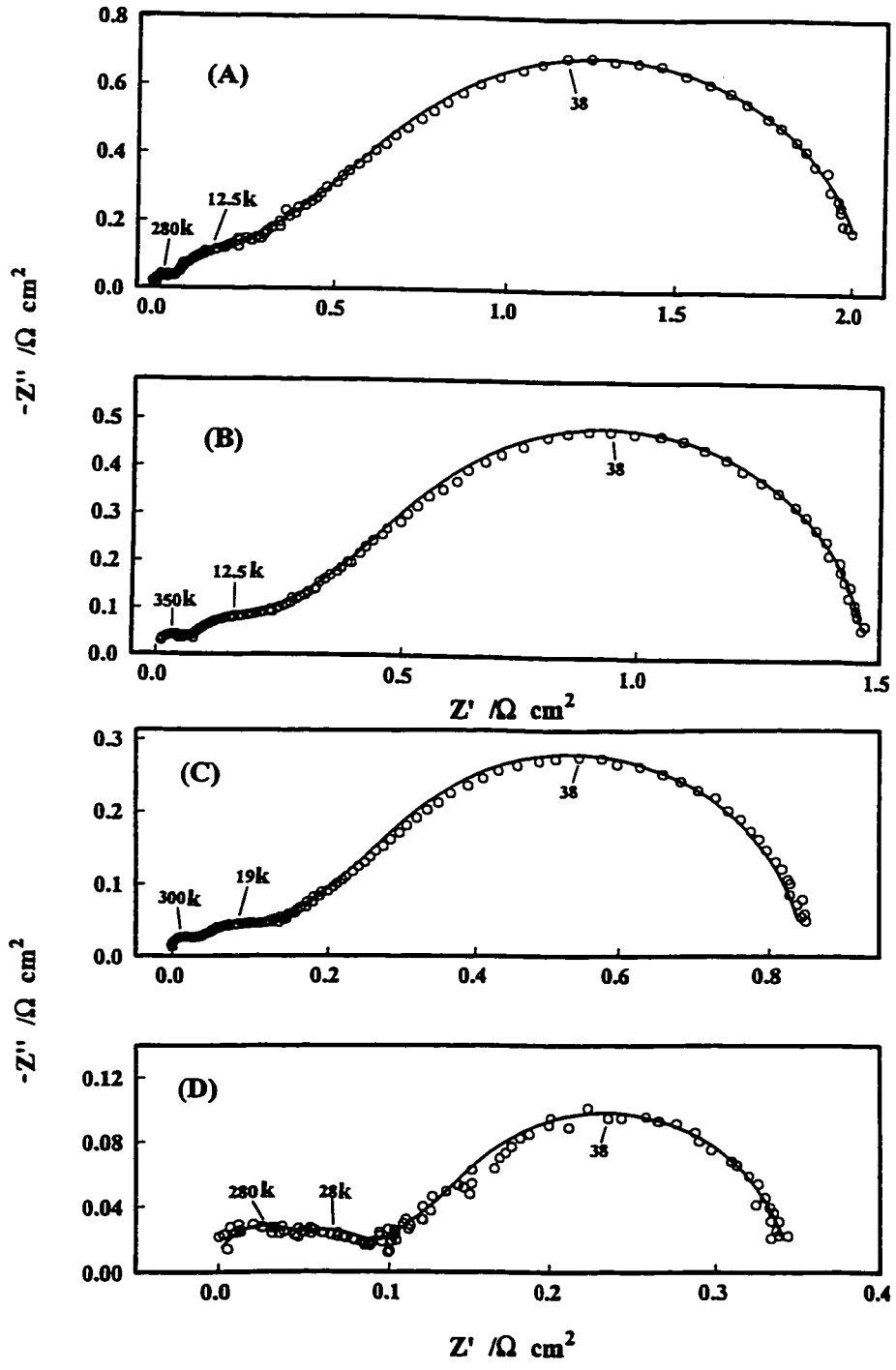

Fig. 5.5. Complex-plane plots for the (511) face at **A)** E = -7.3 mV ; **B)** E = -14 mV; **C)** E = -30 mV; **D)** E = -40 mV. Selected frequencies marked on the plot are in rad s^{-1}.

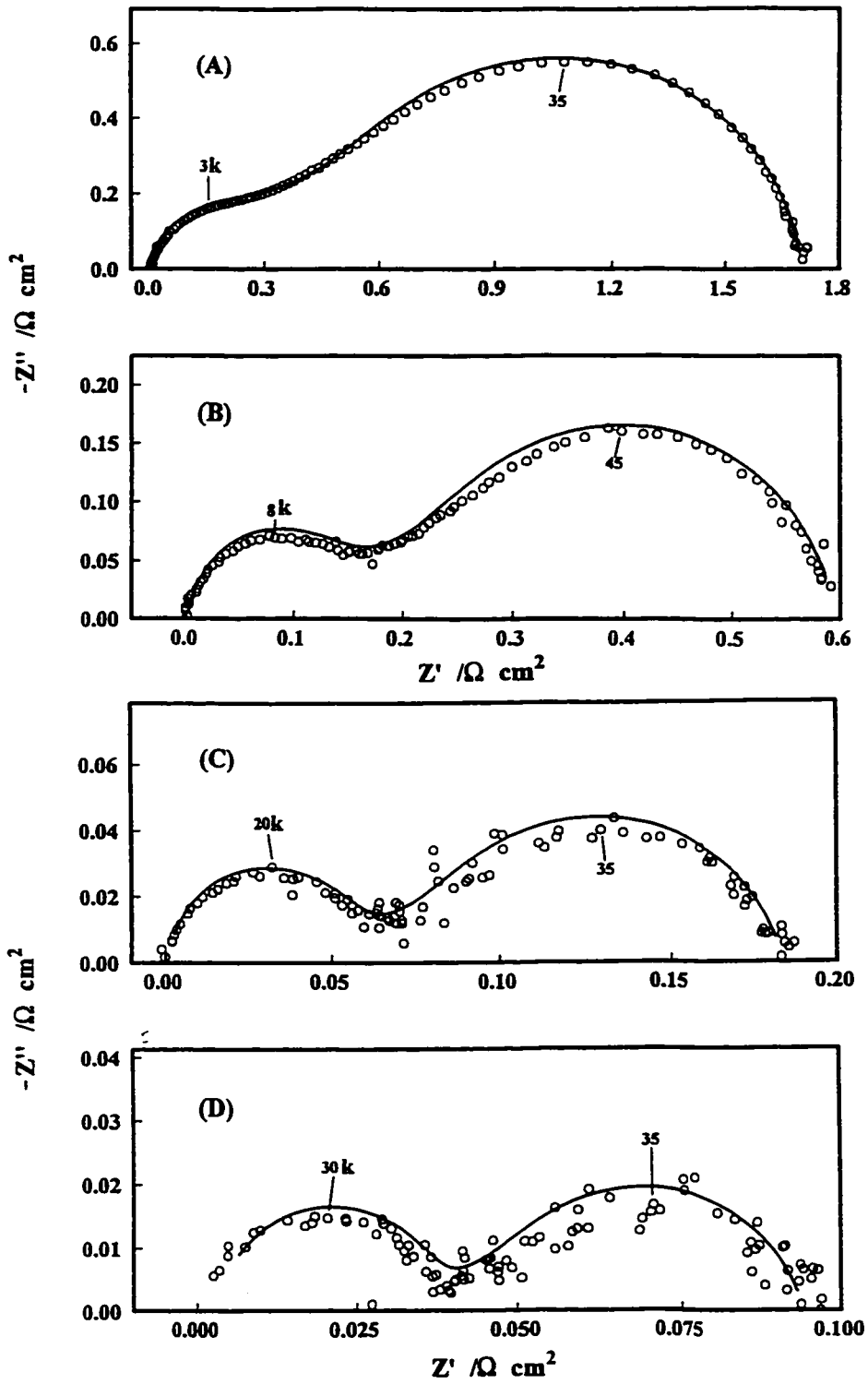

Fig. 5.6. Complex-plane plots for the (111) face at **A)** E = -8.6 mV ; **B)** E = -25 mV; **C)** E = -42 mV; **D)** E = -52.5 mV. Selected frequencies are in rad s^{-1}.

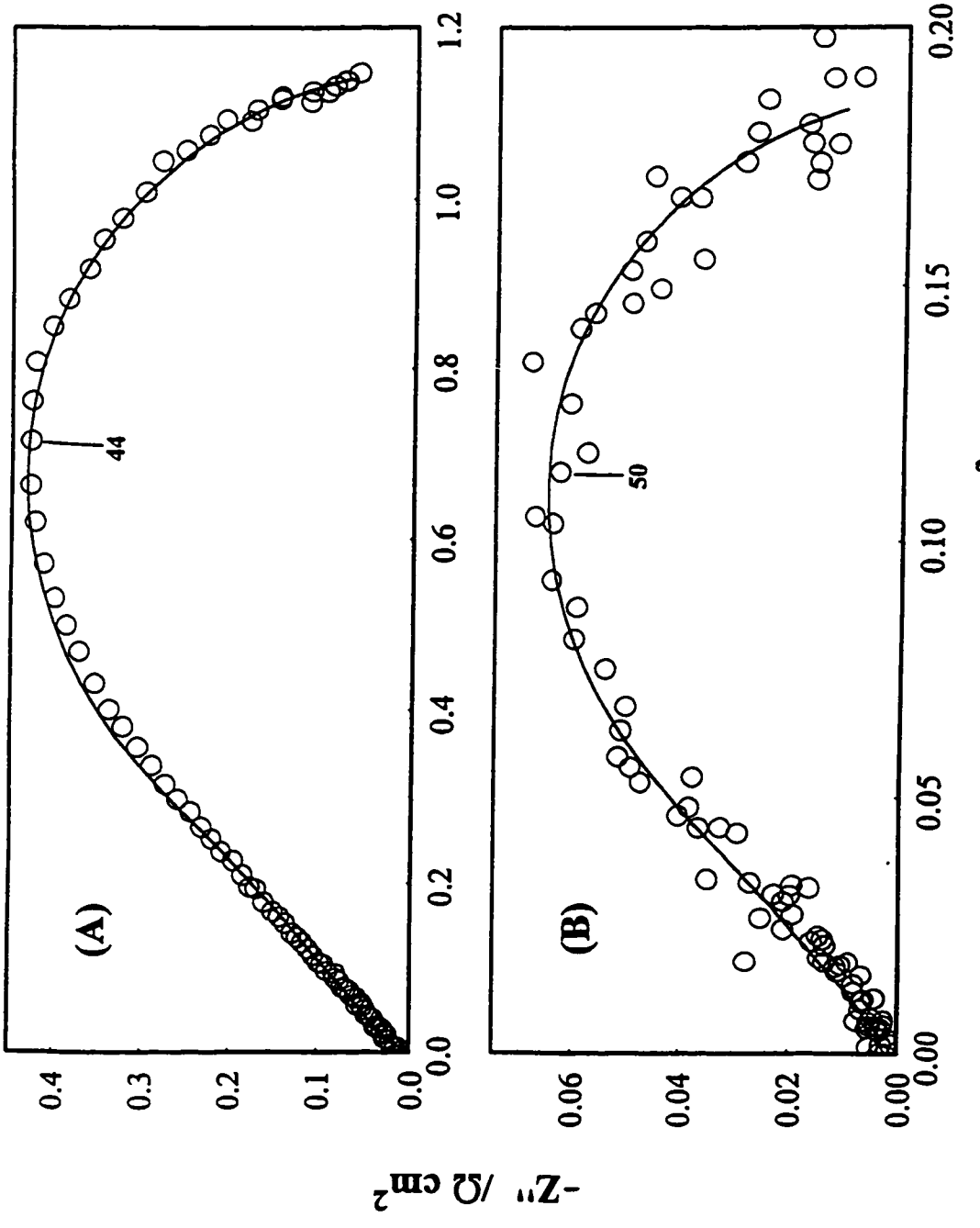

Fig. 5.7. Complex-plane plots for the (110) face at **A)** E = -10.9 mV ; **B)** E = -36 mV *vs.* RHE. Selected frequencies marked on the plot are in rad s^{-1}.

$(100)S_{II}$, (511), (111) and (110) faces, respectively. For the $(100)S_{II}$ and the (511) face cooled in an H_2+Ar mixture, three dispersion processes are observable. For the (111), (110) and the $(100)S_I$ faces the response corresponding to the high frequency charge-transfer resistance was not detectable. At high frequencies the double-layer capacitance relaxes through the charge-transfer resistance (1/A) (Eq. 4.42); at intermediate frequencies the relaxation is that of the adsorbed H as represented by parameters B and C in Eq. 4.42; and in the low frequency region the dispersion process is that for the oscillation of the H_2 concentration at the electrode|electrolyte interphase, represented by parameters E and s in Eq. 4.42. Comparing the impedance spectra for the various faces we observe, as would be expected, that as the overall rate of the HER decreases, going from (110) to $(100)S_{II}$, the prominence of the H_2 diffusion process decreases. The contribution to the overall impedance due to the H_2 diffusion process, represented by the third semicircle in the complex plane plot, increases as the level of reactivity increases from $(100)S_{II}$ to the (110), whereas the impedance for the electron-transfer and adsorption processes decreases in the same order. It is seen, e.g. in Figs. 5.5 or 5.7, that the third semicircles have a shape close to that for the finite layer diffusion case (compare Fig. 4.2b in chapter 4).

Fig. 5.4c shows the Bode phase angle plot for the H_2+Ar cooled (100) face. The maxima associated with H_2 diffusion and H deposition decrease significantly with more negative cathodic potential. This dependence shows that the adsorbed H coverage and H_2 surface-concentration, and their relationships to potential, $(\partial\theta/\partial E)$ and $(\partial c^s(H_2)/\partial E)$, are all changing with potential. The values found for the double-layer capacitance ranged between 20 and 50 $\mu F\ cm^{-2}$. The slower rates at the (100) H_2+Ar cooled face allowed the

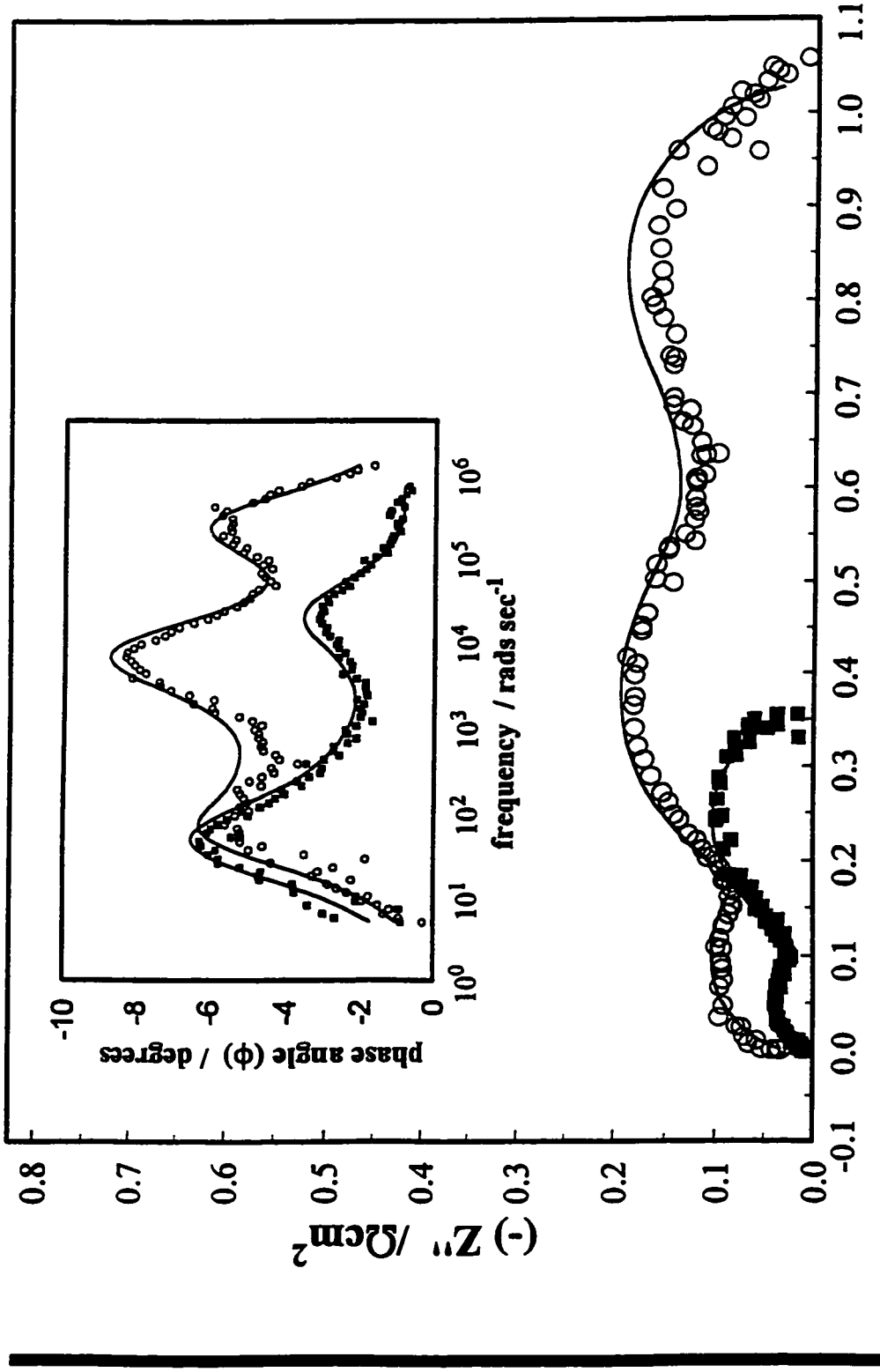

Fig. 5.8. Complex-plane plot showing the effect of the conditions of cooling; Pt(100) 3500 rpm E = -33 mV *vs.* RHE, ○ H_2+Ar cooled (100)S_{II}, ■ air cooled (100)S_I. Inset: Bode phase angle plot, conditions as above.

most accurate evaluation of C_{dl}, and a small decrease with decreasing potential was found.

Some interesting qualitative features of the EIS data for the different faces are to be noted. Firstly, it is seen that as (111) steps are added to the (100) surface in the (19 11) ≡ 10(100) x (111) and (511) ≡ 3(100) x (111) faces the features of the ac responses become more like those of a (110)-like spectrum than for a spectrum comprised of a mixture due to (100)S_{II} and (111) contributions. Surprisingly, this is contrary to what is obtained in the CV responses for the UPD of H (in 0.5 mol dm^{-3} H_2SO_4) at these faces, i.e., in the CV's, introduction of (111) steps directly leads to an increase in the (111) characteristic features in the voltammograms.

In the case of the impedance spectrum for the air-cooled (100)S_I, which from its CV appears to have a less ordered structure than the H_2+Ar cooled surface, it displays almost identical features to those of the (111) face.

Also of interest for the (100)S_I face was the observation of a large difference in the charge-transfer kinetics between the UPD and OPD H regions: UPD R_{ct} = 0.12 - 0.6 Ω cm^2 while the OPD R_{ct} was not observable. This was the only surface where large differences were seen and might be indicative of possible changes taking place in the surface structure between the UPD and OPD H regions.

The differences in the electrode kinetics, specific to the faces examined, as indicated from the Tafel plots in Fig. 5.3, are also quite apparent in the complex-plane EIS representations of the behaviour of the faces. Thus the charge-transfer resistance for the (100) S_{II} face, R_{ct} ≈ 0.2 Ω cm^2, is three times larger than that for the (511) face for which R_{ct} ≈ 0.07 Ω cm^2; also, these values are much larger than those for the (100) S_I, (111) and

(110) faces. The differences between these values are consistent with those seen for H electrosorption in the H UPD potential region [2]: for the (100) S_{II} face an average value of 0.37 Ω cm^2 and for the (311) an average value of 0.09 Ω cm^2 was found [2].

The value of the charge-transfer resistance was substantially affected by the conditions of cooling after annealing, i.e. whether cooling was conducted in O_2 or Ar, as is seen for the (100) face, Fig. 5.8. This drop in charge-transfer resistance, and corresponding increase in electron transfer rates, may be related to defects on the surface which decrease the metal-H bond adsorption energy, and are observable in STM topographical images of the two surfaces, which show the S_{II} structure to have wider, atomically flat, (100) domains, as reported by Clavilier et al.[42].

5.2.4 Analysis of the EIS fitting results

Each parameter in Eq. 4.42, along with the steady-state current *vs.* voltage measurements, was analysed as a function of potential using the kinetic model outlined above. By means of this quantitative analysis we are able to obtain the individual rate constants, the charge q_1 for full coverage of OPD H and the diffusion-layer length. First the rate constants k_1, k_{-1}, and k_3 were obtained by fitting the current-density, A, and B for each single-crystal surface[2]. Using these sets of rate constants the values of q_1 were determined by fitting parameter C as a function of potential. For self-consistency, parameter E was also fitted with this same set of rate constants and the measured diffusion

---

[2] For the (111), air-cooled (100), and (110) faces, no value of A could be determined: therefore k_1, k_{-1}, and k_3 were found by fitting only the current-density and parameter B. This situation unavoidably places a larger degree of error on the rate constants and q_1 values quoted for these faces.

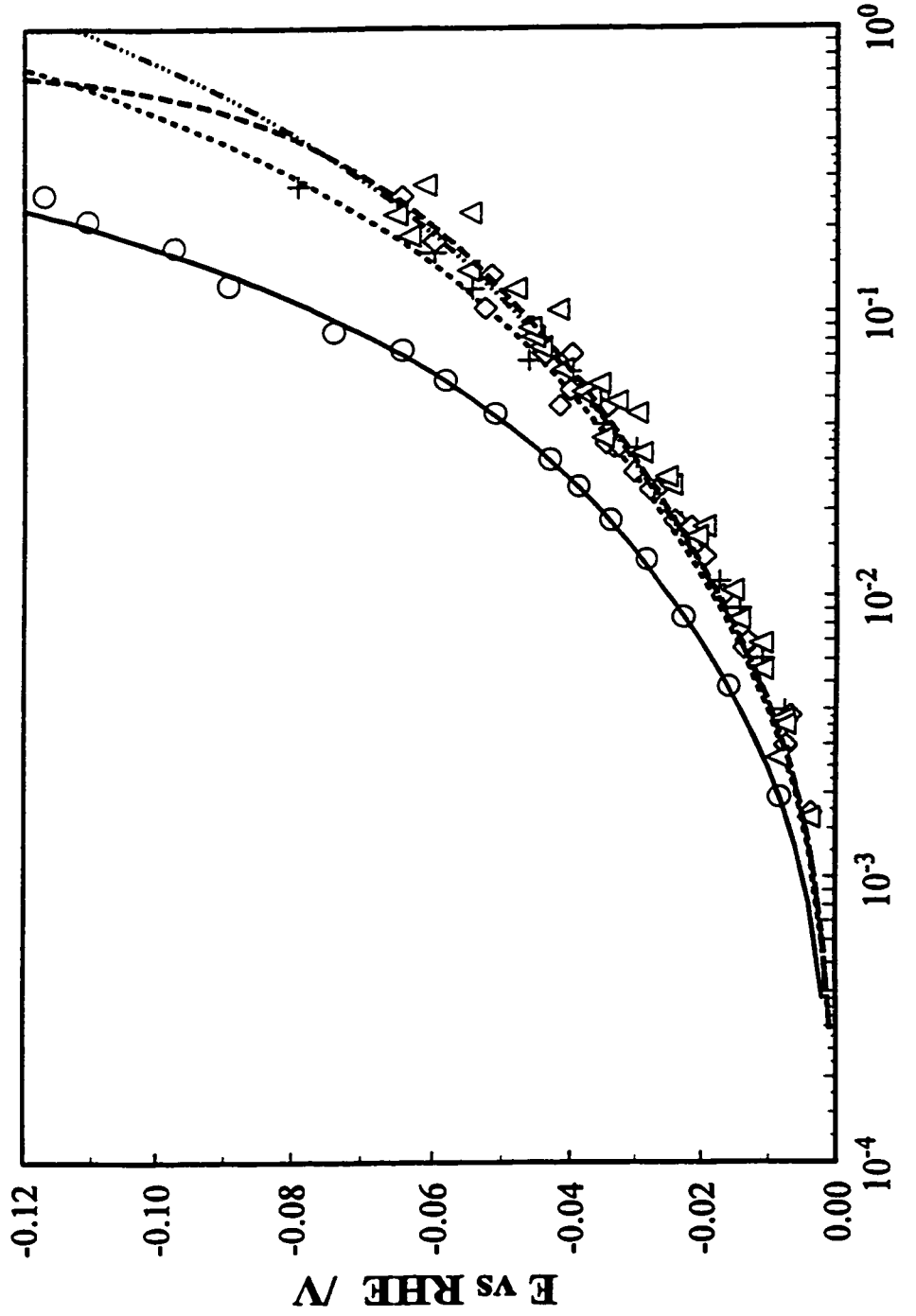

Fig. 5.9. Comparison of the potential dependence of the HER current-density for the (100)S_I ○, (19 11) +, (511) ◇, and (111) Δ faces in 0.5 mol dm^{-3} H_2SO_4, plus the best-fit lines calculated from the rate constants in Table 5.1.

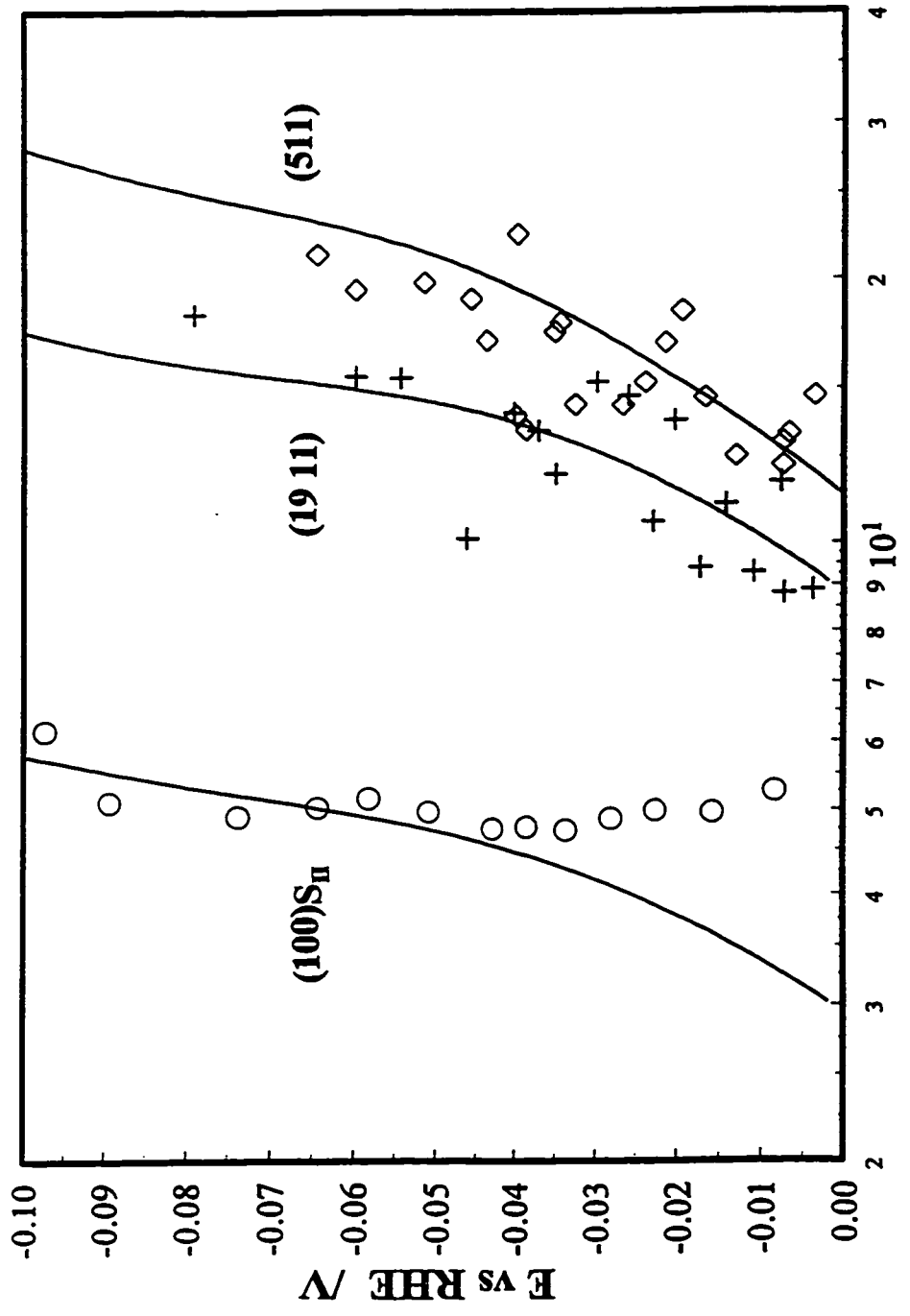

Fig. 5.10. Comparison of the potential dependence of the EIS parameter **A** for the (100)S_{II} (19 11) and the (511) faces, as indicated on the plot, plus the best-fit lines calculated from the rate constants in Table 5.1.

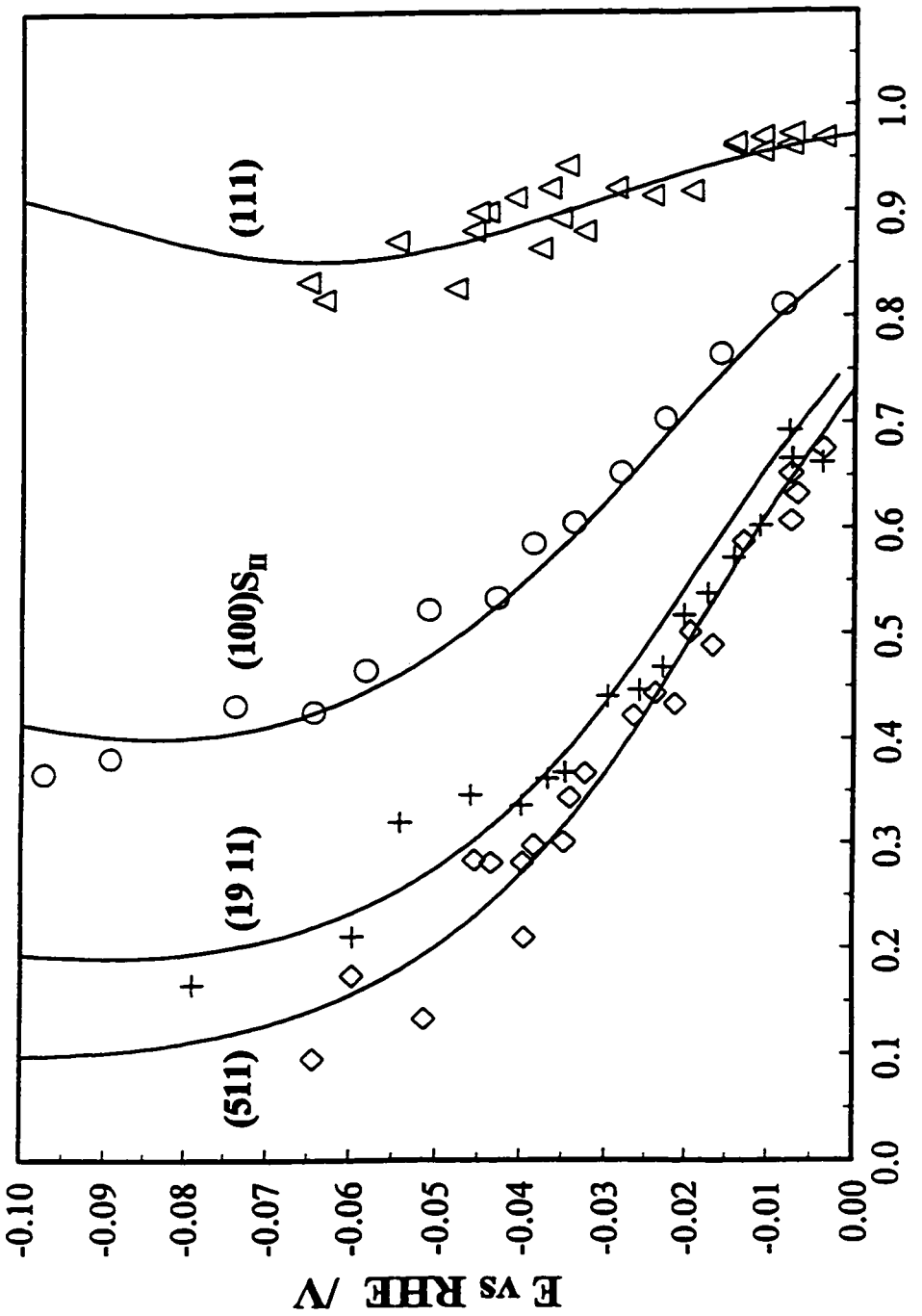

Fig. 5.11. Comparison of the potential dependence of the EIS parameter **B** for the (100)S_{II}, (19 11), (511) and (111) faces, as indicated on the plot, evolving H_2 in 0.5 mol dm^{-3} H_2SO_4, plus the best-fit lines calculated from the rate constants in Table 5.1.

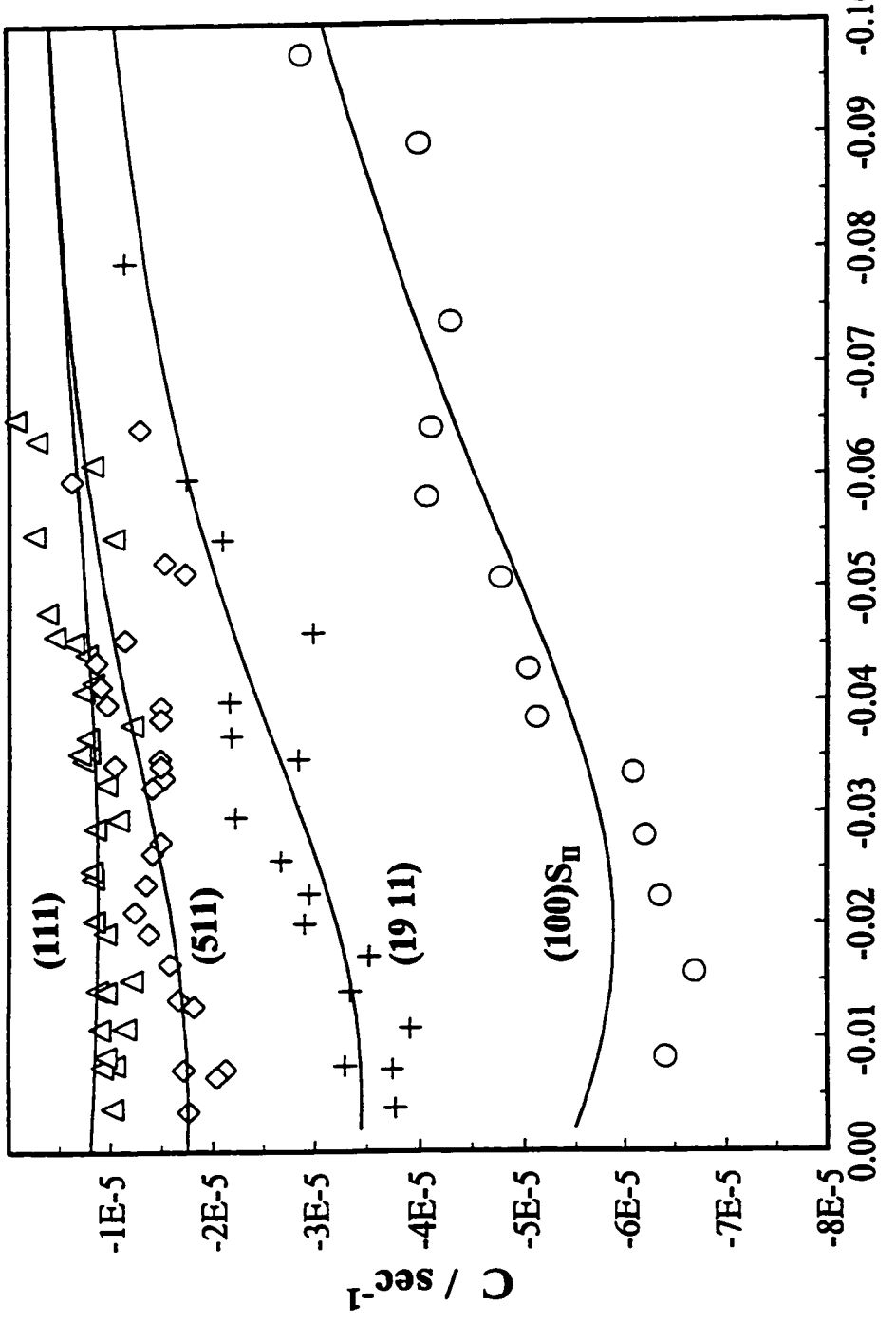

Fig. 5.12. Comparison of the potential dependence of the EIS parameter C for the (100)S_{II}, (19 11), (511) and (111) faces, as indicated on the plot, evolving H_2 in 0.5 mol dm^{-3} H_2SO_4, plus the best-fit lines calculated from the rate constants in Table 5.1.

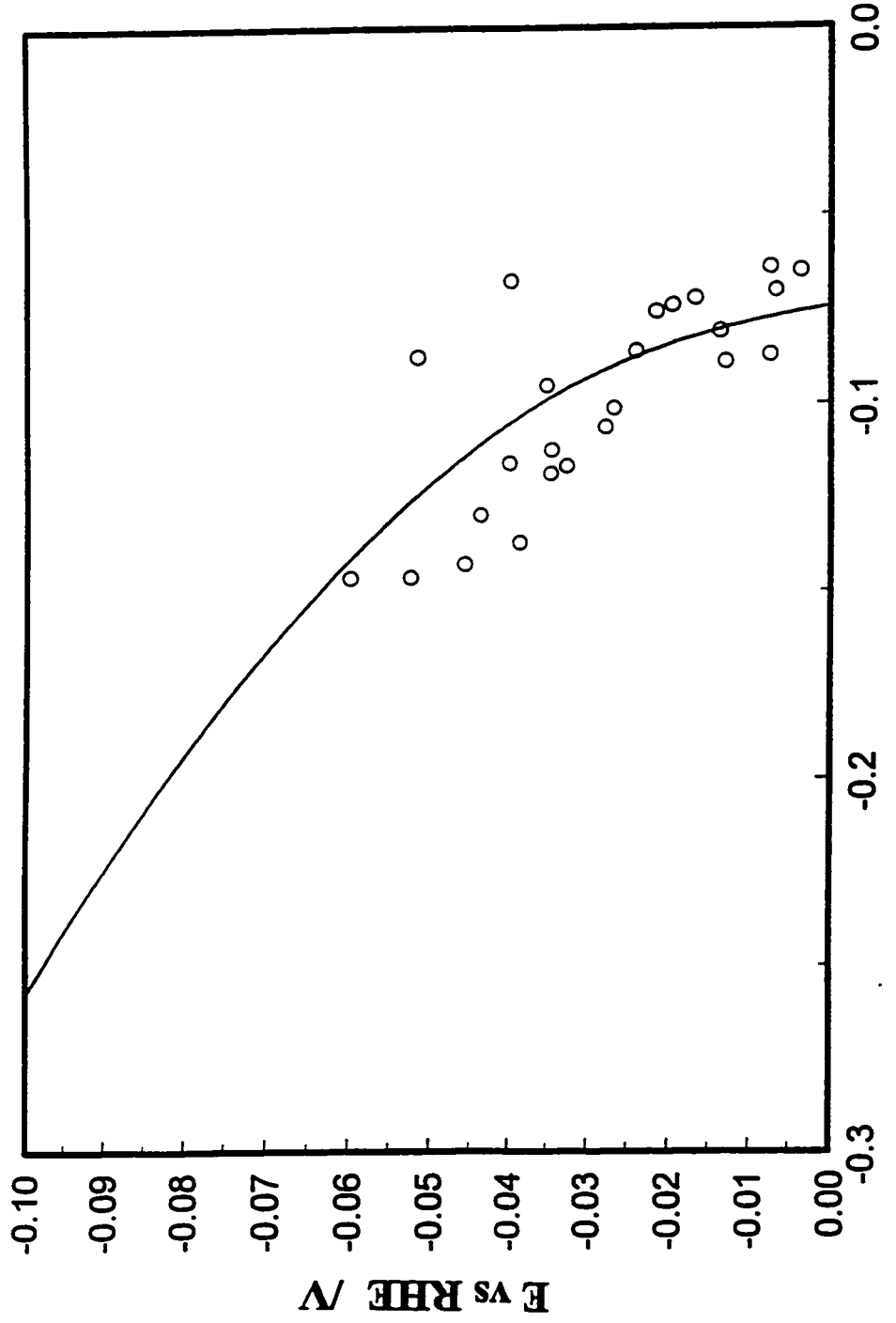

Fig. 5.13. Potential dependence of the EIS parameter **E** for the (511) face showing the best-fit line calculated using parameters in Table 5.1 and a diffusion layer thickness value calculated from the Levich relation.

coefficient to determine the diffusion length L. This value, in all cases, compared well with that calculated from the Levich relationship as is shown in Fig. 5.13. The plots of current-density, A, B, and C are shown in Figs. 5.9, 5.10, 5.11 and 5.12, respectively for the (100)S_{II}, (19 11), (511), and (111) faces. The best-fit curves shown in the above figures were generated using the values in Table 5.1 for the rate constants and q_1.

Table 5.1

orientation	1 x 10^5 k_1 /mol $s^{-1}cm^{-2}$	1 x 10^4 k_{-1}/mol $s^{-1}cm^{-2}$	1 x 10^5 k_3 /mol $s^{-1}cm^{-2}$	1 x 10^4 q_1 (OPD)/C cm^{-2}	1 x 10^4 q_1(UPD)/C cm^{-2}
(100) S_{II}	0.087 ± 0.002	0.077 ± 0.004	0.31 ± 0.02	0.52 ± 0.01	1.97
(100) S_I	1.3 ± 0.3	0.88 ± 0.1	1.1 ± 0.3	0.74 ± 0.04	1.81
(19 11)	0.26 ± 0.01	0.24 ± 0.03	1.9 ± 0.4	1.15 ± 0.04	N/A
(511)	0.32 ± 0.04	0.51 ± 0.1	7.9 ± 4	1.25 ± 0.04	N/A
(111)	4.6 ± 1	1.4 ± 1	0.39 ± 0.2	1.5 ± 0.5	1.61
(110)*	6	1	9	N/A	1.43

* Values estimated from HER kinetics measured in 0.5 mol dm^{-3} NaOH.

The relationship between B and the potential is governed by the ratios of the rate constants k_1 , k_{-1}, and k_3 and is not dependent on their absolute values. The smaller the ratio k_1/k_{-1}, the smaller are the values of B. For the (511) surface, $k_1/k_{-1} = 6.3 \times 10^{-2}$ and for the (111) surface $k_1/k_{-1} = 2.0 \times 10^{-1}$ which is a significant difference as seen in Fig. 5.11.

For the (100)S_{II} surface a mostly satisfactory fit between the EIS parameters and current-density is found at all potentials shown in Figs. 5.9, 5.10, 5.11 and 5.12, yet at more negative overpotentials deviations between the simulation and experimental data

occur. These deviations are directly linked to the simplifications made in deriving the impedance behaviour of the proposed model, i.e. exclusion of the electrochemical desorption (Heyrovsky) step. Deviations from the model due to exclusion of the electrochemical desorption process were only observed for the (100)S_{II} face because, for this face, as was stated earlier, data can be obtained at much larger (more negative) overpotentials than for the other faces. At these relatively high overpotentials the Heyrovsky step then becomes a competing pathway with the recombination (Tafel) step, due to its exponential dependency on overpotential (compare eqs. 5.2 and 5.3).

In order to obtain an estimate for the rate of this step, complex nonlinear least squares fittings were performed on several individual impedance spectra using the full impedance equation 4.40 in equation 4.43, with only k_2 as a free variable. The other fixed parameters (k_1, k_{-1}, k_3 and q_1 (OPD)) were taken from Table 5.1. The estimate of k_2 is 1 ($\pm$ 5) x 10^{-8} mol cm^{-2} s^{-1}. Comparing this value with those in Table 5.1 for the (100)S_{II} face we see that it is two orders of magnitude less that k_3, 3.1 x 10^{-6} mol cm^{-2} s^{-1} showing that the Heyrovsky pathway does not contribute appreciably to the current-density except beyond η = - 100 mV.

From the EIS and steady-state data it was not possible to obtain estimates of the kinetic rate constants for the (110) face and the (poly) surface because of the domination of the overall rate by the H_2 diffusion process (cf. Fig. 5.7). Attempts were made to slow down the electrode kinetics by a temperature reduction but little if any difference was seen between the results at 0 and 25 °C. By comparative extrapolation from experiments conducted in 0.5 mol dm^{-3} NaOH we were able to estimate the orders of magnitude of the

rate constants for the (110) and (poly) surfaces. The estimated values for the (110) face are shown in Table 5.1. We see that the estimated rate constants for the (110) face show that the rates for the electrosorption (Volmer) step and the chemical recombination (Tafel) step will both be large, unlike the other faces where the rate constant of one step is smaller than that of the other step, e.g. at Pt(511) the electrosorption rate constant k_1 is significantly smaller than k_3, the rate constant for recombination, while for the (111) k_3 is significantly smaller than k_1.

The q_1 values, taking the charge for a full monolayer as 210 $\mu C\ cm^{-2}$, correspond to OPD H surface coverages of about 25, 55, 60 and 71% for the (100)S_{II}, (19 11), (511), and (111) faces, respectively. Note that these q_1 values represent charge (for OPD H) *additional to* that for the UPD H already accommodated on the surface lattices below the hydrogen reversible potential. It can now be seen that these OPD H coverages (charges) are relatively small compared to those previously reported in the literature [4,9] and could probably be accommodated on the surface without having to invoke (cf. refs. 4, 9) the formation of a subsurface hydride layer or sorbed H. How then can we account for these significant differences in q_1(OPD) values? Firstly, looking at the q_1(UPD) data quoted by Clavilier et al. [32] given in Table 5.1, it can be seen that the (100)S_{II} face has the highest q_1(UPD) charge and (111) the lowest due to a larger amount of coadsorbed HSO_4^- present on the (111) surface [32]. Secondly, the fact that the (111) face has twice the number of hollow sites as the (100) indicates that at full UPD H occupancy the (111) face would

have half of its hollow sites[3] vacant while the (100) face would have almost all of its hollow sites filled. The OPD species may then fill the remaining hole sites, enabling a much larger q_1(OPD) charge to be realized for the (111) than for the (100) face. The alternative explanation, with the on-top site active for OPD of H, can equally well explain our findings but, no matter which interpretation is correct, the q_1 values will not be affected, and there is a definite increase in the amount of OPD H formed with increasing (111) character of the surface plane.

A further possibility is that the extra OPD H beyond the "monolayer" of UPD H, is accommodated in a new *communal* non-commensurate lattice arrangement. While the formal chemical identities of UPD and OPD H are, of course, the same, their electronic, bonding and coordination relations on the surface lattice must be different once nominal full coverage, "$\theta_H = 1$," is exceeded.

Another aspect in which the UPD H can affect the amount or bonding energy of the OPD H is the location of the UPD H species with respect to the image plane of the metal surface. Adsorbed H species outside the image plane will be expected to lead to a negative shift in the work function while species buried beneath the image plane will produce a positive shift in the work function [43]. The more open structure of the (100) surface will allow the UPD H species to penetrate into the surface more so than on the (111) plane, producing a greater shift in the work function. The (110) surface which possesses adsorption sites both above and below the image plane will most likely give

---

[3] Note that on the (111) face the trigonal holes are of different kinds: those with and those without an immediately underlying metal atom of the 3-d structure.

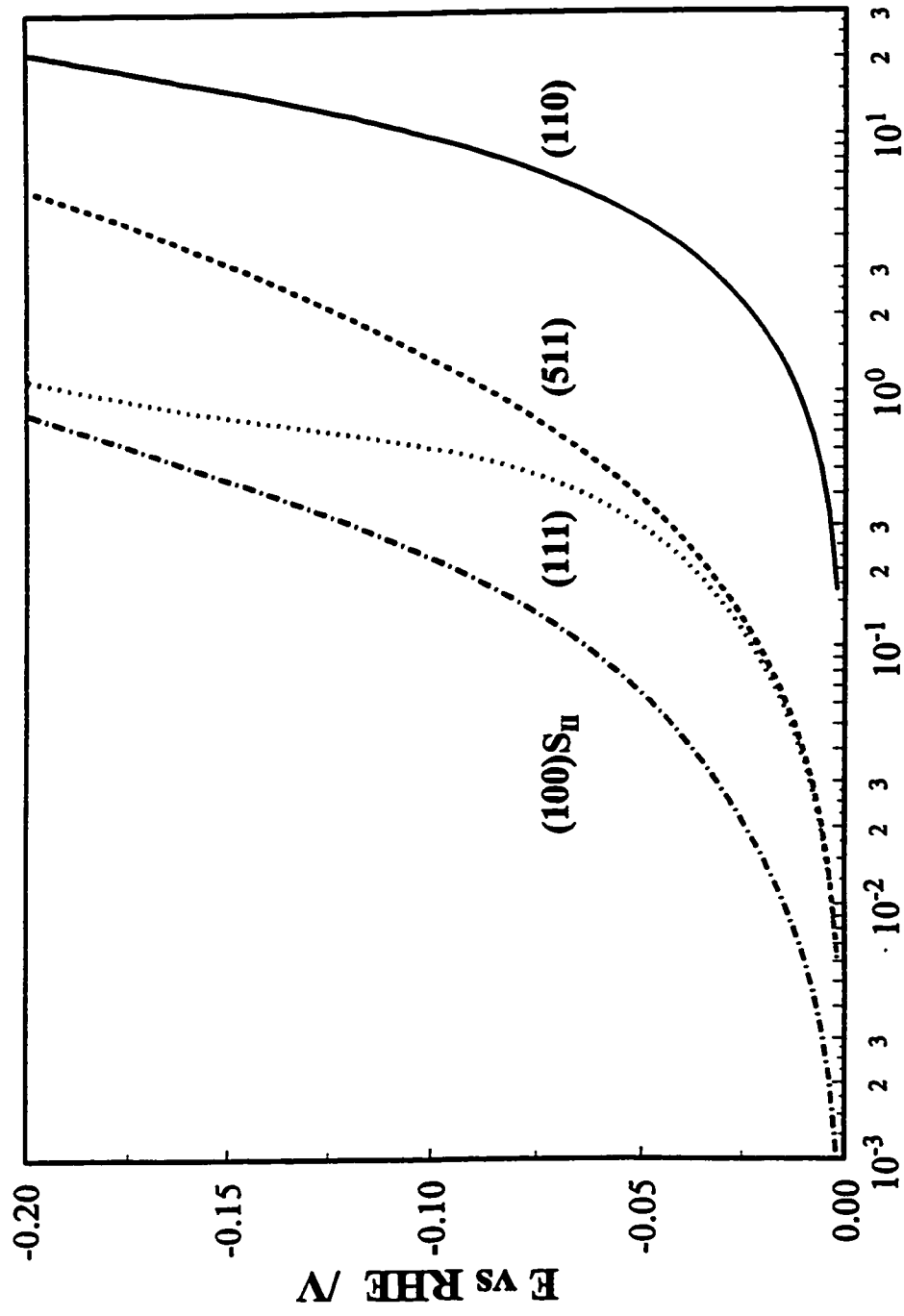

Fig. 5.14. Simulated Tafel plots of the HER at Pt(hkl) electrodes in 0.5 mol dm^{-3} H_2SO_4, less the diffusion contribution, for the faces (100)S_{II}, (511), (111) and (110) faces as marked on the plot.

positive or negative shifts in the work function depending on which adsorption sites are filled, in turn depending on the coverage. Of course other considerations must also be made when discussing the H-induced work function change such as: the extent of electron donation from the metal to the H^+ during the adsorption process which will be a factor determining the surface dipole moment of the adsorbed H complexes; and the effect on the work function arising from the adsorption of the OPD H species.

From the present results it can be stated that the (110) plane appears to have the most favourable work function value, i.e. a value which gives a standard Gibbs energy of adsorption (for OPD H) closest to zero, (i.e. for the top of the volcano curve) in combination with a large number density of adsorption sites for the H intermediate while the $(100)S_{II}$ face, exhibiting the lowest rates, likely has a combination of fewer adsorption sites per cm^{-2} for the OPD of H and a work function value able to produce a stronger M-H bond in the HER region.

It should be mentioned that the extent of prior "full coverage" by UPD H in relation to the onset of deposition of the OPD H intermediate in the H_2 formation reaction is not an absolute or fixed quantity in the sense that the H_2 reversible potential could be made more negative at H_2 pressures greater than the standard value, or in the opposite direction for lower $p(H_2)$. Then it could be expected that larger UPD coverages might be attained up to the H_2 reversible potential if experiments could be conducted up to, say, $p(H_2) \approx 100$ or 1000 atm. On the other hand, similar changes of the HER reversible potential could also be achieved at pH's less than the standard value; however, then reversible potentials for all UPD coverage values would be similarly shifted, so the relation

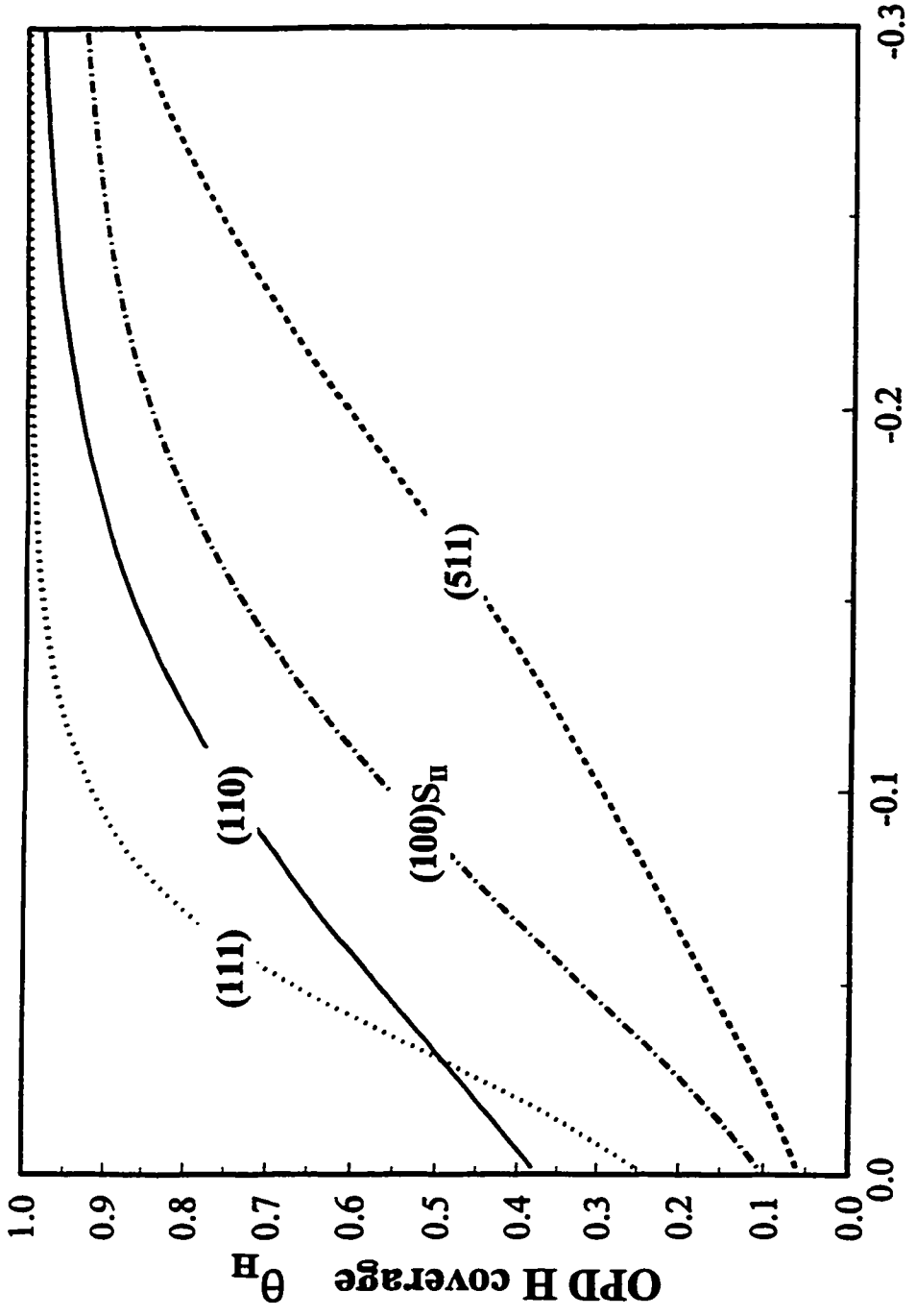

Fig. 5.15. The OPD H coverage *vs.* overpotential calculated from rate constants in Table 5.1. Note that although the coverage on each face approaches 1, the value of q_1 corresponding to the charge to obtain $\theta_H = 1$ is significantly different for each face.

between full UPD H coverage and onset of the OPD of H would be unaffected by pH.

From the derived rate constants given in Table 5.1 we are able to generate Tafel plots depicting the electrode kinetic (H_2 diffusion component removed) behaviour of each face towards the HER This is shown in Fig. 5.14 for the three low-index planes plus the (511) surface. Comparing the kinetics at the (111) and (100)S_{II} faces it is seen that the main difference lie in the values of k_1 and k_{-1} whereas k_3 values are quite similar. These differences are well illustrated in Fig. 5.14 where at low overpotentials, i.e. 0 to -100mV, large differences in the rates are found while at high overpotentials, -100 to -200mV, the rates approach each other as the recombination step becomes rate controlling as θ_H(OPD) $\Rightarrow$ 1, as is shown in Fig. 5.15. It is also of interest to compare the Tafel plots for the (111), (511), and (110) faces, where the effect of k_3 in determining the reaction rates can be clearly seen. The influence of a large recombination (Tafel) rate for the (511) face allows θ_H (OPD) to remain low (Fig. 5.15), which results in a greater rate of the electrosorption step (Volmer); see Eq. 5.1. This situation is exemplified in Fig. 5.14 for the (111) and (511) faces which have identical rates at the lower overpotentials, i.e. 0 to -25 mV, while the Volmer rate constant k_1 is an order of magnitude larger for the (111) plane. Again the influence of k_3 is seen when comparing the (111) and (110) which have similar values for k_1 and k_{-1}, yet the current-density at the (110) is over an order of magnitude larger, as is k_3, than that at the (111).

Finally, it can be unequivocally stated that the electrode kinetics of cathodic H_2 evolution are diverse for the faces studied, and both the rates of the Volmer and Tafel steps, as well as the ratios of the rate constants, are sensitive to surface structure.

---

* An extended discussion of the above points, with reference to *in situ* spectroscopic studies is presented in appendix (5-A) at the end of this chapter.

5.3. Interm conclusions for HER at Pt(hkl) electrodes in 0.5 M H_2SO_4

The most significant general conclusion from this work is that the derived values of the rate constants for the HER at various Pt surfaces show that the electrode kinetics of cathodic H_2 evolution are clearly a function of surface geometry, contrary to the conclusions of some earlier works [9, 10], where this dependence was, it now seems, obscured by the H_2 diffusion effect. Such new conclusions are now consistent with the previously well known major dependence of HER kinetics on the chemical nature of the cathode metal through its chemisorption properties. Although differences in the kinetics can be seen by steady-state polarization methods, it is shown that a quantitative analysis of the *electrode kinetics* can only be accomplished with the use of a complementary technique (EIS, potential relaxation), which allows the diffusional component of the overall rate to be accounted for and factored out. The Volmer step rate constants, k_1 and k_{-1}, increase with increasing (111) character, i.e. $(100)S_{II} < (19\ 11) < (511) < (111)$, of the surface structure. This concurs with the kinetic results found in our previous work on the UPD of H at the (100) and (311) surfaces [2]. For the Tafel step, the largest measured value of k_3 is found for the (511) face. We can speculate that this is due to the atomic "roughness" (terraced nature) of the surface, allowing more favourable interactions for the adsorbed H species to reside at step sites. Apart from this atomic roughness effect, two major influences of the surface geometry are to be noted; 1) differences in ΔH_{ads} for overpotential deposition of H; this is a function of the adsorption site which can be electronically different (work function and d-orbital emergence [23]) for the different faces, e.g. the (100) face has four-fold hollow sites and the on-top sites, whereas the (111)

face has the octahedral and tetrahedral three-fold hollow sites and the on-top sites ; and 2) the number density and inter-atomic distance of nearest neighbouring sites active for OPD of H which increases the probability for H + H combination in the overall reaction kinetics.

5.4 HER at Pt(poly) in Weakly Acidic Solutions

5.4.1 Influences of reactant diffusion (H_3O^+) on the HER

In the course of the study of the HER at single-crystal Pt electrodes in acidic media, the question concerning the nature of the diffusing species was raised. This query is quickly answered when the differences in the current-density/potential behaviour for reactant and product diffusion are examined, see § 1.2.2, but the idea of using the methods we had developed in our laboratory to examine this phenomenon had sufficient merit to justify a preliminary investigation at polycrystalline Pt electrodes.

Other works in which this matter has been examined can be found in the literature [44-46] but there are few. Some of the studies have related local pH changes at the surface, which were experimentally measured, to the current-density/potential behaviour [44] whereas others have utilized transient techniques which supposedly avoid any local pH changes [46]. In the present investigation an approach similar to that used to treat H_2 diffusion away from the electrode will be used, i.e. the surface concentration of H_3O^+ will be determined using EIS and steady-state dc methods. In some of the previous studies [46,47] it was found that the HER kinetics could be evaluated in acidic solutions with concentrations down to 3.6×10^{-4} mol dm^{-3} without a supporting electrolyte. After many trials it was concluded that the impedance results were suffering on account of the large impedance between the working and reference electrode at these low concentrations so a

supporting electrolyte of 0.5 mol dm^{-3} Na_2SO_4 was used. The results for the HER at a polycrystalline Pt electrode, presented below, correspond only to the conditions where the electrolyte (0.5 mol dm^{-3} Na_2SO_4) was at a pH of three.

5.4.2 Data Treatment and Analysis

The HER kinetics, as before, follow the three-step Volmer, Heyrovsky and Tafel mechanism. In order to account for effects associated with mass transfer of H_3O^+ from the bulk of the electrolyte to the surface, a diffusion step is included as represented by:

$$(H_3O^+)^b \overset{J_{diff}}{\rightleftharpoons} (H_3O^+)^s \qquad \textbf{(5.V)}$$

Again a rotating disk electrode was used, therefore J_{diff} can be calculated from the Levich equation:

$$J_{diff} = 0.620 D^{2/3} \nu^{-1/6} \Omega^{1/2} (c^{b}_{H_3O^+} - c^{s}_{H_3O^+}) \qquad \textbf{(5.8)}$$

The constants have already been defined earlier. The surface concentration of H_3O^+ is also explicitly included into the equations for υ_1 and υ_2, with $f = F/RT$ as:

$$\upsilon_1 = k_1 (1-\theta) \left[\frac{c^{s}_{H_3O^+}}{c^{b}_{H_3O^+}}\right] \exp(-\beta\eta f) - k_{-1}\theta \exp((1-\beta)\eta f) \qquad \textbf{(5.9)}$$

and

$$\upsilon_2 = k_2 \theta \left[\frac{c^{s}_{H_3O^+}}{c^{b}_{H_3O^+}}\right] \exp(-\beta\eta f) - k_{-2}(1-\theta) \exp((1-\beta)\eta f) \qquad \textbf{(5.10)}$$

For the previous case where H_2 was diffusing away from the electrode, calculations using the steady-state condition were needed in order to solve for the values of $c^s(H_3O^+)$ and θ_H which allowed the mass-transport and electrode-kinetic parts of the overall rate to be

separated. In the present situation, where H_3O^+ diffuses to the electrode, a different track can be followed which simplifies the analysis but leads essentially to the same kind of results. Remembering from section 1.2.2.1 that reactant diffusion produces a limiting current-density (i_L), the surface concentration can be calculated from eq. 1.4a:

$$\frac{c^{s}_{H_3O^+}}{c^{b}_{H_3O^+}} = 1 - \frac{i}{i_L} \qquad (5.11)$$

since both i and i_L are determined experimentally. Using this ratio of concentrations, the overpotential due to this difference in concentration (concentration overpotential) is calculated as:

$$\eta_{conc} = \frac{RT}{nF} \ln\left[\frac{c^{s}_{H_3O^+}}{c^{b}_{H_3O^+}}\right] \qquad (5.12)$$

where R, T, n and F have their usual meanings. With this value, the mass-transfer effect is factored out by subtraction of the concentration overpotential (η_{conc}) from the measured potential (η_{exp}), giving the activation potential (η_{act}) that drives the surface electrochemistry.

At this point, the data can then be analysed in terms of the three-step HER process taking into account explicitly the H_3O^+ concentration, as was described in detail in § 1.2.3 and later in § 5.5.

5.4.3 EIS and steady-state measurements under the influence of H_3O^+ diffusion

The procedures used in this examination again employed steady-state dc and ac impedance measurements. The surface cleanliness was monitored by cyclic voltammetry over the potential range for UPD of H potential region. In section 1.3.1.2 the influence of H and anion adsorption on the shape of the voltammetry curves was discussed. While exploring the H_3O^+ diffusion effect, several different electrolytes of varying pH and

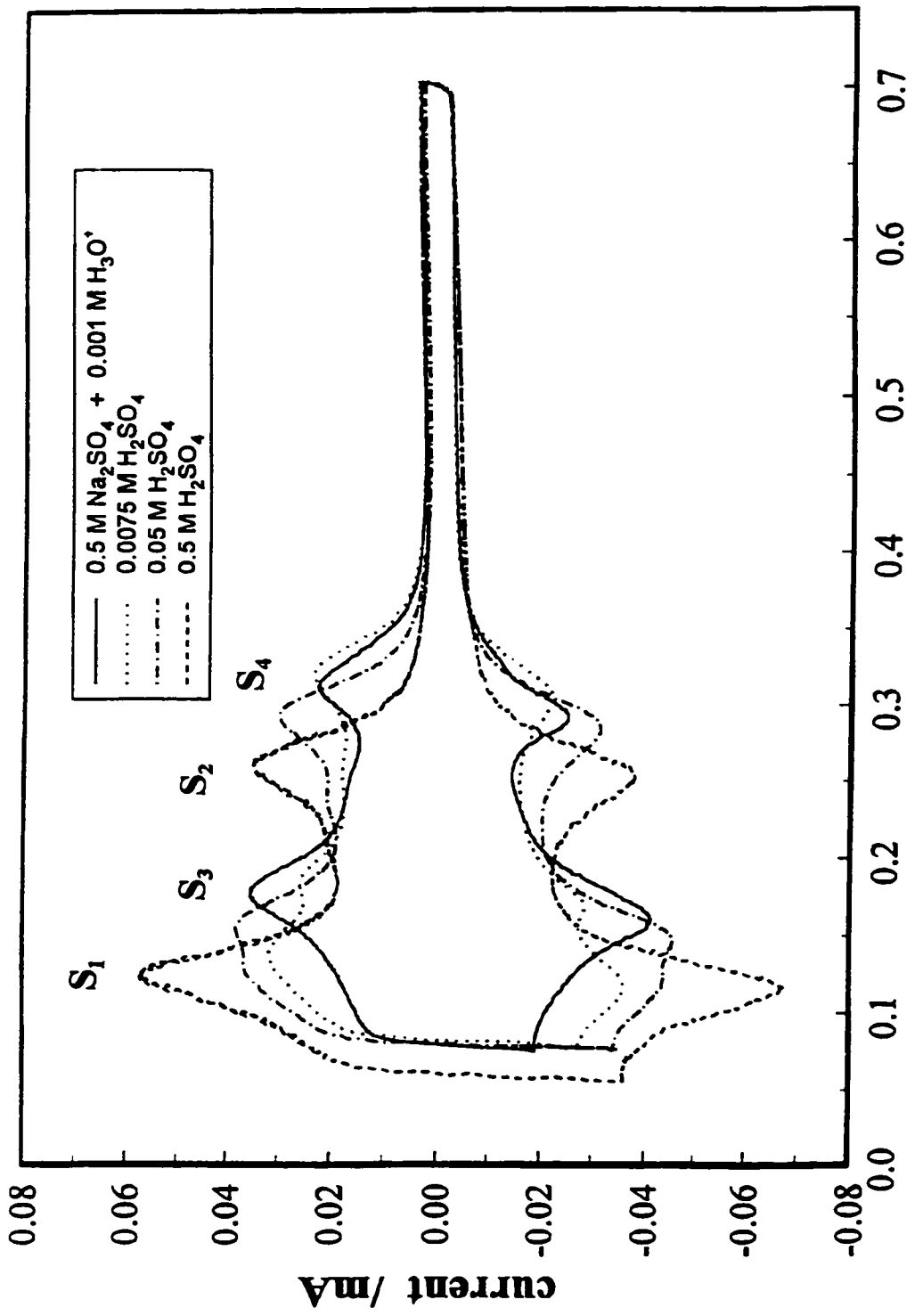

Fig. 5.16 Cyclic voltammograms of the UPD of H at polycrystalline Pt electrodes illustrating the effects of pH and sulphate concentration. Electrolyte concentrations given in caption; scan rate 50 mV s^{-1}.

sulphate concentrations were surveyed. The cyclic voltammograms of the UPD of H from each solution studied are shown in Fig. 5.16 Qualitatively, the shifting of the peaks and generation of new peaks are seen to be influenced by both pH and anion concentration. Of course more systematic studies focussed directly on this effect have been conducted [48], but the general features in Fig. 5.16 can be summed up as follows: as the pH and/or sulphate concentration decreases a new peak (S_3) is seen at the lower potentials and also (S_4) at the higher potentials. This is consistent with what is observed when the electrolyte is changed from 0.5 mol dm^{-3} H_2SO_4 and 0.5 mol dm^{-3} NaOH (compare Figs. 1.4 and 3.4 specifically for the (111) surface). Having ascertained that clean operating conditions had been achieved from the CV's, EIS measurements were conducted at a series of overpotentials. Between each EIS measurement the electrode was reactivated by cycling into the oxide region up to 1.4 V for a duration of 1 minute at 50 mV s^{-1}. This treatment lead to the solid-line CV over the H region in Fig. 5.16.

The EIS results plotted in the complex-plane are shown in Fig. 5.17 for several different overpotentials. The first, and most important aspect to note from this plot, is the direction in which the impedance shifts as a function of overpotential and current-density. Unlike that found for H_2 diffusion away from the electrode, the electron transfer and diffusion impedances *increase* with increasing overpotential and current-density. The second aspect is that only two dispersion processes are resolved, i.e. the high frequency process is that for electron transfer and the low frequency process is associated with the oscillation of the surface H_3O^+ concentration with potential. No dispersion region for H_2 diffusion, and no ac response for the adsorbed H intermediate, unlike what was observed

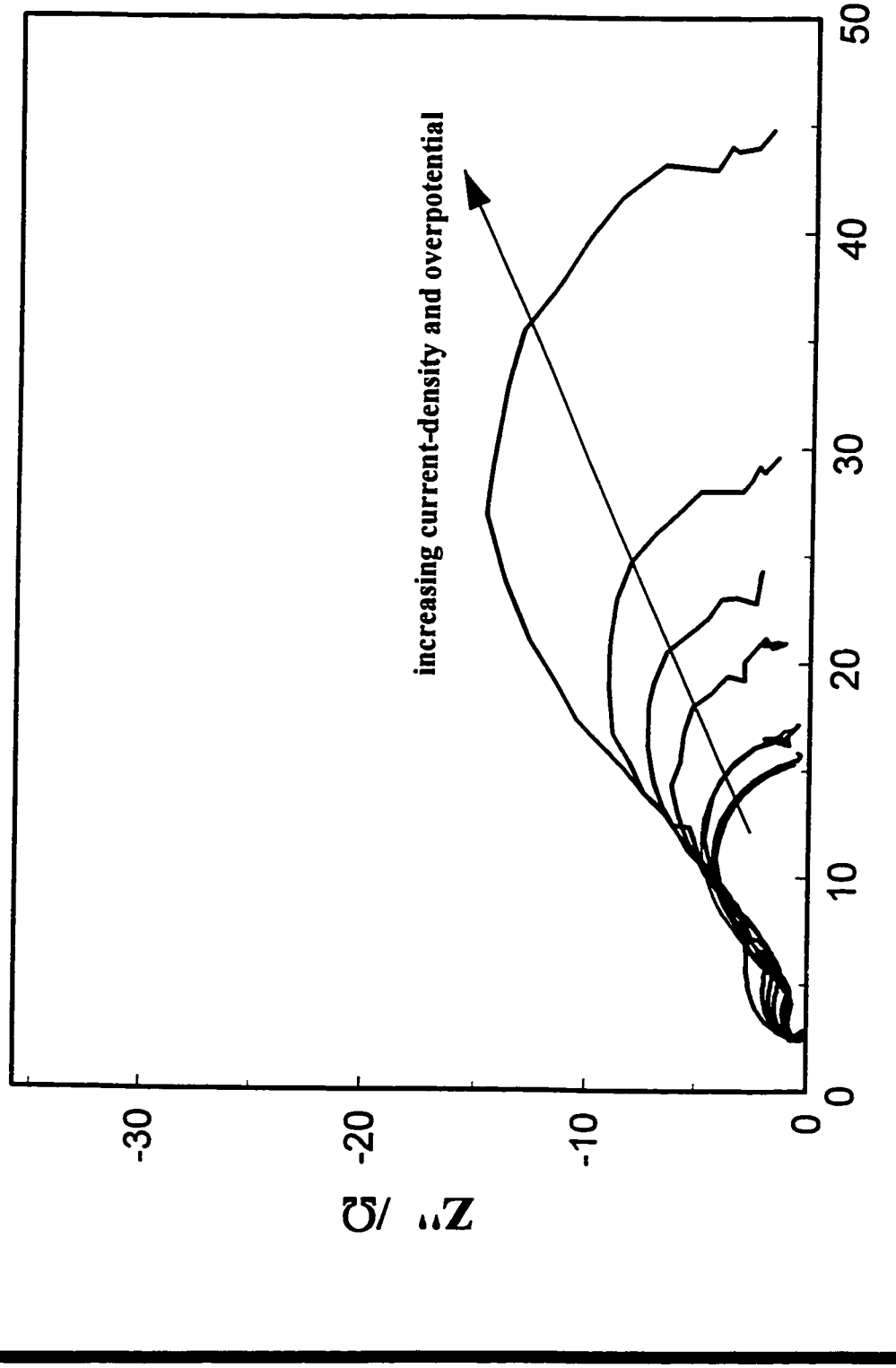

Fig. 5.17 Complex-plane plots of the HER at polycrystalline Pt in 0.5 mol dm^{-3} Na_2SO_4(pH=3) showing the effect of cathodic overpotential. Potential range: -10 mV to -100 mV *vs.* RHE; Rotation rate - 3500 rpm; Electrode area - 0.45 cm^{-2}.

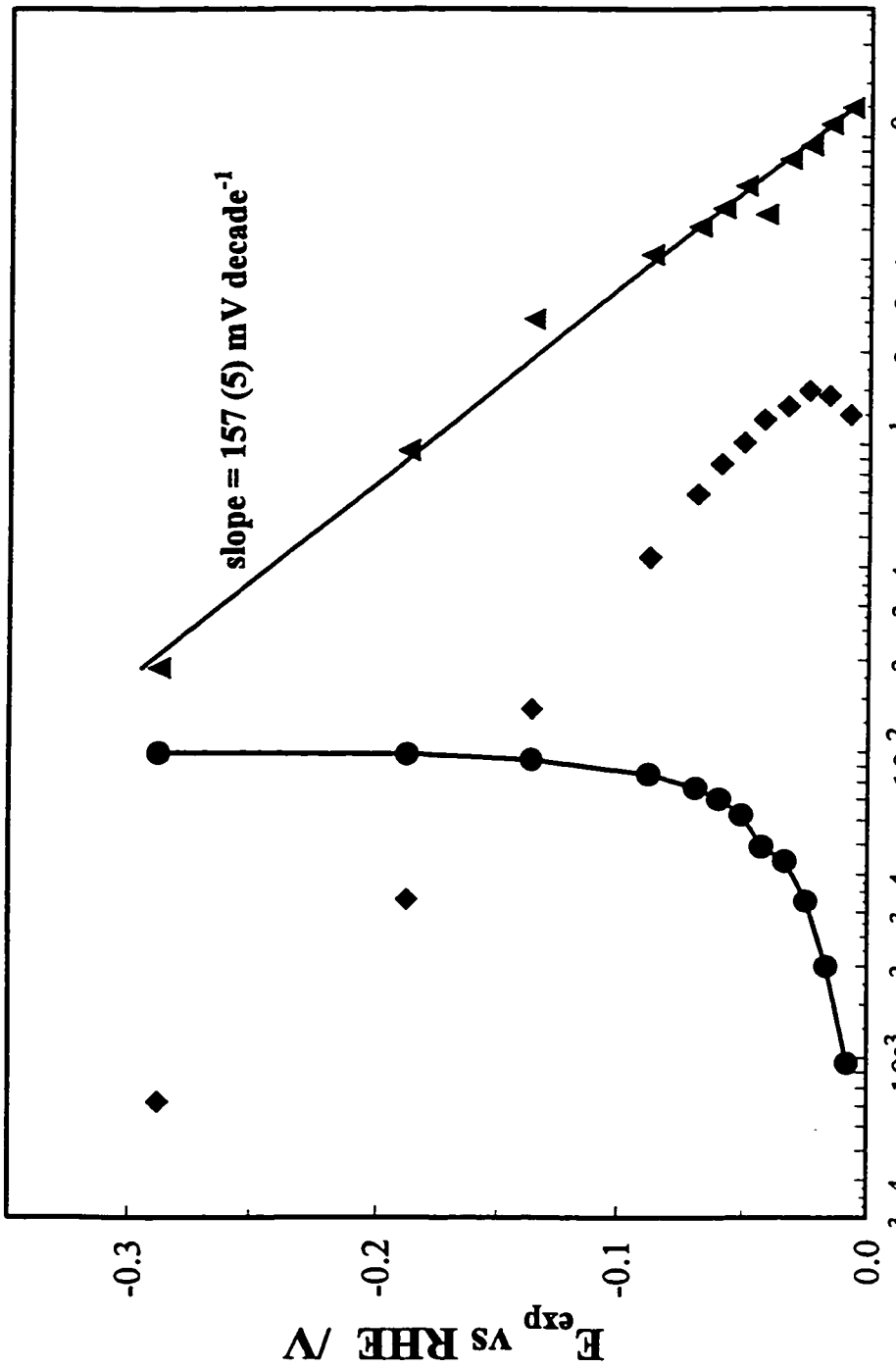

Fig. 5.18 Tafel type plot of current-density (●), R_w^{-1} (◆) and R_{ct}^{-1} (▲) *vs.* measured electrode potential. Electrolyte 0.001 mol dm^{-3} H_3O^+ + 0.5 mol dm^{-3} Na_2SO_4; rotation rate - 3500 rpm; slope for R_{ct}^{-1} curve = +157 mV decade^{-1}; Limiting current-density = 0.0099 A cm^{-2}.

in the EIS results of Pt(hkl) electrodes in acidic and basic electrolytes, see Figs. 5.4 - 5.7 and 5.22 - 5.23 respectively, arises in this case[4].

The increase in magnitude of the impedance may at first seem odd but if it is remembered that $Z = \Delta V/\Delta I$ then it is easily rationalized if the change in potential (ΔV) increases faster with increasing cathodic overpotential than does the change in current-density (ΔI). Another way of thinking about this is that the rate of electron transfer, for example in the Volmer step, decreases with increasing pH, so, as the potential is increased cathodically, the decrease in the rate constant caused by local surface pH change are greater than the increase in rate caused by the increase in the real activation overpotential.

Each curve in Fig. 5.17 was analysed by means of a modified version of eq. 4.22. Modifications are: $r_o = (\upsilon_1 + \upsilon_2)$; the $(j\omega D)^{1/2}$ term is replaced by $(j\omega D)^{1/2}$ coth $(j\omega/D)^{1/2}L$; and Ox ≡ H_3O^+ and Red ≡ H_2 = constant (species not diffusing). The results of this analysis yield two kinetic parameters $A(R_{ct}^{-1}) = F(\partial r_o/\partial E)$, which has already been defined, and R_W which is a generalized diffusion resistance proportional to $(\partial r_o/\partial E)$ and, after dropping the subscript, H_3O^+, $(\partial r_o/\partial c^*)$. These two parameters and the current-density are plotted as a function of potential in Fig. 5.18. As was shown theoretically in section 1.2.2.1, the Tafel curve goes rapidly to a diffusion-limited current-density as the overpotential is increased more cathodically. No region of activation control can be seen in Fig. 5.18; therefore the appropriate corrections must be made before any electrode-

---

[4]It maybe that the process providing coverage (θ_H) by H is overlapping with the diffusive impedance element, the impedance response of the two processes occur or the same frequency range, or it could be that the real activation potential (η_{act}) oscillates at a much lower amplitude than the effectively measured potential (*viz.* $\eta_{act} + \eta_{conc}$) leading to an extremely low response from θ_H which maynot be resolved.

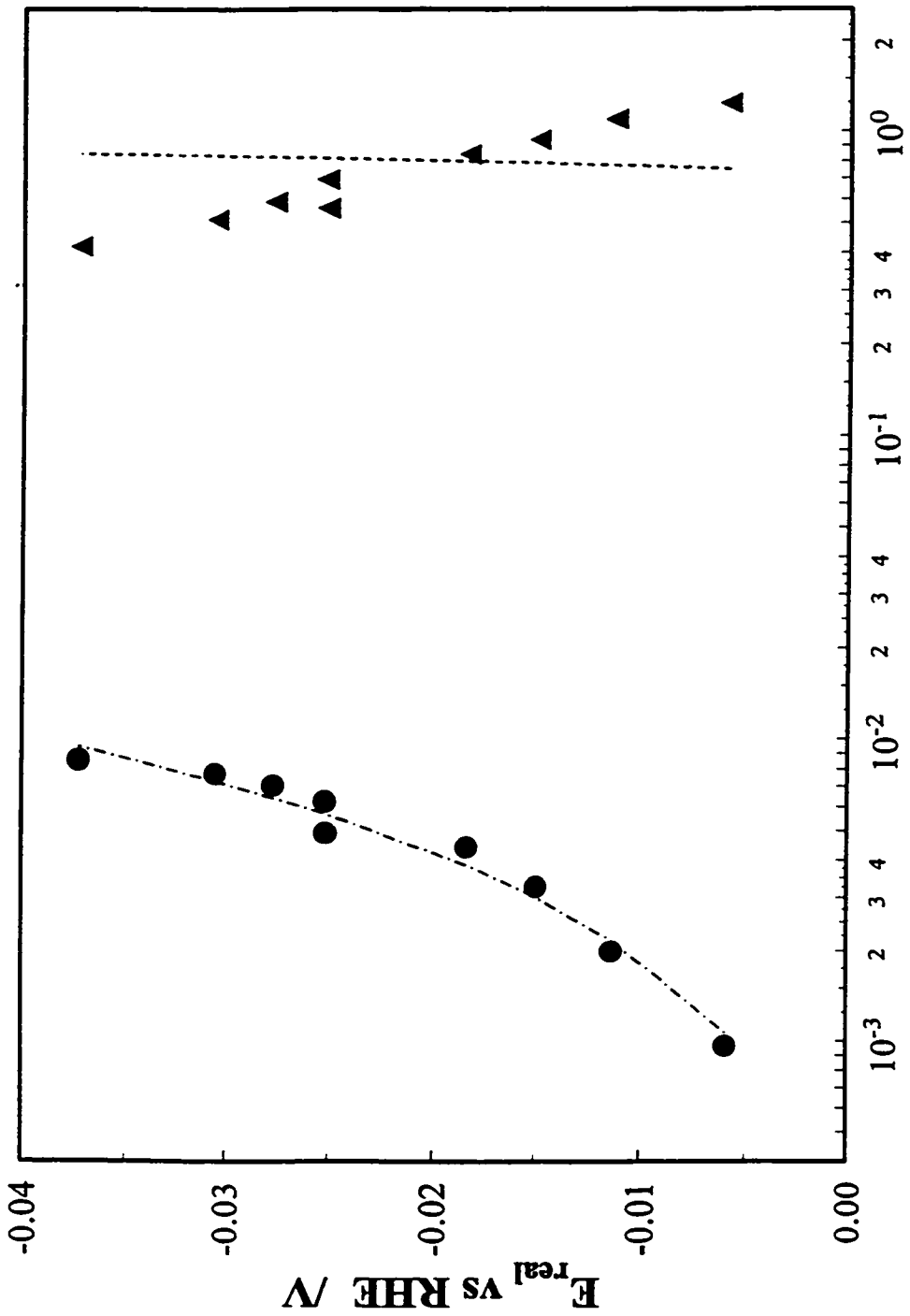

Fig. 5.19 A Tafel type plot of current-density and R_{ct}^{-1} *vs.* the activation overpotential($E_{measured}$ - $E_{concentration}$). Data calculated from Fig 5.18 following that in the text. Best fit lines to the HER model calculated from rate constants given in the text.

kinetic rate information can be obtained.

Consistent with the behaviour shown in Fig. 5.17, the values of R_{ct} and R_W decrease with increasing overpotential, the slope, dE/d log(R_{ct}), being 157 mV decade^{-1}. Since the latter slope for the simplest electron transfer reaction is equivalent to the Tafel slope, in the limiting case, $i = (\beta F/RT)(R_{ct}^{-1})$, the question arises how can this behaviour be accounted for, when the normal Tafel slope for a cathodic reaction is - 118 mV decade^{-1}? As was illustrated in section 1.2.3 the change in coverage of the intermediate with potential can cause the Tafel slope to become lowered from -118 mV decade^{-1} to values of -30 or -40 mV decade^{-1}. A similar term to that of d ln $\theta/d\eta$ for the variation of $c^s(H_3O^+)$ with potential can be entered into the generalized equation for the reciprocal Tafel slope yielding:

$$b^{-1} = \frac{d \ln \theta_H}{d\eta_{act}} - \frac{\beta F}{RT} + \frac{d \ln c^s_{H_3O^+}}{d\eta_{act}} + \frac{d \ln c^s_{H_3O^+}}{d\eta_{conc}} \qquad (5.13)$$

If the values for the two concentration terms are larger than $\beta F/RT$ then the Tafel slope will change from negative to positive values. Qualitatively this is an interesting way of looking at this slope but, since the measured slope is evaluated relative to the experimental potential (activation plus concentration potentials), it is quantitatively useless unless the relationship between η_{meas} and η_{act} is known.

As was shown in the previous section the concentration overpotential is corrected for using the ratio of i/i_L. Following the analysis outlined above, the activation-controlled current-density *vs.* potential relationship can be derived and is shown in Fig. 5.19. These results can then be analysed and the best fit lines values for the rate constants for the three HER steps obtained; see the lines in Fig. 5.19 which are generated from the set of rate-

constants: $k_1 = 2.5 \times 10^{-7}$ mol s^{-1} cm^{-2} , $k_{-1} = 8.6 \times 10^{-7}$ mol s^{-1} cm^{-2}, $k_2 = 1 \times 10^{-13}$ mol s^{-1} cm^{-2} and $k_3 = 2.8 \times 10^{-7}$ mol s^{-1} cm^{-2}.

Although, the current-density *vs.* potential behaviour is well represented by the model, discrepancies between the experimental and simulated R_{ct}^{-1} *vs.* potential behaviour are seen. They can be accounted for by the assumption, in our model, that the electrochemical discharge goes exclusively through the H_3O^+ species, whereas, in actual fact, the possibility of discharge of H_2O is great and the degree to which the two processes compete will be a function of potential and also pH. This can be understood knowing that the H_3O^+ concentration will decrease (at the interface) as the overpotential is increased, allowing a larger probability of discharge from H_2O. This is emphasized when the rate constants for the three different electrolytes are compared, i.e. for 0.5 mol dm^{-3} H_2SO_4, 0.001 mol dm^{-3} H_3O^+ + 0.5 mol dm^{-3} Na_2SO_4, and 0.5 mol dm^{-3} NaOH.

The rate constants obtained for the pH 3 solution are very close to those found for the alkaline solution and orders of magnitude different from those obtained in acidic media. This indicates that the majority of the current for the HER process passes via the H_2O discharge (alkaline solutions) type equations. If this is the case then how is the diffusion process to be rationalized since the diffusing species, if the above were the mechanism, would be OH^-, a product, which would not give the observed Tafel behaviour, see section 1.2.2.1. One explanation is that the OH^- is generated at the surface, through the alkaline HER process, and does not diffuse but is neutralized by H_3O^+ ions diffusing to the electrode surface, with this H_3O^+ species entering into the rate equations as a reactant, therefore giving the observed diffusion behaviour, i.e. a diffusion-limited current-density.

5.5 The HER at the Pt(hkl) Low-index Plane Electrodes in 0.5 mol dm^{-3} NaOH

5.5.1 Particularities of the experimental behaviour and the subsequent data analysis for the HER in 0.5 mol dm^{-3} NaOH

Unlike the behaviour described in the previous two major sections in this chapter, diffusion did not pose a problem in gathering or interpreting the HER data in the NaOH electrolyte. Experimental details of this section of the work are given in § 3.5. Data analysis followed the simple three-step HER mechanism, for which the electrode kinetics were derived in § 1.2.3. For this process the ac impedance model used in the following analysis follows that given in § 4.3.1 with one modification. It was found in the course of the data analysis that a much better fit of the EIS data could be achieved when the double-layer capacitance element was replaced with a constant-phase element (cpe) which is expressed as:

$$Y_{cpe} = (i\omega)^{\phi} T \qquad (5.14)$$

The total impedance is now calculated as:

$$Z_{tot} = (Y_f(HER_1) + Y_{cpe})^{-1} \qquad (5.15)$$

Although, the requirement for use of the cpe is usually associated with porosity of the working electrode [49], this cannot be the situation here; it was thought this may be related to current distribution in the meniscus, but the effect was also seen for an immersed polycrystalline electrode. The results from the analysis showed that the phase-angle was close to 90°; therefore whatever the process is its effect is small. It is unlikely also that the depression of the high frequency semicircle could have been due to the deactivation processes which arose to a limited extent as was discussed in the experimental section. The reason is that the cpe was required either when the steady-state

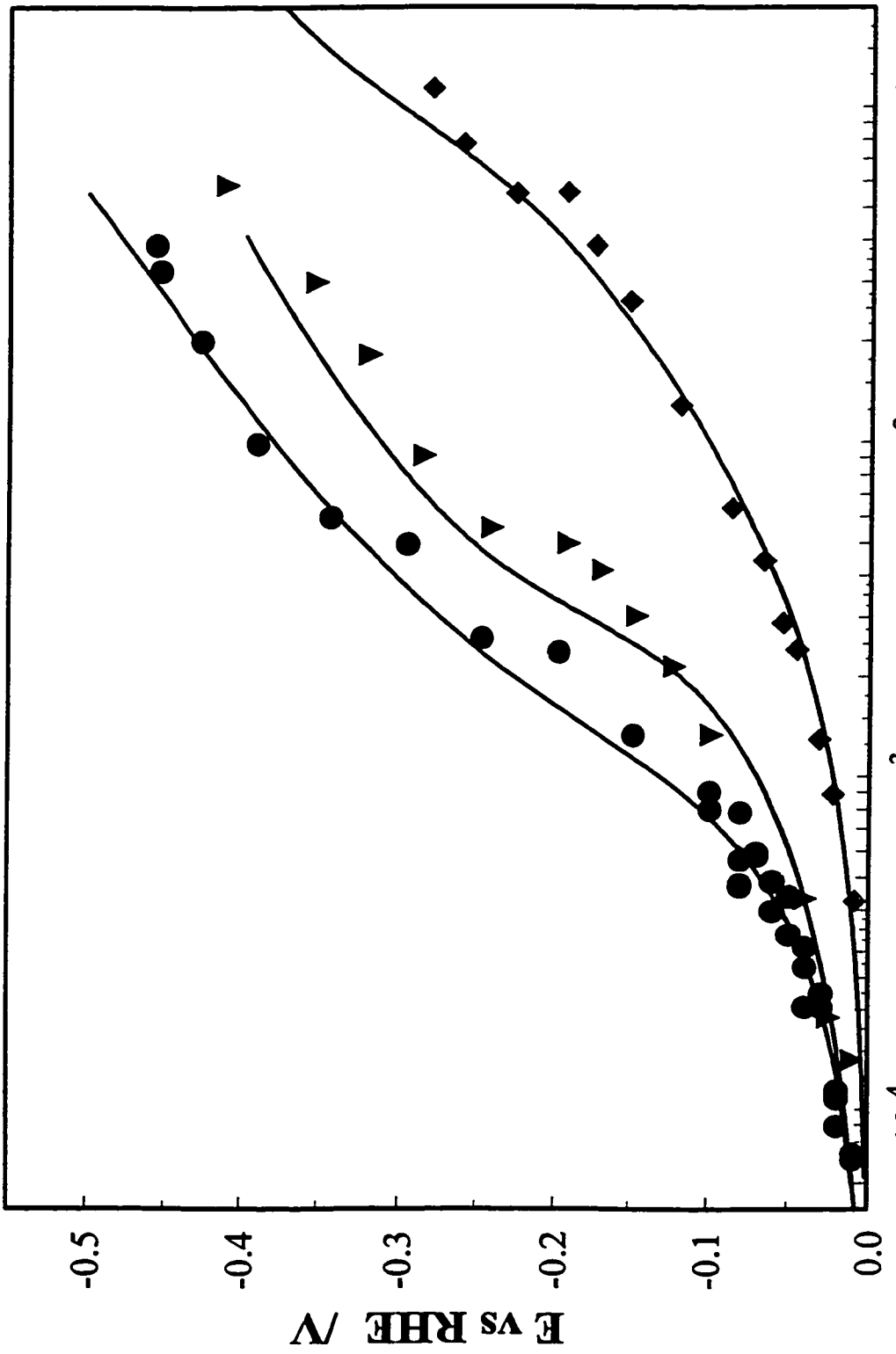

Fig. 5.20 Tafel plots for the HER at the three low-index planes of Pt, ● - (100), ▼ - (111) and ◆ - (110) in 0.5 mol dm^{-3} NaOH. Each point corresponds to one EIS measurement. Rotation rate 3000 rpm; best fit line calculated from the rate constants in Table 5.2.

current-density was slightly decreasing (as for Pt(100) at low η and (111)) or slightly increasing (as for Pt(110) and (100) at high η).

5.5.2 Results and Discussion of the HER kinetic results at the low-index planes of Pt(hkl)

In Fig. 5.20 the steady-state current-density *vs.* potential relationships are compared in Tafel plots. Each current-density/potential point in Fig. 5.20 corresponds to one ac impedance frequency scan, the results from this analysis being shown later. The lines in Fig. 5.20 are calculated from the values of the derived rate constants listed in Table 5.2, which were evaluated by means of simultaneous fitting of the current-density *vs.* potential and the A ($1/R_{ct}$) (see definition below eq. 4.28) *vs.* potential relationships.

Table 5.2 Rate constants for the HER derived from Tafel and impedance analysis as a function of Pt(hkl) surface geometry in 0.5 mol dm^{-3} NaOH

orientation	1×10^{8} k_1 /mol cm^{-2} s^{-1}	1×10^{7} k_{-1} /mol cm^{-2} s^{-1}	1×10^{10} k_2 /mol cm^{-2} s^{-1}	1×10^{7} k_3 /mol cm^{-2} s^{-1}	1×10^{4} q_H(OPD)/C cm^{-2}
(100)S_{II}	0.66 ± 0.07	0.195 ± 0.03	1.5 ± 0.2	0.07 ± 0.02	.3?
(111)	1.3 ± 0.2	7.0 ± 1	0.86 ± 0.1	0.15 ± 0.02	0.58
(110)	2.5 ± 0.2	2.9 ± 0.6	4.3 ± 8	4.9 ± 2	1.14 ± 0.2
(poly)*	1.0	3.0	2.0	2.8	0.7

* Result obtained from ref. 6.

The salient features of Fig. 5.20 are: 1) the order of kinetic reactivity; at all potentials it is seen that the (100) surface has the slowest HER kinetics, with an increase in rate on going to the (111) which is followed by a major jump in the current-density for the (110) face behaviour; 2) the shape of the curves; at low overpotentials, $\eta >$ *ca.*

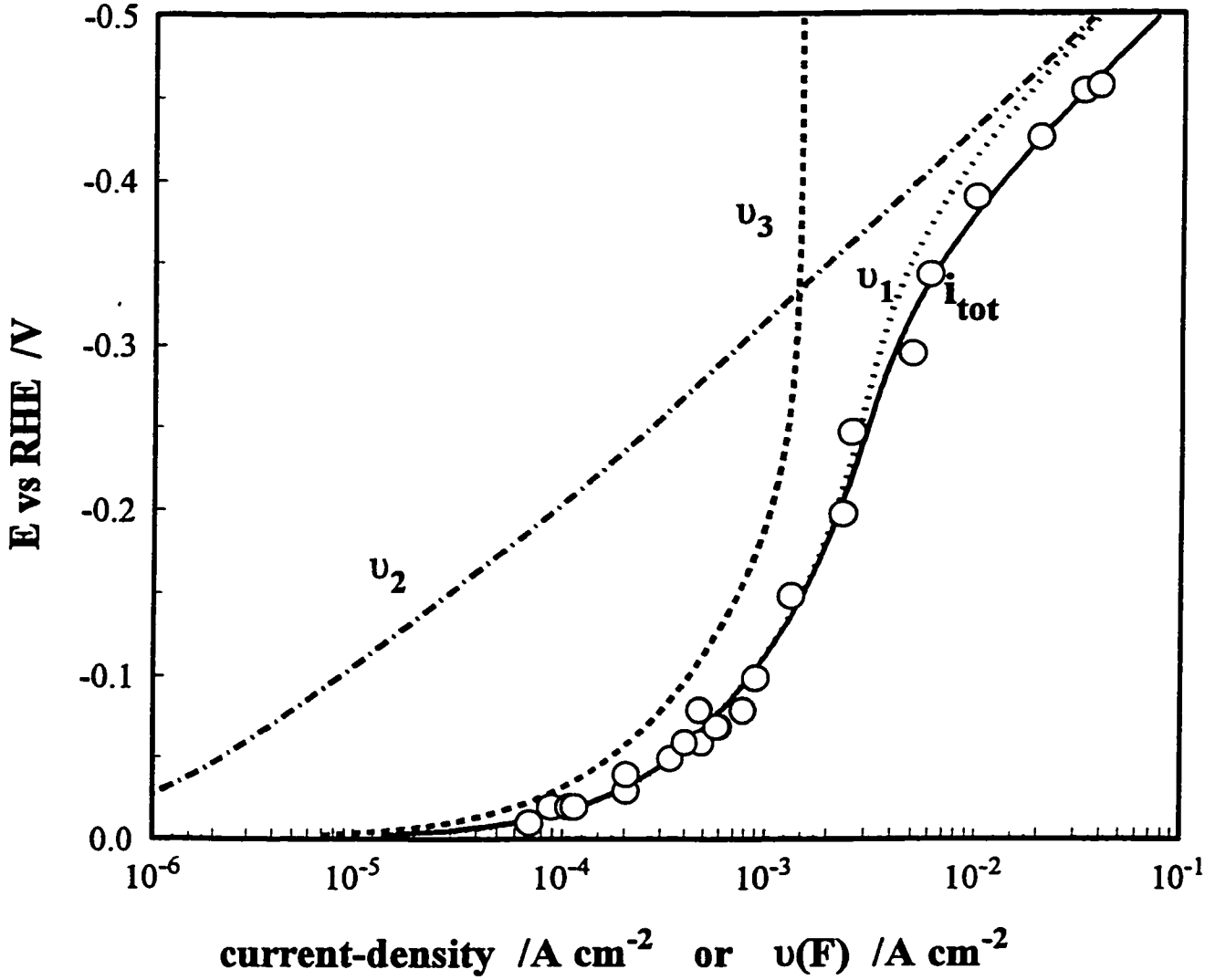

Fig. 5.21 A Tafel plot for the (100)S_{II} surface in 0.5 mol dm^{-3} NaOH as in Fig. 5.20, including the contributions of the three steps in units of current-density (A cm^{-2}).

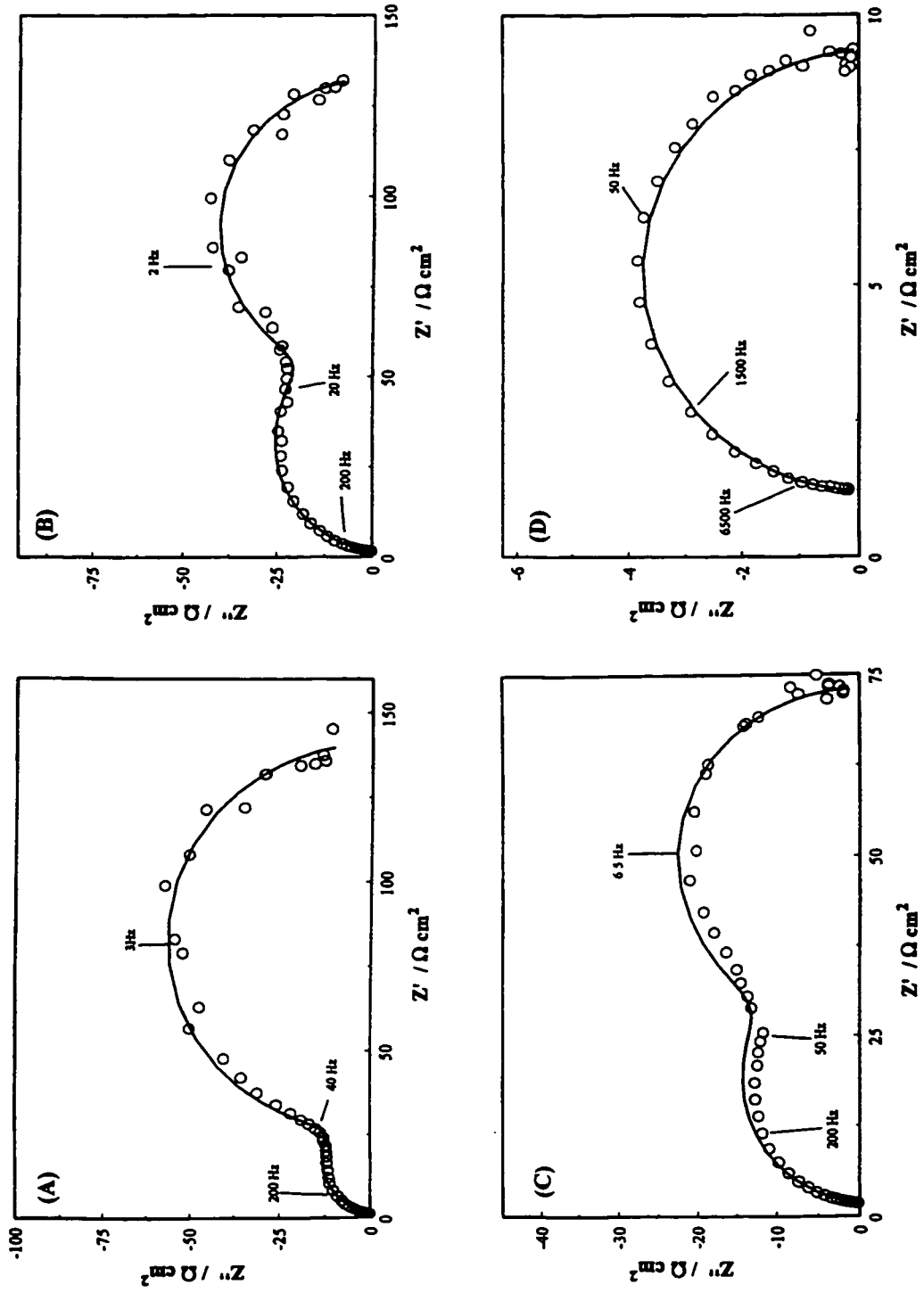

Fig. 5.22 Complex-plane plots of the EIS results for the (100) surface measured at four overpotentials; rotation rate 3000 rpm; frequency range covered 100 kHz to 0.1Hz. **A)** -30 mV *vs.* RHE; **B)** -60 mV *vs.* RHE; **C)** -100 mV *vs.* RHE and **D)** -400 mV *vs.* RHE.

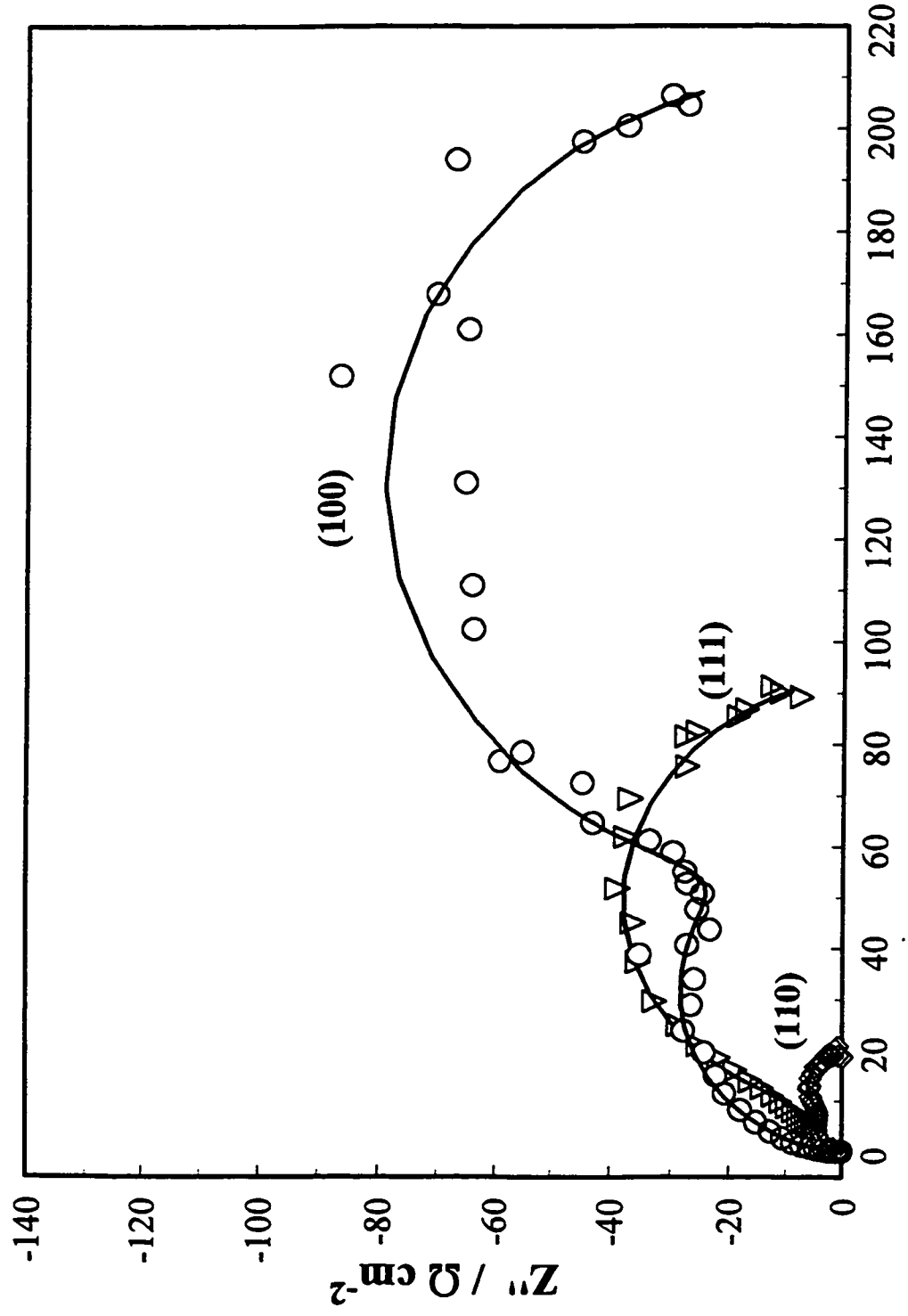

Fig. 5.23 A complex-plane plot comparing the EIS results for the three low-index planes at an overpotential of -40 ± 2 mV *vs.* RHE. Frequency range 100 kHz to 0.1 Hz; rotation rate 3000 rpm; indentification of Miller-indices is given on the plots.

-70 mV, a low Tafel slope, less than 60 mV decade^{-1}, is observed for all three planes. This is an indication of a potential dependence of the OPD H coverage in that region. As the potential is increased an inflection is seen, the Tafel slope beyond this inflection achieving values *greater* than -120 mV decade^{-1} (2.303 RT/βF for $\beta = 0.5$) which can be attributed to the chemical combination (Tafel) step becoming rate influencing, i.e. in this region the rates of the respective steps in the HER mechanism are in the order: $\upsilon_2 < \upsilon_3 < \upsilon_1$, see Fig. 5.21.

The potential range of this behaviour has a larger span for the Pt(100) and (111) planes than for the (110). After the potential is taken to even larger cathodic values a second inflection is seen. This is the transition from step III being rate-influencing to step II becoming rate-controlling[5], which is inevitable due to the different potential dependences of steps II and III. The potential dependence of the rate of step III arises from the potential dependence of θ_H alone as opposed to step II which has both the θ_H dependence and the Butler-Volmer charge-transfer term which enters the potential explicitly in the equation for the rate (compare eqs. 1.10 and 1.11). A summary of how each step behaves over the whole measured potential range is shown in Fig. 5.21 for the (100) face in relation to the total (i_{tot}) current-density.

Representative complex-plane plots showing the impedance data for the (100) face and the best fit curves to an Eq. 5.15 are shown in Figs. 5.22 a, b, c and d. The results for

---

[5] These types of inflections in the Tafel measurements have also been interpreted as resulting from the (actually unlikely) underpotential adsorption of the alkali metal ion [50] (here Na^+). In the present study the proposed three-step HER model represented the data very well so the process of metal ion underpotential deposition was not considered.

the other faces, Pt(111) and (110) showed features similar to those seen for Pt (100) in Fig. 5.22, yet the magnitudes were different.

The impedance spectra for all of the single-crystal surfaces studied consisted of the following components: i) a higher-frequency process assignable to electron transfer relaxing through the double-layer capacitance and ii) a lower-frequency component associated with the modulation of the OPD H coverage, θ_H, with the potential oscillation. At low overpotentials, both dispersion processes are resolved (Fig. 5.22 a, b and c) and at higher overpotentials (surface-dependent) only the high-frequency process is seen (Fig. 5.22d). The decrease and eventual disappearance of the second dispersion process (the semicircle at higher real impedances (Z') on the complex-plane plot), indicates that, at higher overpotentials, the coverage of OPD H is reaching a constant value, in the present case, its saturation limit, i.e. θ_H (OPD) $\rightarrow$ 1.

A comparison of the EIS data, plotted in the complex-plane, for the three low-index faces is given Fig. 5.23 for a constant overpotential of approximately -40 mV *vs.* RHE. It should be noted that the charge-transfer resistance is smallest for the (110) face with a value of approximately 2 Ω cm^2 at η = -150 mV followed by a large increase in R_{ct} yielding, for the (111), face a value of 16 Ω cm^2 with the (100) having the largest R_{ct} value which, at η = -150 mV is 36 Ω cm^2, see Fig. 5.24.

Once the values of A, B and C had been obtained from the CNLS fitting of the impedance data, the rate-constants and q_1 value were obtained by a quantitative analysis of these values as a function of overpotential. The results of this analysis are shown in Figs. 5.24 and 5.25 for the A *vs.* potential and B and C *vs.* potential relationships, the lines on

these plots having been calculated from the best fit-rate constants and q_1 values shown in Table 5.2. For the (100) surface, as was noted in the experimental section, the current-density decreased significantly during the time needed to conduct the ac frequency scan. This did not lead to an unreasonable amount of scatter in the current-voltage or A *vs.* potential relationships, but a large dispersion in the values for the parameters B and C did arise (Fig. 5.26). This problem of scatter was compounded by the fact that the fitting of either B or C led to substantially different q_1 values and that a value satisfying both parameters could not reliably be found. Many trials studying the ac behaviour of this face were performed in order to obtain consistent B and C *vs.* potential relationships, but they were of no avail. Fig. 5.26 shows a plot of C *vs.* potential illustrating the extent of the scatter. Also shown in Fig. 5.26 are the values of q_1 which encompass the limits of this scatter in C which gives an average q_1 value equal to 4 ($\pm$4) x 10^{-4} C cm^{-2}, yielding a maximum OPD H coverage between 0.17 and 3.6 apparent monolayers. The lower value seems more appropriate when compared to the value of 0.25 monolayers which was found in the work of table 5.1 for acidic solutions, where the stability of the current-density was significantly better and much less scatter was observed in the relation of the ac parameters to potential pertaining to the H adsorption process.

Fig. 5.27 shows the calculated dependence of OPD H coverage (θ_H) as a function of the electrode overpotential for the three low-index planes of Pt. The fractional OPD H coverage at the reversible potential is related to the ratio of the rate-constants, i.e of the steps producing adsorbed H *vs.* those in which it as a reactant, as in Eq. 1.12. From Fig. 5.27 it is seen that, at equilibrium, the order of OPD H fractional coverage values is

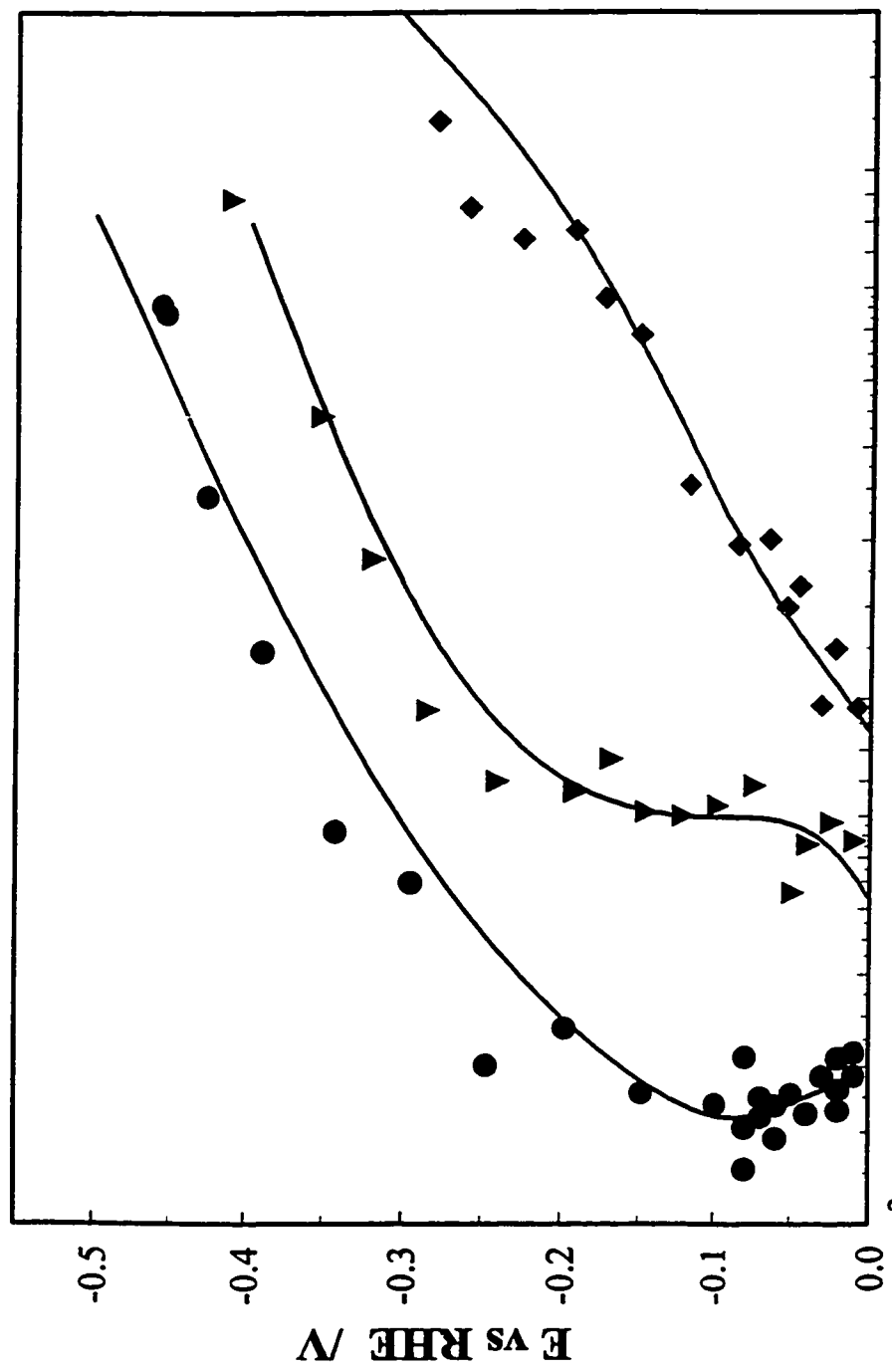

Fig. 5.24 A semilogarithmic plot of $A(R_{ct}^{-1})$ *vs.* potential for the HER at the three low-index planes of Pt ● - (100), ▼ - (111) and ◆ - (110) in 0.5 mol dm^{-3} NaOH. Rotation rate 3000 rpm; best fit line calculated from the rate constants in Table 5.2.

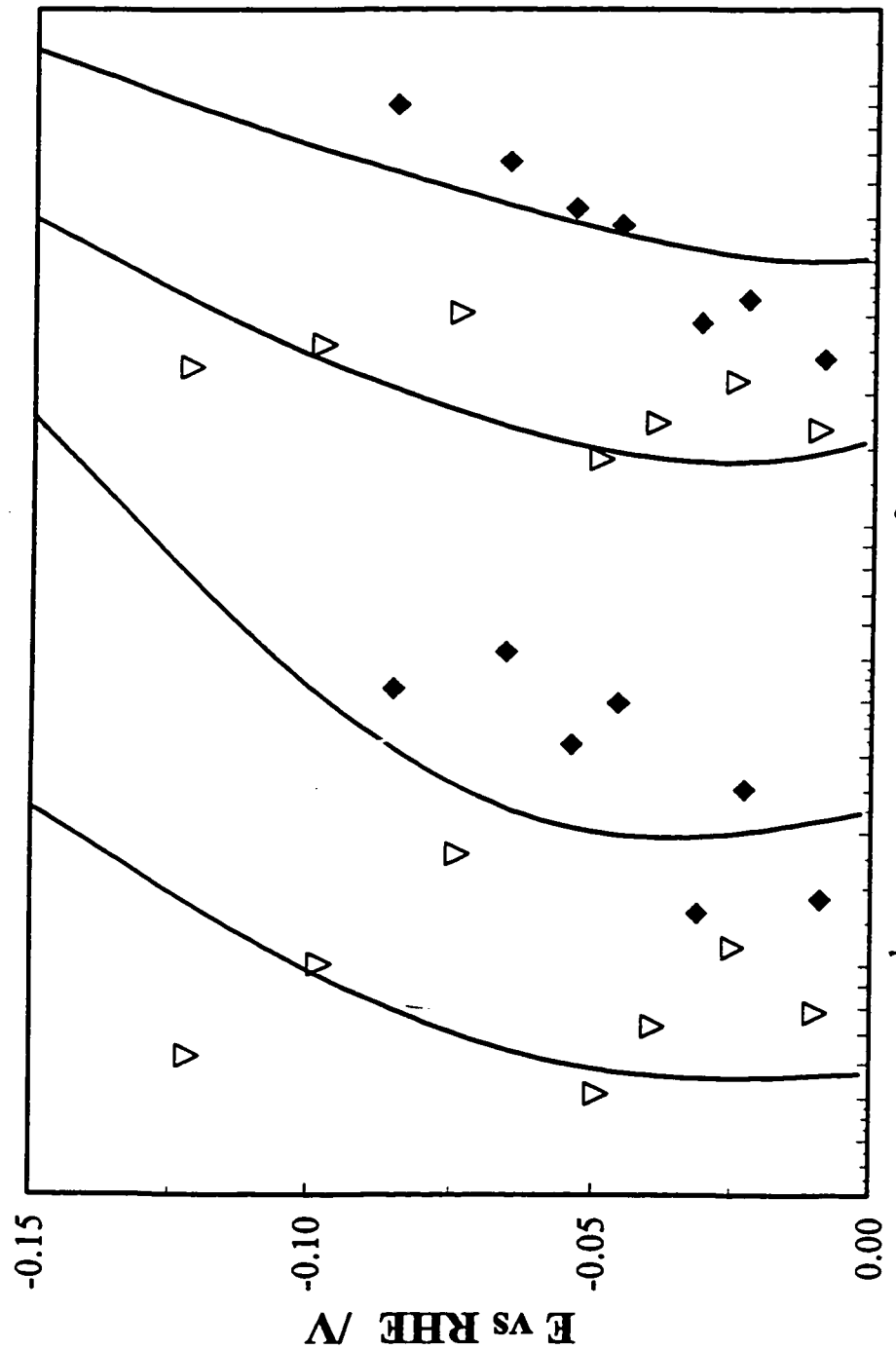

Fig. 5.25 A plot of the ac parameters (-)B and C *vs.* overpotential for the ∇ - (111) and ◆ - (110) surfaces. The best-fit lines were calculated from the rate-constants and q_1 given in Table 5.2. Note that the parameters B and C correspond to the second semicircle in the EIS complex-plane plots and that this process was only resolved at lower overpotentials (η = 0 to -100 mV), see Fig. 5.22.

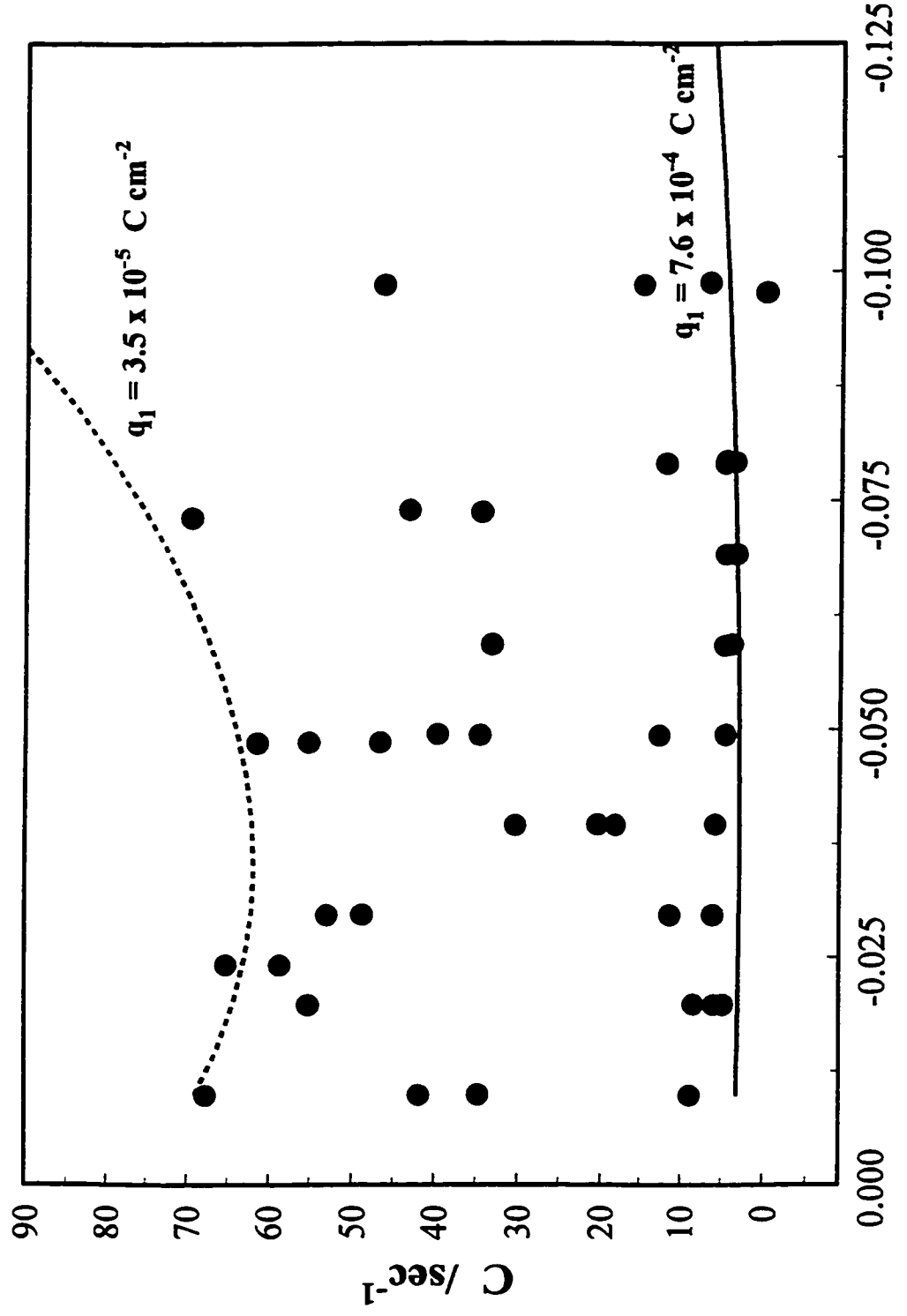

Fig. 5.26 A plot of C *vs.* overpotential for the (100) surface, illustrating the degree of scatter that arises. The lines on the plot indicate the range of q_1 values which the scatter encompasses.

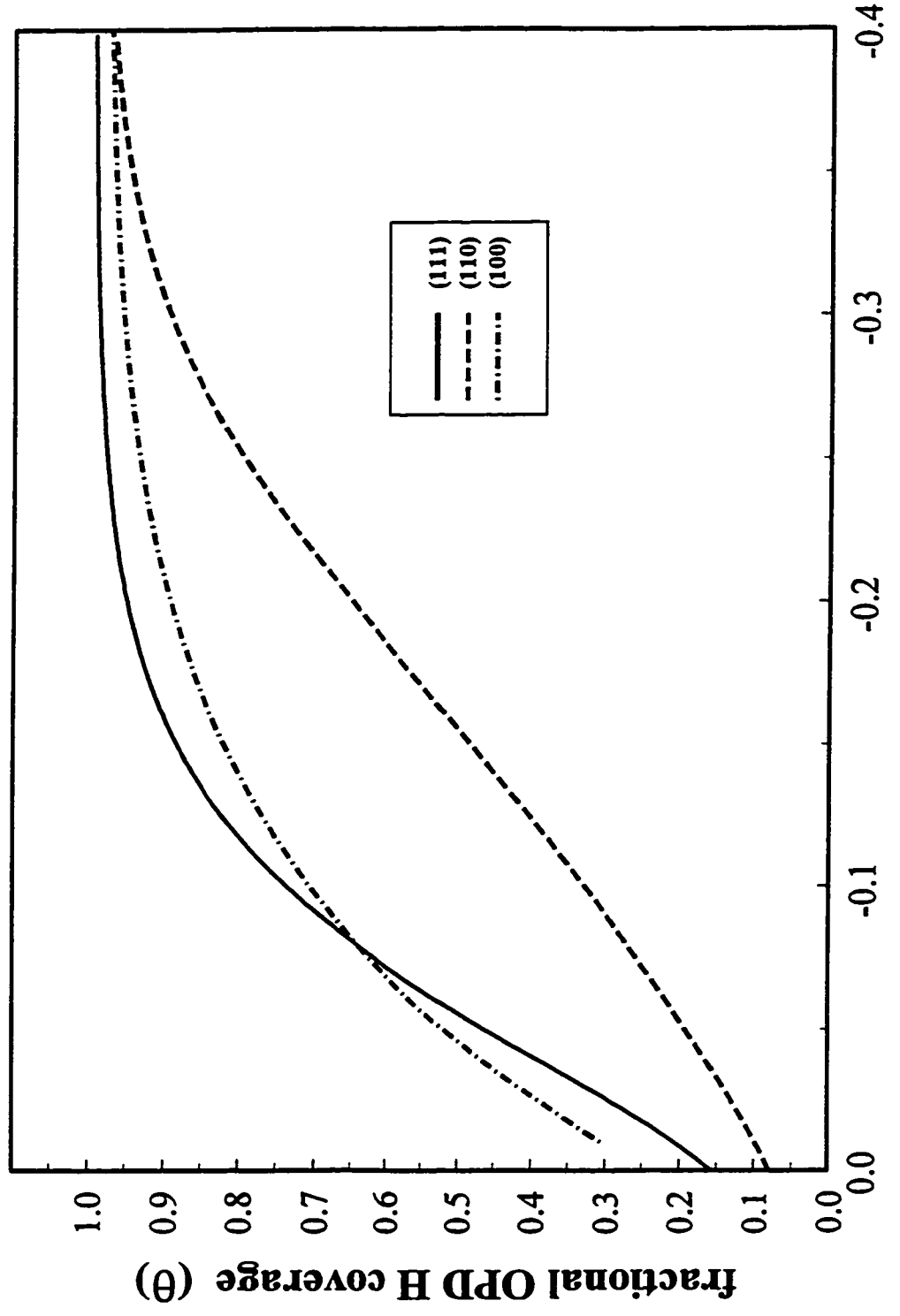

Fig. 5.27 A plot of fractional surface coverage of overpotentially deposited H as a function of overpotential for the three low-index planes. Note that to obtain the real surface H concentration the fractional coverage is to be multiplied by q_1.

(100) > (111) > (110) but if one takes into account the concentration of active sites on the surface, which is measured by q_1, the absolute OPD H coverage values become, almost equivalent for the three faces, within the experimental error for the q_1 value.

The ratio of the rate constants for the steps in the HER mechanism is also seen (Fig. 5.27) to influence the rate of change of θ_H with potential. The largest determining factor in this is the relative magnitudes of k_2 and k_3 in comparison with k_1. The sharper rise of θ_H for the (111) electrode compared with that for the (100) surface is mainly a result of the k_1/k_2 ratio being over 3 times greater for the (111) electrode (i.e., the rate in which θ_H reaches its maximum value is 3 times greater for the (111) surface relative to the (100) surface). The $\theta_H(\eta)$ curve for the (110) surface, on the other hand, has a much lower rate of change than either the (100) or the (111) surfaces due to the much greater activity of the Tafel step (k_3), relative to the Volmer step (k_{-1}) at the (110) surface. The ratio, k_1/k_3, is seen, from the values in Table 5.2, to be over an order of magnitude smaller for the (110) surface compared to that calculated for the (100) or (111) surfaces.

It can then be stated that not only does the overall rate depend on the Pt single-crystal surface geometry, but the distribution of the reaction affinity amoungst the three steps is also surface sensitive.

5.5.4 Discussion of previous results

In order to thoroughly assess the present data and the conclusions drawn from it, it is necessary to discuss these findings in the light of previous work. It is unfortunate that, to our knowledge, only one other paper in which the HER at Pt(hkl) surfaces was studied

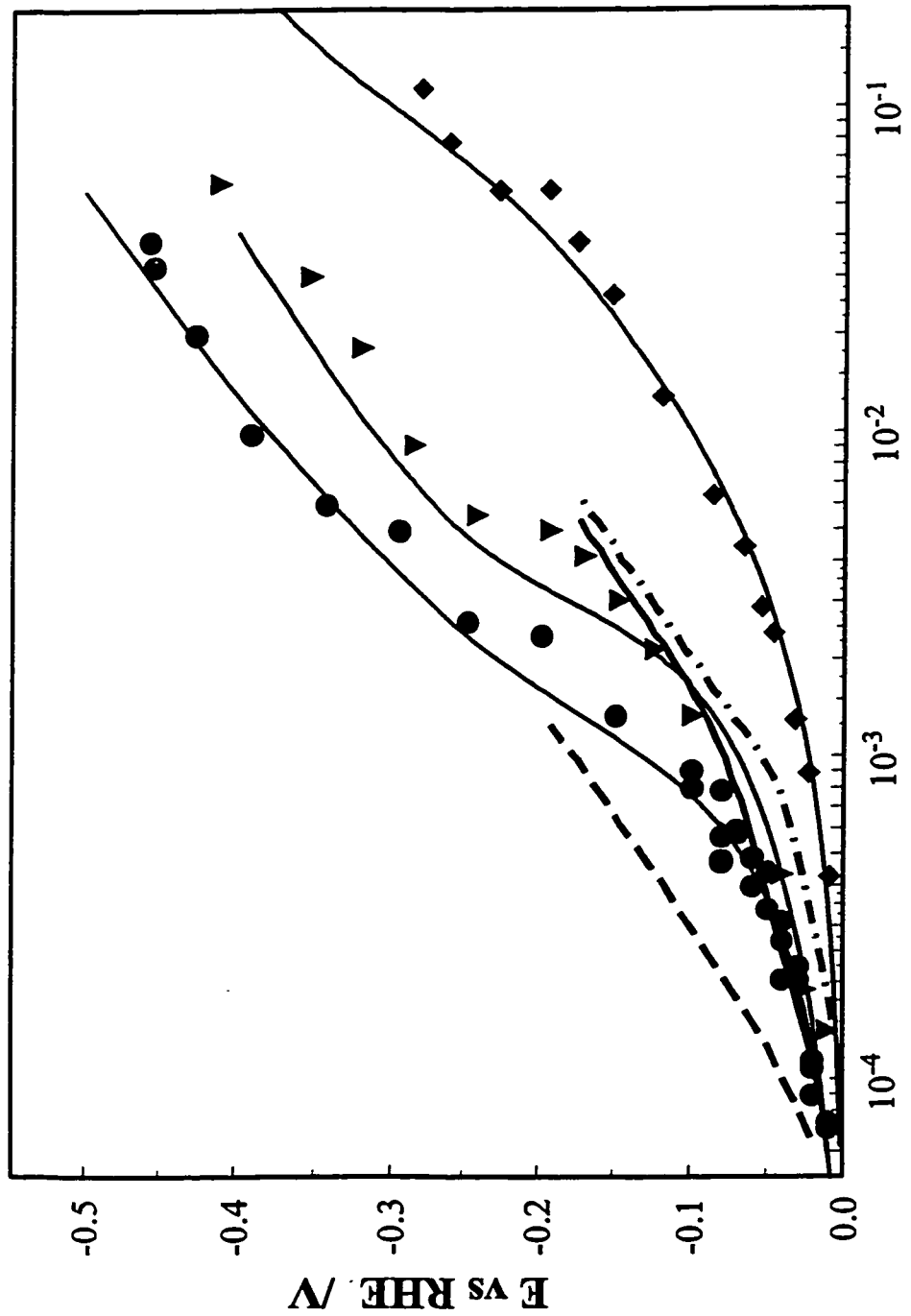

Fig. 5.28 A Tafel plot as in Fig. 5.20, ● - (100), ▼ - (111) and ◆ - (110), but with the addition of the results from Marković et al. [12], (111) ---, (100) — and (110) - · - · -.

in alkaline solutions has been published, *viz.* that of Marković et al. [12]. Upon comparison of the present results with those in ref. 12 (see Fig. 5.28), it is readily noticed that the orders of electrocatalytic activity are different, i.e. in Marković, ref. 12, (111) > (100) > (110) compared to the present results which show an order (100) > (111) > (110). The problem therefore is to find a factor or factors which can account for this difference.

First of all there are differences in the two experimental procedures employed. The most significant difference is how the single-crystal face is isolated from the remainder of the electrode surface. In the present work the rotating meniscus (rm) technique was used whereas, in ref. 12, a Teflon sleeve (ts) covered the sides of the crystal. Both techniques have advantages and disadvantages.

1) Using the rm method the preparation and installation of the electrode into the cell is simple and results can be obtained within seconds of the annealing/cleaning step whereas the ts procedure takes a longer time and much more manipulation of the electrode is required before it can be entered in a clean condition into the cell. This factor favours the rm method.

2)The isolation of the surface is guaranteed in the ts method (if no leakage occurs) whereas, as was stated in § 3.4 and 3.5 using the rm method, the isolation of the desired surface is less assured and careful adjustment of the dimensions of the crystal, the meniscus and its positioning with regard to the Luggin capillary are important. For the face exhibiting the slowest kinetics a small kinetic influence from the sides was found as descibed in § 3.4, but this was minimized to a large degree by the above mentioned

precautions, see § 3.4. This factor somewhat favours the ts method.

3) Providing a constant pressure of H_2 gas to the electrolyte is also a factor; in the ts method H_2 can be bubbled continuously through the solution during measurements, whereas in the rm technique gas can only be bubbled before the crystal is placed in the cell and, after its installation, a constant pressure of H_2 is provided over the electrolyte. However, this did not seem to pose any problem and, if the H_2 flow was sufficiently large, a stable rest potential of 0.0 V *vs.* RHE could be achieved using the rm method.

Tafel plots comparing the two sets of data are shown in Fig. 5.28 which clearly indicate that the origin of the differences runs deeper than just the order of reactivity. In the present work the current-density covered is at least one decade more than that in ref. 12. This extra current and associated overpotential allows the transition between the rate-controlling processes to be seen, i.e. the Tafel to Heyrovsky (step II to step III) transition. Analysis of the data in ref. 12, (linear Tafel plots which have a slope near 120 mV decade^{-1}), could falsely lead to a conclusion that the contribution from step III is negligible. For the (111) and (110) surfaces, the present results show greater activity than those from ref. 12. The only coincidence occurs at low overpotentials for the (100) surface and it is interesting that the current densities in ref. 12 are larger at higher overpotentials for this plane.

Actually it was observed that if the (100) electrode was cooled in air it gave similar behaviour to the results shown in ref. 12 for the (100) plane. This difference in the cooling conditions for the (100) surface is also consistent with the observations in acidic solutions (see the above sections, 5.1 to 5.3). The coincidence of the two (100) curves (Fig. 5.28)

is also surprising due to the fact that (as seen from the results obtained by the rm method in 0.5 mol dm^{-3} H_2SO_4) because the (100) face suffers the most from edge effects although, taking the necessary precautions, it could be minimized. If edge effects had been important, this would have increased the measured apparent current-densities to larger values (due to greater accessible area) and a discrepancy going in the opposite direction would have been observed for the two (100) curves.

The differences seen in Fig. 5.28 between the two (110) results may be a result of the activation effect that was observed at this face over the first minute or so of application of potential. Although we are unsure of exactly what this activation process is, it was felt that the correct Tafel behaviour is found after this activation process has become completed. The reasoning behind this conclusion stems from the following observations: i) the Tafel behaviour after this activation process is identical with that of the polycrystalline surface (electrode sealed in a Teflon sleeve and immersed in solution, as in ref. 4) which is also consistent with the findings when the 0.5 mol dm^{-3} H_2SO_4 electrolyte was used, see Figs. 3.2 and 5.3 and ii) the CV for the (110) surface, after this activation process has taken place does not indicate reconstruction, only a slight deactivation[6]. It was also essential to our ac impedance measurements that a stable current-density was achieved, as was the case after this activation process had gone to completion.

The only behaviour which is inexplicable is the difference between the two plots

---

[6] It maybe the case that *reconstruction* takes place over the HER potential region and then is lifted when the potentials are brought back to the potential range for the UPD of H.

(here and in ref. 12 for the (111) surfaces), which is unfortunate since this is the result that leads to the apparent difference in order of reactivities.

5.5.5 Conclusions

The results presented in this section of the chapter provide a clear indication that the kinetics of the HER are dependent on the surface geometry of the low-index planes of Pt single-crystal electrodes. Consistency with the results of our previous work performed in acidic media is very good. In both instances the order of reactivity is (100) < (111) < (110).

From both steady-state Tafel type and ac impedance measurements it was found that all three steps in the reaction mechanism participate significantly and a transition from step III to step II as rate-influencing is clearly shown to arise at each surface. The rate-constants for each reaction step were determined with good accuracy and reasonable values of the charge required for full coverage of OPD H, q_1, were obtained for the (111) and (110) surfaces. Using 210 $\mu C\ cm^{-2}$ as our reference, it is found respectively, that, 27% and 54% of the (111) and (110) surfaces are maximally covered with OPD H. At the (100) surface, much scatter was observed in the impedance parameters (B and C) pertaining to the H adsorption process and a definite q_1 value could not be found. A comparison with the results found above, Table 5.2, would indicate that the maximum fractional coverage of the surface is below 25%.

One issue that arises from this work is that a substantial difference between the present results and those published by Marković et al [12] exists. It appears these discrepancies arise from differences in experimental technique. Discussion of this matter

was presented, but still some points need resolution.

Lastly, the three single-crystal surfaces were found to behave quite differently upon application of cathodic overpotential, i.e. the current-density decreased or increased with time, depending on potential, for the (100) face; it remained approximately constant for the (111) face and increased significantly at all potentials for the (110) electrode surface. The reasons for these changes are, as yet, unknown but some ideas concerning this phenomenon were given. The use of high-purity solutions and preparation techniques (cf. ref. 51) makes it unlikely that the deactivating effects are due to poisoning impurities. They were not observed in similarly prepared acid solutions.

References

1. J. Clavilier, A. Rodes, K. El Achi and M.A. Zamakhchari, J. Chim. Phys., 88 (1991) 1291.

2. S. Morin, H. Dumont and B.E. Conway, J. Electroanal.Chem., 412 (1996) 39, see also S. Morin, Ph. D. Thesis, University of Ottawa (1996).

3. S. Motoo and N. Furuya, J. Electroanal. Chem., 172 (1984) 339.

4. L. Bai, J. Electroanal. Chem., 355 (1993) 37; L. Bai and B.E. Conway, Electrochim. Acta, 31 (1986) 1013.

5. D. Schonfuss and L. Muller, Electrochim. Acta, 39 (1994) 2097.

6. D.A. Harrington and B.E. Conway, Electrochim. Acta., 32 (1987) 1703; L. Bai, D.A. Harrington and B.E. Conway, Electrochim. Acta, 32 (1987) 1713.

7. M.W. Breiter in E. Yeager (Ed.) Symposium on Electrode Processes, The Electrochemical Society, Wiley, New York (1961) pp. 307-324.

8. R. Durand, Electrochim. Acta, 24 (1979) 1095.

9. S. Schuldiner, J. Electrochem. Soc., 106 (1959) 891.

10. K. Seto, A. Iannelli, B. Love and J. Lipkowski, J. Electroanal. Chem., 226 (1987) 351.

11. Hanwei Lei, Bengliang Wu and Chuansin Cha, J. Electroanal. Chem., 332 (1992) 257.

12. N.M. Marković, S.T. Sarraf, H.A. Gasteiger and P. Ross Jr., J. Chem. Soc., Faraday Trans., 92 (1996) 3719.

13. V. V. Losev, Electrokhimiya, 17 (1981) 733.

14. M. Breiter, J. Electrochem. Soc., 109 (1962) 549.

15. B.E. Conway and J. O'M. Bockris, J. Chem. Phys., 26 (1957) 532.

16. P. Ruetschi and P. Delahay, J. Chem. Phys., 23 (1955) 195.

17. B.E. Conway, "Theory and Principles of Electrode Processes.", Ronald Press, NewYork (1964).

18. J.A.V. Butler, Proc. Roy. Soc. London, Ser. A, 157 (1936) 423.

19. J. Horiuti and M. Polanyi, Acta Physicochim. URSS, 2 (1935) 505.

20. G.C. Bond, "Heterogeneous Catalysis", Clarendon Press, Oxford (1974).

21. S. Trasatti, J. Electroanal. Chem., 39 (1977) 163.

22. R. Parsons, Trans. Faraday Soc., 34 (1958) 1053.

23. B.E. Conway and B.V. Tilak, Adv. in Catalysis, 38 (1992) 1.

24. G. Jerkiewicz and A. Zolfaghari, J. Electrochem. Soc., 143 (1996) 1240.

25. I.I. Physhnogrva, A.M. Skumdin, Yu. B. Vasiliev and V.S. Bagotsky, Electrokhimiya, 6 (1970) 142.

26. S. Schuldiner, M. Rosen and D. Flin, J. Electrochem. Soc., 117 (1970) 1251.

27. H. Kita, S. Ye and Y. Gao, J. Electroanal. Chem., 334 (1992) 351.

28. J. O'M Bockris and H. Mauser, Can. J. Chem., 37 (1959) 475.

29. B.E. Conway and G. Jerkiewicz, J. Electroanal. Chem., 357 (1993) 47.

30. R. Piontelli, G. Poli and G. Serravalle, Symposium on Electrode Processes, Ed. E. Yeager, The Electrochemical Society, John Wiley, New York, 1961, pp. 67-103; R. Piontelli, L. P. Bicelli and A. Vecchia, Lineci - Rend. Sc. fis. mat. e nat., 28 (1960) 139.

31. A. Hamelin, Modern Aspects of Electrochemistry, Eds. BE Conway, J.O'M. Bockris and R.E. White, Plenum Publ. Co., NewYork, 16 (1985) 1.

32. J. Clavilier, J.M. Orts, R. Gómez, J.M. Feliu and A.Aldaz, Proc. Symp. on Electrochemistry and Materials Science of Cathodic Hydrogen Adsorption and Absorption , Eds. B.E. Conway and G. Jerkiewicz, 94-21 (1994) 167, The Electrochemical Society Inc.

33. E. Herrero, J. Clavilier, J. M. Feliu and A. Aldaz, J. Electroanal. Chem., 410 (1996) 125.

34. H. Angerstein-Kozlowska, Comprehensive Treatise of Electrochemistry, Eds. B.E. Conway, J.O'M. Bockris, S. Sarangapani and R.E. White, Plenum, New York, 9 (1984) 15.

35. D.K. Kahaner, C. Moler and S. Nash. "Numerical Methods and Software.", Prentice Hall, Englewood Cliffs, NJ (1989).

36. C. Delouis, I. Epelboin, M. Keddam and J.C. Lestrade, J. Electroanal. Chem., 28 (1970) 57.

37. D. Franceschetti and J.R. MacDonald, J. Electroanal. Chem., 101 (1979) 307.

38. D. Franceschetti, J.R. MacDonald and R.P. Buck, J. Electrochem. Soc., 138 (1991) 1368.

39. J. O'M. Bockris, S. Srinivasan and D.B. Mattews, Disc. Faraday Soc., 39 (1965) 239; J. O'M. Bockris and D.B. Matthews, J. Chem. Phys., 44 (1966) 198.

40. J. R. MacDonald and D. Franceshetti, "Impedance Spectroscopy.", Ed. J.R. MacDonald, John Wiley and Sons, New York, (1987) p. 122.

41. A. Frumkin and E. Aikasjan, Doklady Akad. Nauk. SSSR, 100 (1955) 315; also see Izvest. Akad. Nauk., 202 (1959).

42. J. Clavilier, J.M. Orts and J.M. Feliu, J. Phys. IV, 4 C1 (1994) 303.

43. K. Christman, Surf. Sci. Rev., 9 (1988) 1.

44. T. N. Anderson, B.S. Dandapani and J.M. Berry, J. Electroanal. Chem., 357 (1993) 77.

45. J. O'M. Bockris and R.E.H. Watson, J. Chim. Phys. 49 (1952) C70.

46. D.R. Flin and S. Schuldiner, Electrochim. Acta, 19 (1974) 421.

47. D.R. Flin, M. Rosen and S. Schuldiner, Colln. Czech. Chem. Comm., 36 (1971) 454.

48. W. Savich, S-G. Sun, J. Lipkowski and A. Wiechowski, J. Electroanal. Chem. , 388 (1995) 233.

49. A. Lasia, in "Proc. Symp. on Electrochemistry and Materials Science of Cathodic Hydrogen Adsorption and Absorption", Eds. B.E. Conway and G. Jerkiewicz, Vol. 94-21, The Electrochemical Society NJ., 261 (1994).

50. T. Yamazaki and M. Enyo, Electrochimica Acta, 35 (1990) 523.

51. B.E. Conway, H. Angerstein-Kozlowska, W.B.A. Sharp and E. Criddle, Anal. Chem., 45, (1973) 1331.

A

Appendix 5-A
Comparison of the present results with the findings of *in situ* and *ex situ* spectroscopic studies of OPD and UPD H at Pt(hkl) substrates

In § 5.2.4 and 5.5.2 discussion was forwarded on the nature of the intermediate species in the HER. This discussion was based on our knowledge of the single-crystal metal surface structure, electrochemical studies of the UPD H species and the present electrochemical insights into the coverage of the OPD H species as a function of electrode potential and surface structure. As was stated in the above mentioned sections, electrochemical studies can give general information concerning the quantity of electroactive species which have reacted or adsorbed on the surface. Integration of single-crystal electrodes into electrochemical techniques allows one to sketch out the most likely bonding sites of the quantity under study, but still an absolute configuration can usually not be obtained; i.e. in § 5.2.4 it was shown that either position, the ontop site or a multi-coordinated hole site could not be distinguished from each other. Reaction at either site requires the flow of one electron of charge, yet the potential at which they react maybe different. It is fortunate then that much effort has been expended on *in situ* and *ex situ* electrospectroscopic studies into the reaction of H with single-crystal Pt surface. Here we will discuss results from *in situ* FTIR and surface x-ray scattering (SXS) studies and make comparisons to the present results.

In situ vibrational spectroscopic studies of the Pt-H bond of the electrochemically generated ad-species have been reported by Nicols [1], Bewick [2] and Ogasawara [3] using SNIFTIRS and by Tadjaddine et al. [4,5,6] using the sum frequency generation (SFG) technique. In all of the above studies ir bands attributable to UPD Pt-H adbond vibrations were exclusively found in the 1800-2200 cm^{-1} range which have been assigned to a

terminally bonded species. In the 500-1700 cm^{-1} range where multi-coordinated H/Pt species are found to adsorb in UHV/EELS studies [7], no bands were detected from either the UPD or OPD H. The vibrational spectroscopic results are then directly opposed to what is known from other studies that indicate a multi coordinated Pt-UPD H species.

The support for this is:

1) Results from UHV, FTIR and EELS studies of H adsorbed ($0<\theta<1$) on a large variety of metals has only shown multi-coordinated M-H adspecies.
2) Thermodynamic analysis of the Pt UPD H bond strength [8,9] corresponds extremely well with the bond strength of the multi-coordinated Pt-H found using UHV techniques [7].
3) *In situ* SXS studies [10,11] shows relaxation of the first Pt layer away from the bulk metal lattice upon UPD H adsorption, this has been interpreted as H adsorption into the interstitial, multi-coordinated surface sites.

The vibrational spectroscopic studies, although their assignments of the UPD H species are in conflict with the other evidence, have been successful in resolving a new band at potentials lower than 50 mV vs. NHE which corresponds to OPD H, the intermediate in the HER. The absorption peak is observed at 1750-1770 cm^{-1} [6] this energy is outside the usual spectral limits of both the multi-coordinated adspecies (500-1700 cm^{-1}) and the terminally bonded adspecies (1800-2200 cm^{-1}). This band was tentatively assigned to a dihydride adsorption configuration (H_2-Pt) [4,5,6] and it was also seen that its peak wavenumber was sensitive to the single-crystal surface structure. The lower energy of this band vs. the UPD H ir bands provides evidence that the OPD H species has distinctly different energetics than that the UPD H species. And also that the M-H bond energy of this OPD H species is

sensitive to single-crystal surface structure and should as was seen in the present results, correlate to surface sensitive HER kinetics.

The SGF technique used Tadjaddine et al. [4,5,6] allowed negative potentials down to –0.15V vs NHE (probably not corrected for solution resistance) to be accessed and increases in the absorption signal from the OPD H species was seen as the potential became more negative. This observation and the fact that these bands appeared at potentials greater than 0.0 V vs. NHE corresponds well to the OPD H coverage / electrode potential relationship derived from the present EIS study shown in Figs. 5.15 and 5.27. It seem very promising that a coupled EIS/SGF study of the OPD H species at Pt(hkl) electrodes would yield not only new information concerning the nature of the OPD H species but possible a more detailed view of the steps involved in the HER process itself; e.g. correlating electrochemically determined coverages to IR peak area would enable the determination of the transition dipole moment of the Pt-H bond and therefore enhance the assignment of the OPD H adsorption site.

SXS studies [10,11] have shown that the relaxation of the surface layer follows the order (110)>>(100)>(111) this is indicative of multi-coordinate adsorption in the H UPD range. Unlike SFG though, this method relies on subtraction from a reference potential and the relative relaxation given above, maybe different than the absolute relaxation magnitudes. Still it is possible that these results can be translated into a variation of the work function as a function of UPD H coverage and ultimately give a indication of the Pt-H OPD H bond strength as a function of single-crystal surface structure.

In conclusion, it seems very likely that progress in this area can be achieved by the combination of electrochemical and *in situ* spectroscopic techniques.

References

1. R.J. Nichols and A. Bewick, J. Electroanal. Chem., 243 (1988) 445.
2. A. Bewick and J.W. Russell, J. Electroanal. Chem., 132 (1982) 329.
3. H. Ogasawara and M. Ito, Chem. Phys. Lett., 221 (1994) 213.
4. A. Tadjaddine and A. Peremans, J. Electroanal. Chem. 409 (1996) 115.
5. A. Tadjaddine, A. Peremans and Guyot-Sionnest, Surf. Sci., 335 (1995) 219.
6. A. Peremans and A. Tadjaddine, J. Chem. Phys. 103 (1995) 7197.
7. K. Christmann, Surf. Sci. Rep. 9(4) (1988) 1.
8 G. Jerkiewicz and A. Zolfaghari, J. Electrochem. Soc. 143 (1996) 1240.
9. B.N. Grgur, N.M. Marković and P.N. Ross, J. Phys. Chem.B, 101 (1997) 5405.
10. I.M. Tidswell, N.M. Marković and P.N. Ross, J. Electroanal. Chem. 376 (1994) 119
11. N.M. Marković and P.N. Ross, J. Electroanal. Chem. 330 (1992) 499.

Chapter 6

Competitive Effects of S-containing Catalyst Poisons on the UPD of H in Relation to H_2 Evolution Kinetics and OPD of H at Pt

6.1 Adsorption of the Catalyst Poisons, Thiourea, Cysteine and 2,2' diethanol-sulphide at the Pt Electrode

The adsorption of poisons (P) leads to: a) diminution of coverage by underpotentially deposited H; and b) changes of the kinetics of the HER and associated diminution of coverage by the overpotential-deposited H; and additionally, c) possibly enhancement of sorption of H into the cathode at certain transition metals.

In a number of the experiments to be descibed below addition of the poison was made to an initially poison-free solution. This results in the desorption of previously adsorbed H (UPD-H and OPD-H), and anions (see § 1.3.1.2), the amount being dependent on the electrode potential during poison adsorption. The resulting voltammograms over the H UPD potential region, after this adsorption process had been completed, are shown as a function of bulk thiourea concentration in Fig. 6.1. In the UPD potential range, the anodic H desorption effect [1] is observed, i.e., at a constant potential, H is desorbed in a recordable anodic current (charge) transient, see § 1.3.1.2 for Pt and § 8.1 for Pd. The coverage by the poisons on Pt, determined from the decrease in the UPD of H as measured from the charges under the cyclic voltammetry current-peaks, is concentration and time dependent. The process of "P" adsorption can be written for conditions where adsorption of P is competitive with that of H, as follows, where $\theta_{H(P)} < \theta_H$, is the H coverage in the presence of P, and $(1-\theta_H, \theta_H)$ represents the initial state of

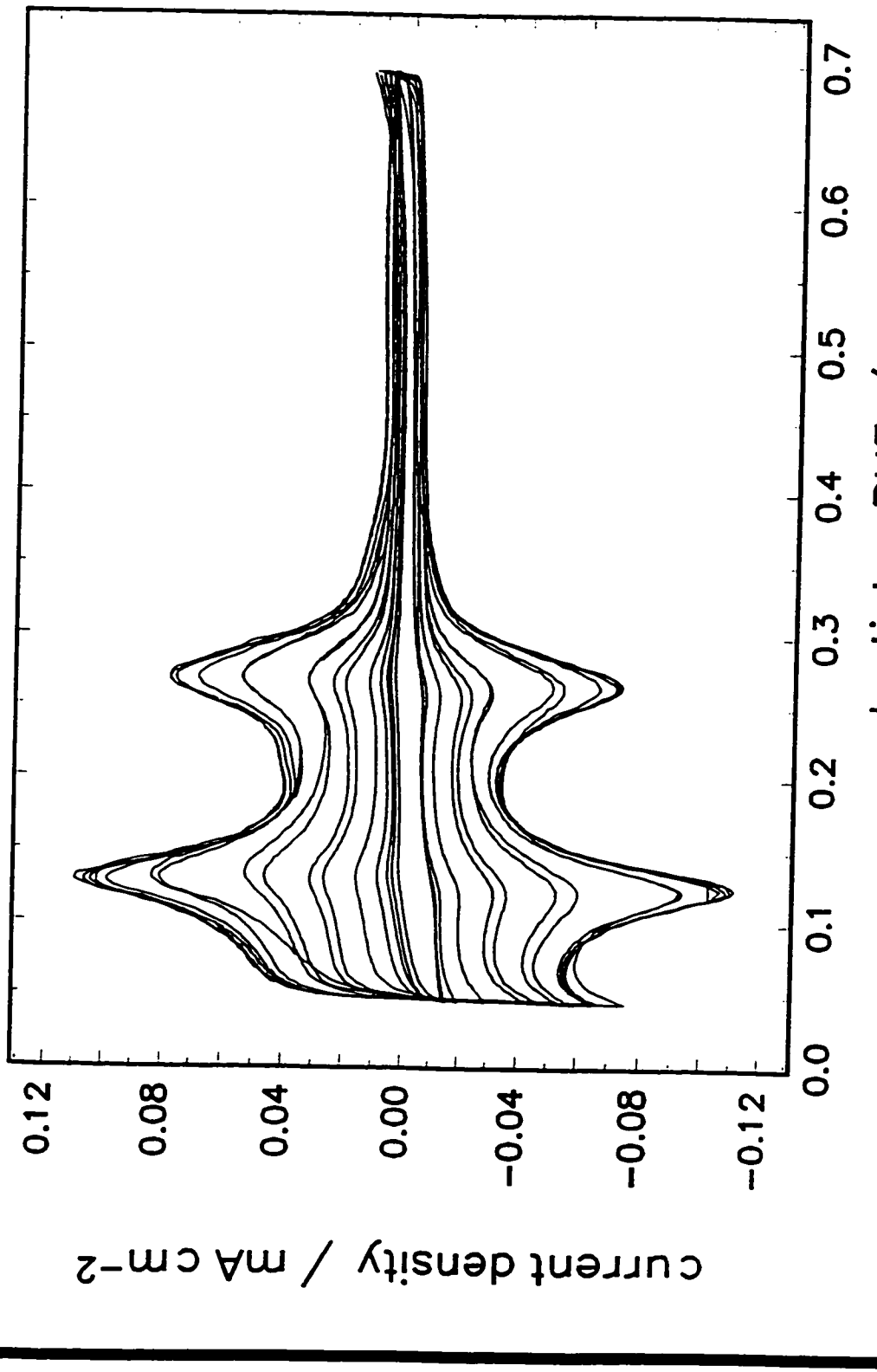

Fig. 6.1 Cyclic voltammograms of UPD H at Pt(poly) in 0.5 mol dm^{-3} H_2SO_4 + x mol dm^{-3} thiourea: 5 x 10^{-6} mol dm^{-3} < x < 1 x 10^{-4} mol dm^{-3}, scan rate 50 mV sec^{-1}.

free sites and the H coverage on the electrode when $\theta_P = 0$:

$$\underset{1-\theta_H,\,\theta_H}{Pt} + \underset{[P]}{poison} \xrightarrow{k_A} \underset{(1-\theta_{H,P}-\theta_P),\,(\theta_{H(P)}+\theta_P)}{Pt - poison} \qquad \textbf{(6.I)}$$

The variation of θ_P expressed as the change, $\Delta\theta_H$, caused by the poison at a constant adsorption time but for various P concentrations, is shown for cysteine and thiourea in Fig. 6.2. The maximum blocking of underpotentially deposited H which can be achieved by thiourea adsorption on Pt in 0.5 M H_2SO_4 reaches *ca.* 99%. Due to the complications from time and concentration factors when the poisons are present in the electrolyte, the preferred procedure, mentioned in § 2.3, was adopted. This consisted of first adsorbing the poisons onto the electrode in a separate vessel, *ex situ*, from an initial solution, 0.1 mol dm^{-3} in concentration, for adsorption times of 10 min. for thiourea and 1 h. for cysteine and 2,2'diehanolsulphide (DES); then the electrode was transferred to the test cell in which kinetic and coverage experiments were conducted. For thiourea at the above concentration, the time allowed for adsorption had little effect past the one minute value.

Cyclic voltammograms (inset in Fig. 6.3) were taken subsequently to this *ex situ* adsorption and indicate that, for adsorbed thiourea under the conditions employed, the coverage by underpotentially deposited H becomes almost zero but for cysteine and DES, the blockage of UPD H is incomplete. For these poisons, adsorption times greater than 4-5 h. were needed for a "complete" film to be formed but θ_P's of 80 - 90 % were attained quickly. These differences probably result from specific configurational surface bonding requirements [2,3] similar to those for self-assembled monolayers [4].

All the voltammetric responses for pre-adsorbed poisons were found to be stable

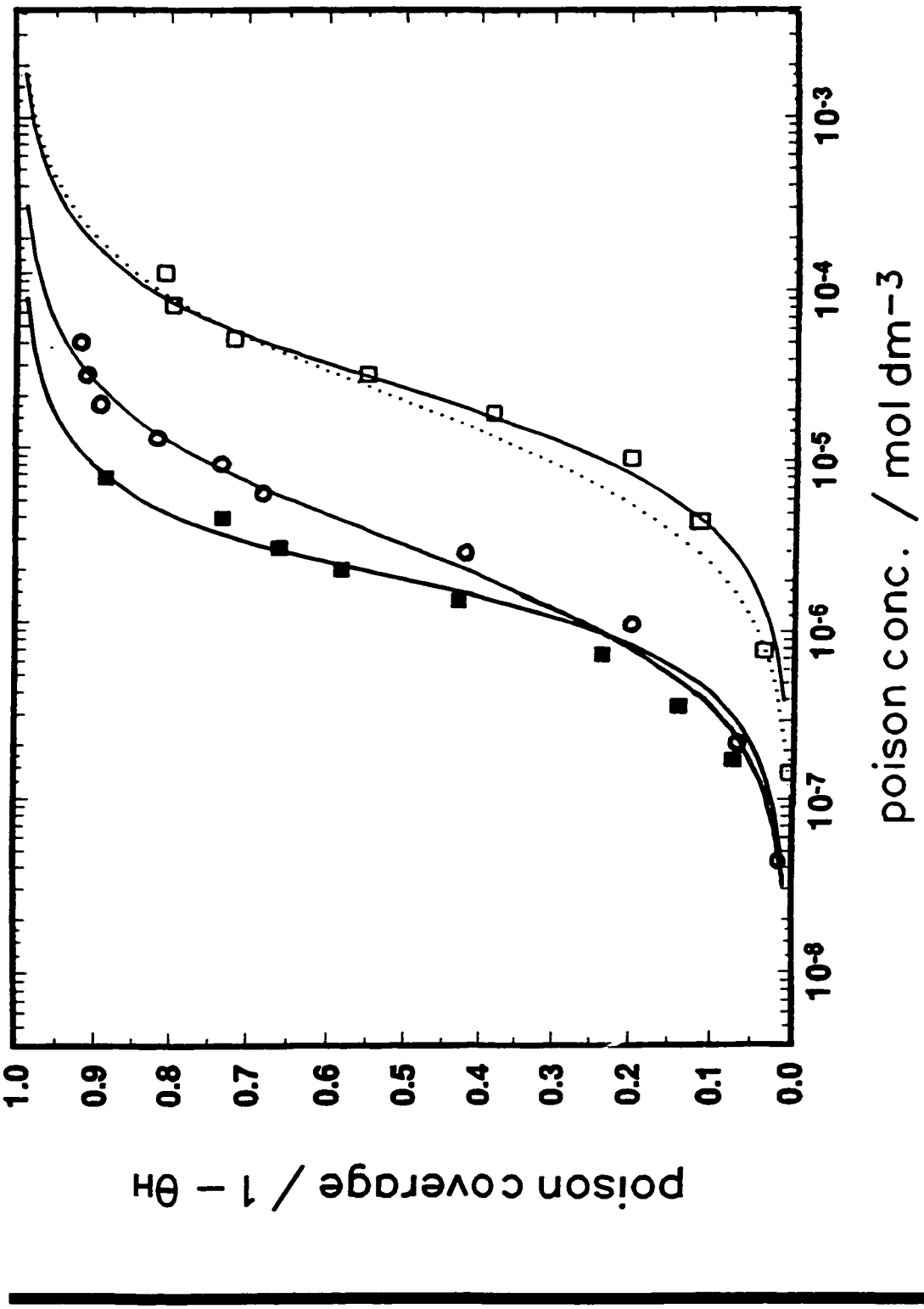

Fig. 6.2 Coverage of UPD H as a function of poison concentration in 0.5 mol dm^{-3} H_2SO_4 on Pt. (o) thiourea; (■) cysteine; (□) cysteine (HCl); (----- or —) indicate langmuir or frumkin isothermal behaviour.

over 100's of cycles in the UPD H region, demonstrating a state of virtually constant poison coverage.

6.2 Poison Effects on the Steady-state Polarization Behaviour of the HER At Pt Electrodes Bearing Preadsorbed Poison Films

The steady-state cathodic polarization measurements on the HER in the presence of thiourea, cysteine and DES reflect the effects of the relative values of poison coverage determined in the UPD H region, *viz.* i(thiourea) < i(cysteine) < i(DES), as shown in Fig. 6.3 in terms of current-densities (i) *vs.* overpotential (η) plots.

These Tafel relations were recorded for a series of increasing, and then subsequently decreasing, overpotentials up to, or down from, *ca.* -0.2V *vs.* RHE. The resulting currents were always larger on the "descending" than on the "ascending" curve, (see Fig. 6.3) due to irreversibility associated with the changes of θ_P with potential. Thus the poison becomes progressively desorbed with increasing η allowing a greater fraction of free sites to be available for H accommodation in the HER. However, at each point along the Tafel curves, an apparent steady-state had been reached in the time-scale of the measurements, *ca.* 1 min.

Quantitative measurements of H-blocking by thiourea, as a function of η for the HER, were made by determining the charge for UPD of H by the procedure described in § 2.3 after a steady-state cathodic current at each overpotential had been attained. As η was increased cathodically, θ_H was found to increase semi-logarithmically with η, yielding a slope ($d\eta/ d \log \theta_H$) of -81 mV per decade (inset in Fig. 6.4). Placing this reciprocal value in eq. 1.8 for d ($\ln \theta_H$)/$d\eta$, a Tafel slope of -48 mV per decade results, similar to the

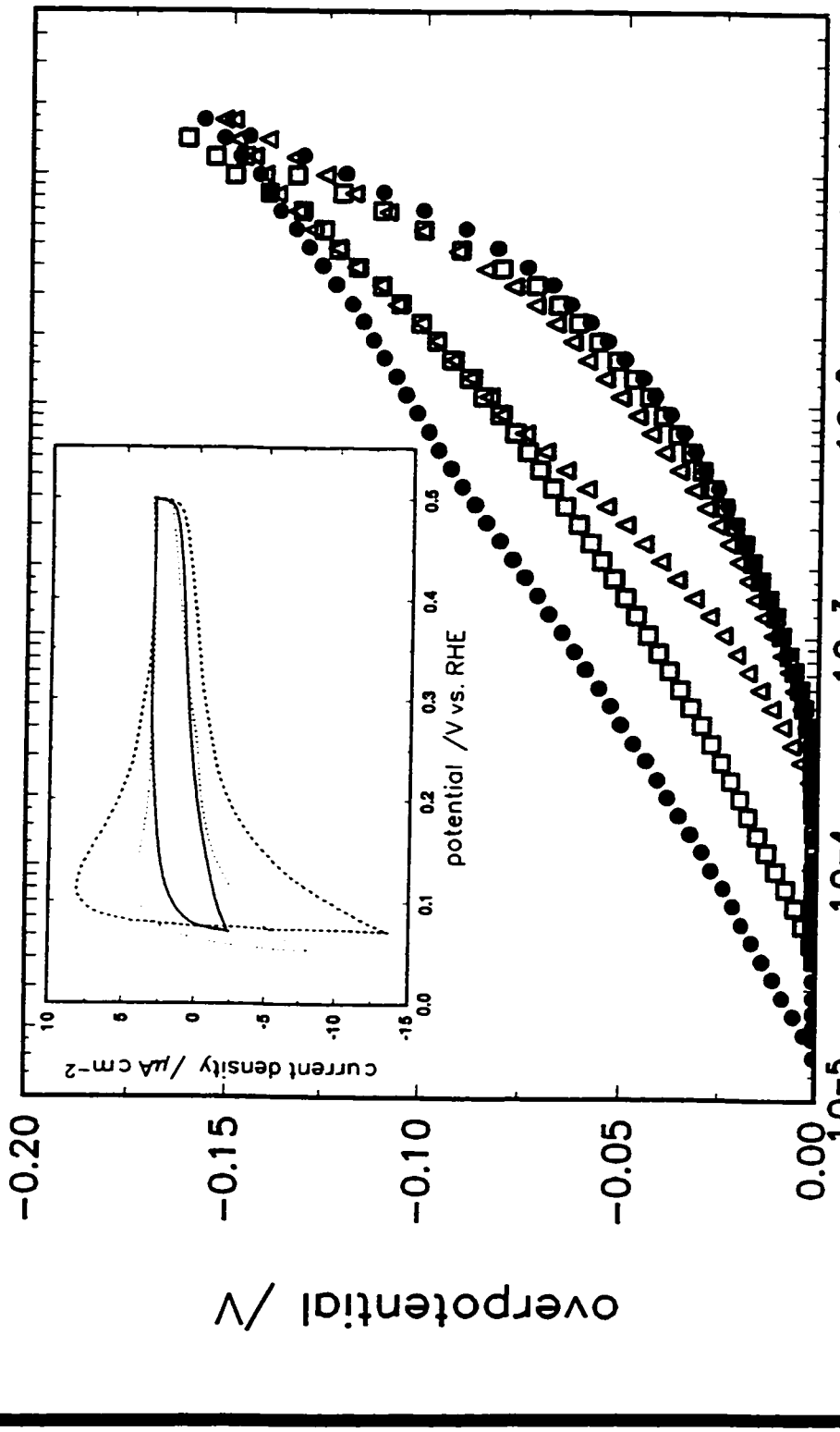

Fig. 6.3 Tafel plots of the HER showing ascending and descending polarizations taken after *ex situ* adsorption; (●) thiourea; (□) cysteine; (Δ)DES; Inset; Cyclic voltammograms taken before the cathodic polarizations shown. (—) thiourea; (· · ·) cysteine; (-----) DES, scan rate 50 mV sec^{-1}.

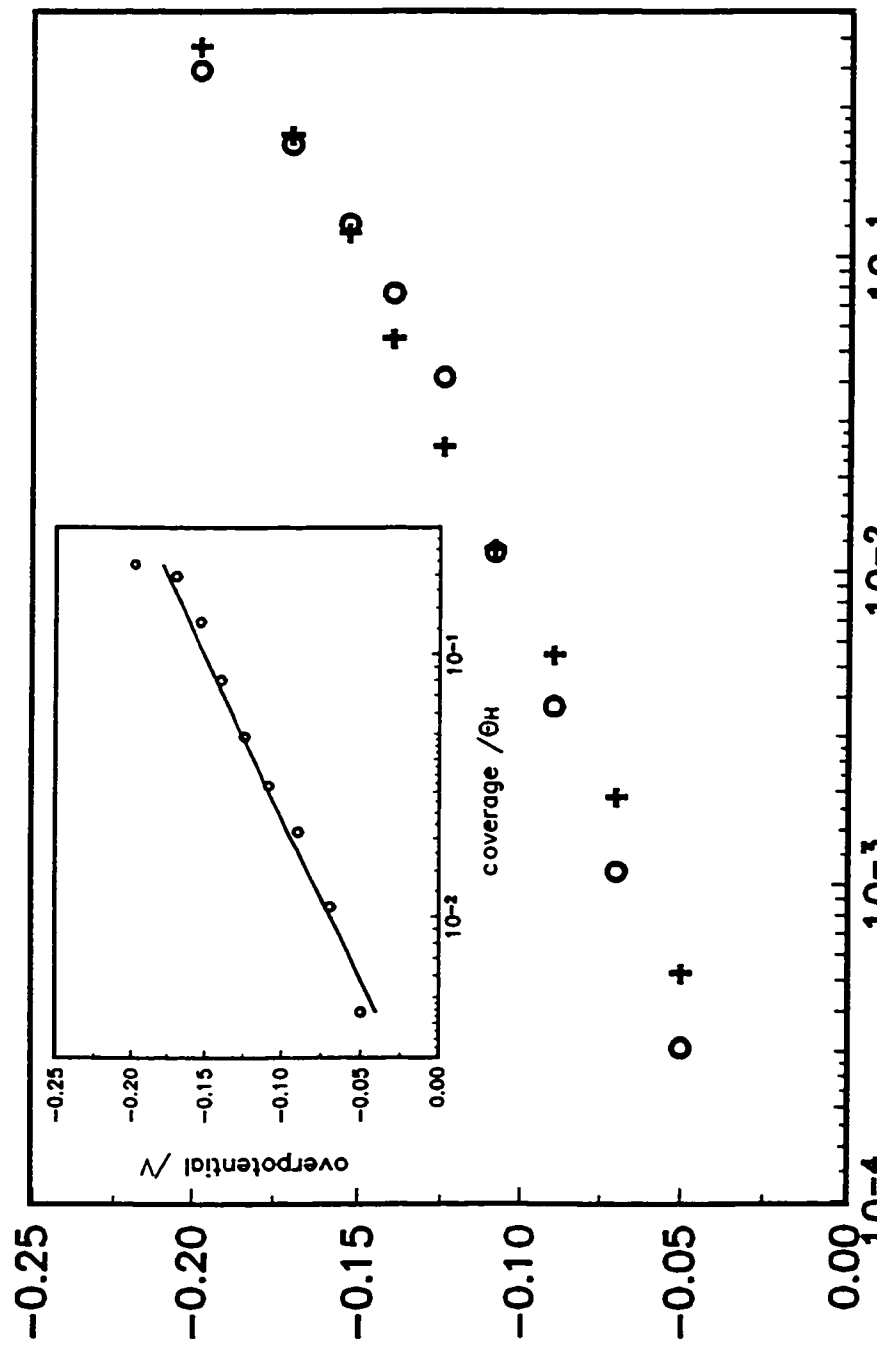

Fig. 6.4 Experimental (○) and simulated (✚)Tafel plots of the HER after *ex situ* adsorption of thiourea. Inset; Measured UPD H coverages at each corresponding overpotential in the main figure (slope = -81mV).

experimental value of -41mV per decade (Fig. 6.4). Correspondingly a calculated Tafel plot can be constructed using the $\eta(\theta)$ relationship and compared with the experimental behaviour as in Fig. 6.4.

6.3 Tafel Relations for Pt with the Poison Present in the Electrolyte

6.3.1 Thiourea

The effects of poisons on the kinetics and mechanisms of the HER should be considered in relation to both the changes in exchange current-density (i_o) and Tafel slope values. Especially the latter can be indicative of the effects of the poisons on the potential dependence of θ_H (eq. 1.8), and on the mechanism of the overall HER.

At active, clean Pt electrode surfaces, the Tafel relations, as discussed in Chapter 5, are significantly influenced by effects of H_2 diffusion, especially at lower overpotentials, but approach kinetic control as the overpotential is increased cathodically (see Chapter 5 and § 1.2.2). With thiourea present in the electrolyte, a linear Tafel region is observed over several decades of current-density (Fig. 6.5) having a slope near -60 mV. Such a value is difficult to account for conventionally (cf. eq. 1.8) through any of the steps 1 to 3 except with an unrealistic value of β or by invoking H surface diffusion [31]. However, the -60mV slope could be accounted for through a progressively changing coverage (θ_P) of the poison or a product of its reduction, e.g. H_2S, as for the *ex situ* results, that is dependent on η over the range of the observed Tafel plot. Corrections of Tafel curves for changes in θ_P with overpotential have been applied by several authors [7,8] to account for Tafel slopes numerically < -118 mV when thiourea is adsorbed on Hg.

Thiourea and its selenium analogue have been the poisons of choice in a number of

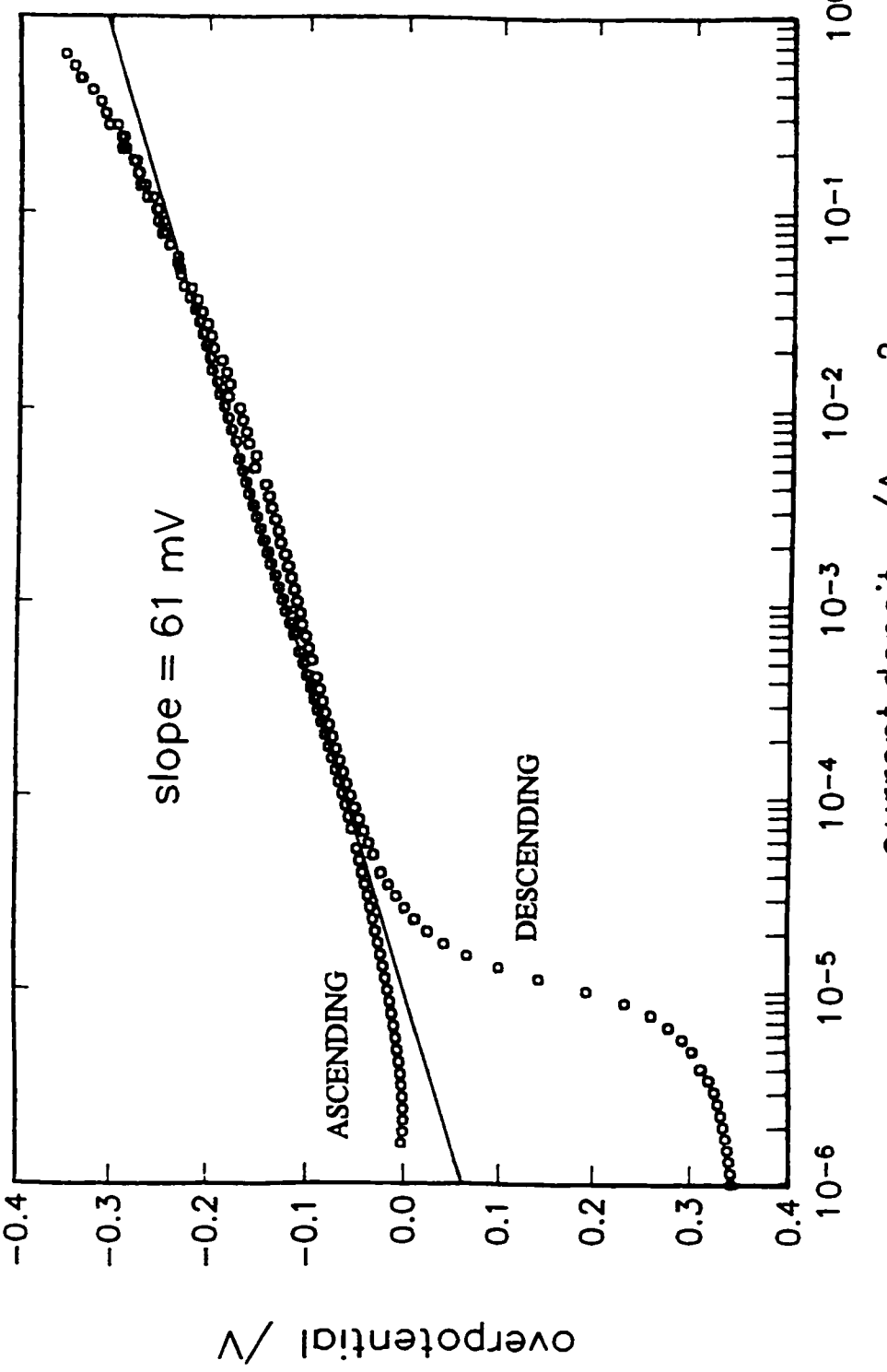

Fig. 6.5 Tafel plot of the HER in 0.5 mol dm^{-3} H_2SO_4 + 1.3 x 10^{-4} mol dm^{-3} thiourea, demonstrating the -60 mV Tafel slope and the 0.35 H_2S rest potential.

previous studies on hydrogen *ab*sorption into metals [9,10,11] and corrosion inhibition [12]. The double C-to-S bond is reactive in both reduction and oxidation [13] of thiourea. Reduction takes place during the HER at Pt to produce (at -50mV vs RHE) H_2S, PtS, PtS_2 and traces of colloidal sulphur [14,15] on the Pt surface[1], together with methylamine. However, thiourea is not reduced in the UPD H region contrary to N=O, and C=C groups which observably become reduced [16,17] by the UPD H species.

The reduction of thiourea [eqs. 6.IIa and 6.IIb] has a pronounced effect on the kinetics of the HER which cannot be explained by site blockage alone. Alternative steps are as follows, one involving chemisorbed OPD H:

$$M - thiourea_{(ads)} + 4\,M - H_{(ads)} \rightarrow H_2S + H_2C(NH_2)_2 + M \qquad \textbf{(6.IIa)}$$

and the other an electrochemical step involving proton discharge:

$$M - thiourea_{(ads)} + 4H_3O^+ + 4e^- \xrightarrow{k_P} H_2S + H_2C(NH_2)_2 + 4H_2O \qquad \textbf{(6.IIb)}$$

Neutral or protonated methylenediamine and H_2S are the products, the latter being also a strong poison. Elimination of NH_3 from methylene diamine would give $CH_2 = NH$ (the N- analogue of formaldehyde) the structure of which has been considered in the literature.[18] The H_2S produced in 6.IIa or 6.IIb could remain adsorbed, especially as it would arise directly from the centre, C=S, by which thiourea is adsorbed. However, because the solution was being bubbled with H_2, H_2S would tend to be expelled.

We now examine if the kinetic behaviour of the HER in the presence of thiourea can be attributed to the potential dependence of θ_P which determines the maximum

---

[1] PtS, PtS_2, and colloidal sulphur may not be a direct product of thiourea reduction but can result from the interaction of the resulting H_2S with the Pt surface.

attainable coverages by H. Literature on the electrochemical hydrogenation reaction (EHR) of nitro compounds and unsaturated hydrocarbons [16,19,20] suggests that at UPD potentials a mixed mechanism of catalytic and electrochemical hydrogenation is operative, *viz.* eqs. 6.IIa and 6.IIb for the reaction of thiourea. At overpotentials in the HER region, the electrochemical mechanism is predominant [20], i.e. eq. (6.IIb) for thiourea. Therefore, accepting eq. (6.IIb) as the mechanism of hydrogenation of thiourea we can write:

$$\frac{d\theta_p}{dt} = 0 = \upsilon_A - \upsilon_P \qquad \textbf{(6.1)}$$

where, for process 6.IIb,

$$\upsilon_P = k_P\,[H_3O^+]^4\;\theta_p\;\exp(-\beta\eta F/RT) \qquad \textbf{(6.2)}$$

and

$$\theta_p = \frac{k_A}{k_A + k_P\,\exp(-\beta\eta F\,/\,RT)} \qquad \textbf{(6.3)}$$

The effect of the potential dependence of θ_P in eq. (6.3) on the kinetics of the HER follows by writing the rate equations for the steps in the HER with the inclusion of θ_p; thus[2],

$$\begin{aligned}\upsilon_1 &= k_1\,(1-\theta_H-\theta_P)\exp(-\beta\eta f) - k_{-1}\theta_H\exp((1-\beta)\eta f) \\ &= k_1'\,(1-\theta_H-\theta_P) - k_{-1}'\theta_H\end{aligned} \qquad \textbf{(6.4)}$$

$$\upsilon_2 = k_2\,\theta_H\,\exp(-\beta\eta f) = k_2'\,\theta_H \qquad \textbf{(6.5)}$$

and

$$\upsilon_3 = k_3\,(\theta_H)^2 \qquad \textbf{(6.6)}$$

---

[2]We recognize that in a more sophisticated analysis, some dependence of k values on θ_P, due to lateral H/P interaction effects, could be included. However, comparison (see Table 6.1) of its fitted rate constants for the HER at a poison-free surface indicate that such interaction effects are not important or may have been engulfed into the fixed parameters defining the poison reaction.

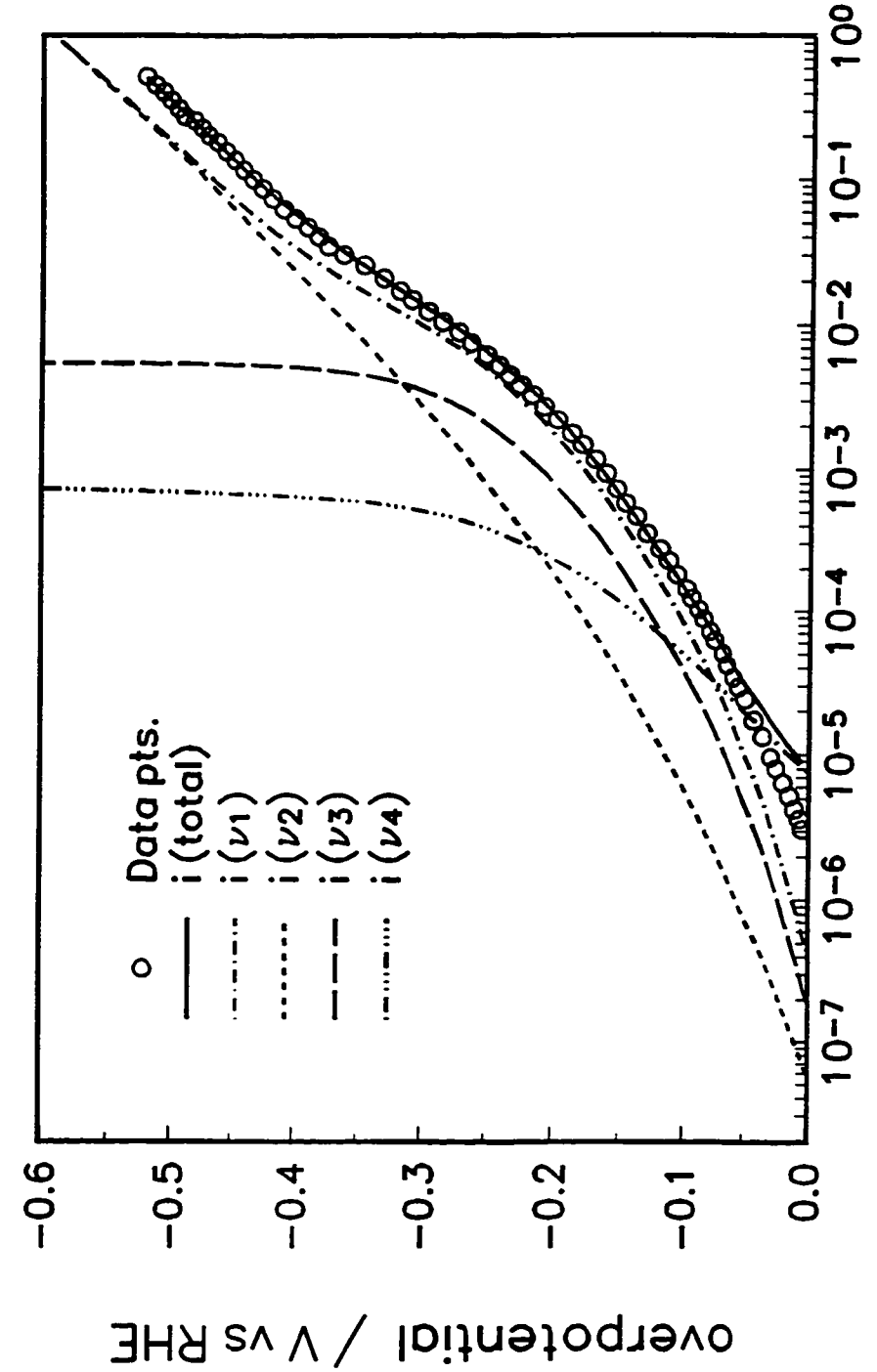

Fig. 6.6 Tafel plot for the HER and EHR in 0.5 mol dm^{-3} H_2SO_4 + 5.1 x 10^{-3} mol dm^{-3} thiourea. (O) experimental data; (—) best fit line; the broken lines represent the contributions of each of the reaction steps; (υ_1, υ_2, and υ_3) for the HER; (υ_4) for the EHR, in units of A cm^{-2}.

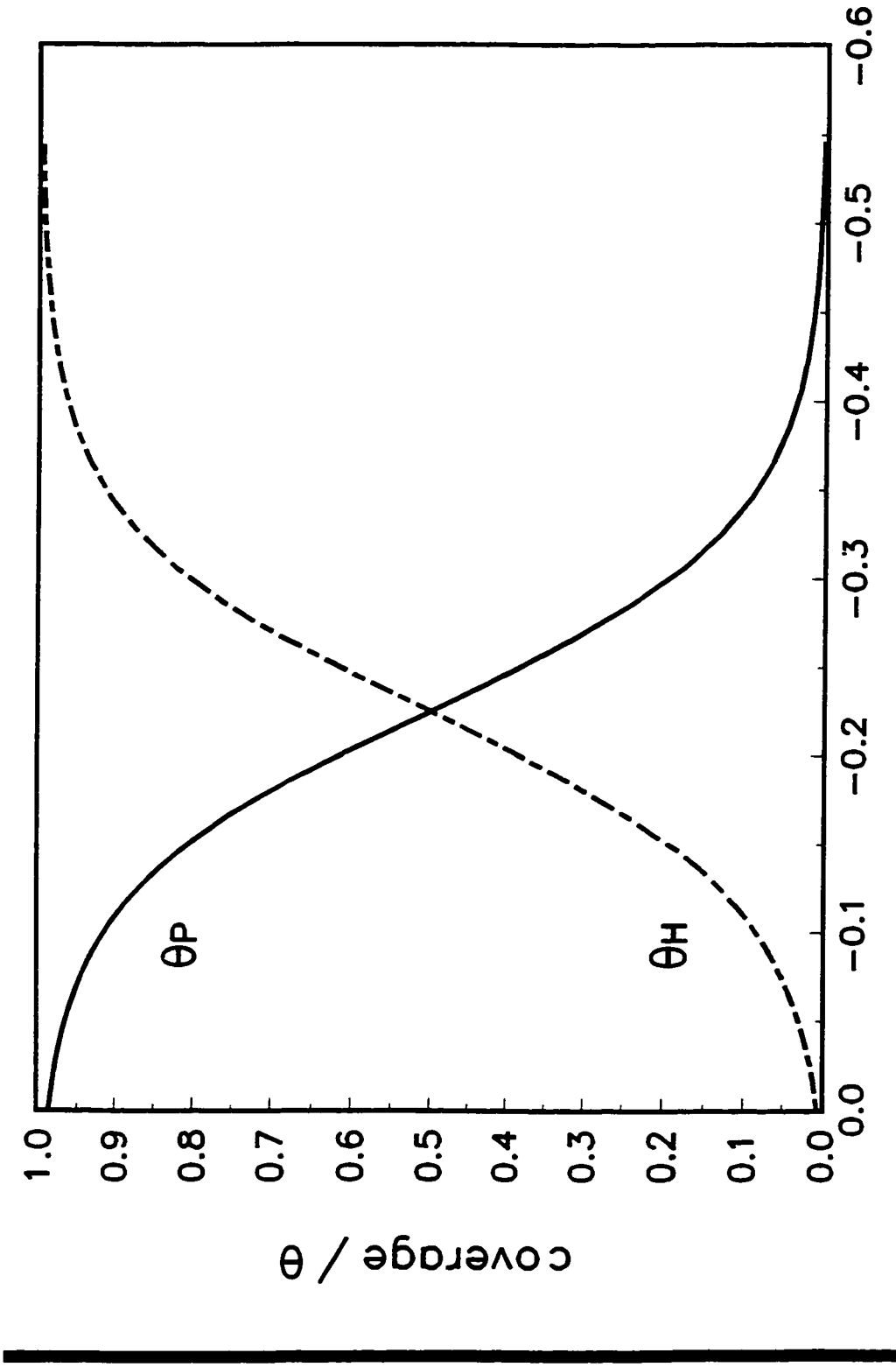

Fig. 6.7 Coverage *vs.* overpotential calculated from the rate constant determine from the fitting of the experimental data in Fig. 6.6 as listed in Table 6.1.

The steady-state value of θ_H can then be determined using eqs. (6.4)-(6.5) and eq. (6.3), giving:

$$\theta_H = \frac{-(k_1' + k_{-1}' + k_2')}{4k_3} - \frac{\sqrt{(k_1' + k_{-1}' + k_2')^2 - 8\,k_1'(1 - \theta_P)\,k_3}}{4k_3} \qquad (6.7)$$

The η *vs* log i Tafel behaviour can then be calculated from:

$$i = F(\upsilon_1 + \upsilon_2) + 4F\upsilon_P \qquad (6.8)$$

On the basis of the above approach, the experimental i(η) behaviour for thiourea hydrogenation in 0.5 mol dm^{-3} H_2SO_4 , occurring during the HER, was fitted using a non-linear least squares calculation as shown in Fig. 6.6 for which the rate constants required for a good fit are given in Table 6.1.

Table 6. 1 **Rate constants derived from NLS fitting of equation 6.8 to the i(η) data shown in Fig. 6.6**

			k (mol cm^{-2} s^{-1})		
k_1	k_{-1}	k_2	k_3	k_A	k_4
3.8×10^{-7}	5.1×10^{-7}	1.0×10^{-10}	5.6×10^{-8}	1.4×10^{-9}	1.95×10^{-11}

The resulting relative coverage *vs.* potential relationships for both thiourea and the OPD H are shown in Fig. 6.7. Evidently this treatment gives a good account of the observed poisoning effect of thiourea (or derived H_2S, eqs. 6.IIa or 6.IIb) on the kinetics of the HER. The rate constants in Table 6.1 for the HER kinetics are all in good respective agreement with those found in the literature [21] for the HER on a clean Pt

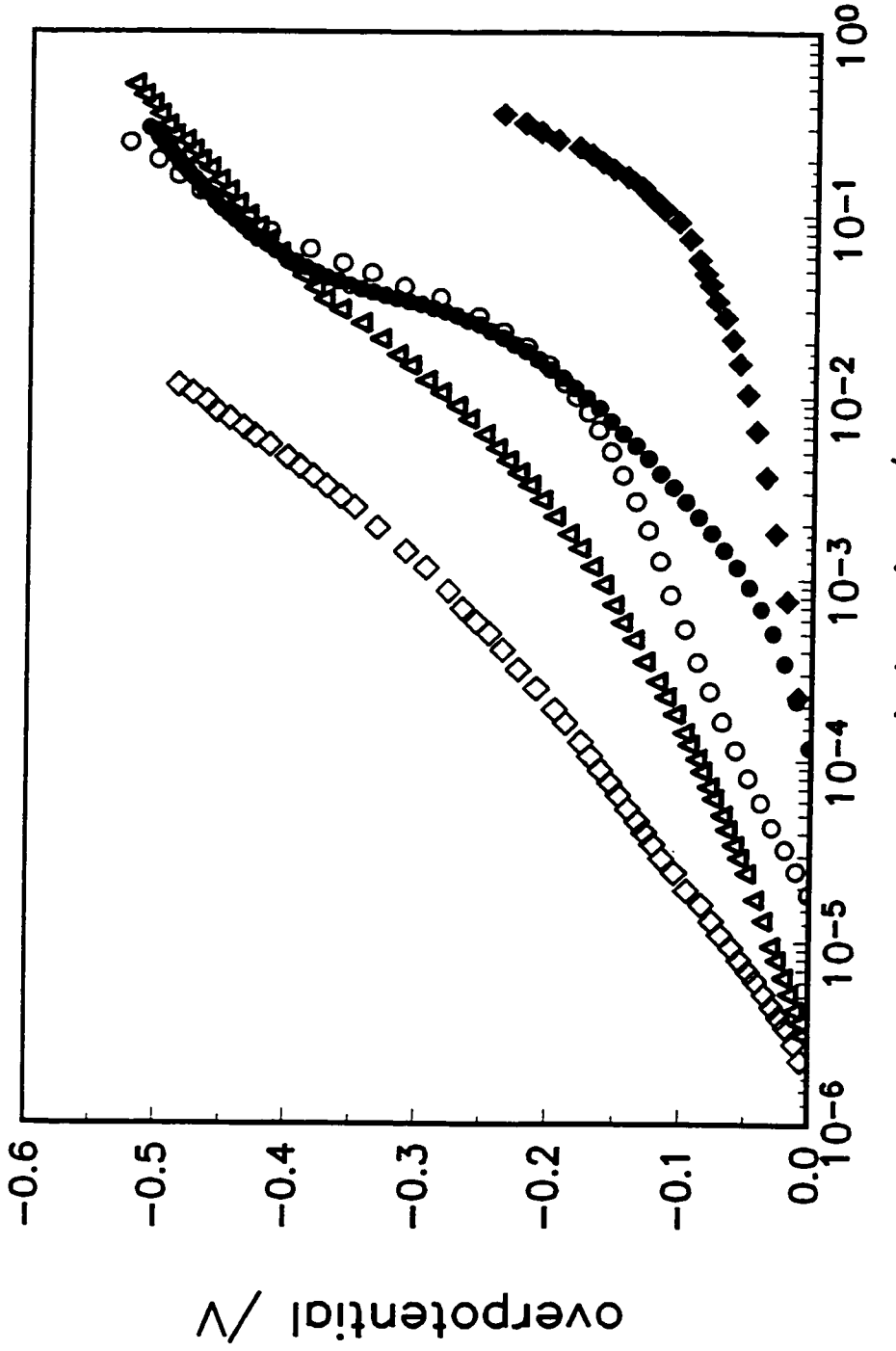

Fig. 6.8 Tafel plots for the HER in various supporting electrolytes plus 5×10^{-3} mol dm^{-3} thiourea. (◇) 2 mol dm^{-3} H_2SO_4; (Δ) 0.5 mol dm^{-3} H_2SO_4; (○) 0.5 mol dm^{-3} NaOH; The corresponding "clean" behaviour in (●) 0.5 mol dm^{-3} NaOH; and (◆) 2 mol dm^{-3} and 0.5 mol dm^{-3} H_2SO_4.

cathode. The rate constants for the EHR, k_A and k_P, are for the step of adsorption of the poison (eq. 6.I), and for the coupled hydrogenation\desorption step (eq. 6.IIb). The value of k_A derived from the fitting of the experimental kinetic results obtained at the rotated electrode (2500 rpm) is 3-4 orders of magnitude lower than the value calculated for mass transfer of the thiourea to the rotating sphere. This indicates clearly that the EHR, proceeding through an adsorbed intermediate, is not diffusion controlled.

Another factor which must be addressed for the case of thiourea is its acid/base properties; its protonation constant is pK = 1.44 [22] . Figure 6.8 demonstrates the effect this has on the behaviour of the HER in three different electrolytes: 2 mol dm^{-3} H_2SO_4, 0.5 mol dm^{-3} H_2SO_4, and 0.5 mol dm^{-3} NaOH, having pH values of -0.30, 0.292, and 11.7 respectively. In 2 mol dm^{-3} H_2SO_4 the fraction of thiourea protonated is 10~20 percent. The polarization behaviour for this case indicates that the coverage by thiourea does not change with potential and the adsorption of the protonated species is likely to be enhanced at higher overpotentials. In 0.5 mol dm^{-3} NaOH, on the other hand, where thiourea is not protonated, we observe, at overpotentials < -100 mV, $i(\eta)$ behaviour similar to that in the absence of the poison indicating complete desorption of thiourea from the active sites for the HER (i.e. equivalent OPD H coverages in the clean and poisoned electrolytes). Using 0.5 mol dm^{-3} H_2SO_4 the fraction protonated is 2-4 percent.

It is seen (Fig. 6.8) that the behaviour when 0.5 mol dm^{-3} H_2SO_4 is used, is intermediate between that in 0.5 mol dm^{-3} NaOH (unprotonated) and 2 mol dm^{-3} H_2SO_4 (15 percent protonated), which provides some evidence that in 0.5 mol dm^{-3} H_2SO_4 a mixture of both species could cover the surface. For thiourea in aqueous HCl for Hg as

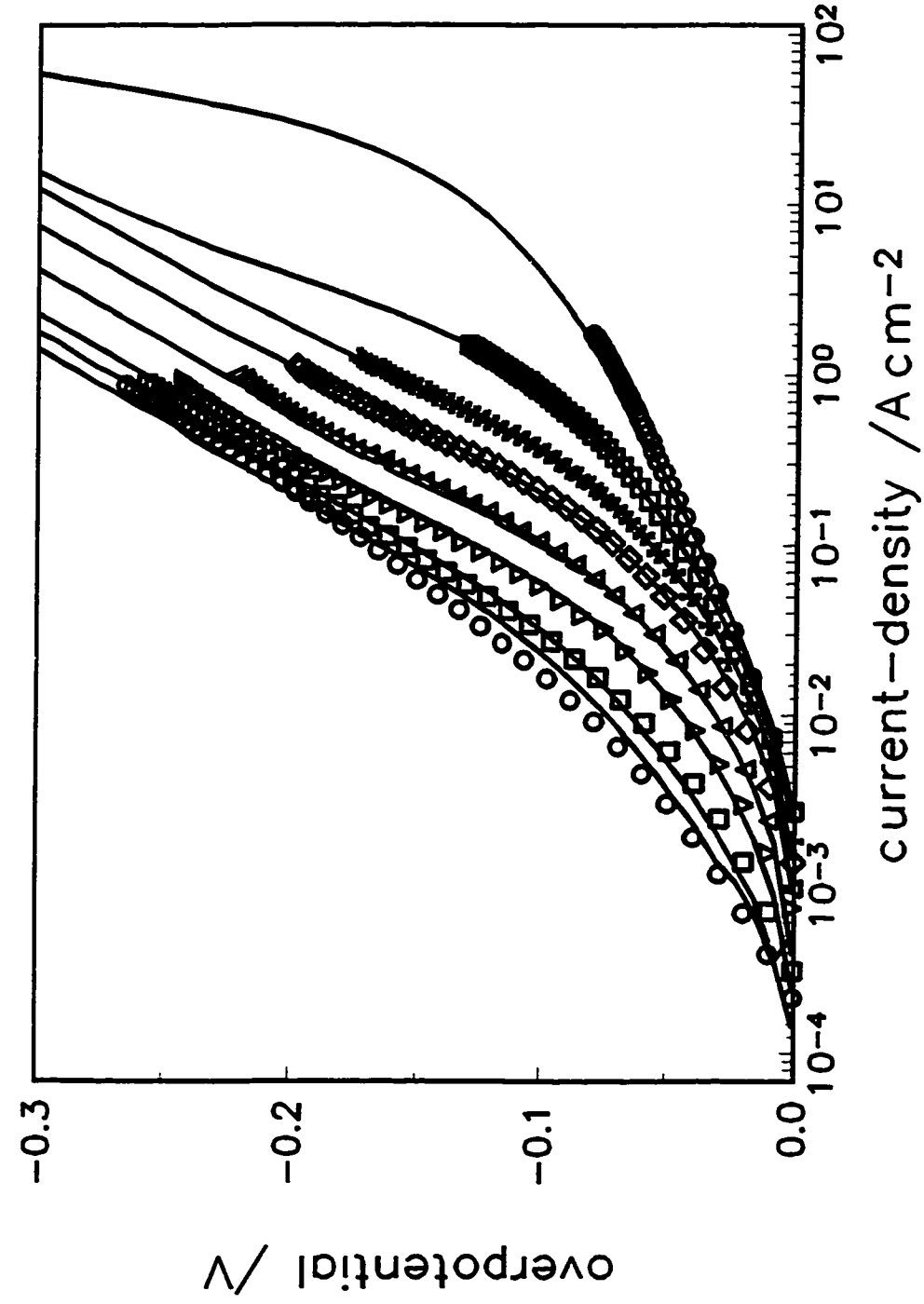

Fig. 6.9 Tafel plots and best fit lines for the HER with stable coverages of thiourea (see text). Thiourea conc. = 2 x 10^{-7} mol dm^{-3} to 4 x 10^{-6} mol dm^{-3}.

the substrate it was proposed [7] that the adsorbed protonated species acted as a catalytic centre for rapid H_3O^+ discharge. On Pt the HER on the bare substrate occurs at a faster rate than discharge from the adsorbed protonated species; the latter therefore only plays the role of a site blocker at Pt. In summary then it appears that the protonated form, being able to remain on the surface up to elevated cathodic overpotentials, is a more effective poison than the neutral form, which becomes desorbed with increasing overpotential in the way usually expected for a neutral molecule adsorbate.

In order to obtain a better understanding of the role of thiourea coverage on the kinetic parameters of the HER, experimental conditions were set so that the coverage *did not* change with potential. This was achieved by first applying a cleaning cycle in the

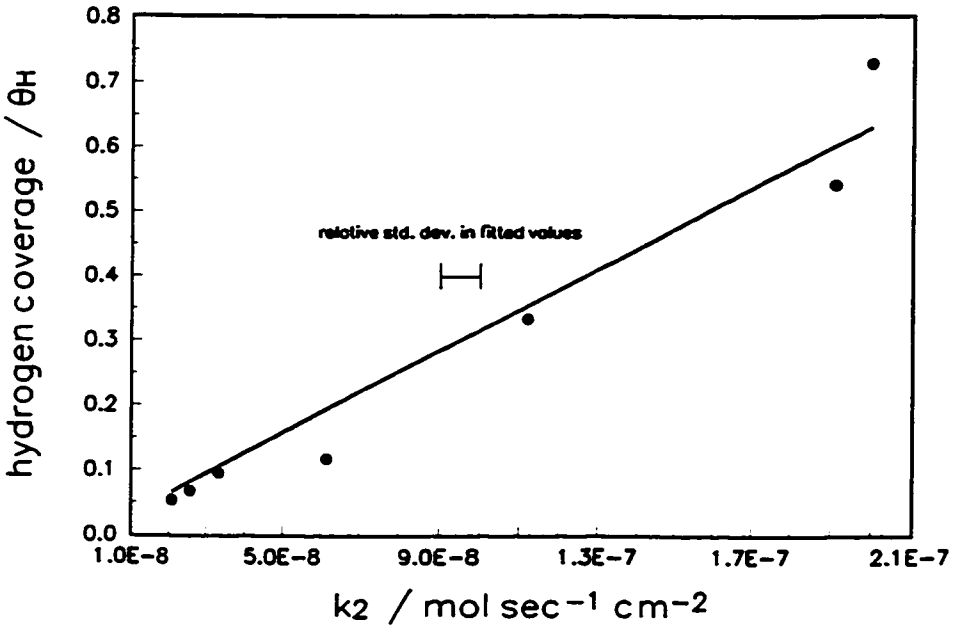

Fig. 6.10a UPD H coverage *vs.* the rate constant for step 2 in the HER mechanism. Rate constants obtained from fitting of the data in Fig. 6.9.

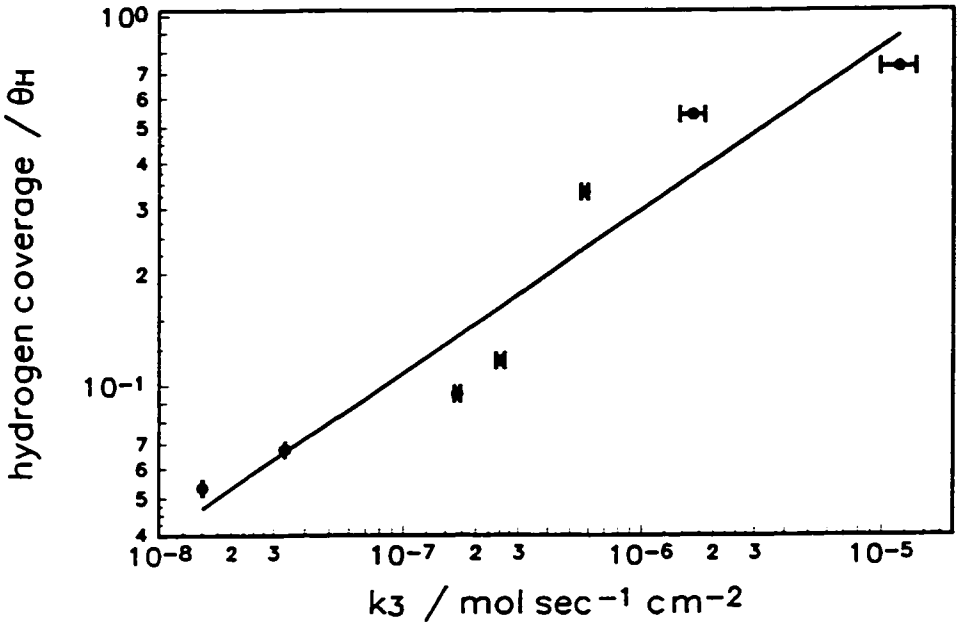

Fig. 6.10b UPD H coverage *vs.* the rate constant for step 3 in the HER mechanism (slope = 2.2). Rate constants obtained from fitting of the data in Fig. 6.9.

oxide region followed by an adsorption step in the double-layer potential region which produced a surface coverage defined for a given concentration by a relationship similar to that shown in Fig. 6.2 for each point on the polarization curve; also the time of polarization was restricted so that hydrogenation and desorption would not significantly take place. In this way a family of Tafel type measurements could be collected, Fig. (6.9), which corresponded to series of surface coverages by thiourea, under these conditions constant with overpotential. Note the larger current-densities for the HER in the clean 0.5 mol dm^{-3} H_2SO_4 in Fig. 6.9 compared with Fig. 6.8. These differences are a result of differing electrode geometries used to obtain the two measurements (Fig. 6.8, rotating

disk *vs.* a rotating micro-sphere electrode Fig. 6.9), with the case in Fig. 6.9 having the better hydrodynamic conditions, and having a Tafel curve closer to that in the absence of H_2 diffusion (see Fig. 5.3 and 5.14). Figure 6.9 also shows the results from the fitting of the kinetic equations for the HER to each curve in the absence of EHR. For the fitting, it was not necessary for θ_P to be specifically included since it was absorbed into the rate constants, being almost constant with respect to potential.

Comparing the variation in the fitted rate constants for the individual reaction steps as a function of the surface coverage of UPD H as determined from cyclic voltammetry (Figs. 6.10a and 6.10b), it is found that the rate constants for the alternative rate-limiting steps (Heyrovsky and Tafel steps) have direct relationships to θ_H while, for the electrochemical H adsorption/desorption step (Volmer), the rate constant values seem independent of coverage.

6.3.2 Cysteine and 2,2' diethanolsulphide (DES)

Cysteine is a common amino acid with a thiol group which has a chemistry intermediate between that of the C=S group in thiourea and the C-S-C group in 2,2' diethanolsulphide (DES). Cysteine will carry a positive charge on its NH_2 group in 0.5 M H_2SO_4. The charged nature of the cysteine species could give rise to some double-layer effects, but these are probably much weaker than the effect of site blockage. At shorter adsorption times, i.e. for less than complete poison coverages, the forward and reverse scans of overpotential were similar, which indicates only a minor dependence of poison coverage on η. If sufficient time is given, *ca.* 16-24 h., cysteine and DES produce films which virtually eliminate UPD of H. A dependence of θ_P, for cysteine and DES, on

η is observed when $\theta_P \approx 1$ (full coverage) initially before any H_2 has been evolved; this is similar to the behaviour with thiourea but in that case such a dependence was seen regardless of the initial surface coverage.

In order to explore this behaviour a series of potential-relaxation transients (Fig. 6.11) were recorded corresponding to various initial overpotentials, on an electrode fully covered with a cysteine film. For a brief introduction to the potential-relaxation technique, see § 9.4. Note that similar trends were observed using thiourea and DES on Pt in 0.5 M H_2SO_4 and also on a Pd substrate with an adsorbed thiourea film. Numerical simulations were undertaken (Fig. 6.12) using the parameters given in Table 6.2 but non-linear least squares fitting of the experimental data was unsuccessful due to the anomalous potential dependence, $d\eta/d(\log t) \neq 118$ mV, of the process of double-layer capacitance relaxation which would result when either of the normal 2-step HER mechanisms are operative [23]. This anomalous behaviour may arise from a charge-transfer reaction occurring between the poison and the Pt substrate during the double-layer relaxation. Although a good fit could not be achieved, the simulation illustrates how the effect of the potential dependence of θ_P on the HER kinetics accounts for the salient features of the experimental results.

A correlation was achieved between the simulated and experimental results, by taking constant "chemical", potential-independent, rate constants; other potential-dependent terms were the C_{dl} (double-layer capacitance), q_1 (charge for maximum H coverage in the presence of P), and θ_P (poison coverage). These three parameters are not independent and, as expected, q_1 decreases with increasing θ_P , and the increase in the

double-layer capacitance may also be accounted for by a decrease in the separation of the charges across the interface, especially if charge is held by the poison itself, e.g. as for the case of cysteine at acid pH's.

Table 6.2 Rate constants[3] (k) in mol cm^{-2} s^{-1}, adsorption parameters and double-layer capacitance values used for the simulation of the potential-relaxation curve in Fig. 6.12

k_1	k_{-1}	k_2	k_3	C_{dl} ($\mu F\ cm^{-2}$)	q_1 ($\mu C\ cm^{-2}$)	θ_p
4.7×10^{-7}	9.35×10^{-7}	4.6×10^{-8}	6.6×10^{-7}	84	8.7×10^{-4}	0.94
"	"	"	"	74	9.7×10^{-4}	0.89
"	"	"	"	42	1.25×10^{-3}	0.8
"	"	"	"	20	2.0×10^{-3}	0.68
"	"	"	"	19	2.1×10^{-3}	0.41
"	"	"	"	19	3.24×10^{-3}	0.045

In order to deal with the possibility that θ_p may change during the potential relaxation process, we have studied the impedance behaviour (Fig. 6.13) over a frequency range of 300 kHz to 0.1 Hz for the HER in the presence of low concentrations of cysteine and thiourea (incomplete coverages). Three dispersion processes were observed

---

[3] The diffusive terms for H_3O^+ and H_2, e.g. the ratio of the surface-concentration to the bulk-concentration seen in the rate-equations in Chapter 5, are implicit in the rate-constants in Table 6.2. As stated in the above text the diffusion influence of H_2 drops off dramatically with an increasing degree of poisoning, this therefore allows the ratio of concentrations, i.e. surface to bulk, to be taken as one. Also the rate constants throughout this thesis implicitly contain any double-layer effects which may be present. This effect will be very small because a large excess of supporting electrolyte was used in *all* the experiments.

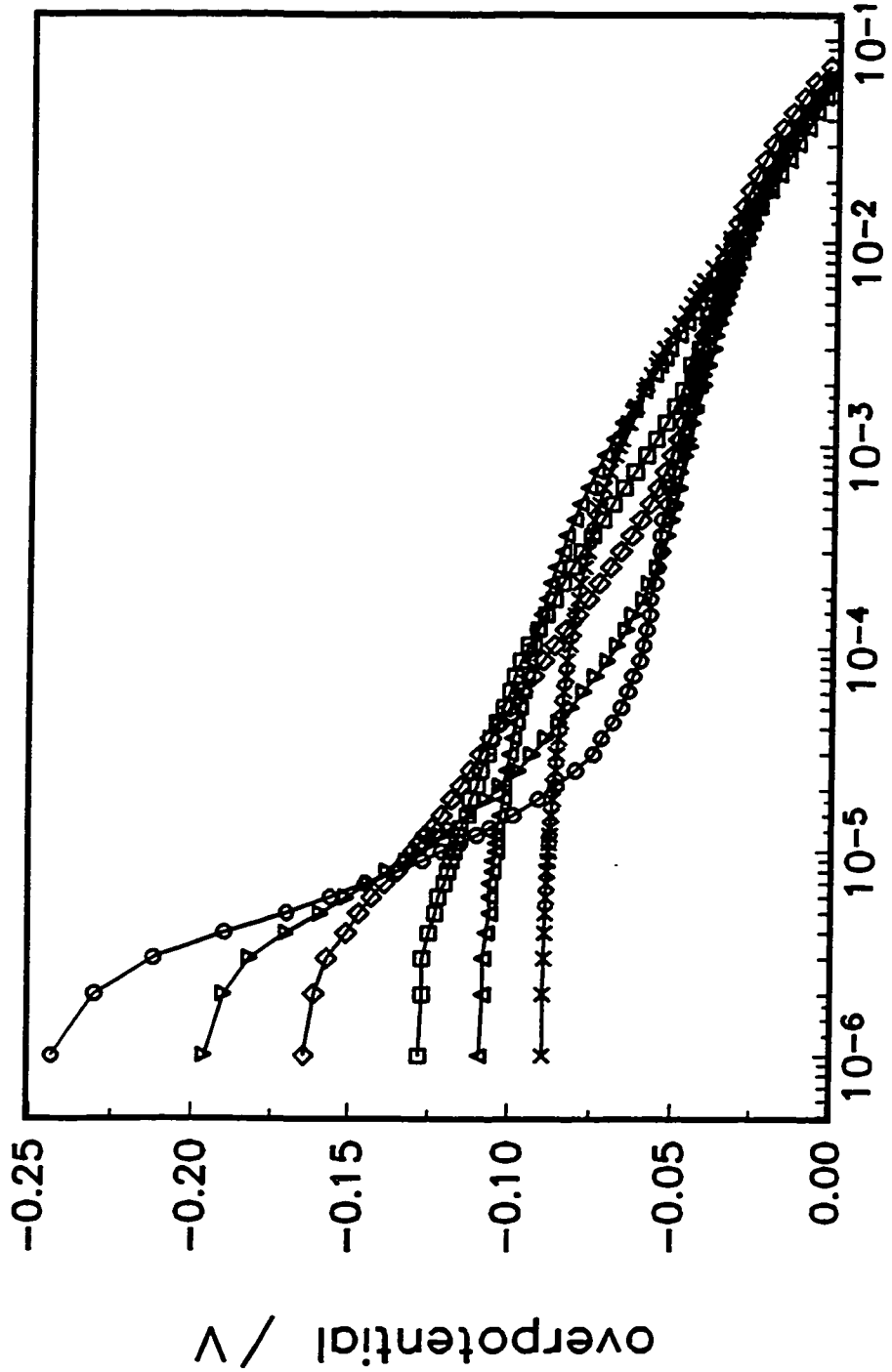

Fig. 6.11 Potential relaxation transients taken in 0.5 mol dm^{-3} H_2SO_4 + 1.4 x 10^{-4} mol dm^{-3} cysteine at current densities (X) 2.5 x 10^{-3}, (Δ) 6.3 x 10^{-3}, (□) 2.5 x 10^{-2}, (◇) 8.8 x 10^{-2}, (▽) 2.5 x 10^{-1} and (○) 8.8 x 10^{-1} A cm^{-2}. Lines are drawn for clarity.

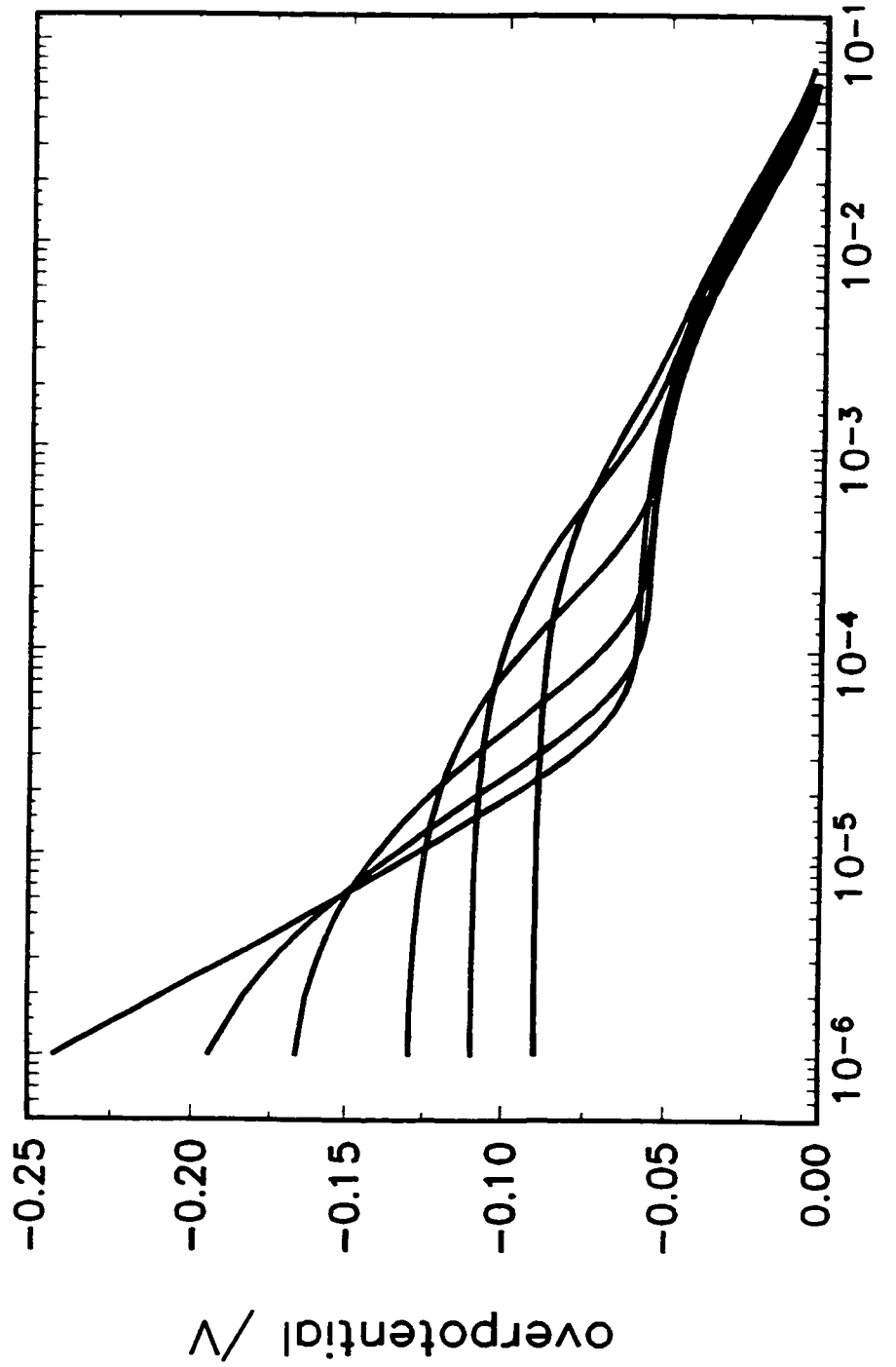

Fig. 6.12 Simulated potential relaxation curve using the rate constants given in Table 6.2 and initial potentials corresponding to those of the experimental data from Fig. 6.11.

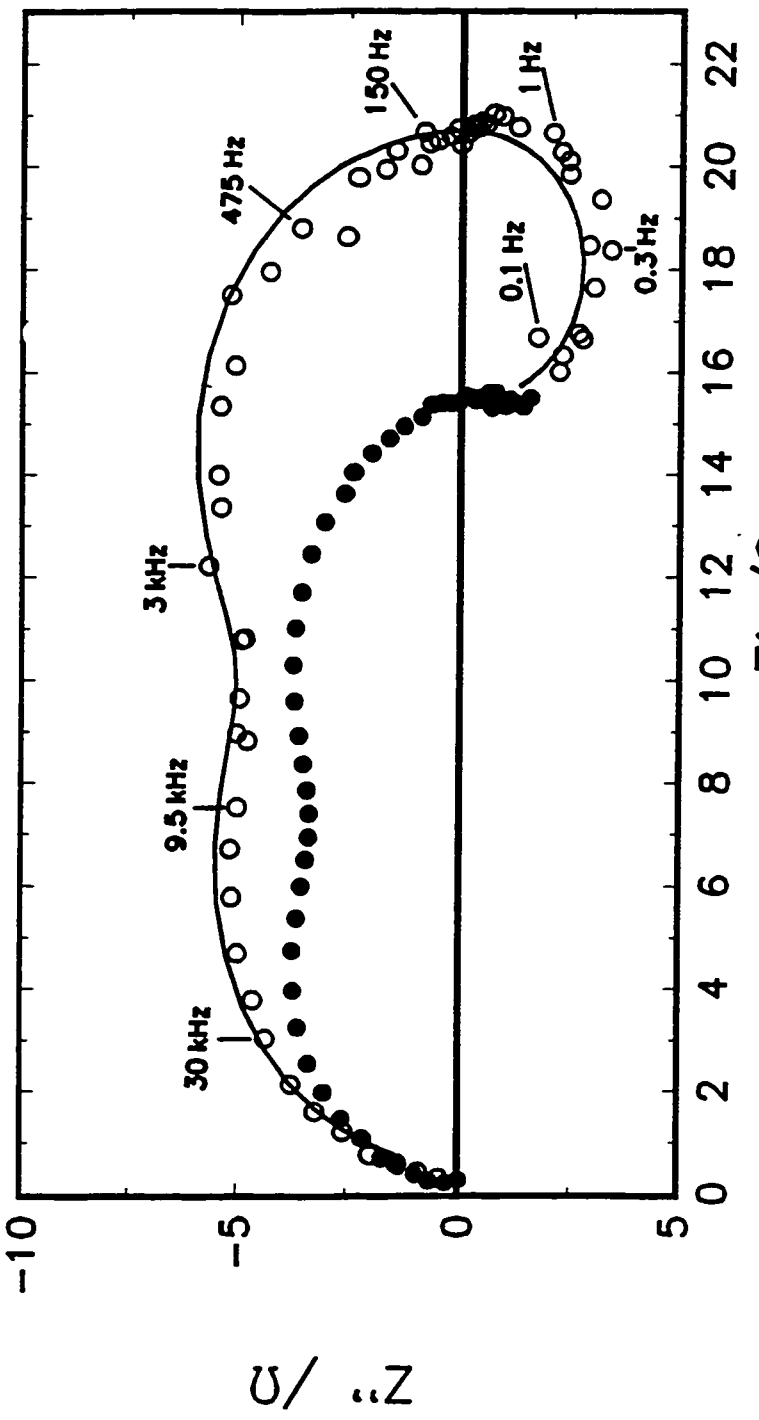

Fig. 6.13 Complex plane plot taken at η = -125 mV in 0.5 mol dm^{-3} H_2SO_4 + 5 x 10^{-6} mol dm^{-3} (●)cysteine and (○) thiourea; (—) best fit lines calculated using eq. 4.34 derived in § 4.3.2 for the two adsorbate system.

which can be assigned to the relaxation of the double-layer capacitance, the OPD H pseudocapacitance through the charge-transfer impedance and a pseudoinductance for the relaxation of θ_P. This is consistent with the two-adsorbate (H and P) impedance model derived in § 4.3.2 and also with theoretical investigations on similar systems by Zoltowski [24] and by Bai and Conway [24-27] which indicate that such inductive behaviour arises when one or both of the adsorbate coverages (here P) decrease with increasing overpotential, with the condition that the current is also increasing. Recognizing that the relaxation of θ_P is associated with the third time-constant (i.e. for the inductive semicircle), we can evaluate semi-quantitatively the relaxation rate of θ_P. For thiourea the relaxation process occurs at frequencies < 1 Hz and for cysteine < 0.1 Hz. This indicates that θ_P will be stable within the time frame of the potential relaxation process, i.e. times < 0.1 sec, and validates the approach of using constant θ_P terms when simulating each potential relaxation transient.

6.4 Conclusions

1. Experimental procedures based on cyclic voltammetry, potential-step transients and potential relaxation measurements at Pt have enabled the competitive adsorption of three S-containing catalyst poisons *vis à vis* H to be quantitatively evaluated.

At Pt, both the UPD and the OPD of H are substantially blocked by the three poisons studied, the effects being strongest with thiourea. Measurements of the blocking of adsorption of the underpotential deposition of H by thiourea, cysteine and DES enable competitive adsorption isotherms for the three poisons to be constructed.

2. Thiourea can, however, undergo reductive desorption that makes its coverage dependent on overpotential, resulting in a Tafel relation for the HER having an unusual slope value of *ca.* -60mV. Cysteine and DES suffer desorption only from high surface coverages and consequently this effect is smaller than with thiourea.

3. At sufficiently low pH, thiourea is protonated, resulting then in a diminished potential dependence of its adsorption.

References

1. B. MacDougall, B.E. Conway and H. Kozlowska, J. Electroanal. Chem., 32 (1971) 15.
2. E. Protopopoff and P. Marcus, Surf. Sci., 161 (1985) 533.
3. E. Protopopoff and P. Marcus, Surf. Sci., 169 (1986) L237.
4. K.D. Troung and P.A. Rowntree, J. Phys. Chem., 100/51 (1996) 19917.
5. B.E. Conway and L. Bai J. Electroanal. Chem., 198 (1986) 149.
6. B.E. Conway and B.V. Tilak, Adv. in Catalysis, 38 (1992) 1.
7. E. Dayalan and R. Narayan, J. Electroanal. Chem., 179 (1984) 167.
8. N. Mauree and L. Gierst, Collect. Czech. Chem. Com., 36 (1971) 389.
9. B. Baranski and M. Smialowski, J. Phys. Chem. Solids, 12 (1959) 206.
10. Z. Sklarska-Smialowski and M. Smialowski, J. Electrochem Soc., 110 (1963) 444.
11. M. D. Archer and N.C. Grant, Proc. Roy. Soc. Lond. A, 395 (1984) 165.
12. K. Pillai and R. Narayan, J. Electrochem. Soc., 125 (1978) 1393.
13. V.P. Vasil'ev, V.I. Shorokhova, A.V. Katrovtseva and G.S. Lamakina,

Electrokhimiya, 19 (1983) 453.

14. A.A. Sutyagina, N.I. Il'chenko, M.N. Semenenko and G.D. Vovchenko Electrokhimiya, , 15 (1979) 1094.

15. A.A. Sutyagina, I.L. Volchkova and M.N. Semenenko, Rus. J. Phys. Chem., 63 (1989) 714.

16. Y.B. Vassiliev, V.S. Bagotzky, O.A. Khazova, T.N. Yastrebova and T.A. Sergeeva, Electrochim. Acta, 26 (1981) 563.

17. H. Ebert, R. Parsons, G. Ritzoulis and T. VanderNoot, J. Electroanal. Chem., 264 (1989) 181.

18. A. Streitwieser and C.H. Heathcock, "Introduction to Organic Chemistry", MacMillan, NewYork, 1976, p.13.

19. G.A. Bogdanovsky, G.P. Khomchenko and A.I. Shlygin, "Catalytic Reactions in Liquid Phase", Alma-Ata, Acad. Sci. Kayakh SSR, 1963, p. 276.

20. G.A. Bogdanovsky and G.D. Vovchenko, Kinetika Kataliz., 10 (1969) 923 and Electrokhimiya, 6 (1970) 318.

21. L.Bai, D.A. Harrington and B.E. Conway, Electrochim. Acta, 32 (1987) 1713.

22. V.P. Vasil'ev, V.I. Shorokhova, N.K. Grechina and L.V. Katrovtseva, Russian J. of Inorg. Chem., 23 (1978) 1274.

23. D.A. Harrington and B.E. Conway, J. Electroanal. Chem., 221 (1987) 1.

24. P. Zoltowski, J. Electroanal. Chem., 240 (1988) 53.

25. L. Bai and B.E. Conway, Electrochim. Acta, 38 (1993) 1803.

26. L. Bai and B.E. Conway, J. Electrochem. Soc., 138 (1991) 2897.

27. L. Bai and B.E. Conway, J. Electrochem. Soc., 137 (1990) 3737.

28. G. Jerkiewicz, J.J. Borodzinski, W. Chrzanowski and B.E. Conway, J. Electrochem. Soc., 142 (1995) 3755; G. Jerkiewicz, J.J. Borodzinski, W. Chrzanowski and B.E. Conway in, Proc. Symp. Electrochemistry and Materials Science of Cathodic Hydrogen Absorption and Adsorption, 94-21 (1995) 44.

29. P. Marcus and E. Protopopoff, J. Chim. Phys., 88 (1991) 1423.

30. P. Marcus and E. Protopopoff, C.R. Acad. Sci., Paris, 308 (1989) 1127.

31. J. O'M Bockris and H. Mauser, Can. J. Chem., 37 (1959) 475.

Chapter 7

Electrochemical Permeation of H Through Metal Membranes

7.1 Mechanism and Numerical Treatments

The following two simple conditions can be envisioned for the diffusion of H into and through metal membranes, e.g. Pd, Fe and Ni.

A) *constant concentration of H at the entrance face*

$$t \le 0 \qquad E = E_1 \qquad c(x,t) = 0 \qquad \textbf{(7.1a)}$$

$$c(0,t) = c_1$$

$$t > 0 \qquad E = E_2 \qquad c(0,t) = c_2 \qquad \textbf{(7.1b)}$$

where c(0,t) is the H concentration just inside the surface of the metal (x = 0), and with c_1 and c_2 denoting the value of c(0,t) before and after the application of the cathodic polarization; c_1 can have a finite value or zero depending on the initial potential setting (E_1), see Fig. 8.9. These conditions can be realized when θ_H and therefore c_2, following from eqs. 1.24 and 1.25, are constant in time after the application of the potential step for the purpose of inducing a transient of H diffusion flux into the metal. We denote this condition as (c) standing for constant surface concentration. Before solving the second diffusion equation of Fick, it is convenient to introduce the following reduced variables:

$$\tau = Dt/l^2$$

$$\chi = x/l$$

$$\sigma(\chi,\tau) = c(x,t)/c_o$$

$$\text{and} \qquad i(\tau) = [i(t)-i_1]/[i_\infty - i_1]$$

with D = the H diffusion coefficient, t = time, c(x,t) = the concentration at any plane x

inside the metal and at any time (at $t = 0$, $c(x,t) = c_1$), i_∞ is the steady-state permeation current-density and i_1 is the steady-state permeation current-density at $t < 0$; i_1 may or may not be zero, as it is dependent on the value of E_1.

Fick's second law is then solved[1] with the above boundary conditions in dimensionless form giving the dimensionless permeation current *vs.* time response as:

$$i(\tau) = -(\partial\sigma/\partial\chi)_{\chi=1} = 1 + 2\sum_{1}^{\infty}(-1)^n \exp(-n^2\pi^2\tau) \qquad (7.2)$$

B) *constant flux of H at the entrance face*

The initial boundary condition is the same as that expressed above in eq. 7.1a and the boundary condition after application of the polarization is:

$$t > 0 \qquad (\partial c(0,t) / \partial x) = \text{constant} \qquad (7.3)$$

This condition states that upon application of the cathodic potential or current step a constant flux of H into the metal is generated. This case is denoted as **(f)** standing for constant surface flux. Again solving Ficks' second law with the above reduced parameters, the dimensionless current *vs.* time relationship is now expressed as:

$$i(\tau) = -(\partial\sigma/\partial\chi)_{\chi=1} = 1 - \frac{4}{\pi}\sum_{0}^{\infty}\frac{(-1)^n}{2n+1}\exp(-¼(2n+1)^2\pi^2\tau) \qquad (7.4)$$

---

[1] In the literature both Laplace [2,3] and Fourier [1,4] transforms have been used to derive the current *vs.* time behaviour. It is our experience that the solution obtained by the Fourier method is better behaved at long times and was the solution used exclusively for the present data analysis

Conditions **c** and **f** can be associated with either potentiostatic or galvanostatic control, as was pointed out by Archer and Grant [2]. Deciding which diffusion situation (**c** or **f**) is appropriate for the analysis of a particular data set was shown [2,6] to be dependent on factors such as membrane thickness, cathodic electrolyte composition and the value of the applied cathodic current or potential.

7.2 Results and Analysis of Typical H Permeation Transients at Ni and Pd

Two typical i(t) transients for H permeation through Pd and Ni membranes are shown in Figs. 7.1a and b. As discussed in ref. 2, in some of the earlier work it was assumed that a potentiostatic experiment would guarantee the **c** condition and a galvanostatic experiment would guarentee the **f** condition. The approach used here to analyze these transients consisted of the fitting of eqs. 7.2 and 7.4 to the data using NLS methods, comparing the goodness of each individual fit using standard NLS statisitical methods and then examining if the experimental condition could support the chosen model's diffusion conditions. In many cases this procedure, to differing, degrees, would break down due to the fact that neither eqs. 7.2 or 7.4 could adequately simulate the current *vs.* time behaviour.

The largest descrepancies, from these models, were seen when poisons were adsorbed on to the cathodic surface, i.e. the most common feature was a current-maximum observed before the steady-state condition was reached. In the literature this maximum has been associated with H entering and filling small voids caused by defects in the metallic stucture. These voids are referred to as H traps [7]. In the

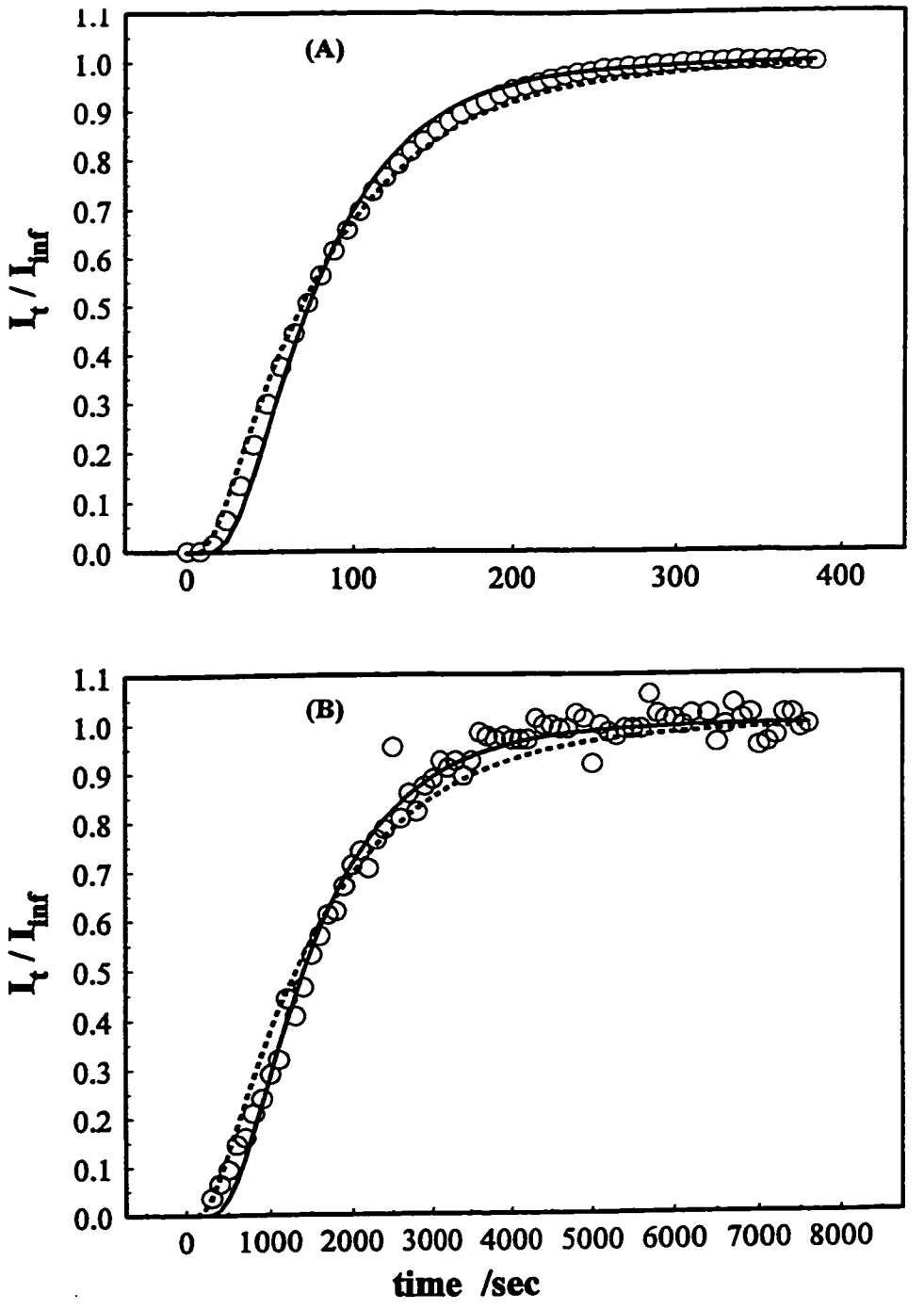

Fig. 7.1 H permeation transients for: **A)** Pd membrane 0.01 cm thick; E was stepped from + 300 to +150mV *vs.* RHE; eletrolyte entrance and exit sides, 0.5 mol dm^{-3} H_2SO_4; **B)** Ni membrane 0.0025 cm thick; E was stepped from -200 to -250 mV *vs.* RHE; electrolyte entrance side 0.5 mol dm^{-3} H_2SO_4, exit side 0.5 mol dm^{-3} NaOH.

present context, though, these maxima are believed to be associated with fluctuations of the poison coverage in time after the cathodic polarization was applied. Support for this view is seen in the time variation of thiourea coverage at Pt electrodes as was discussed in chapter 6. Mention of this phenomenon, i.e. poison coverage variation, is found in the literature [8], where the poison coverage was monitored using a potential pulse/H permeation technique.

The experimental conditions producing the two results shown were, for Fig. 7.1a - a Pd membrane stepped from +300 mV to +150 mV *vs.* RHE, thickness = 0.01 cm; and for Fig. 7.1b - a Ni membrane stepped from -200mV to -250mV *vs.* RHE, thickness 0.0025 cm. The most obvious difference found between these two transients is the length of time needed for the current to reach its maximum value; this is directly related to the diffusion coefficient of H in each metal. As illustrated in Figs. 7.1a and b, both equations provide reasonably good fits to the data. For the Pd experiment a choice based on the NLS goodness-of-fit parameters, (see LEVM 6.0 users manual) could not be made; this finding is consistent with that found in ref. 2. The average diffusion coefficient is (D_{Pd}) of 3.7×10^{-7} cm^2 s^{-1}; a value which is well within the range given in the review by Pound [6], *viz.* 1.05 to 6.3×10^{-7} cm^2 s^{-1}. For the H permeation through the Ni membrane (Fig. 7.1b), eq. 7.2 clearly fits the data better than eq. 7.4; this statement is supported by the statisitical analysis provided by the NLS software. The derived diffusion coefficient (D_{ni}) is $6.13 \pm 0.09 \times 10^{-10}$ cm^2 s^{-1} which again falls in the range of values found in the literature [6], *viz.* 2 to 6.8×10^{-10} cm^2 s^{-1}. With these results and others we were able to verify that the experimental system for H permeation measurements was working properly.

Once the H permeation current-density has reached its steady-state value, i_∞, the latter is recorded and then used in conjunction with the cathodic i(V) relationship to elucidate information concerning the interfacial H transport kinetics, step IV in § 1.4. These results will be discussed in § 8.2 and § 9.2.

References

1. P.K. Subramanyan, in Comprehensive Treatise on Electrochemistry, Eds. J. O'M Bockris, B.E. Conway, E. Yeager and R. E. White, Plenum, New York, vol. 4 (1980), p. 11.

2. M.D. Archer and N.C. Grant, Proc. Roy. Soc. London, A 395 (1984) 165.

3. J. Crank, "The Mathematics of Diffusion", Clarendon Press, Oxford (1956).

4. J. McBreen, L. Nanis and W. Beck, J. Electrochem. Soc., 113 (1966) 1218.

5. P.H. Pumprey, Scripta Metall., 14 (1980) 515.

6. B. Pound, in "Modern Aspects of Electrochemistry", Eds. J. O'M. Bockris, B.E. Conway and R.E. White, Plenum Press, N.Y. vol. 25 (1993) 63.

7. J. O'M Bockris and P.K. Subramanyan, J. Electrochem. Soc., 118 (1971) 1114.

8. P. Kedzierzawski, Z. Sklarska-Smialowska and M. Smialowski, J. Electrochem. Soc., 127 (1980) 2550.

Chapter 8

Co-adsorption of Thiourea and H at Pd Cathodes in 0.5 mol dm^{-3} H_2SO_4 as it Affects H *Ad*sorption and *Ab*sorption

8.1 General Effects as Studied at Micro-Cylindrical Electrodes

Pd is one of the most interesting cathode materials, electrochemically, because it possesses many of the favourable qualities of Pt which aid in its electrochemical examination and, additionally, it is able to sorb large quantities of H into the metal lattice, up to an atomic extent, Pd:H = 0.6. A comparison of the cyclic voltammograms for Pt and Pd surfaces in 0.5 mol dm^{-3} H_2SO_4 is shown in Fig. 8.1. Both electrodes exhibit a well defined, quasi-irreversible oxide region and an almost reversible region corresponding to the UPD of H. However, at smooth Pd electrodes thicker than, say 0.25 μm. [2], the current associated with the UPD process is dwarfed by that arising from H sorption *into* the metal lattice; therefore the UPD of H cannot be directly measured by the usual cyclic voltammetry procedure. Various other methods though are available for the measurement of the UPD of H at Pd, e.g. use of extremely thin films of Pd plated on Au [1,2], fast linear potential scan methods [3], ac impedance spectroscopy [4] or H displacement methods [5] (see § 1.3.1). The latter two procedures were used for some preliminary characterization of the system under study here.

Injection of thiourea into a clean solution of 0.5 mol dm^{-3} H_2SO_4 after fully charging a Pd electrode at a given potential in the UPD of H region by the method described § 1.3.2 for CO adsorption on Pt, produces the current *vs.* time transient shown as Fig. 8.3. Note that measurements of displacement of UPD H at Pd can only be properly performed when the

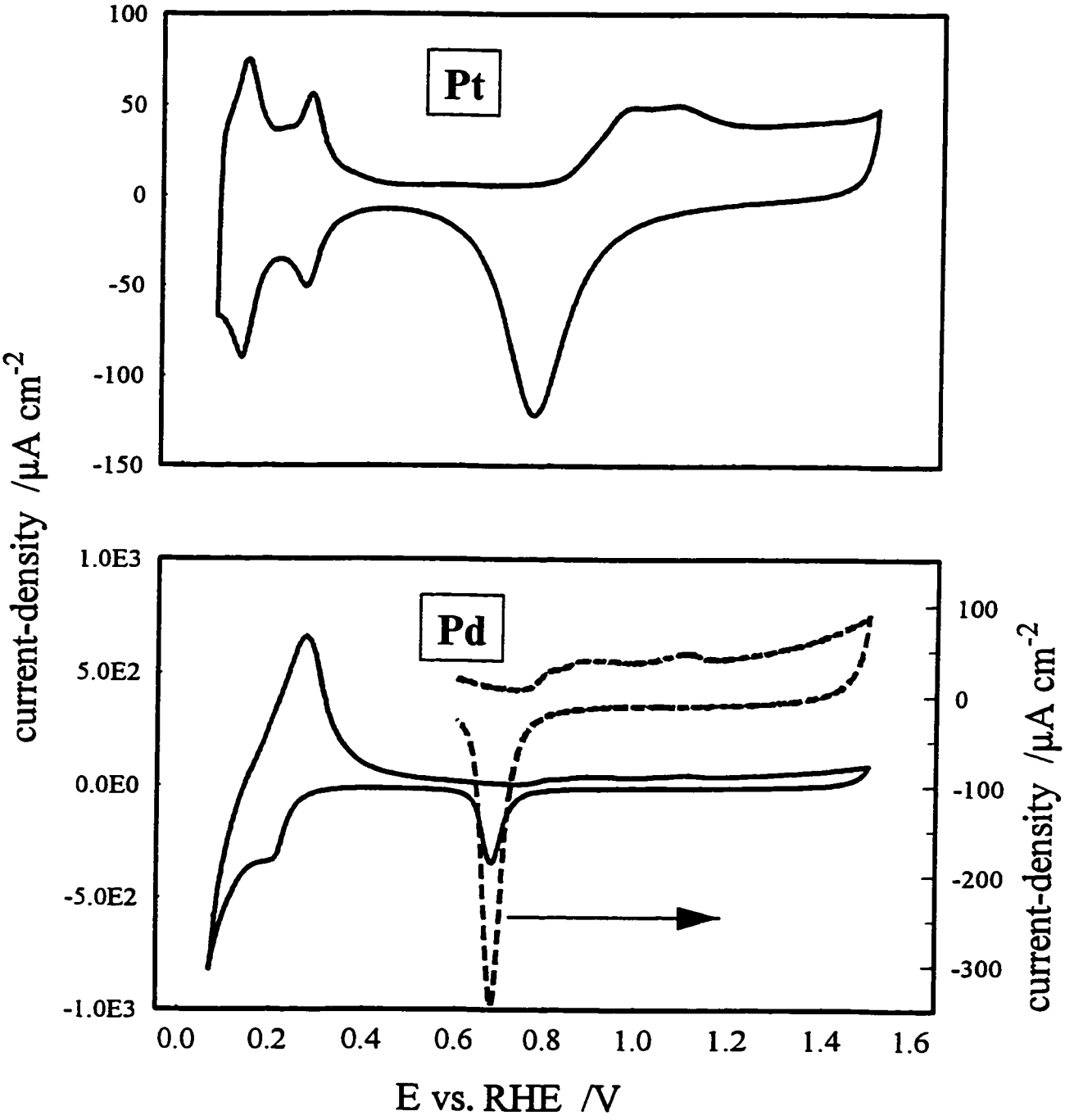

Fig. 8.1 Cyclic voltammograms of polycrystalline Pt and Pd electrodes in 0.5 mol dm^{-3} H_2SO_4. Scan-rate, 50 mV s^{-1}; Pt electrode, 0.5 mm diameter wire; Pd electrode, 25 μm diameter wire; T=25°C.

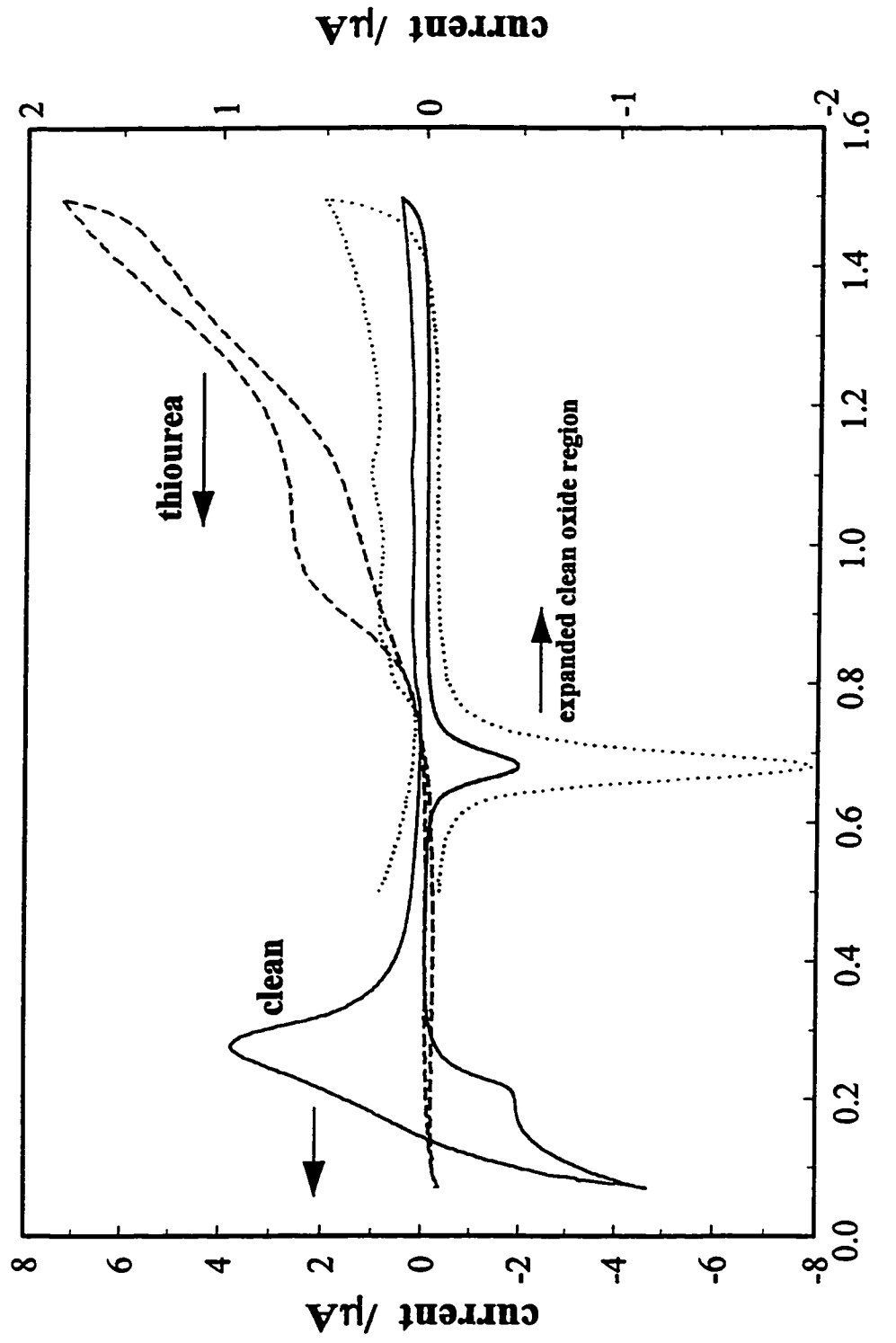

Fig. 8.2 Cyclic voltammograms of a thin Pd wire electrode (diameter 20μm) in 0.5 mol dm^{-3} H_2SO_4 with and without 5×10^{-5} mol dm^{-3} thiourea.

current corresponding to H entry into the Pd lattice has reached zero, e.g. for the 25 μm wires used in the present work, the time required for $i \rightarrow 0$ was approximately 600 seconds. The process taking place which gives rise to this anodic current *vs.* time transient is represented by the following quasi-chemical reaction:

$$Pd\text{-}H_{ads} + H_2O + thiourea \rightleftarrows Pd\text{-}thiourea_{ads} + H_3O^{+} + e^{-} \qquad (8.I)$$

Integration of the i(t) transient in Fig. 8.3 can give an estimate of the charge corresponding to the UPD of H. Performing this experiment over a range of different potentials, enables an isotherm for adsorption of UPD H to be constructed, as in ref. 7 where the displacing molecule was CO [5-7].

Given enough time and a sufficiently large thiourea concentration ([thiourea] > 1×10^{-5}) the fractional thiourea surface coverage on the Pd surface will approach unity ($\theta_P \rightarrow 1$). Full coverage by thiourea on the Pd surface influences the Pd cyclic voltammetry (Fig. 8.2), in ways which are similar to what was found at Pt electrodes (see chapter 6) covered with thiourea: i) the H adsorption (absorption) processes are completely suppressed over the potential-region for the UPD of H in clean 0.5 mol dm^{-3} H_2SO_4 and ii) thiourea oxidation, producing much larger currents, takes place, suppressing oxide formation at potentials E > 0.8 V *vs.* RHE in 0.5 mol dm^{-3} H_2SO_4.

The effect thiourea has on the H transport across the electrode|electrolyte interface is clearly illustrated in Fig. 8.4 which shows linear (anodic) potential scans for the oxidation of H absorbed in Pd following cathodic charging at 67 mV *vs.* RHE for 600 s in thiourea-*free* 0.5 mol dm^{-3} H_2SO_4. In Fig. 8.4 the oxidation of absorbed H occurs into

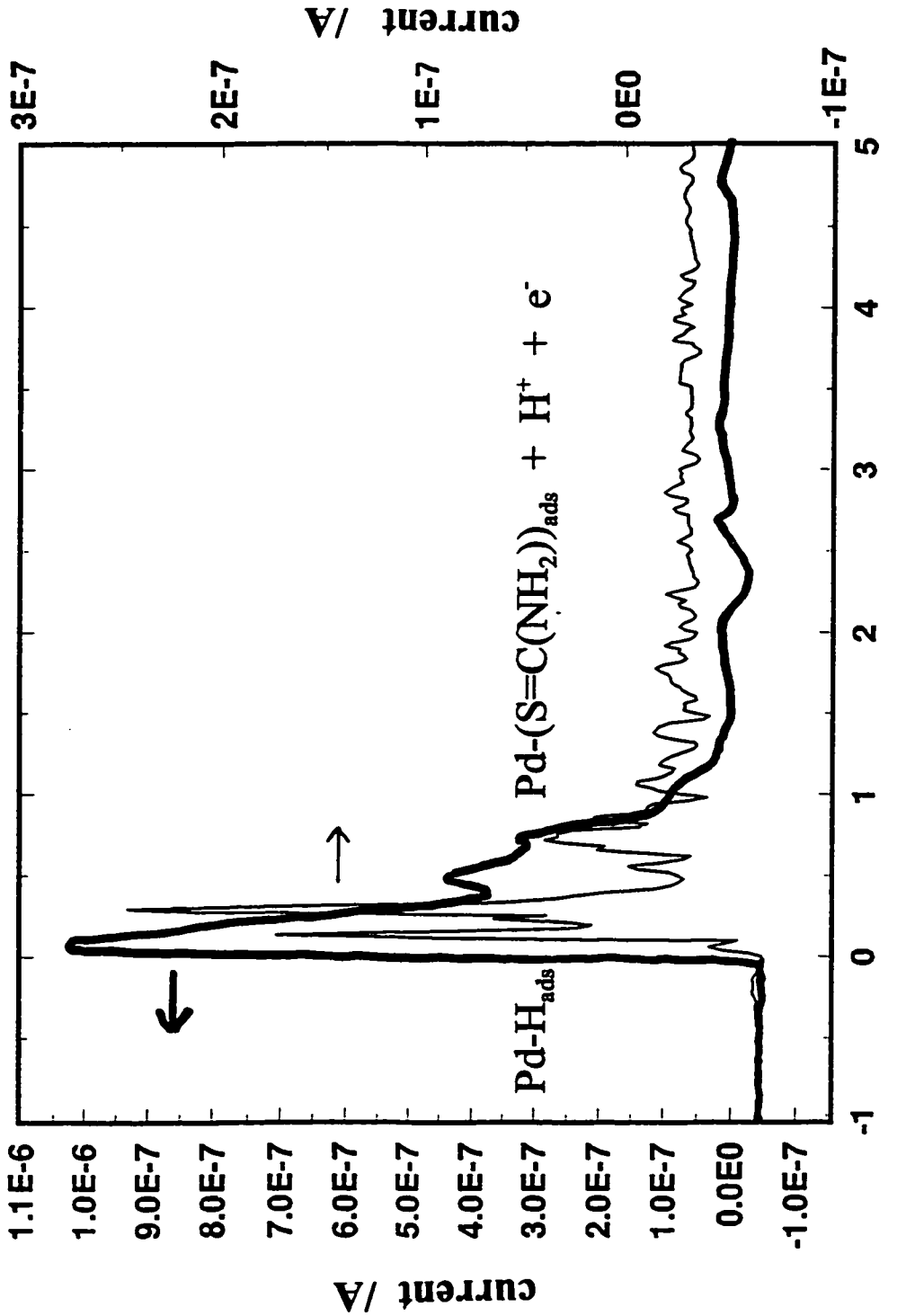

Fig. 8.3 Current *vs.* time transient, after the injection of thiourea into the electrolyte, of H desorption from a thin Pd wire electrode which had been charged for 600 s at 70 mV *vs.* RHE in "clean" 0.5 mol dm^{-3} H_2SO_4; T = 22°C.

either a clean, 0.5 mol dm^{-3} H_2SO_4 or the same solution after injection of thiourea (see Fig. 8.3), therefore displacing the underpotentially deposited H. The same charge for H desorption is recovered (90 μC) in both the clean and poisoned electrolytes but the H desorption/oxidation process in the presence of thiourea occurs at much more positive potentials, 0.8 to 1.6 V. As seen in Fig. 8.2 this is the region where oxidative desorption of thiourea takes place. Thus anodic desorption of H is effectively inhibited so long as thiourea *remains on the surface* and the process is also shifted to the potential region where thiourea becomes oxidized, corresponding to a voltage shift of over 600 mV. Also the shape of the H oxidation CV profile changes from the bell-shaped curve seen in clean 0.5 mol dm^{-3} to a curve with a shape corresponding to the two waves as seen for thiourea oxidation alone (Fig. 8.2).

The blocking effect by thiourea on H desorption/oxidation is also seen for H entry into the metal. Using the technique outlined above, involving charging/discharging of a thin wire, this effect can be studied. Correspondingly, the curves in Fig. 8.5 show the H oxidative desorption charges for H previously sorbed into the Pd wire at various potentials, in the range 0.07 V to -0.25 V, for a charging time of 600 s.

The two sets of results in Fig. 8.5 were recorded in the presence and absence of thiourea. It is seen that by increasing the potential, the blocking effect of thiourea can be overcome, producing significant H sorption when charging potentials, more negative than *ca.* 0.00 V *vs.* RHE, are applied. Note, however, that limiting H desorption charges are approached in both cases as increasing cathodic polarization is applied. This H desorption charge limit, compared with the findings of Mizuno and Enyo [11], corresponds to the

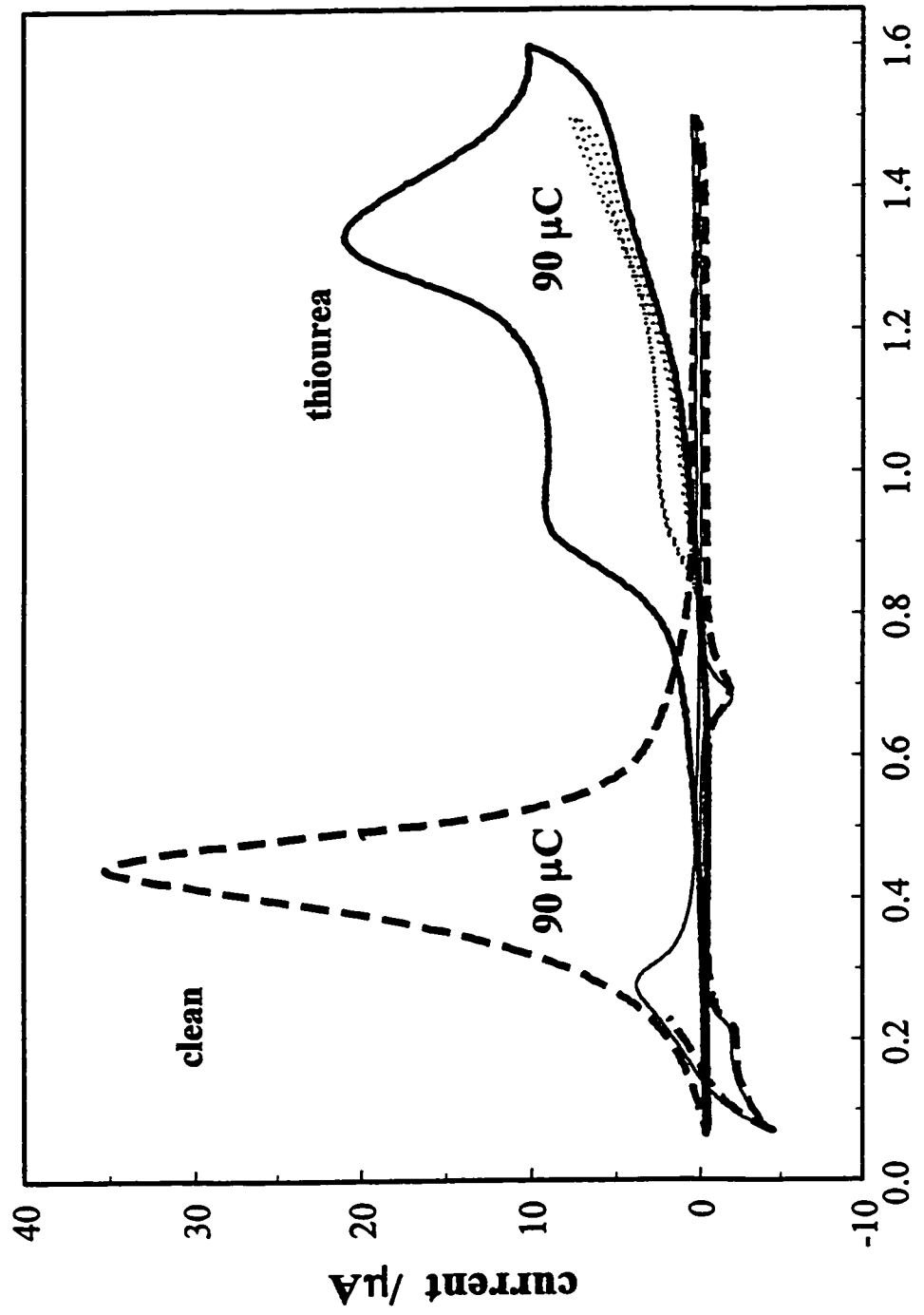

Fig. 8.4 Cyclic voltammograms of H_{ads} oxidation after charging a Pd wire with H at 70 mV *vs.* RHE for 600 s in 0.5 mol dm^{-3} H_2SO_4; discharged in (——) 0.5 mol dm^{-3} H_2SO_4 and (——) 0.5 mol dm^{-3} H_2SO_4 + 1 x 10^{-3} mol dm^{-3} thiourea. Total desorption charge = 90 µC in each case.

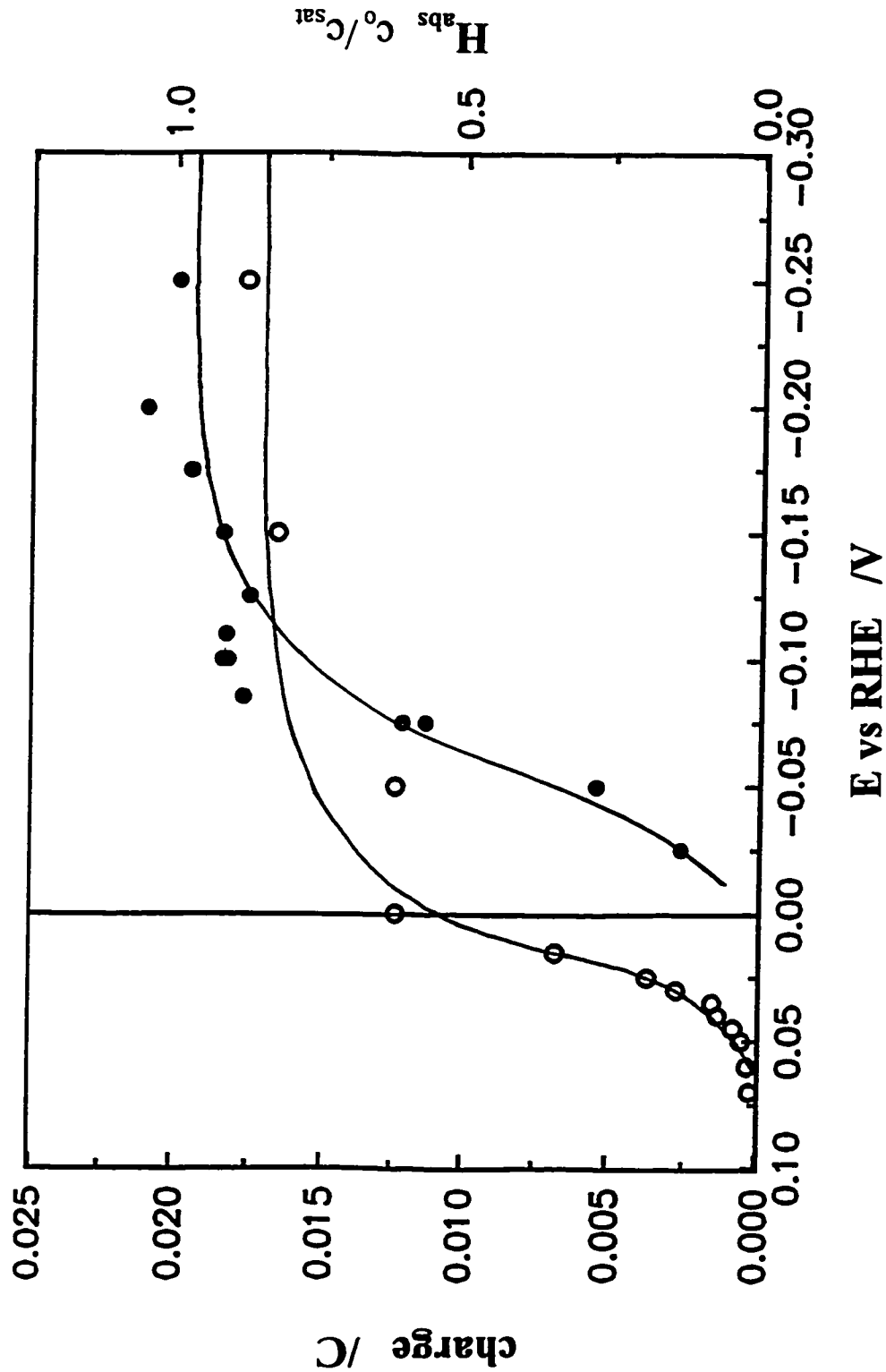

Fig. 8.5 Quantity of H absorbed into a thin Pd wire cathode (diameter 25 μm) as a function of cathodic charging potential in 0.5 mol dm^{-3} H_2SO_4 with (●) and without (○) 3.65 x 10^{-5} mol dm^{-3} thiourea; charging time 600 s; T = 22°C.

formation of the pure Pd-H β phase, H:Pd ≈ 0.5. In their work [11] it was found that the Pd-H α phase and a mixed α/β phase could be charged/discharged very rapidly compared with the γ phase (H:Pd > 0.5), i.e. the time frame for the present H discharge, *viz.* several potential cycles at 50 mV s^{-1} (total time 400 sec), is sufficient for the discharge of the α and β phases. This increase in H sorption at the more negative overpotentials (when thiourea is present) can be associated with the following three factors, which may or may not be interrelated.

1) The reduction of thiourea which occurs at higher cathodic overpotentials (see chapter 5, where thiourea reduction on Pt was seen not to occur in the potential-region of the UPD of H), opens up the Pd surface (decreasing θ_p) for the H absorption process;

2) The participation of the so-called OPD H species at these overpotentials (although here very little H_2 is evolved and the OPD H will be associated more with the H sorption process), as it is related to thiourea reduction and H sorption;

3) The increase in the driving force for the H absorption process by the increase of the hydrogen overpotential; directly if the process occurs via direct discharge of H_3O^+ and indirectly when H_{abs} is formed via an adsorbed H intermediate.

From these results it could be stated that the role played by thiourea adsorbed on the Pd surface is to block H from going into and out of the metal lattice, but the question arises is this blocking effect a thermodynamic property of the system or is it a consequence of a modification of the surface electrode kinetics? The thermodynamics of this problem have been dealt with theoretically by Jerkiewicz and Conway [8], and independently by Protopopoff and Marcus [9,10]. The principles of these studies are as follows:

The chemical potentials of H in the absence (μ_H) and in the presence ($\mu_{H(P)}$) of P are, for Langmuir adsorption,

$$\mu_H = \mu_H^o + RT \ln\left(\frac{\theta_H}{(1-\theta_H)}\right) \quad \textit{and} \quad \mu_{H(P)} = \mu_{H(P)}^o + RT \ln\left(\frac{\theta_{H(P)}}{(1-\theta_{H(P)}-\theta_P)}\right) \qquad \textbf{(8.1)}$$

where $\theta_{H(P)}$ is normally $< \theta_H$ at a given potential.

However, considering kinetically the steps I and II in the HER mechanism, it is readily found, for steady-state conditions, that

$$\frac{\theta_H}{(1-\theta_H)} = \frac{(\bar{k}_1 + \bar{k}_{-2})}{(\bar{k}_{-1} + \bar{k}_2)} = \bar{K}_H \ (say) \qquad \textbf{(8.2)}$$

for $\theta_P = 0$ and also

$$\frac{\theta_H}{(1-\theta_{H(P)}-\theta_P)} = \frac{(\bar{k}_1 + \bar{k}_{-2})}{(\bar{k}_{-1} + \bar{k}_2)} = \bar{K}_{H(P)} \ (say) \ for \ \theta_P > 0, \qquad \textbf{(8.3)}$$

where $\bar{k}$'s are the *electrochemical* rate constants ($\bar{k}_i = k_i \exp(\alpha\eta f)$)for the indicated steps. Evidently then $\bar{K}_H = \bar{K}_{H(P)}$, so the presence of P in altering the "configurational" term in μ does not change or increase the chemical potential of H. Hence, only when there are lateral (repulsive) interactions between H and P can P influence the "driving force" for H sorption, from adsorbed H, into a metal electrode. Physically this could arise from dipole/dipole interactions and related surface electron-density changes determined by the difference of electronegativities of P and the substrate metal.

An original approach to the above problem was suggested by Protopopoff and Marcus [9] who proposed that the *effective* coverage by H in the presence of P should be a normalized value, τ, defined as $\theta_H / \theta_{H,s}$ where $\theta_{H,s}$ is the *local* saturation value for H on

the sites remaining unblocked (*i.e.* $1-\theta_P$) by adsorption of P (occupying 1 H site per P). On this basis the *local* chemical potential of H's amongst P's in terms of τ, would be

$$\mu_{H(\tau)} = \mu^{o}_{H(\tau)} + RT \ln \frac{\tau}{(1-\tau)} \tag{8.4}$$

$$= \mu^{o}_{H(\tau)} + RT \ln \frac{\theta_H / (1-\theta_P)}{1-\theta_H / (1-\theta_P)} \tag{8.5}$$

Rearrangements give

$$\mu_{H(\tau)} = \mu^{o}_{H(\tau)} + RT \ln \frac{\theta_H}{(1-\theta_H-\theta_P)} \tag{8.6}$$

which turns out to be equivalent to eq. (8.3) which, as shown above, does not lead to a difference between μ_H in the absence and presence of P, unless interaction effects, are significant. Noting that the chemical potential of H inside the metal lattice is:

$$\mu_{H,b} = \mu^{o}_{H,b} + RT \ln \frac{X_H}{1-X_H} \tag{8.7}$$

and also that it is unaffected by the adsorption of P, it is therefore seen that the driving force for transfer of hydrogen from the metal surface into the bulk lattice ($\Delta\mu_{sorption} = \mu_{H,b} - (\mu_H \equiv \mu_{H(P)} \equiv \mu_{H(\tau)})$ is a constant, under Langmuir conditions, regardless of the value of θ_P.

The main consequence of this analysis is that when the fractional coverages of H in the absence and presence of poison are equivalent, the fractional M:H ratios will also be identical. Since the M:H ratio is unaffected by a poison when it is acting simply as a site blocker, the situation arises, for the above Langmuir conditions, that although the absolute surface H coverage is greatly reduced when the poison is coadsorbed, the M:H ratio will remain constant. For example a hypothetical situation, with and without coadsorbed P, at equilibrium could produce values:

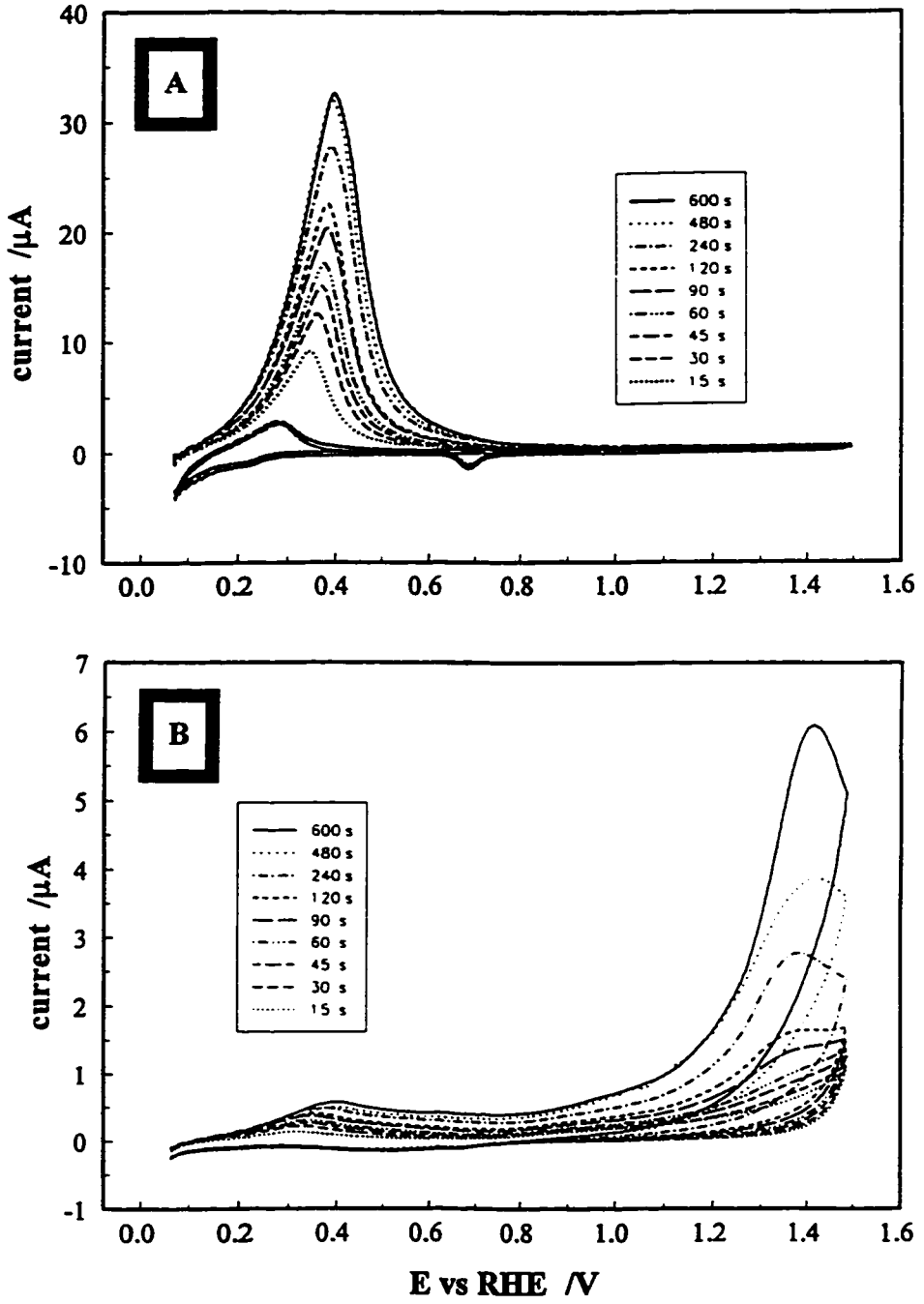

Fig. 8.6 Cyclic voltammograms for the oxidation of H, desorbing from a thin Pd cathode which was previously charged at 67 mV *vs.* RHE, as function of charging time. Scan-rate 50 mV s^{-1} ; electrolyte used for charging/discharging in **(A)**, 0.5 mol dm^{-3} H_2SO_4; or in **(B)**, 0.5 mol dm^{-3} H_2SO_4 + 3.65 x 10^{-5} mol dm^{-3} thiourea; T = 22°C.

Clean	$\theta_H = 0.5$	θ_H (absolute) = 0.5	$X_H = 0.5$
Poisoned	$\tau = 0.5$, $\theta_P = 0.8$	θ_H (absolute) = 0.1	$X_H = 0.5$

What then, are the causes for the decreased H sorption effects seen above; kinetic effects or thermodynamic arguments based on the inclusion of lateral interaction terms in our adsorption isotherm?

In order to distinguish between these factors the sorption process was examined as a function of charging time at thin Pd wire electrodes by the charging/discharging technique outlined above. Figs. 8.6a and b show the cyclic voltammograms for H desorption as a function of the time of charging of the electrode with H at E = 67 mV *vs.* RHE for the electrode in 0.5 mol dm^{-3} H_2SO_4 with and without 3.65×10^{-5} mol dm^{-3} thiourea respectively. As was discussed above the potential range in which H desorption takes place is shifted anodically by ≈0.6 V when thiourea is present in the electrolyte. For the clean electrolyte the charge under the desorption peak increased with charging time until 480 s, after which point (600 s) no further increase was seen. For all the previous charging/discharging results which were obtained to examine the effect of potential, a charging time of 600 s was used as suggested by the above result. With thiourea in solution and adsorbed on the Pd surface, the evolution of H desorption charge under the current-peak at ≈ 1.4 V *vs.* RHE is changing continuously throughout the 0 to 600 s charging-time range, indicating that equilibrium has not yet been reached.

Comparing the charge for 600 s, when the charging had been performed in clean

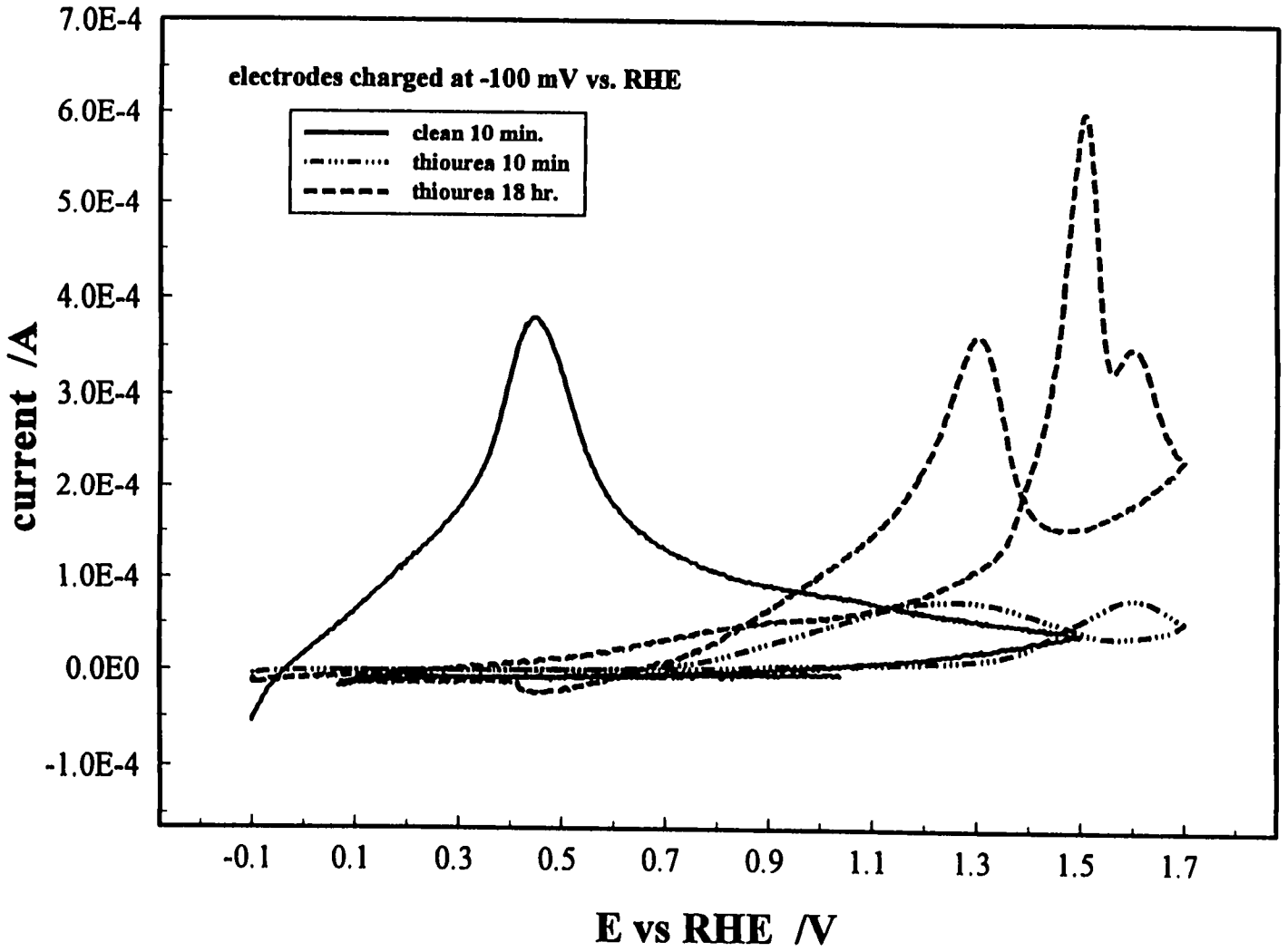

Fig. 8.7 Cyclic voltammograms for the oxidation of H previously adsorbed in a thin Pd wire at -95 mV *vs.* RHE; charging conditions: (——), 0.5 mol dm^{-3} H_2SO_4 for 600 s; (- ··· -) charged in 0.5 mol dm^{-3} H_2SO_4 + 4.2 x 10^{-4} mol dm^{-3} thiourea for 600 s and (——) 18 hr. Scan-rate for desorption cycles = 50 mV s^{-1}; T = 22°C.

and poisoned electrolyte, it is found that for the poisoned case the charge is equal to 35% of that of the clean-solution case. Holding for longer times decreases this difference, e.g. at t(charge) = 12,000 s, a charge corresponding to 54% of that of the maximum seen for the clean-solution case is found and for t(charge) ≈ 12 hr the charge for the poisoned electrode can exceed that for the clean-solution case, giving a percentage of 131%.

This time effect is illustrated in Fig. 8.7 which shows the H desorption voltammograms after charging at a potential of -0.1 V *vs.* RHE. The three voltammograms represent the cases where charging was performed for 10 min. in 0.5 mol dm^{-3} H_2SO_4, with and without thiourea (cases **A** and **B**) and for a charging time of 18 hr. with the electrolyte containing thiourea (case **C**). Calculating the charges and assuming that the charge for **A** is the equilibrium value at this potential, the following charge ratios are found: **A/B** = 0.30 and **A/C** = 1.0. The above two examples, showing the time effect of H entry into Pd, gives conclusive evidence that the poisoning effect of thiourea is *not* based on thermodynamic factors; rather it is due to significant decreases in the rates of the interfacial H transport.

It appears from these results that the change in the chemical potential of the adsorbed H species in the absence and presence of adsorbed thiourea ($\Delta\mu_{H_{ads}} = \mu_H - \mu_{H(P)}$), if in fact it is involved in the H sorption process, is not large, i.e., at least for the case of Pd, Pd:H ratio is approximately *the same* in the presence and absence of thiourea. In order to reach a definite understanding of the thermodynamic factors involved, certain information, which at this point is undetermined, would have to be gathered: i) The extent of participation of an adsorbed H species in the H sorption process; ii) If the adsorbed H

does play a role then are there differences in the H coverage between the clean and poisoned surfaces, i.e. θ_H *vs.* $\theta_{H(P)}$ or τ; 3) The magnitude and sign of any lateral interactions between adsorbed species on the surface in both the clean and poisoned surface, e.g. H–H and H–P interactions.

Assumptions can be made and values inferred using the observed differences in charge ratios between the charging results in clean and poisoned electrolytes but, since the above three factors are interconnected, a complementary technique should be employed.

8.2 H Permeation Studies

The kinetics of this H sorption process were investigated using the H permeation technique as discussed in chapter 7. Unlike the analysis in chapter 7, we are now interested in the behaviour of the anodic and cathodic current-densities under steady-state conditions (current-density at the plateau in the i(t) transient) as a function of the cathodic voltage. The H permeation data recorded when the cathodic side of the membrane was exposed to 0.5 mol dm^{-3} H_2SO_4 solution with and without 1.5×10^{-4} mol dm^{-3} thiourea are shown in Fig 8.8 in terms of Tafel-type plots. At all potentials studied, both the cathodic and anodic currents are significantly lower when thiourea is present in the electrolyte. Also for each individual set of data (clean and poisoned electrolyte) there is, at almost all overpotentials, a 1:1 correspondence between the cathodic and anodic current-densities. This indicates that the rate of transfer of H from one face of the membrane to the other is not limited in the steady-state by the diffusion of H through the metal but, it is directly related to the *kinetics of the H entry* at the cathodic side.

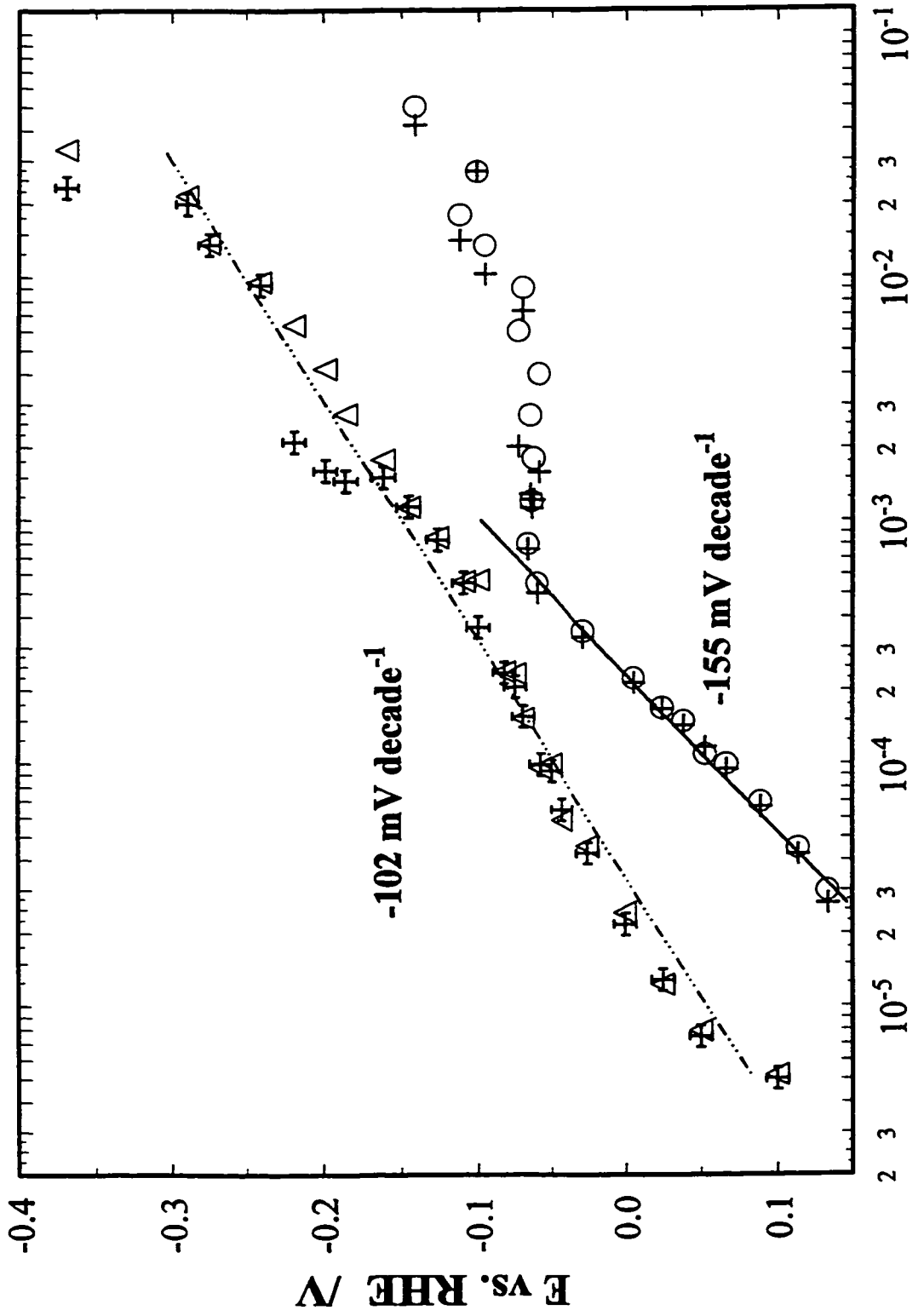

Fig. 8.8 A Tafel type plot of H permeation results, anodic and cathodic current-densities *vs.* cathodic potential (IR corrected); O and Δ cathodic current-densities; + and ✣ anodic current-densities; cathodic electrolyte was 0.5 mol dm^{-3} H_2SO_4 with (Δ ✣) and without (O +) 1.5 x 10^{-4} mol dm^{-3} thiourea; anodic electrolyte was 0.5 mol dm^{-3} H_2SO_4 for both cases.

The flux of H into the metal at the entry side is thus directly proportional to the flux at the output side. This is a typical result which has been observed at other metals such as Ti [12] and Zr [13], but little has been done to relate this to the theoretical consequences of an HER/H sorption model. One interpretation of this observation comes from Popov et al. [14] where the 1:1 ratio is thought to arise from entry of an H atom into the metal via the direct interfacial transfer of a proton.

This being the kinetic situation, it can be directly stated that the presence of adsorbed thiourea on the surface leads, in fact, to a significant *decrease* in the rates of H transfer into the metal. The magnitude of this difference at potentials positive to -0.1 V *vs.* RHE is approximately one order of magnitude, decreasing slightly with increasing negative potential. This decrease in current-density will correspond to a one order of magnitude decrease in either H coverage or effective (i.e. available/active) surface area (depending on the chosen mechanism). This value for the decrease in current-density or coverage is quite reasonable when compared with that for the observed blocking of the UPD of H process by thiourea on Pt (see Fig. 6.2) which suggests, for [thiourea] = 1.15×10^{-2}, a value of θ_H approaching zero.

Also, at potentials positive to -0.1 V *vs.* RHE, their is a substantial difference, 60 mV decade^{-1}, in the Tafel-type slopes measured when H permeation takes place in the presence and absence of thiourea in the electrolyte. In chapter 6 the HER Tafel slope recorded in the presence of thiourea (see Figs. 6.3 and 6.5) was interpreted in terms of a potential dependence of the thiourea coverage, as measured by the change in coverage of UPD H, Tafel, potential decay and by EIS studies. Here the same arguments as in chapter

6 can be applied to explain the decrease in slope caused by thiourea adsorption.

For the two H sorption mechanisms the arguments go as follows:

Direct electrochemical H injection mechanism

As the potential increases cathodically, the poison becomes desorbed or is reduced leading to desorption from the electrode surface, which in turn increases the effective surface area; thus, as the potential increases cathodically, the available area increases; then the Tafel slope can then be defined as: $b^{-1} = d \ln (area)/d\eta - RT/\beta F$.

Mechanism involving the adsorbed H species

As above, when the poison becomes desorbed, the area of clean surface increases, which allows the surface concentration of the adsorbed H species to increase with overpotential, yielding a Tafel slope lower than that observed without thiourea being adsorbed.

The last point to be mentioned concerning the permeation experiments deals with the arrest of current-density seen for both sets of results around $i \approx 1.5 \times 10^{-3}$ A cm^{-2}. The arrest ceases when the cathodic current-densities in Fig. 8.8 reach a value of approximately 6×10^{-3} A cm^{-2}, but it appears that it is more correct to associate this process with a given amount of charge which must pass and, for the experimental conditions used here, this charging goes to completion at a corresponding value of current-density of approximately 6×10^{-3} A cm^{-2}. The evolution of this process in time is

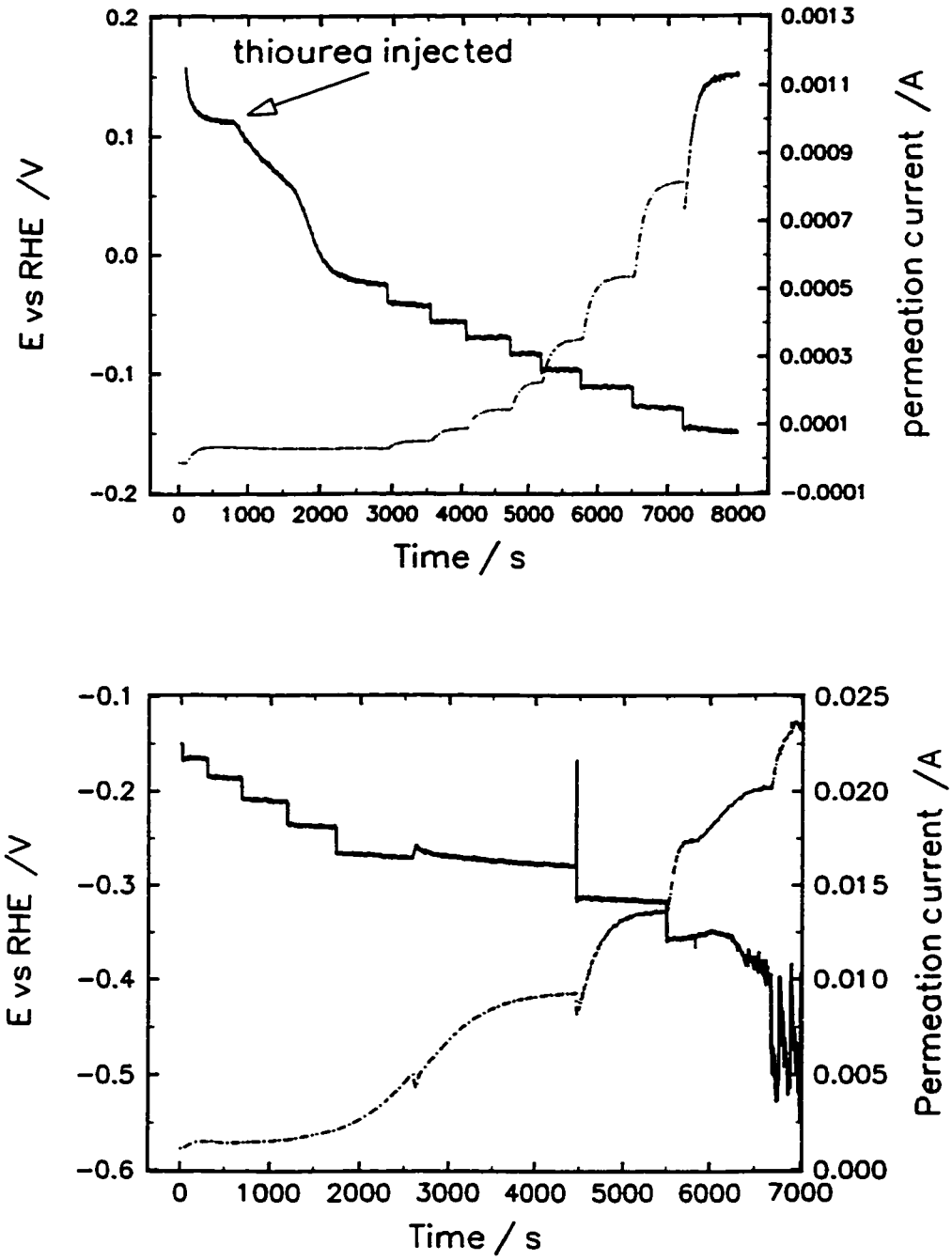

Fig. 8.9 H permeation anodic-current, cathodic-potential time transients, illustrating the behaviour around the region where the β Pd-H phase is formed; experimental conditions as described in fig. 8.8.

shown in Fig. 8.9. By calculation of the H:Pd ratio at the potentials corresponding to this arrest, it can be shown that it correlates with the transition from the mixed α/β phase to the pure β phase. Using the experimental H permeation current-density, 50 mA cm^{-2} (see Fig. 8.8) and eq. 1.23, with $D = 2 \times 10^{-7}$ cm^2 s^{-1} and L = 0.02 cm, a H:Pd ratio of approximately 0.6 is found which corresponds well with the value (*ca.* 0.63) calculated from the results of the thin wire charging experiments at E = -140 mV *vs.* RHE.

The phase changes and their associated H:Pd ratios, as quoted from the data of Lewis [15], are:

H:Pd	Phase
<0.05	α
0.05 to 0.54	α, β mixed
> 0.54	Pure β

Once this arrest has been traversed, irreversible changes in the electrode itself have taken place, e.g. the CV is overlaid on a large resistance originating from the metal (i.e. a large decrease in the conductivity), and an approximately 20 times increase in surface roughness is seen[1]. In some recent reports, the issue of phase change, as it evolves in time, has been considered in terms of the movement of a phase boundary into a cylinder [ref. 11, p. 474] and into a sheet [16]. Hitherto, the more complicated situation of the time evolution of a phase change during steady-state H diffusion through a membrane has not, it seems, received any attention.

---

[1] These effects could only be reversed by prolonged annealing in vacuum.

8.3 Conclusions

1. The adsorption of thiourea on Pd severely reduces the rate in which H can enter the metal lattice. These effects can be discussed in terms of either a decrease in available surface area or equivalently a decrease in absolute coverage by the adsorbed H intermediate.

2. For a constant charging time (600 s), an effect of overpotential is observed on the H concentration in a thin Pd wire when charging is performed in an electrolyte with and without added thiourea. As the potential is increased cathodically, the concentrations of H inside the metal become approximately equivalent for charging in an electrolyte containing thiourea or one that is thiourea-free.

3. The differences in the amount of H absorbed into the thin Pd wires charged as per the conditions given in conclusion 2, are shown to be caused only by kinetic effects and if enough time is given for equilibrium to be attained in both cases, the Pd:H ratios are comparable indicating that the chemical potential of H adsorbed on the Pd surface is not being influenced greatly by the coadsorption of thiourea. This was discussed in terms of theoretical work published in the recent literature [8].

4. Results of H permeation studies corresponded well with those obtained by the charging/discharging technique, that is substantial decreases in current-density (H absorption rate) arose when thiourea was adsorbed on the electrode surface;
and

5. Theoretical considerations show that co-coverage of electrode surfaces with P and H does not lead to change of the chemical potential of H (μ_H) and hence cannot

provide a thermodynamic basis for the enhancement of H absorption into cathodes. Only when interaction effects are included in the μ_H function can such an enhancement effect arise. Similarly, a treatment of the chemical potential of H in terms of a reduced surface coverage fraction, based on fractional occupancy of the free sites left after some extent of poisoning, θ_P, also cannot lead to an increase of μ_H. Thus poisoning effects cannot modify μ_H when only the "configurational" component is considered.

References

1. J. Horkans, J. Electroanal. Chem., 106 (1980) 245.

2. M. Baldauf and D.M. Kolb, electrochim. Acta, 38 (1993) 2145.

3. M.W. Breiter in, Proc. of the Third Symposium on Electrode Processes, Eds. S. Bruckenstein, B. Miller, J.D.E. McIntyre and E. Yeager, The Electrochemical Society Inc., N.J. 80-3 (1979) 410.

4. Chan Lim, Su-IL Pyun and Jeh-Beck Ju, J. Alloys and Comp., 176 (1991) 97.

5. J. Clavilier, J.M. Orts, R. Gómez, J.M. Feliu and A.Aldaz, Proc. Symp. on Electrochemisty and Materials Science of Cathodic Hydrogen Adsorption and Absorption, Eds. B.E. Conway and G. Jerkiewicz, The Electrochemical Society, NJ., 94-21 (1994) 167.

6. B. MacDougall, B.E. Conway and H. Angerstein-Kozlowska, J. Electroanal. Chem., 32 (1971) App.15.

7. A. Czerwiński, J. Electroanal. Chem., 379 (1994) 487.

8. G. Jerkiewicz, J.J. Borodzinski, W. Chrzanowski and B.E. Conway, J. Electrochem. Soc., 142 (1995) 3755; G. Jerkiewicz, J.J. Borodzinski, W. Chrzanowski and B.E. Conway in, Proc. Symp. on Electrochemistry and Materials Science of Cathodic Hydrogen Absorption and Adsorption, The Electrochemical Society, N.J., 94-21 (1995) 44.

9. P. Marcus and E. Protopopoff, J. Chim. Phys., 88 (1991) 1423.

10. P. Marcus and E. Protopopoff, C.R. Acad. Sci., Paris, 308(II) (1989)1127.

11. T. Mizuno and M. Enyo, in Modern Aspects of Electrochemistry, Eds. R.E. White, B.E. Conway and J.O'M. Bockris, Plenum Press, N.Y., 30 (1996) 415.

12. J.J. Phillips, P.Poole and L.L. Shreir, Corros. Sci., 14 (1974) 533.

13. T. Morozumi, T. Mizuno and T. Kurachi, Boshoku Giyutu, 28 (1979) 285 (In Japanese).

14. G. Zheng, B.P. Popov and R.E. White, J. Electrochem. Soc. 142 (1995) 154.

15. F.A. Lewis, Platinum Metals Rev., 4 (1960) 132.

16. R. Durand, M. Srour, N. Adhoum, D. Aberdam and Y. Joly, Proc. Symp. on Electrochemical Surface Science of Hydrogen Adsorption and Absorption, Eds. G. Jerkiewicz and P. Marcus, Electrochemical Soc., N.J., 97-16 (1997).

Chapter 9

Effects of Adsorption of Thiourea on the H_2 Evolution Reaction and H Absorption at Nickel in 0.5 mol dm^{-3} H_2SO_4

9.1 Effects of Catalyst Poisons on Electrochemcial Processes Involving Hydrogen

The effects of catalyst poisons, such as thiourea on the cathodic H_2 evolution reaction at various metals have attracted much interest over many years. Basically, three aspects have been investigated: 1) the effect of the adsorbed poison on the actual kinetics of the HER; 2) the origin of supposed enhancement of sorption of H generated in the HER, into certain transition metals, e.g. Ni, Ti, Fe and Pd, by adsorbed catalyst poisons, an effect, hitherto, which has not been at all well understood; and 3) the behaviour of H adsorbed at the electrode surface, either as the chemisorbed intermediate in the HER or, in the underpotentially deposited (UPD) state at noble metals such as Pt, Pd, Rh, Ru and Ir, and the influence of co-adsorbed poisons on the behaviour of the UPD H.

In this section of the thesis, results of studies of effects of thiourea on the HER at Ni cathodes will be presented and discussed, together with the coupled phenomenon of H sorption into Ni and the effect of thiourea on the latter process. As will be explained later, thiourea is also found to influence the corrosion of Ni in acidic media; this behaviour is examined in terms of Wagner-Traud mixed potential diagrams, especially the effect of thiourea on the cathodic partial process (in O_2-free solution) of the Ni corrosion reactions. Also the effects of thiourea on the HER are not simple due to reductive desorption that can occur, leading to formation of other poison species, H_2S or HS^-.

The use of Ni and Ni alloys in electrochemical applications, e.g. industrially (electrolyzer cathodes) and commercially (Ni/ metal-hydride batteries), can be accounted for partly by its favourable interactions with hydrogen, especially when it is alloyed with certain metals ($NiMo_x$ and Raney Ni[NiAl alloy], both are found to be good HER catalysts [1,2]) and partly by its large natural abundance. A Ni cathode in its bulk form has an intermediate activity for cathodic hydrogen evolution; it lies in the middle of the left-hand branch of the volcano plot for electrocatalysis of the HER, Fig 1.7. Preparation techniques which lead to highly porous surface structures of Ni, e.g. using electrodeposition techniques, usually with codeposition of Co, Fe or Mo, can produce composite materials having excellent catalytic properties for the HER [1,2], manifested by low Tafel slopes and high i_0 values, which can only partially be attributed to the, usually enhanced, surface area factor [3].

Interest in the study of H sorption into, and the HER at, Ni has recently grown with the advent of Ni-based H storage alloys such as, $LaNi_5$ type materials, which can host a large atomic fraction of H without severe embrittlement. Absorption and diffusion of H into Ni, as compared to Pd and Fe, is, however, energetically much less favourable [4]. This was illustrated in chapter 7 by the differences found for the H diffusion coefficients; thus, D_H in Pd is 3-4 orders of magnitude greater than D_H in Ni.

The stability of Ni in non-oxidizing, non-complexing solutions as a function of pH, as given by Pourbaix [5], is shown in Fig. 9.1. Under the conditions employed in the present study, 0.5 mol dm^{-3} H_2SO_4, pH = 0.28, a window for Ni corrosion is seen between -0.4 and 0.3 V *vs.* RHE. The rate of this corrosion in "clean" 0.5 mol dm^{-3} H_2SO_4 is slow

compared to the time frame of the HER and H permeation measurements, and was found not to influence the measured results. It will be shown that upon the addition of thiourea the corrosion and HER rate are inhibited and this will be discussed in the light of its effect on H sorption.

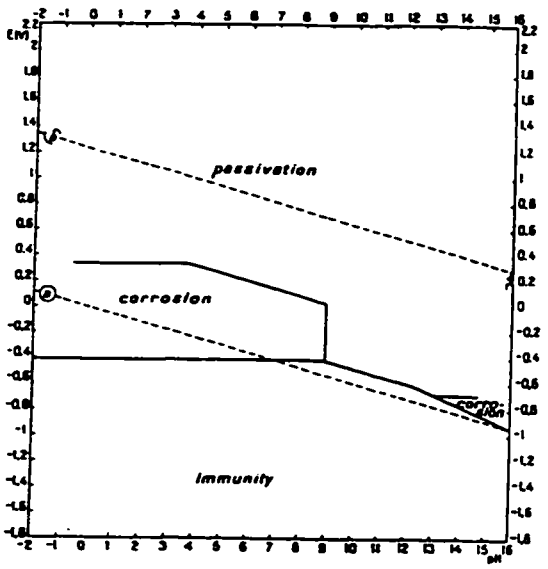

Fig. 9.1 Pourbaix Diagram, potential *vs.* pH, showing the regions of stability of Ni in aqueous solutions, free from chloride. (From Pourbaix [5])

Szklarska-Smialowska and Smialowski [6] have shown through the use of a electrochemical H charging/H_2 gas desorption technique that the equilibrium Ni-H system, in a limit of material thicknesses less than 30 μm, shows behaviour similar to the Pd-H system, i.e. α and β M-H phases are believed to be present and a limiting H/M ratio of 0.6 - 0.7 was calculated. The Ni or Pd to H ratio has been rationalized both experimentally and theoretically. The valence electron configuration of the both Ni and Pd are believed

to have a 0.55 electron-per-atom vacancy in the d shell. Magnetic susceptibility measurements [7] showing a drop to zero as the H content in Pd reaches 0.6 H/Pd corresponds well with an H sorption process where each H atom donates its electron to a Pd atom in the metal lattice, therefore filling its d shell vacancy at a H to Pd level of 0.6. Other evidence showing the migration of the sorbed H in an electric field [8], indicates that the sorbed H is a proton-like charged species, which again supports this maximum H to Pd or Ni ratio of 0.6 - 0.7.

Three conditions [6] have been stated as being crucial for the generation of the Ni-H species electrolytically: 1) large cathodic charging current densities, e.g. $i > 10$ mA cm^{-2}, 2) the presence of reducible H-promoting species (species which form a hydride on the electrode surface when reduced) and 3) temperatures below 80° C. It was found [6] that the most effective poison for promoting H sorption into Ni is thiourea.

The aims of the present study were to investigate what role thiourea plays in enhancing H sorption into Ni, and how the electrode kinetics of the H *ab*sorption reaction (HAR) and the HER are affected by thiourea and to discuss the results in the light of those found in the present work for Pd and Pt.

9.2 Thiourea Adsorption and Ni Dissolution in Relation to the HER and HAR

In order to study the effect of an adsorbate on the kinetics of a surface process at an electrode, a "clean" reproducible surface must first be formed. It was shown as discussed in § 2.2 that either technique; A) annealing and sealing of a Ni wire in an H_2-filled glass bulb [9], or B) cutting and polishing the electrode prepared in A to produce a Ni disk, gave similar and reproducible HER kinetic results.

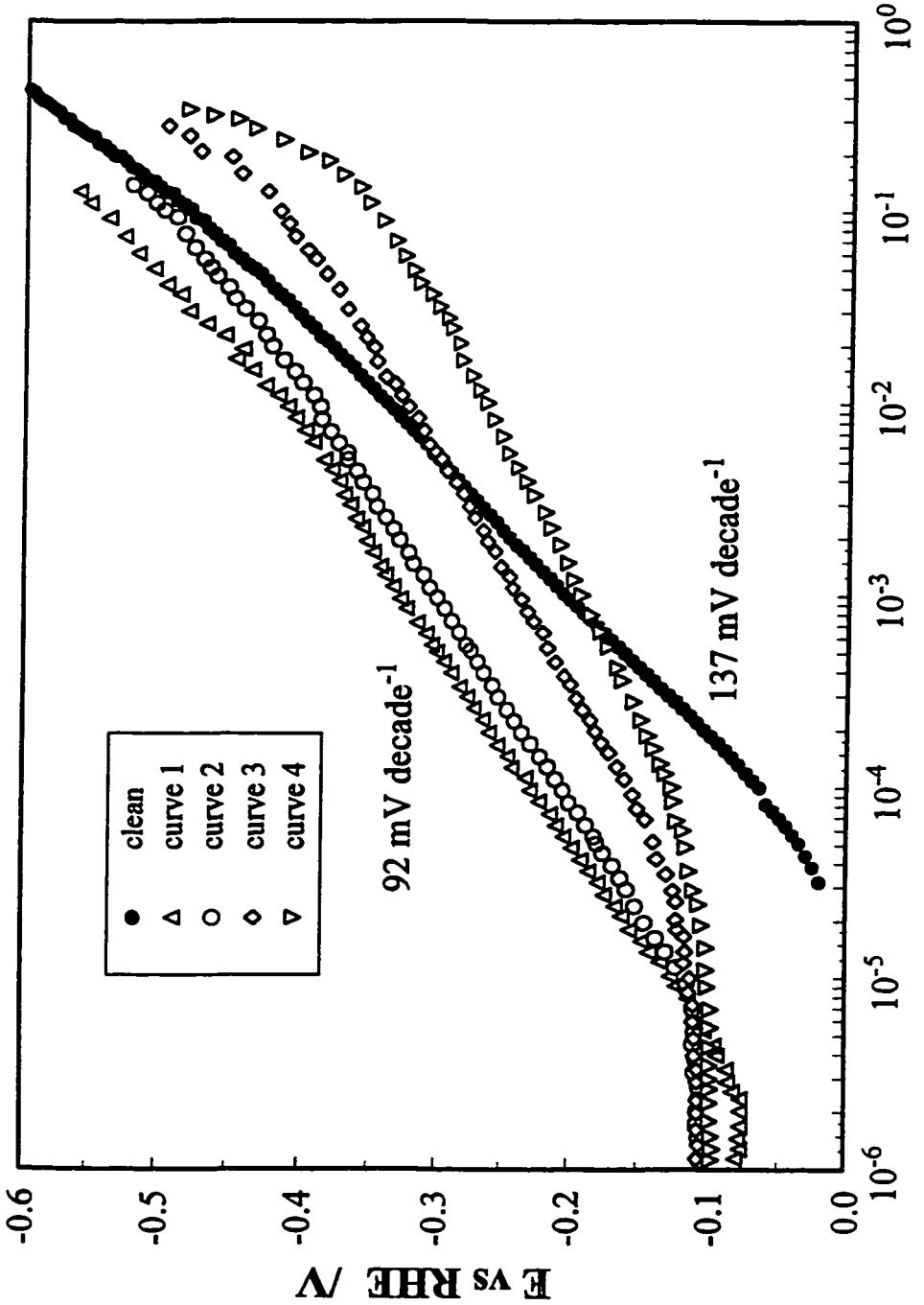

Fig. 9.2 Tafel plots for the HER at a Ni wire electrode in an H_2 saturated 0.5 mol dm^{-3} H_2SO_4 solution. Clean electrolyte: solid symbols; electrolyte containing 7.52 x 10^{-4} mol dm^{-3} thiourea - open symbols. The order in which the curves were recorded after the thiourea had been added are indicated in the legend.

The Tafel plot for the HER at a Ni wire electrode, prepared by method A, is shown in Fig. 9.2. The plot is seen to be linear over almost all of the potential range covered, with measured slopes spanning values from -135 to -140 mV decade^{-1}; for the example shown in Fig 9.2 for the clean-solution case a slope of -137 mV decade^{-1} was found. This value of Tafel slope can be interpreted, see § 1.2.3, as either the Heyrovsky or Volmer step being rate-controlling with the charge transfer coefficient being equal to 0.43. This same type of Tafel behaviour was observed at all electrode rotation rates, for both the Ni rde and the Ni wire electrode and, complementarily no diffusive behaviour was observed in the EIS measurements, verifying that the measured currents were those for the electrode kinetics alone.

The behaviour of the HER at Ni in poison-free 0.5 mol dm^{-3} H_2SO_4 can be represented by the Volmer/Heyrovsky HER mechanism (no Tafel-step, $k_3 = 0$) with either k_1 or $k_2 = 1.8 \times 10^{-10}$ mol cm^{-2} sec^{-1}, i.e. equivalent i(η) relationships are found by exchange of rate-constants, i.e. $k_1 \leftrightarrow k_2$ and $k_{-1} \leftrightarrow k_{-2}$. The difference in these two mechanism configurations is that when the Volmer step is rate-limiting, $k_1 = 1.8 \times 10^{-10}$ mol cm^{-2} cm^{-1} and $\theta_H f(\eta) \rightarrow 0$ while if the Heyrovsky step is rate-limiting, $k_2 = 1 \times 10^{-10}$ mol cm^{-2} cm^{-1} and $\theta_H f(\eta) \rightarrow 1$. The case of the Heyrovsky step being the rate-controlling step is more realistic since the coverage, θ_H, as monitored from measurements of H permeation and electrocatalytic hydrogenation of organics at Ni [10], is indicated as having significant values at negative overpotentials. Although the Heyrovsky-step has been assigned as the rate-limiting step, it will be necessary to revisit this issue later in the chapter, in light of the potential-relaxation results. It is also worth mentioning at this time

that tracer studies of the HER at Ni by Matsushima and Enyo [24], seem to support the Volmer-step as rate-determining.

With the addition of thiourea an immediate jump in the rest potential to more negative values is observed, by *ca.* -20 mV *vs.* RHE. The first, second, fourth and seventh Tafel polarization measurements, after the addition of thiourea, recorded when the current had been progressively stepped to larger values, are shown as curves 1 though 4 in Fig 9.2. The initially poisoned electrode exhibits lower current-densities compared to the clean case at all overpotentials; also the curve has a lower Tafel slope: -90 mV decade^{-1}. This decrease in slope is due in part to a potential-dependent poison coverage, which can produce a significant d log θ_H / dη factor, as was discussed in chapter 6. A more important contribution to the decrease in the Tafel slope, is the continual increase in surface area which is found to occur when thiourea is present in the electrolyte. This effect appears, under some conditions, to be due to corrosion enhanced by the presence of thiourea or one of its hydrogenation products.

The results shown in Fig. 9.2 are those measured when the current was stepped incrementally from the lower to the higher current-limit, where at each step a steady-state potential was maintained for 1 minute[1]. Changing the direction of the current-steps, once the maximum current had been reached, resulted in a steady-state Tafel plot which was always shifted to lower overpotentials. This type of "hysteresis", i.e. differences between

---

[1]At lower overpotentials an absolute steady-state may not have been attained but the time needed to see this transient behaviour is > 4000 s. Since the purpose here is to show the change in Tafel behaviour over time, 1 min. intervals of potential in which the current was stable were used.

the measurements when the current was scanned cathodically (current-up) and when the current was scanned anodically (current-down) over the HER region was also seen at Pt electrodes which had been poisoned with thiourea (chapter 6). There the "hysteresis" was explained as due to the irreversible desorption of the poison from the surface. For Ni electrodes in thiourea-containing electrolytes, the "hysteresis" is found to occur between both the current-up/current-down measurements and also between the current-down/current-up measurements indicating a continually increasing surface area. This behaviour is dissimilar from that at Pt because, although differences are seen between the current-up and current-down Tafel plots at Pt, each consecutive set of measurements, up and down, is superimposible on the former set of measurements. This increase in the surface area could be observed visually; after the measurements, the electrode surface was found to be roughened with black pits (see Fig. 9.3).

The Tafel slopes of the curves for the thiourea poisoned Ni electrode, as shown in Fig. 9.2, do not change greatly until the 7th measurement (curve 4), indicating that the change in surface area occurs without a change in the HER mechanism. The increase in current-densities between the 1st (curve 1) and the 7th (curve 4) polarization measurements at -400 mV *vs.* RHE is $|8.43 \times 10^{-3} - 2.05 \times 10^{-1}|$ A cm^{-2}, this translates into an equivalent surface area increase of 24 times. As the surface roughens it is seen, comparing curves 3 and 4 to that for the clean electrode case, that the apparent electrocatalytic activity of the poisoned electrode surpasses that of the clean electrode.

From the Pourbaix diagram, Fig. 9.1, it follows theoretically that corrosion will arise at potentials up to -0.4 V *vs.* RHE, the reaction being:

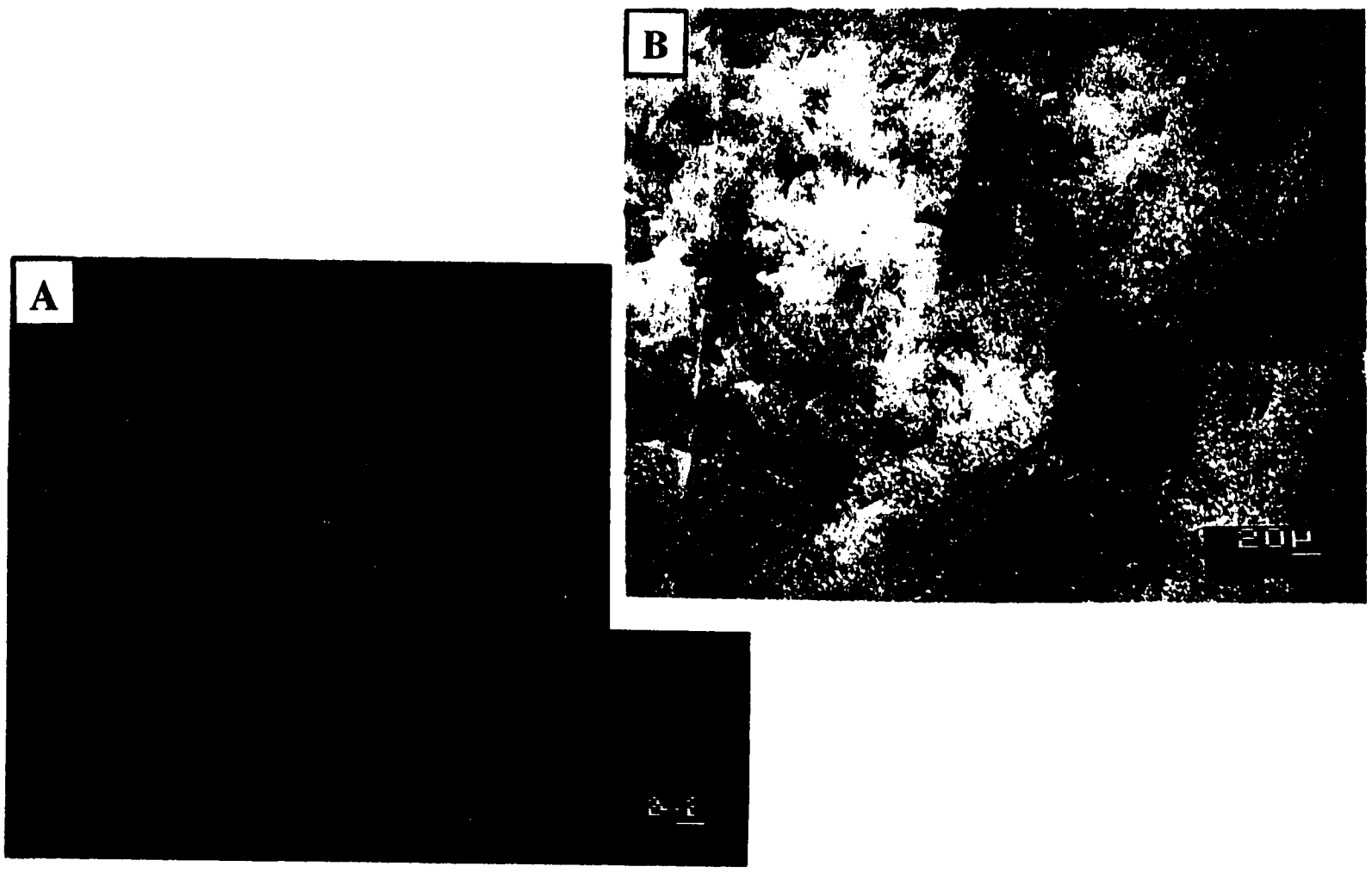

Fig. 9.3 SEM images of Ni electrodes after cathodic polarization in H_2 saturated 0.5 mol dm^{-3} H_2SO_4 solutions containing 5 x 10^{-4} mol dm^{-3} thiourea. A) A Ni rde subjected to 1 hr. of polarization followed by a potential-relaxation transient, another additional hour. B) A Ni membrane electrode subjected to approximately 12 hr. of variable cathodic polarization potentials (used for H permeation measurements). Magnifications A and B 20μm.

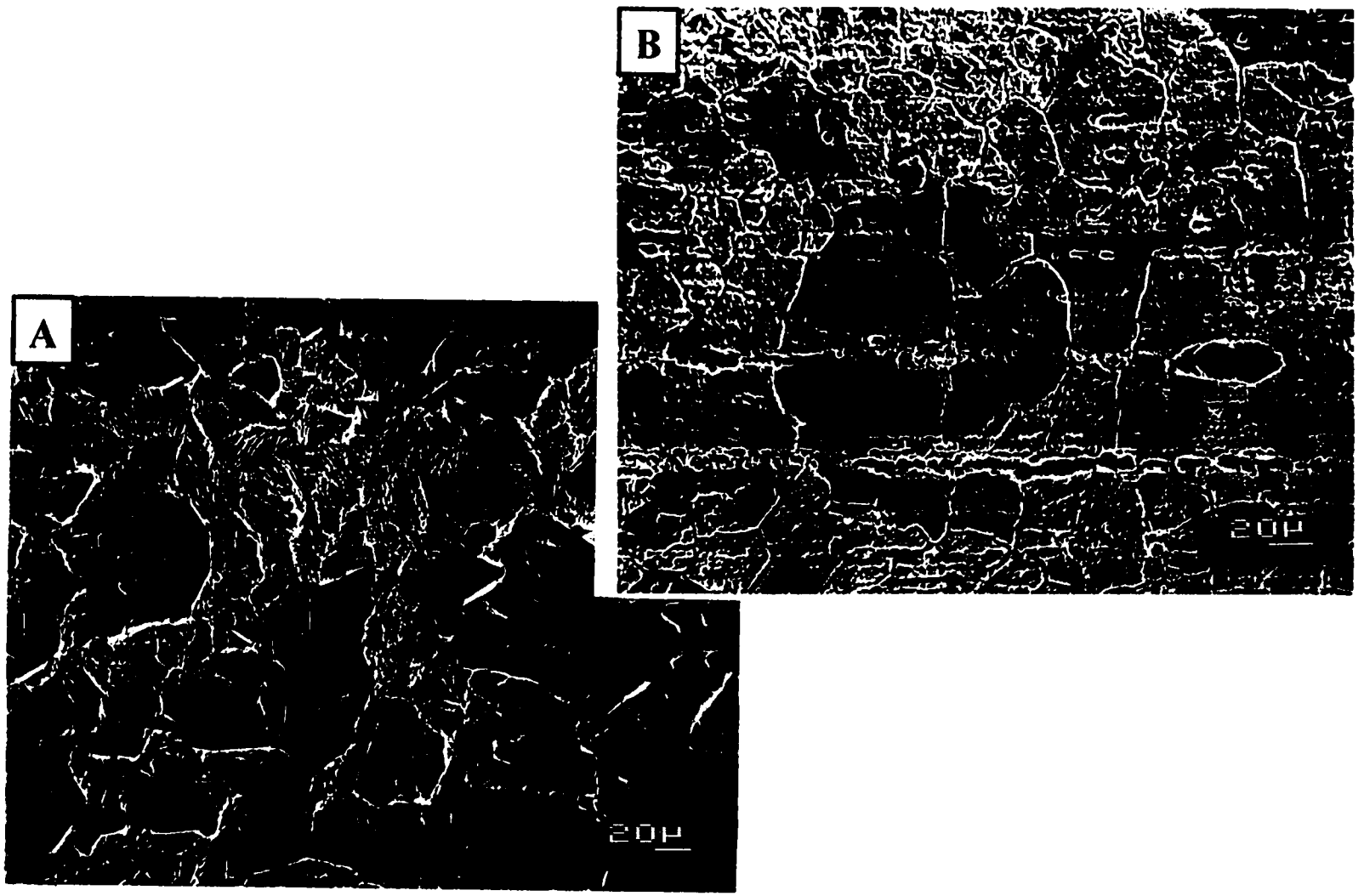

Fig. 9.4 SEM images of Ni wires (H_2 annealed) corroded in various acidic solutions. A and B) 0.5 mol dm^{-3} H_2SO_4 under an air atmosphere; C and D) 0.5 mol dm^{-3} H_2SO_4 under an H_2 atmosphere (1 atm pressure). B and D) the solutions also contained 1 x 10^{-3} mol dm^{-3} thiourea. The magnification on all of the images is 20μm.

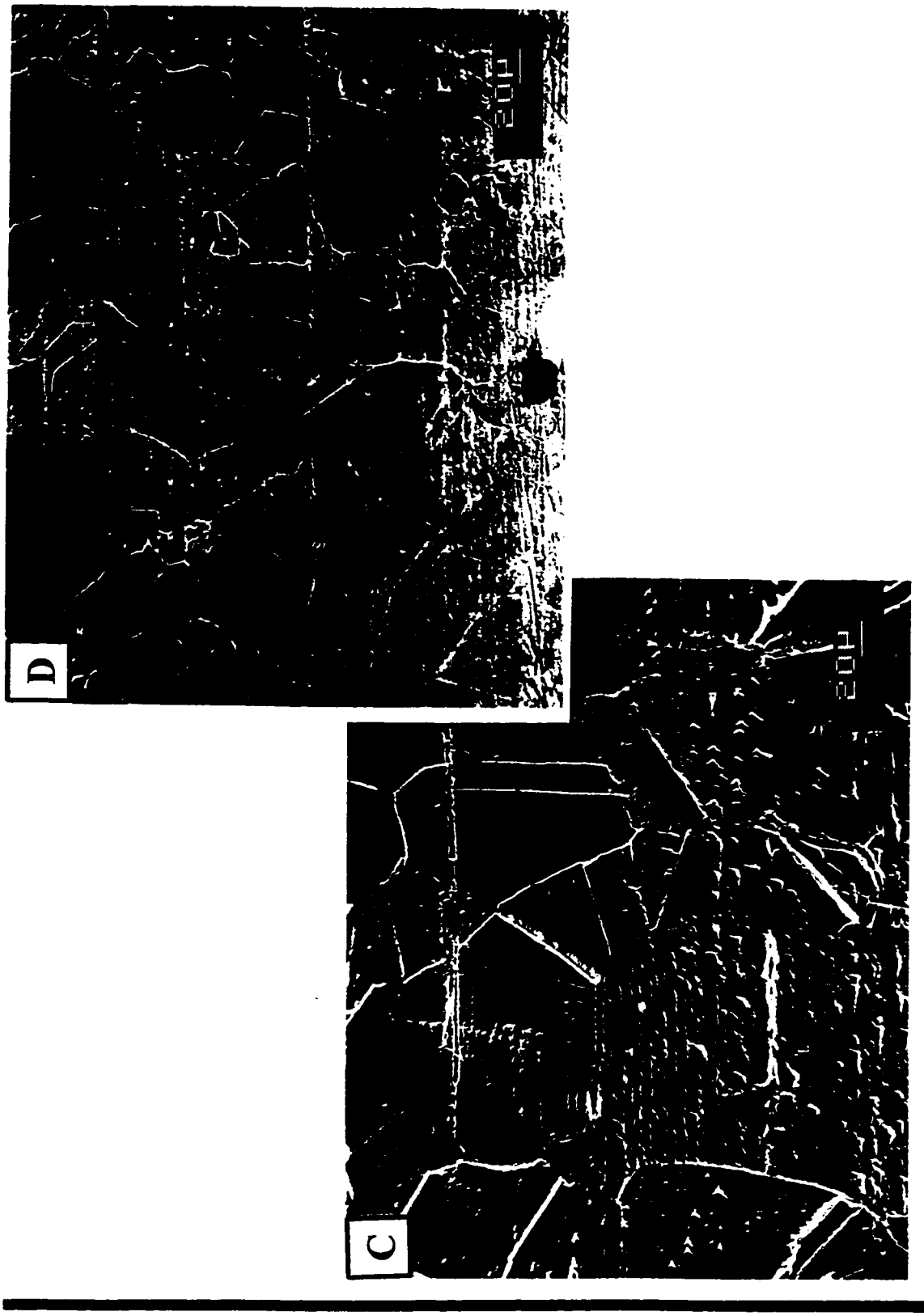

Fig. 9.4 SEM images C and D as described in the caption on the above page.

$$Ni + 6H_2O + SO_4^{2-} \rightleftarrows Ni(H_2O)_6SO_4 + 2e^- \qquad E^o = -0.250\ V \quad \textbf{(9.V)}$$

Under the present experimental conditions, H_2-saturated 0.5 mol dm^{-3} H_2SO_4 solution, the rate of the above dissolution reaction (9.V) is extremely small, allowing stable and reproducible surfaces to be obtained. One measure of the stability of the Ni electrode in the clean 0.5 mol dm^{-3} H_2SO_4, solution was the unchanging Tafel polarization curves which could be recorded over many hours of experimentation. Another measure of the stability was the small amount of corrosion which took place at a Ni wire exposed for four days to the same conditions as the Ni working electrode, and was observable in the SEM pictures, Fig. 9.4c.

The inhibitory influence which thiourea has on Ni corrosion in 0.5 mol dm^{-3} H_2SO_4, observed when Ni wires were allowed to freely corrode in the presence and absence of thiourea, was investigated. SEM pictures, taken after the corrosion was allowed to progress for 2 days when the solutions were open to air and after 4 days when the solutions were placed under an hydrogen atmosphere, are shown in Figs. 9.4a, b, c and d respectively, with 9.4b and 9.4d corresponding to 1 x 10^{-3} mol dm^{-3} thiourea having been added to the 0.5 mol dm^{-3} H_2SO_4. It can be seen that both the atmosphere above the solution and presence or absence of thiourea have dramatic effects on the extent of corrosion. The most severely corroded specimen was the wire which had been placed in a "clean" 0.5 mol dm^{-3} H_2SO_4 solution open to an air atmosphere. The least corroded sample was the wire which was bathed in a 0.5 mol dm^{-3} H_2SO_4 solution containing thiourea and saturated with H_2 gas.

One specific aspect which should be noted from the SEM photos is the regions where the majority of the corrosion takes place, i.e. the location of corrosion is quite specific to the grain-boundary regions and also it appears that one type of grain has a surface which is more sensitive to corrosion than the other type of grain surface. Such behaviour is commonly found in the corrosion literature and is a result of the substantial differences in the surface-energy between the atoms at the grain boundaries and the surface atoms which lay above a uniform metal lattice. This aspect is important when these corrosion pictures are compared with the SEM pictures taken after the Ni electrodes had been subjected to extensive cathodic polarization in the presence of thiourea, Figs. 9.3a, b and c.

The surface structure of the corroded Ni electrodes is found to consist of three regions (Figs. 9.3b and c). The large light and dark regions are, as in the previous SEM pictures, representative of the different grains. Interestingly the grain boundaries between these two types of grains (light and dark areas) do not appear to be selectively corroded over other areas of the Ni surface. The grains with the lighter shade are more severely corroded, appearing bevelled. The third region on this surface consists of black, worm-like pits. Comparison of these SEM pictures with those for the specimens which had not undergone previous cathodic polarization clearly indicates that the corrosion seen in Fig 9.3 is *not* due to the same process as that shown in Fig. 9.4. Although a surface analysis was not performed on the samples showing the two different types of corrosion (Fig. 9.3 and 9.4), indirect chemical and electrochemical evidence can be used to explore further the differences between these two types of corrosion behaviours.

The chemical nature of the two types of specimens, those in Fig. 9.3 and in Fig. 9.4, after corrosion, can be assessed qualitatively. The role of thiourea as an inhibitor can be rationalized since it is noncomplexing with Ni ions [11] and because it has a strong negative influence on the HER reaction rates (see curve 1, Fig. 9.2). If thiourea inhibits corrosion, the question then arises what process is causing the increase in the surface area observed during and after cathodic polarization? The only other species present or produced in solution is sulphide, being a product of the reduction of thiourea [6].

It can be speculated that the black worm-like pits on the sample in Fig. 9.3 are comprised of NiS or possibly a non-stoichiometric form, NiS_x. The reasoning for this assertion is: i) sulphur, in some form, e.g. S_{ads}, H_2S, Ni-SH, etc., is a product of the reduction of thiourea. This was demonstrated at a Pt electrode as described in chapter 6 (seen as a positive shift in the open-circuit potential to a value of 0.3 V *vs.* RHE, indicative of the PtS/Pt H_2S potential), and has been measured as H_2S gas exiting the cathode compartment at large surface area Ni electrodes in ref. 5; ii) the visible nature of NiS is black as are the pits in Fig. 9.3; and iii) It is found that PtS, PdS and NiS can be formed on the surface of the corresponding metal electrodes in acidic solutions [12]. The large stability of the PtS and PdS species allows these films to be formed electrochemically in macroscopic quantities by addition of H_2S to a cell containing the corresponding metal; the films can be subsequently removed easily and analysed [12]. NiS, on the other hand, is relatively reactive in *acidic solutions*, e.g. the equilibrium constants for NiS, PdS and PtS forming there respective ions along with the generating H_2S are 1.1 , 2×10^{-37}, and 1×10^{-52} [13] respectively. It is also known shown that metallic Ni_xS compounds can be

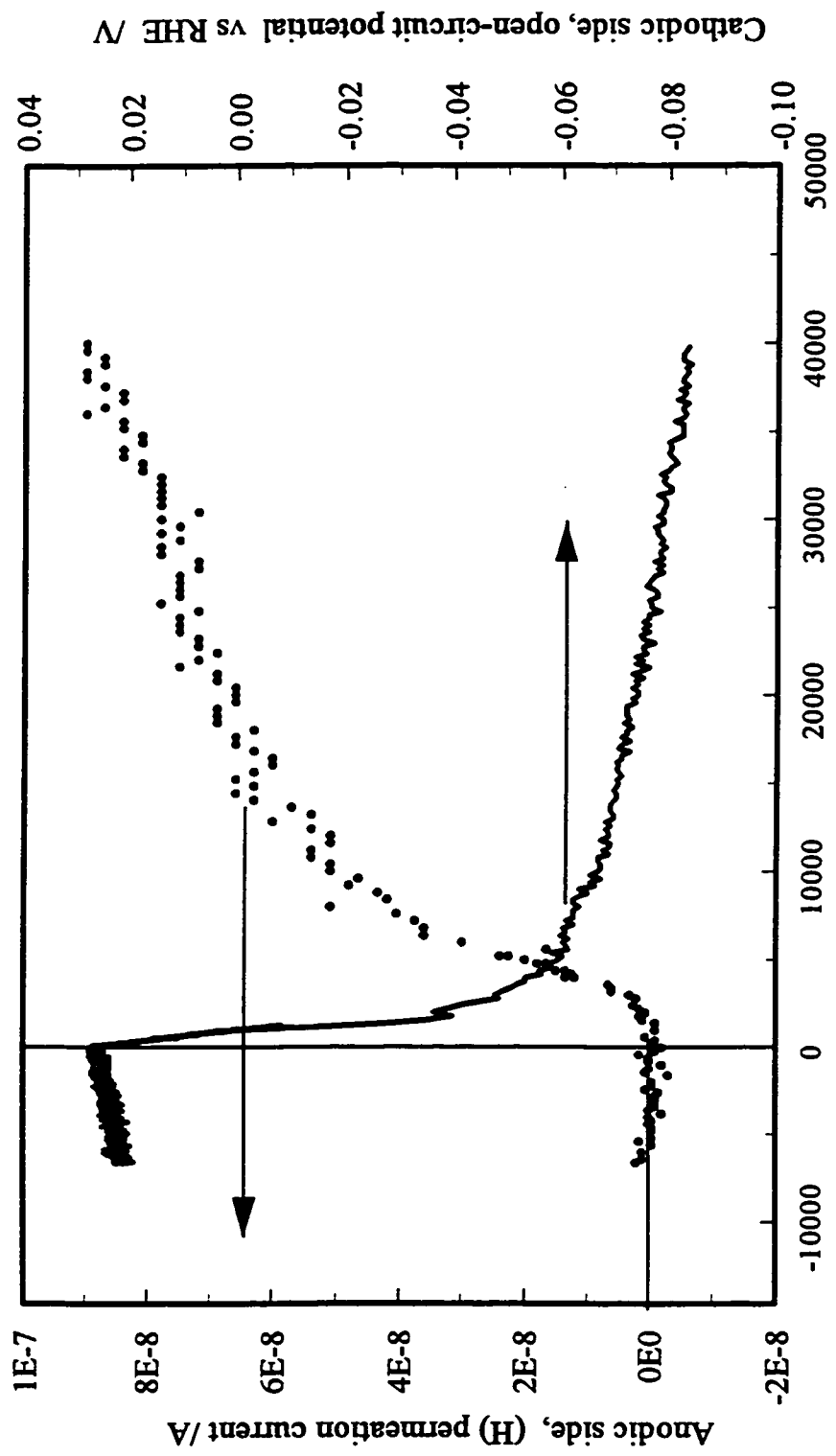

Fig. 9.5 Transient for H permeation through a 25 μm Ni membrane (symbols) and the open-circuit potential of the cathodic side of the membrane (solid line), resulting from the addition of thiourea (1.3×10^{-4} mol dm^{-3}) to the cathodic side of the membrane.

formed in electrochemical plating from a $NiSO_4$, H_3BO_3 and HCl solution containing varying amounts of thiourea which acts as the sulphur source [14]. This is conclusive evidence for the formation of an adsorbed S species after reduction of thiourea and gives some support to the formation of a NiS species . These compounds appeared to be stable during electrochemical HER measurements in alkaline media [15] and it was also stated that the S content, 10-20%, influences the amount of H sorbed inside the electrode, e.g. Ni:H values from 16 to 6 were found.

The effect thiourea has on the corrosion process and on the measured open-circuit potential can be illustrated by constructing a Wagner-Traud [16] diagram, Fig 9.6, using the E *vs.* log i relations for both the anodic and cathodic processes involved. The measured cell potential of the coupled anodic and cathodic reactions, the corrosion potential, then corresponds to the point where the anodic and cathodic polarization lines cross. The current-density at which they cross, corresponds to the equal and opposite individual current-densities of each reaction, as the net reaction current-density is equal to zero. The measured open-circuit potential of the overall process of corrosion of Ni in a clean, H_2-saturated 0.5 mol dm^{-3} H_2SO_4 solution was identical to the hydrogen reversible potential, *ca.* 0.0V *vs.* RHE. From the Wagner-Traud type diagram, this corrosion potential indicates that the dissolution process has a much lower rate and that it is the only reaction of the coupled reactions (dissolution and H_2 evolution) which is polarized, i.e. the velocity of the HER can equal the rate of dissolution without an observable polarization.

When thiourea is added to the solution the dissolution line moves to lower current-densities, which is consistent with the SEM corrosion photos (Figs. 9.3 and 9.4), but now

the dissolution current is coupled to the HER proceeding at the thiourea-poisoned Ni surface. Since the poisoned surface has poorer catalytic properties for the HER than the clean Ni surface, a greater cathodic polarization takes place leading to a diminution of the dissolution rate. This results in a lowered corrosion potential of -20 mV *vs.* RHE, denoted as $E1_{cor}$ in Fig. 9.6.

The other possible cathodic reaction which could be coupled to Ni dissolution when O_2 is not present, is that of H *ab*sorption into the metal. The cathodic reaction, H_2 evolution or H *ab*sorption, which would be preferred is that which couples with the anodic dissolution as the more reversible reaction.

At a disk or wire electrode the H *ab*sorption reaction is *noncontinuous*, analogous to the UPD of H at Pt but in a 3-dimensional sense. The corrosion reaction, which is continuous, will couple to the similarly continuous HER, which is slightly polarized at a thiourea-poisoned Ni surface producing the -20 mV *vs.* RHE open-circuit potential which was measured at the disk and wire electrodes. If the same type of corrosion takes place but now at the surface of the H input side of the H permeation cell, where H entering the metal can diffuse though the membrane and ultimately be oxidized at the anodic side, the H absorption process would now be continuous, allowing it to be a viable reaction in the Ni corrosion process.

The result of injecting thiourea into the working electrode compartment for the cathodic (H input) side of the Ni membrane, when it was at open-circuit (o.c.), is shown in Fig. 9.5. The o.c. potential of the cathodic side shifts negatively after addition of the thiourea, while, at the anodic side of the Ni membrane electrode, an anodic current *vs.*

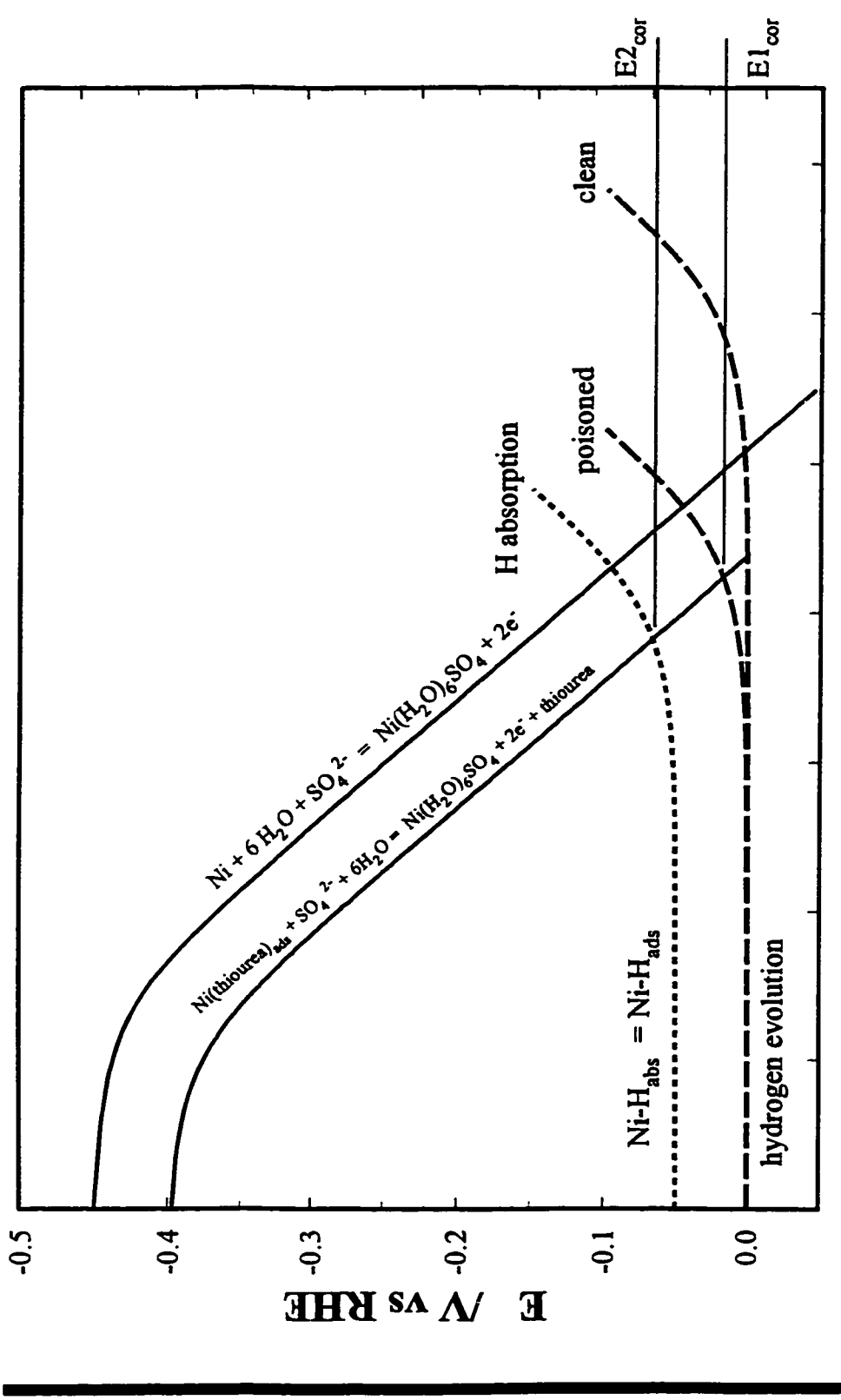

Fig 9.6 A Wagner-Traud plot illustrating the connection between the rates of dissolution and coupled cathodic reaction during corrosion of Ni in 0.5 mol dm^{-3} H_2SO_4 + thiourea. $E1_{cor}$ - the corrosion potential at a Ni disk or wire electrode, $E2_{cor}$ - the corrosion potential the cathodic side of the permeation cell, where permeating H is oxidized at the outlet end.

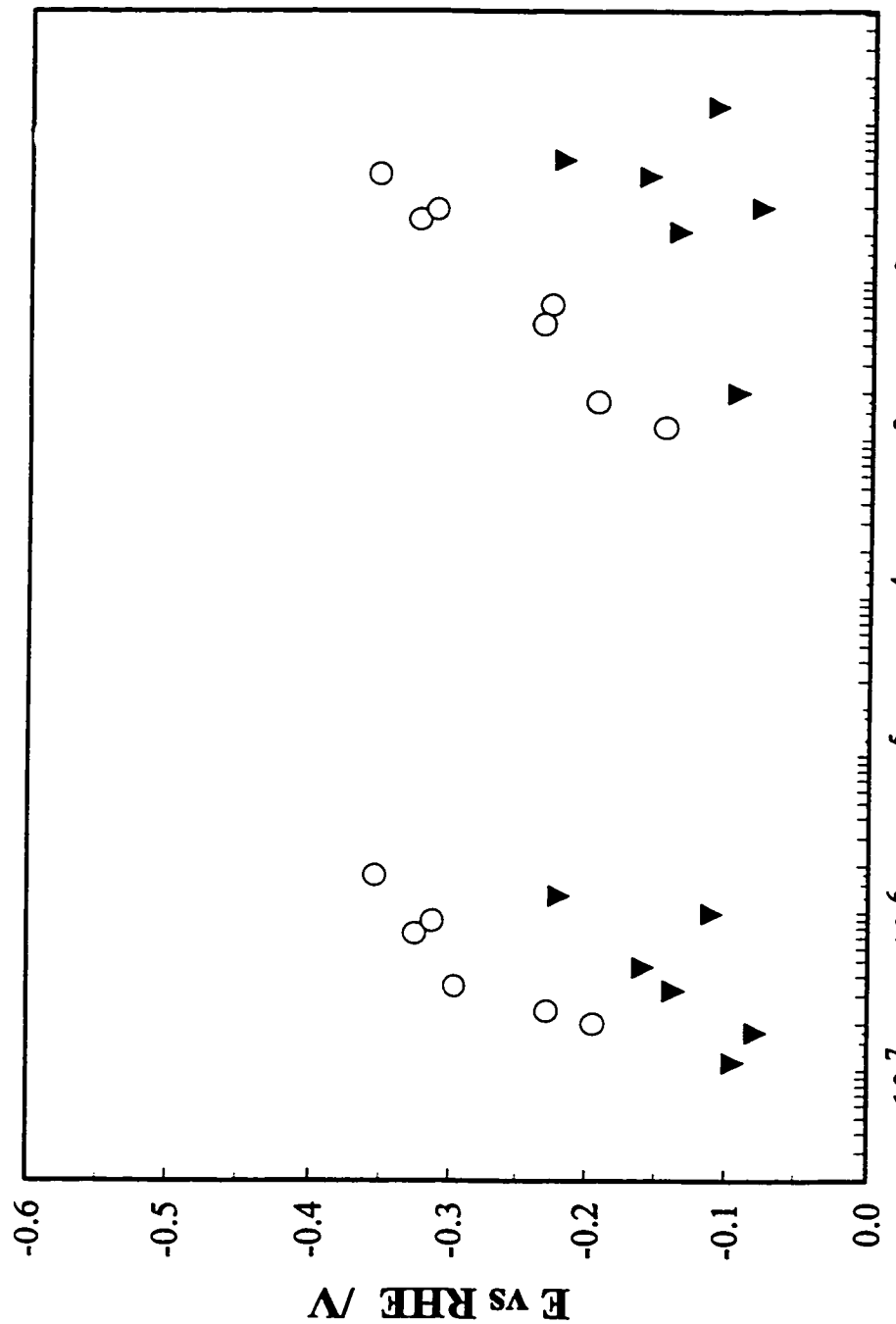

Fig. 9.7 Tafel type plots from the steady-state H permeation, anodic and cathodic current-density *vs.* cathodic potential. Open symbols - 0.5 mol dm^{-3} H_2SO_4; solid symbols - 0.5 mol dm^{-3} H_2SO_4 + 1 x 10^{-4} mol dm^{-3} thiourea, in the W.E. compartment of the cathodic side of the membrane. Anodic side- 0.5 mol dm^{-3} NaOH, E = + 500 mV *vs.* RHE; T = 298 K.

time transient arises. The shift in the o.c. potential of the H input side of the membrane, must arise on account of H permeation into and through the Ni membrane. The increase of negative potential at the cathodic side *with time*, to a value *ca.* -90 mV *vs.* RHE, the value when the measurements were stopped, is connected with an increasing difficulty in sorbing H into the Ni. At time = 0, the Ni metal is free of absorbed H, (i.e. the dimensionless fraction of H inside the metal, $(X_H) = 0$ at t = 0) the overpotential required to sorb H (regardless of mechanism) at a rate equal and opposite to that of the dissolution reaction, which we assume to have a constant rate, will be low since the factors $(1-X_H)$ and X_H in eq. 1.22 favour the forward reaction, but as the metal fills with H the (negative) overpotential must increase cathodically so as to enhance the driving force for H sorption with, depending on the mechanism, a corresponding increase in θ_H on the surface to counteract the declining value of $(1-X_H)$ in the forward direction of the sorption reaction, eqs. 1.24 and 1.25.

A similar argument, justifying the increase in overpotential as the H permeation current increases, can also be presented, supposing the direct H injection process is operative. In this case the H sorption reaction is directly dependent on overpotential through a Butler-Volmer type relation, and the increase in overpotential will increase the driving force of the reaction in the usual way for simple electrochemical processes. The only problem with this explanation is that it is more difficult to take into account how the adsorbed thiourea modifies the reaction energetics.

The H permeation currents in this case are extremely low, *ca.* 80 nA cm^{-2}, which may reflect a low rate of dissolution (the amount of dissolution current going to produce

H_2 is unknown). The relationship between the permeation current-density, i_∞, and the H concentration at the input side, c_o, as determined in § 1.4 is: $i_\infty = F(c_o D_H/L)$; from this relation, a c_o value corresponding to the steady-state permeation current-density, measured from Fig. 9.5, is calculated to be 3.8×10^{-6} mole cm^{-3} taking $D_H = 6.1 \times 10^{-10}$ cm^2 sec^{-1} and the membrane thickness L = 25 m..

Lewis [8], states that the transition from the α to β Pd-H phase occurs at an H concentration > 3.4×10^{-3} mole cm^{-3}. Making the analogy between Pd and Ni, the measured c_o concentration would be characteristic of the formation of 0.11% of the α Ni-H phase. In fact, the largest permeation current-density we were able to measure, Fig. 9.7, corresponded to approximately 2 μA cm^{-2} yielding a value of 8.5×10^{-5} mol cm^{-3}, which is comparable with the limiting c_o value calculated by Archer and Grant [18] of 7.22 $\times 10^{-5}$ mol cm^{-3}; these values are still well within the α Ni-H phase region, i.e. 2.5% of the α phase formed![2] Therefore, the o.c. potential in Fig 9.5, according to the above rationalization, *cannot* be a consequence of an α/β Ni-H equilibrium but is the mixed potential of the coupled Ni dissolution and H sorption reactions. This corrosion potential is identified as $E2_{cor}$ on the Wagner-Traud diagram, Fig 9.6.

Actually the potential of an electrode cannot be governed by a phase change *inside* the metal, but will be regulated by the charge-transfer reaction which discharges the

---

[2]This type of analysis only holds if the limiting process of H permeation is the diffusion step, otherwise if the rate-limiting process is transfer of H from the a*d*sorbed to the a*b*sorbed state then the surface concentration of H would be expected to be lower than the equilibrium value of H (c_o) which is measured at an electrode where all the surfaces are experiencing the same potential. This is usually not assumed to be the case but it would explain the differences in these results as compared to the equilibrium measurements made in ref. 6.

surface products of the phase change, in the present case adsorbed H, at a surface coverage fraction, θ_H.

9.4 Potential-Relaxation Measurements

A quantitative mathematical description of the potential-relaxation technique will not be given due to space restraints. In words, the potential-relaxation experiment can be described as the relaxation of the charge which is built up in the electrochemical interphase after the interruption of a steady-state polarization. The charge which the interphase can hold is that of the electrochemical double-layer, similar to the charge on a capacitor, and also charge which is held by adsorbed intermediates, where an electron has been transferred in the adsorption process. The dissipation of this interfacial charge occurs via the electrochemical steps of the reaction of interest. Implicitly the theoretical problem is defined as two differential equations which when solved gives the potential and coverage relaxations, $d\eta/dt$ and $d\theta/dt$ respectively. For the HER these equations take the form:

$$-(C_{dl}/F)(d\eta/dt) = r_o(\theta,\eta) = \upsilon_1 + \upsilon_2 \qquad \textbf{(9.1)}$$

$$(q_1/F)(d\theta/dt) = r_1(\theta,\eta) = \upsilon_1 - \upsilon_2 - 2\upsilon_3 \qquad \textbf{(9.2)}$$

with C_{dl} being the double-layer capacitance (assumed to be potential independent) and q_1 the charge needed for maximum surface coverage of adsorbed H. The other terms r_i and υ_i define the electrochemical rates as has been seen in previous chapters. The potential-relaxation problem has been studied in depth by a number of authors, for theoretical analyses of the potential-relaxation problem see refs. 21,25 and for a more analytical approach see ref. 26 and, for experimental details and data acquisition procedures, see

refs. 26 and 27.

The apparent shift in the equilibrium potential to values *ca.* -0.1 V *vs.* RHE found in the Tafel measurements, Fig. 9.2, when thiourea was present in the electrolyte, has a value equivalent to the potential plateau observed in potential-relaxation measurements, Fig. 9.8. The stability of this plateau extends over six orders of magnitude of time, at which point (approximately 4000 s) it decays to a value of the potential ≈ -10 to -20 mV *vs.* RHE, i.e. it has reached the same potential value as that observed before cathodic polarization when thiourea was present in the electrolyte. The length of time of this arrest is indicative of an H diffusion rate-limited process where H diffuses through or out of a thin layer of Ni_x-H inside the metal, near the Ni surface. The times involved are comparable to those for H permeation through the 25 μm Ni membrane where 3000 to 5000 s where needed to reach a steady-state anodic H permeation current-density; see Fig. 7.1b. Also shown in Fig. 9.8 are the potential-relaxation transients recorded in a poison-free 0.5 mol dm^{-3} H_2SO_4 solution and one containing additionally L-cysteine. The lines running through the clean-solution data and those for thiourea being present are the results of nonlinear least squares (NLS) fitting of the HER model [20] to the data.

The derived rate constants are shown in Table 9.1, written assuming the Heyrovsky step to be rate-limiting. The plateau of potential set up at the Ni electrode during potential-relaxation after charging in a solution containing thiourea can be accounted for as either in terms of: 1) the quasi-equilibrium potential set up between the α and β Ni-H phases in the near-surface region, 25 to 30 μm deep [6] inside the metal surface, an equilibrium process equivalent to that seen at the α/β Pd-H electrode where

the established equilibrium potential is E ≈ 0.05 V vs RHE, or 2) a mixed potential set up between the anodic M-H decomposition reaction (the direct H ionization mechanism assumed: see below) and cathodic hydrogen evolution [17], expressed as:

anodic reaction

$$Ni_xH + H_2O \rightleftarrows Ni + H_3O^+ + e^- \qquad \textbf{(9.VI)}$$

and the complementary, coupled **cathodic reaction**

$$H_3O^+ + e^- \rightleftarrows \tfrac{1}{2}H_2 + H_2O \qquad \textbf{(9.VII)}$$

or 3) with the potential dependence of the a*b*sorption-desorption reaction being determined by the HER kinetics alone, through a coupling of X_H with θ_H [21,22].

Assuming that the interfacial transfer of H from lattice to surface sites is rapid, and taking into consideration that any bulk to surface diffusion of H_{abs} only influences the duration of the plateau [22] we can write:

$$\underset{X_H}{Ni_xH_{abs}} \quad \underset{k_4}{\overset{k_{-4}}{\rightleftarrows}} \quad \underset{\theta_H}{NiH_{ads}} \qquad \textbf{(9. IV)}$$

with the H surface coverage (θ_H) discharging through the anodic and cathodic HER steps [21,22] coupled according to:

$$NiH_{ads} + H_2O \quad \underset{k_1}{\overset{k_{-1}}{\rightleftarrows}} \quad Ni + H_3O^+ + e^- \qquad \textbf{(9.I)}$$

with

$$NiH_{ads} + H_3O^+ + e^- \quad \underset{k_{-2}}{\overset{k_2}{\rightleftarrows}} \quad H_2 + H_2O \qquad \textbf{(9.II)}$$

Theoretical work based on this type of mechanism [22] has shown that the addition of the HAR into the overall reaction kinetic scheme does not dictate the value at

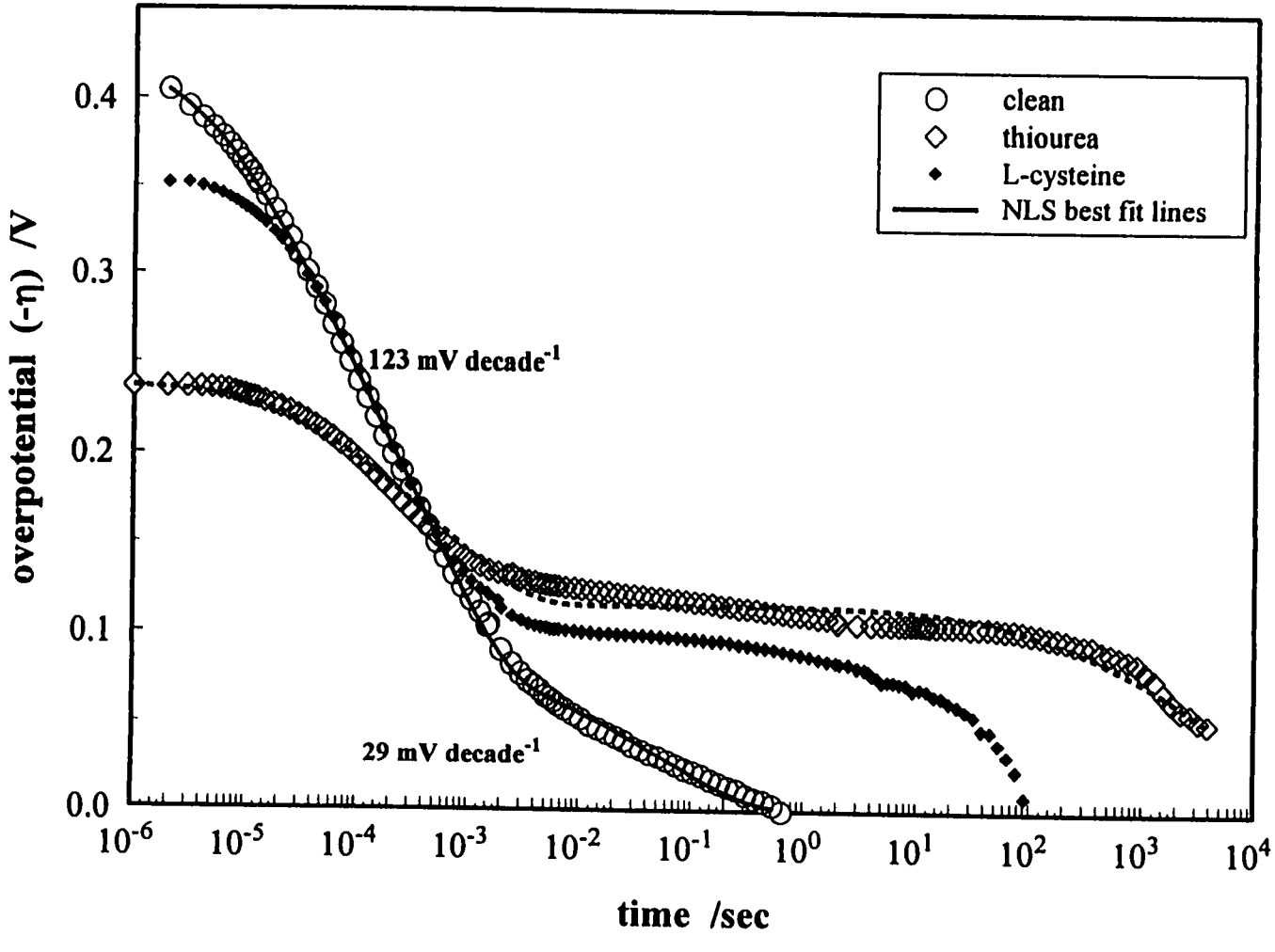

Fig. 9.8 Potential relaxation transients of Ni in 0.5 mol dm^{-3} H_2SO_4. ○ - clean, $i_{t=0}$ = 22.5 mA cm^{-2} ;♦ - 7.5 x 10^{-5} mol dm^{-3} L-cysteine, $i_{t=0}$ = 14 mA cm^{-2} ; ◇ -7.5 x 10^{-5} mol dm^{-3} thiourea, $i_{t=0}$ =5.5 mA cm^{-2} ; —— clean and ------ 7.5 x 10^{-5} mol dm^{-3} thiourea - best NLS fit lines. Polarization times 60 min for clean and thiourea, 5 min for L-cysteine.

which the potential plateau occurs but can only influence the duration of the arrest. The MH_{abs} species acts as an H reserve feeding the MH_{ads} species, θ_H, on the surface external to the bulk lattice. The coverage of the surface species remains constant until the fractional lattice occupancy by H_{abs}, X_H, goes to zero; then θ_H will relax to its equilibrium value through the HER steps I and II.

The relation between the rate constants is found [21] to be one of the controlling factors of the value of the arrest potential, in particular the ratio $(k_1 k_{-2})/(k_{-1} k_2)$, defined from this point onward as K_1/K_2. With the rate-controlling process being the Heyrovsky step, i.e. k_2 smaller than k_1, it is seen from [21] that as K_1/K_2 decreases, the potential at which the arrest occurs increases to more cathodic potentials; with the Volmer step as rate-controlling the opposite is true.

Table 9.1

Conditions	k_1 mol s^{-1} cm^{-2}	k_{-1} mol s^{-1} cm^{-2}	k_2 mol s^{-1} cm^{-2}	k_{-2} mol s^{-1} cm^{-2}	K_1/K_2
0.5 M H_2SO_4 *	3.6± (0.1) x 10^{-8}	1.0± (0.1) x 10^{-8}	5.6± (0.1) x 10^{-10}	2.0± (0.1) x 10^{-9}	13
0.5 M H_2SO_4 + thiourea *, **	8.2± (0.01) x 10^{-11}	1.7± (0.01) x 10^{-7}	9.3± (0.02) x 10^{-12}	1.4± (0.01) x 10^{-15}	2 x 10^{-7}

* C_{dl} held at 20 μF cm^{-2}, ** α = 1.0 (high overpotential slope in Fig 9.8 is 60 mV $decade^{-1}$)

The rate constant values shown in Table 9.1 for the potential-relaxation at poison-free electrodes compare reasonably well with those derived from analysis of the Tafel data and with the results from EIS measurements, *viz.* $i_o(Taf) = 2F(1.8 \times 10^{-10})$ and $i_o(pd) = 2F(5.6 \times 10^{-10})$ A cm^{-2}. The comparison of these values becomes better considering that the results obtained by the potential-relaxation method are given per cm^2 of real surface

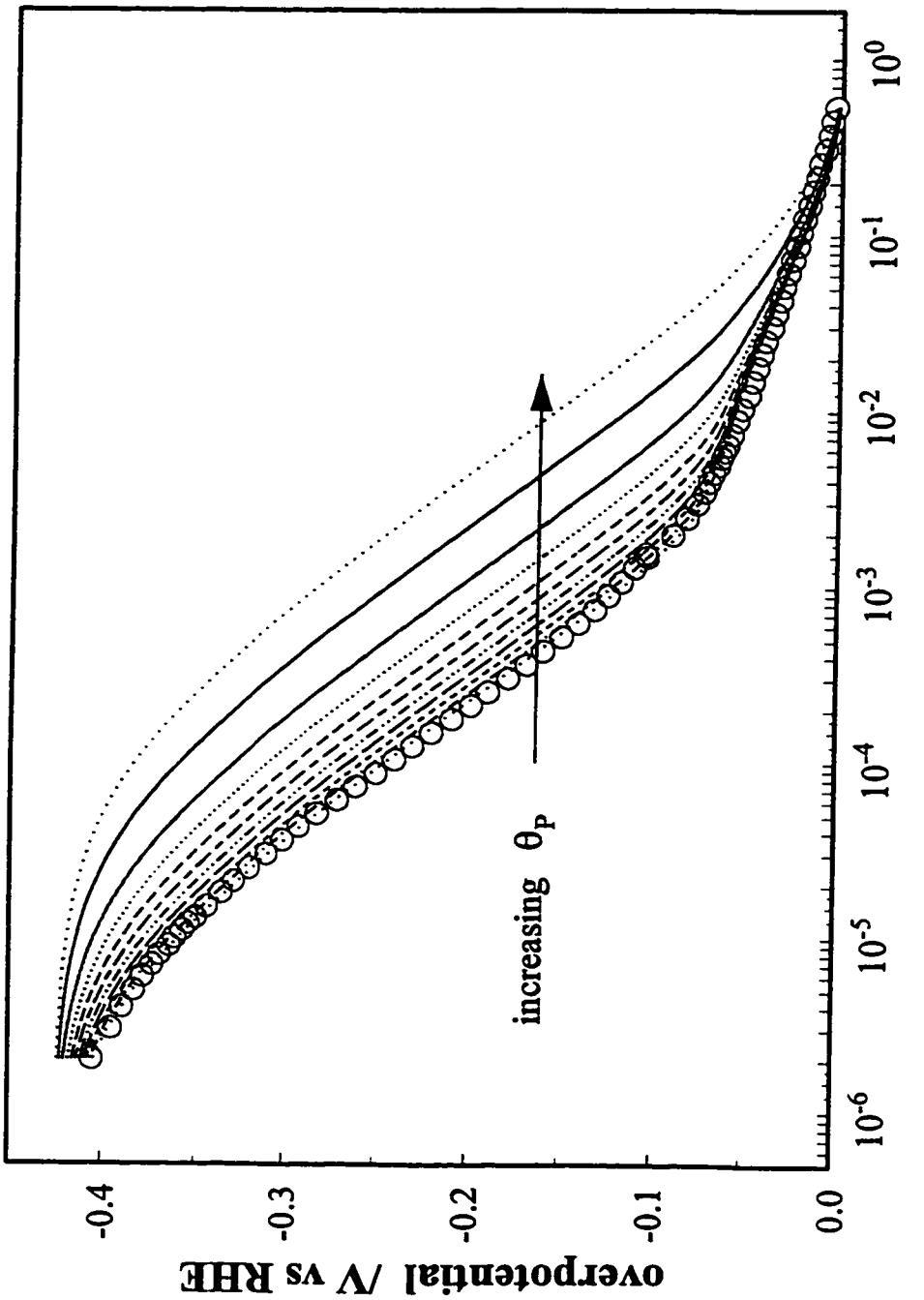

Fig. 9.9 Potential decay transients showing the effect of including a υ_P term in the rate equations for step I and II. Rate constants used in the calculation are taken from Table 9.1 for the clean fit. θ_P values vary from 0 to 0.9 in 0.1 step intervals plus $\theta_P = 0.95$.

area while the results from the Tafel method (here the geometrical surface area was used in the analysis) work out in terms of the actual geometrical surface area. The above results obtained in the poison-free, 0.5 mol dm^{-3} H_2SO_4 solution therefore provide a value for the roughness factor of 3.1, which is reasonable for the surface studied, that of an unpolished, annealed Ni wire.

The magnitudes of the rate constants for the case where the electrode was poisoned with thiourea also give a log i (η) relationship close to that found experimentally, Fig. 9.2 (curve 4), but again a roughness factor, in this case *ca.* 25 must be introduced. This value of the roughness factor is comparable to that found by comparing the current-density increases in the Tafel measurements, see curve 1 to curve 4 in Fig. 9.2. The most important feature of the NLS fitting results found in Table 9.1, is the striking difference between the K_1/K_2 values for the clean and poisoned-electrode *cases, viz. ca.* 8 orders of magnitude which arises because of the appreciable differences in orders of magnitude of the respective rate constants (Table 9.1).

The influence of an adsorbed poison on the potential-relaxation response for hydrogen evolution can be considered in an elementary sense by adding a poison coverage term, θ_P, into the rate equations of the HER, steps I and II, i.e. replacing $(1 - \theta_H)$ with $(1 - \theta_P - \theta_H)$ in the back-reaction Volmer term (υ_{-1}) and the forward Heyrovsky term (υ_{+2}). Using the rate constants from the fitting of the potential-relaxation curve for the electrode in clean, 0.5 mol dm^{-3} H_2SO_4, the effect of adding a θ_P term is shown in Fig. 9.9. The response to the introduction of the θ_P term is a decrease in the overall rate, producing slower depolarization of the C_{dl} and a lowering of θ_H which diminishes the plateau-like

feature at longer times.

From a comparison of the simulation in Fig. 9.9 with the data in Fig. 9.8 it is clear that the presence of thiourea or L-cysteine on the Ni surface acts not only as a site blocking agent but intimately reacts with the surface altering significantly the "chemical" rate constants, k_1, k_{-1} and k_2 by modes specific to each step and step direction. The specific changes are seen when comparing the ratios of each of the rate constants: $k_1(cl)/k_1(P) = 440$, $k_{-1}(cl)/k_{-1}(P) = 0.06$, $k_2(cl)/k_2(P) = 60$ and $k_{-2}(cl)/k_{-2}(P) = 2.0 \times 10^6$ which account for the large differences in the K_1/K_2 ratio and the significant shifts in the plateau potential shown in the potential-relaxation results for Ni in solution with and without thiourea present.

An expression for the chemical potential (μ_H) of adsorbed H at a given steady-state or equilibrium potential was derived in chapter 8. After rearrangement, eqs. 8.1 and 8.2 become:

$$\mu_H = \mu_H^o + RT \ln \overline{K_H} = \mu_H^o + RT \ln \frac{\overline{k_1} + \overline{k_{-2}}}{\overline{k_{-1}} + \overline{k_2}} \qquad (9.3)$$

Using the rate constants from the potential-relaxation fitting the difference in the chemical potential of H when it is adsorbed at clean and poisoned Ni electrodes can be calculated from:

$$\Delta\mu_H = \mu_H^{cl} - \mu_H^P = RT \ln \frac{\overline{K_H^{cl}}}{\overline{K_H^P}} \qquad (9.4)$$

The $\Delta\mu_H$ value resulting from this calculation is +22 kJ mol^{-1}.

It is also useful at this point to explore the alternative potential-relaxation analysis. As was discussed in § 9.1 an identical current-voltage response can be calculated when the rate constant value of k_1 is interchanged for k_2 and as well k_{-1} for k_{-2}; this is also found to

be true for the potential-time behaviour in a potential-relaxation experiment [20]. When the rate constants are interchanged, using the analyses of the potential-relaxation behaviour in both the clean and poisoned electrolytes (Table 9.1), a new calculated ($\Delta\mu_H$) value of -22 kJ mole^{-1} results.

The two values of ($\Delta\mu_H$), +/- 22 kJ mole^{-1}, will therefore give opposing views on the thermodynamics of the H sorption process. In the first arrangement, which gives $\Delta\mu_H$ = +22 kJ mole^{-1}, a decrease in the chemical potential of adsorbed H results when H is adsorbed at an electrode which is in contact with a 0.5 mol dm^{-3} H_2SO_4 solution which contains thiourea. This causes an increase in the reaction energy for the transfer of H from the *ad*sorbed state to the *ab*sorbed state thus decreasing the driving force for absorption of H. This arrangement of the rate constants corresponds to θ_H increasing with potential and also it is found that at $\eta = 0$, θ_H (clean) is greater than θ_H (poisoned).

The second case, $\Delta\mu_H$ = -22 kJ mole^{-1}, leads to an increase in the driving force for the H absorption process when thiourea is present in the electrolyte but this configuration of the rate constants leads to a situation where θ_H will decrease with potential for both the cases with and without thiourea in the electrolyte.

The difficulty is then to determine which arrangement of the rate constants, that producing a larger θ_H or smaller θ_H as η becomes more negative, best describes the system[3]. As was noted in § 9.1 evidence for both situations, θ_H decreasing or increasing

---

[3]It is also possible that the direction of the change of the coverage of the OPD H species with respect to overpotential differs when thiourea is present in the electrolyte, e.g. the HER in clean 0.5 mol dm^{-3} H_2SO_4 might have θ_H(OPD) increasing with overpotential but when thiourea is added θ_H(OPD) might decrease with overpotential, or vice versa.

with overpotential, have been presented in the literature [10,24].

An approach which was developed by Cheong *et al.* [10] for differentiating between these two limiting cases is to relate the rate-determining step of the HER to the shift in the open-circuit potential which takes place in the presence of organics which can be actively reduced by adsorbed H. Following the mechanism proposed by Cheong *et al.* [10], the o.c. potential shift occurs because the symmetry between the reaction steps which produce and the reaction steps which use adsorbed H is broken. According to the mechanism presented by Cheong *et al.* [10], a positive shift in the o.c. potential indicates that $k_1 > k_2$, i.e. the Heyrovsky step is rate-controlling and θ_H will increase with an increasingly negative overpotential. A negative shift indicates $k_1 < k_2$, i.e. the Volmer step is rate-controlling and θ_H will decrease with an increasingly negative overpotential.

This treatment of an organic reduction reaction which is running in parallel with the HER is different from that presented for the reduction of thiourea at Pt in chapter 6. The view of Cheong *et al.* [10] has the organic in a nonadsorbed state reacting with adsorbed H. The treatment presented in chapter 6 had adsorbed thiourea being reduced via an electron transfer/proton transfer (from the bulk solution) type mechanism, not involving adsorbed H and hence the symmetry of the HER, in terms of θ_H is preserved. In the study of Cheong *et al.* [10], compounds which appeared to be nonadsorbing on the Raney Ni electrocatalysts used, i.e. THF, t-cinnamic acid and benzoic acid, were shown to produce positive shifts in the o.c. potential in 0.5 M NaOH solutions; these results indicate that $k_1 > k_2$. In the present work, when both L-cysteine and thiourea are present in the electrolyte a negative shift in the o.c. potential was observed which, according to

the treatment of Cheong *et al.* [10], indicates that the Volmer-step is rate-controlling ($k_1 < k_2$) and therefore θ_H decreases with increasingly negative overpotential.

From the two above analyses of the potential-relaxation transients, 1) the analysis of the shift in μ_H, determined from kinetic fitting with the +ve $\Delta\mu_H$ value, corresponds to promotion of the H absorption reaction and 2) from the shift in the o.c. potential (arrest potential), analyzed using the treatment of Cheong *et al.* [10], it would appear that the rate-limiting step is the Volmer, H adsorption, step resulting in θ_H decreasing with increasingly negative overpotential. This result though is inconsistent with the previous observation of the change in the o.c. potential of the H input side in the H permeation transient in Fig. 9.5, which arose in response to the addition of thiourea to the electrolyte in the input side.

From this result two conclusions can be drawn: 1) if the addition of thiourea enhances H sorption, μ_H must have a more *positive* value than that when clean 0.5 mol dm^{-3} H_2SO_4 is used and 2) the increase of the o.c. potential to more negative values as the H permeation current increases (Fig. 9.5) can only be explained (assuming H absorption goes through the adsorbed H intermediate) if the Heyrovsky step is rate-limiting, which leads to θ_H and also μ_H increasing with overpotential. Since the potential-relaxation analysis is heavily dependent on the specific model used it is subject to greater uncertainty, and therefore the choice of which step in the HER is rate-limiting must be based on the H permeation results shown in Fig. 9.5. As a consequence, the potential-relaxation analysis is left in an incomplete state awaiting increased sophistication of the model and an extension of the experimental work.

A more exact potential-relaxation analysis would need to include parameters for, 1) the adsorption and reaction of thiourea (through a mechanism of direct electron transfer or a mechanism where it reacts with adsorbed H), 2) the effect of any products which are formed by the reduction of thiourea and 3) the H *ad*sorbed to H *ab*sorbed transfer reaction, along with bulk-to-surface diffusion.

9.5 Conclusions

The HER at Ni in 0.5 mol dm^{-3} H_2SO_4 is well behaved and its kinetics follows the Volmer-Heyrovsky mechanism. The addition of thiourea to the electrolyte produces an adsorbed layer of thiourea on the Ni surface; this adsorption initially decreases the rates of the HER by *ca.* 1 order of magnitude of current at a given hydrogen overpotential. Additional to this influence on the HER rate, the adsorption of thiourea is found to increase the stability of a Ni specimen, not under potential control, to corrosion in 0.5 mol dm^{-3} H_2SO_4. Upon cathodic polarization, sulphur (most likely in the form of H_2S or an adsorbed S species) is produced from the electrocatalytic reduction of thiourea. This species is then found to *enhance* the dissolution rate of the Ni electrode, decreasing the stability of the Ni surface. The surface structure, after this type of dissolution process, was found to be significantly different from that produced on freely corroding Ni wires in 0.5 mol dm^{-3} H_2SO_4 solutions, with and without thiourea present.

It was shown that the main influence of thiourea on the H sorption and H_2 evolution reaction, results from substantial modification of the reaction rates of each HER or H-sorption reaction step. This was directly measured from H permeation and potential-

relaxation measurements. It was shown that the modification of the HER rates by thiourea is significant enough that an increase of H entry into the metal can be seen at open-circuit, as measured using the H permeation technique. This increase in H entry at o.c. attests to the vast modification of the HER kinetics and chemical potential of adsorbed H which arises because the increase in H entry is coupled with a dissolution reaction, following the usual corrosion mechanism, which runs at a greatly impaired rate.

The *enhanced* corrosion rate seen after cathodic polarization performed in the presence of thiourea is evident from the HER Tafel measurements. The indicated surface area changes can also be observed as pitting of the Ni surface as found by SEM. Different corrosion potentials at Ni disk and membrane (used in the permeation cell setup) electrodes are explained by the coupling of the Ni dissolution reaction to the HER at disk electrodes and to the HAR at the membrane electrodes.

Clear evidence of thiourea acting as an H-entry promoter at Ni during active cathodic polarization is marred by the instability of the Ni surface when thiourea is present in the electrolyte, (see scatter in the H-permeation results, Fig. 9.7). The role of thiourea in modifying the HER kinetics is clearly seen from the potential-relaxation results. The changes in the HER kinetics produce a decrease in the chemical potential of the adsorbed H species, which is linked, as was shown in chapter 8, to the amount of H sorbed into the metal.

References

1. B.E. Conway and Bai, J. Electrochem. Soc., 142 (1995) 3393.

2. L. Chen and A. Lasia, J. Electrochem. Soc., 139 (1992) 3214.

3. B.E. Conway and L. Bai, Proc. Fifth World Hydrogen Energy Conference, Toronto, Canada, July (1984) 879.

4. D.P. Smith, "Hydrogen in Metals", Chicago University Press, Chicago (1948).

5. M. Pourbaix, "Atlas of Electrochemical Equilibrium in Aqueous Solutions", National Association of Corrosion Engineers, 1974.

6. Z. Sklarska-Smialowska and M. Smialowski, J. Electrochem. Soc., 110 (1963) 444.

7. H. J. Bauer and E. Schmibbauer, Zeit. Physik, 164 (1961) 367.

8. F.A. Lewis, " The Palladium Hydrogen System", Academic Press, London, 1967.

9. J. O'M Bockris and B.E. Conway, J. Sci. Instrum., 25 (1948) 205; J. O'M Bockris and B.E. Conway, J. Chem. Phys., 28 (1958) 707.

10. A. Kam Cheong, A. Lasia and J. Lessard, J. Electrochem. Soc., 141 (1994) 975.

11. W.M. Szulman and S.W. Larionov, Zhur. Neorg. Chim., 11 (1966) 1076.

12. N. Ramasubramanian, J. Electroanal. Chem., 64 (1975) 21.

13. C. Linde , CRC Handbook of Chemistry and Physics, 75th edn., CRC Press, Cleveland, Ohio (1994/95) pp. 8-58.

14. R.Sabela and I. Paseko, J. Appl. Electrochem., 24 (1992) 376.

15. I. Paseka, Electrochimica Acta, 38 (1993) 2449.

16. Wagner and Traud, Zeit. Elektrochem., 44 (1938) 391.

17. B.E. Conway, H. Angerstein-Kozlowska, M.A. Sattar and B.V. Tilak, J. Electrochem.Soc., 130 (1983) 444.

18. M.D. Archer and N.C. Grant, Proc. Roy. Soc., London, A 395 (1984) 165.

19. A.C. Riddiford, in "Adv. in Electrochem. and Electrochem. Eng.", Eds. P. Delahay and C.W. Tobias, Vol. 4, Interscience Publishers, New York (1966), 47; see also D. Jahn and W. Vielstich, J. Electrochem. Soc., 127 (1962) 849.

20. A. Lasia and A. Rami, J. Electroanal. Chem., 294 (1990) 123.

21. D.A. Harrington and B.E. Conway, J.Electroanal. Chem., 221 (1987) 1.

22. A. Lasia and D. Grégoire, J. Electrochem. Soc., 142 (1995) 3393.

23. P. Marcus and E. Protopopoff, J. Electrochem. Soc., 140 (1993) 1571.

24. T. Matsushima and M. Enyo, Electrochim. Acta, 21 (1976) pp. 241, 823 and 1029.

25. B.V. Tilak and B.E. Conway, Electrochim. Acta, 21 (1976) 745 and also Electrochim. Acta, 22 (1977) 1167.

26. B.E. Conway, L. Bai and B.F. Tessier, J. Electroanal. Chem., 161 (1984) 39.

27. J. Giguère, H. Ménard and E. Potvin, Anal. Instr., 19 (1990) 87.

Contributions to Original Research

The processes involved in the reactions of hydrogen electrochemically at metal cathodes (evolution, adsorption and absorption) has received attention from researchers for over 90 years. This extensive body of work has provided a large base of knowledge from which one must progress in order to make significant contributions in this field. The accomplishments of the present researcher have been predicated by key ideas and concepts from the literature on hydrogen evolution and electrocatalysis; which can be categorized as follows:

1) Early ideas concerning the basis of electrocatalysis, and specifically the HER.

Key contributors: P. Delahay, M. Bagotosky, J.O'M. Bockris, B.E. Conway, R. Parsons, W. Vielstich and R.R. Adzic.

2) The recognition of H_2 diffusion as a process having an influence on the HER at active electrode surfaces.

Key contributors: M. Breiter and I. Losev.

3) The development and application of impedance techniques to electrochemical systems generally, and in terms of HER kinetics in particular.

Key Contributors: J.E.B. Randles, Epelboin, Keddam, R.D. Armstrong, J.H. Sluyters, M. Sluyters-Rehbach, D.D. MacDonald, B.E. Conway, L. Bai and D.A. Harrington

and

4) The recent work by J. Clavilier et al. which enabled researchers to be able to prepare and use Pt(hkl) electrodes having clean surfaces in a simple and reliable

way.

Having said this, these ideas and concepts had *not* previously been put together in such a way that the HER kinetics at Pt(hkl) surfaces could be quantified. Therefore, the most important contribution to original research by the author of this thesis is precisely the way in which this knowledge was manipulated, combined and extended in order to derive and analyze results for the HER at single-crystal Pt surfaces, a direction of electrode-kinetic research which, until now, had not been properly explored. A list of the most critical and original discoveries in the present work is as follows:

i) The quantification of the kinetics of diffusion, adsorption and electron-transfer processes as involved in the HER at single-crystal Pt electrode surfaces. The use of impedance spectroscopy, coupled with determination of electrode relation effects, enabled the strong influence of diffusion of H_2 away from the electrode on the overall kinetics of the HER at Pt and other noble metal electrodes to be factored out so that the surface-specific electrode kinetics of the reaction could be unveiled. This situation determines the manner in which HER results are to be analyzed; i.e. data other than those from steady-state polarization measurements must be gathered in order to evaluate accurately the actual electrode-kinetic behaviour. The additional finding that a subsurface hydride region could *not* be detected by electrochemical means at Pt electrodes in acidic electrolyte put to rest a long standing controversy. The most important contribution to arise from this section of the portion of the work at single crystal Pt surfaces is the finding that electrocatalytic reaction rates of steps in the HER process *are* dependent on electrode surface geometry contary to earlier conclusions in the literature and are consistent with the

basic fundamental understanding of electrocatalytic reactions and their marked dependence on the electrode metal.

Other significant contributions are summarized as follows:

ii) Introduction and quantificative analysis of the idea of a potential-dependent poison coverage in the HER potential region at Pt and its application in terms of interpreting the measured steady-state Tafel polarization curves and the dependence of H sorption and desorption measurements on this potential dependent poison coverage.

iii) Determination that an adsorbed catalyst poison such as thiourea, becomes reductively desorbed at Pt, giving rise to a potential-dependence of H coverage and thereby a contribution to the dependence of H coverage on potential, this influencing the Tafel slope of the HER, as in (ii) above.

iv) Important general work on the application of EIS analysis to electrochemical systems involving both adsorption and diffusion phenomena, especially illustrating the rarely identified situation of product diffusion away from an electrode surface and its comparison with the more usual situation where diffusion of reactants takes place towards the surface.

v) The presentation of an understanding (although not yet a complete understanding) of how certain catalytic poisons affect the process of H sorption at Pd and Ni electrodes. The two matters which were defined are: 1) A kinetic influence of the poison which slows the H sorption and desorption rates and 2)Thermodynamic aspects of the poisoning effect, illustrating the importance of the μ_H factor (the chemical potential of adsorbed H) in determining the *equilibrium* fraction of sorbed H.

And lastly:

vi) Determonstration that adsorption of a S-containing poison at a Pd electrode inhibits rather than enhances H sorption (contrary to the situation at Ni? and Fe) and that the desorption of prviously sorbed H is inhibited at a Pd electrode by such poisons, the desorption only becoming possible after removal of the poison film has taken place upon surface oxidation of the Pd electrode at potentials greater than *ca.* 0.9 V *vs.* RHE.

Appendix A

A1. Procedure Preparation and Use of Pt Single-crystal Electrodes

1. Clean approx. 5 cm of high purity, AESAR puratronic grade or its equivalent, (99.9996 metal basis) 1 mm diameter Pt wire in hot nitric acid.

2. Hang the cleaned wire on a T-shaped quartz holder by bending one of its ends to make a small hook.

3. Light torch, adjust flame and don the quartz glass-blowing glasses.

4. Slowly bring the gas/oxygen torch with a blue flame up to the hanging end of the Pt wire, then increase the temperature of the wire by raising the flame by adjusting the lab jack to which the torch is mounted.

5. Proceed as above until a sphere of the desired size is obtained. Notice the liquid solid phase boundary, it is residing at the sphere/wire junction.

6. At this point either lower the flame with the jack or decrease the O_2 flow, which ever allows the most sensitive control. While reducing the temperature by the above procedure, carefully watch the liquid|solid phase boundary as it should take about 1 to 2 min. for it to move to the end of the sphere.

7. If the sphere is cooled too fast it may not produce a good single-crystal. The quality of the crystal can be determined by checking the placement of the (111) planes (flat spots on the single-crystal sphere). The planes should be at 90° to each other. This determination can be aided by briefly etching the crystal in hot aqua regia; the (111) and (100) planes will not etch, therefore producing smooth and rough patches on the sphere.

8. If the above check fails, remelt the sphere and try to cool it at a slower rate. If air pockets in the single-crystal sphere are a problem (revealed later on when polishing) remelting several times before the final cooling can be employed.

9. The single-crystal electrode once obtained, is then mounted loosely into the plastic holder with a small blob of plasticine "femo". This plastic holder then fits snugly into the goniometer. While mounting the crystal, the desired face can be zeroed in on by *carefully* bending the wire in the correct manner, remembering that the flat spots are the (111) planes.

10. The maximum deflection of the goniometer is 10° so the wire attached to the crystal should be bent so that the face of interest is within approx. 6° from the position perpendicular to the sides of the goniometer. A preliminary x-ray examination can be performed if this is in doubt.

11. With the crystal in the appropriate position, it is then solidly mounted, using Struers cold mounting epoxy. See the box for mixing instructions. It is best to wait to use the epoxy until it is extremely viscous.

12. After the epoxy has set the crystal is ready for aligning using x-ray diffraction.

A2. Procedure for acquiring an x-ray diffraction picture

1. Mount the goniometer in the holder on top of the x-ray diffractometer, making sure that the line on the goniometer and that on the holder match up and that the back of the goniometer is flush with the back of the holder. With these conditions met, lock it in with the screw on the holder.

2. Place the adjustment rod inside the x-ray outlet, move the holder close to the end of this rod, then centre the crystal in the path of the x-ray beam with aid from the adjustment rod by means of the horizontal and vertical adjusts on the holder.

3. Remove the adjustment rod from the x-ray outlet, and move the holder along its track so that the crystal is 6 cm from the surface of where the x-ray film will be placed.

4. Turn on the cooling water tap.

5. Turn on the main power of the x-ray machine; a fan will then start.

6. Turn on the red lamp and turn off the main room lights.

7. Obtain a film from the box (Kodak DEF 5 CAT # 155 9145); *remember close the film box afterwards*. Punch a hole in the centre of the film using the supplied tool and slip it into the black cardboard envelope. Note the position of the washer as it indicates how the film was positioned in the x-ray machine.

8. Mount film (in envelope) in the x-ray machine; the washer should be in the lower left-hand corner and locked into place.

9. Using a low intensity flashlight, illuminate each of the pinholes, 2 sec. each, at the four corners of the film holder. This will produce spots on the film which will allow the centre to be determined.

10. Close the lid of the protective lead box, then turn on the room lights. "Did you remember to put all the films back in their box?".

11. Provide power to the x-ray machine by: i) pushing the x-ray button, ii) adjusting the tube current and voltage in that order, so that 1/2 tube intensity is achieved, 35 kV and 25 mA (levels marked on the current and voltage gauges).

12. Adjust the timer for the 3rd shutter to a value of approx. 15 min.(longer if low intensity spots are to be seen on the film), then press the button to open the shutter.

13. Although no radiation is found to escape from the x-ray machine while it is on, it is a common practice to leave the room until the shutter is closed and power to the x-ray tube is killed (when the timer is finished).

14. Fill each of the trays with 1/2 litre of:

Tray 1	developer
Tray 2	water
Tray 3	fixer
Tray 4	water

15. With exposure time complete, reduce the tube current and voltage to their zero values. (If it is the last x-ray to be taken then turn off the main x-ray power and shut off the cooling water), turn *off* the room lights, turn *on* the red light, then remove the film from the x-ray.

16. Remove the film from its envelope and place it in tray 1 (the developer). Mix it around gently for 1 to 2 min., depending on how old your developer is.

17. Take the film from the tray 1 and place it in tray 2, and mix again for another half minute, then transfer to the fixer.

18. Once in the fixer the room lights can again be turned on. Remove the film from the fixer once all the yellow regions on it have become transparent, and then rinse well in the water in tray 4.

19. Dry film; use the blow dryer on the medium setting to speed up this

process but be careful not to warp or damage the film.

20. Once dry, tape the film to a transparency sheet, of the nonphotocopier kind.

A3. Analysis of the x-ray film

1. Find the centre of the film by connecting the dots on the opposing corners, draw lines using a ruler and a transparency marker.

2. Draw lines through two or three series of the dots corresponding to the crystal planes; they should all intersect at the plane of interest. If you are trying to find a certain plane, then measure several angles (along the lines drawn above) *vs.* a reference point (the (100) or (111) planes work the best).

3. Then using the charts and maps given in [1] the points can be labelled as the planes they represent.

4. Once the point of interest has been identified, simply measure its distance (horizontally and vertically) from the centre of the film using the chart given in [1]; note every section on the chart is equivalent to 2°.

5. Make the appropriate adjustments with the screws on the goniometer and, if necessary, take another x-ray diffraction picture.

The above steps 1 - 5 in part 3 are based on the assumption that the x-ray apparatus is perfectly aligned, but if it is found that this may not be the case, an alternative method of film analysis is suggested, as follows:

A1. First, following the above procedure obtain two x-ray pictures of the same crystal, but for the second x-ray have the goniometer rotated 180° from its initial position.

B1. As above, find the centre of each film.

C1. Rotate one of the films 180° and then match it to the other film by superimposing the reference lines.

D1. At perfect alignment the spots of interest should also become superimposed on one another.

E1. If this is not the case then draw a line through the two points and find the

midway point on that line.

F1. Using one of the films, measure the distance between the spot and the midway point (horizontally and vertically), make the appropriate adjustments on the goniometer, and take two more x-ray pictures, line up and line down.

G1. Repeat the adjustments until the spots from up and down are superimposed, at which point the crystal will be ready for polishing.

A4. Polishing

1. Place goniometer into the polishing ring, (the goniometer should be able to rotate in the ring but should not be able to wiggle).

2. Holding on only to the polishing ring, start polishing using 1200 grit SiC wet grinding paper and grind away over half of the sphere (watch for the disappearance of the flat sides of the (111) planes); move the ring/goniometer in a figure 8 fashion.

3. Sonicate and move to a finer grit, 2400, polish until the 1200 scratches are removed, sonicate, move to the 4000 grit and polish until the 2400 scratches are replaced entirely with those corresponding to the 4000 grit paper.

4. Now move on to polishing with 1 μm diamond grinding paste smeared on to a suitable cloth which is dowsed with the polishing lubricant; polish until the 4000 grit scratches have disappeared, then sonicate and proceed to polishing with a 1/4 μm diamond suspension deposited on a the cloth designated for the this step alone.

5. After this, remove the plastic holder from the goniometer and dissolve the epoxy by placing the holder into a plastic beaker full of $HCCl_3$.

6. Clean the crystal as best as you can, then remove all of the rest of the contamination by placing the crystal in hot HNO_3, for a couple of minutes.

A5. Use of Crystal for Electrochemical Studies

1. First, spot weld the crystal electrode to a clean Pt wire electrode (0.5 mm for conventional studies, 1 mm wire for rotating disk studies).

2. Read ref. 2 fully.

3. Assemble and dearate the electrolyte inside the electrochemical cell.

4. Light the gas/O_2 torch (fairly low flame), and start bubbling the Ar/H_2 mixture through the cooling apparatus.

5. Anneal the electrode in the flame (at most 30 sec.), cool in either air or the Ar/H_2 (being careful not to ignite the H_2). When using the Ar/H_2 mixture, the steps after the annealing step are:
   - Allow the crystal to cool down from the red-hot state.
   - Place in the flow of the Ar/H_2 mixture, which is now richer in H_2, and allow the Pt to get hot again from the surface reaction of H_2 with O_2 from the air.
   - When it has reached red heat, then flood the gas flow with Ar, allow it to cool down a little, then quench it in millipore water and when removing it, see that a drop of the millipore water remains attached to it.

6. If not cooling in Ar/H_2, then allow the crystal to cool in the air; quench with millipore water making sure a drop remains attached upon completion of the cooling.

7. It is found that it is convenient to dry the upper part of the wire with a kimwipe before entering it into the cell, leaving a small drop still attached to the surface of interest. This procedure is not absolutely necessary, especially if the wire is not roughened. When aligning the crystals for rotation, it was unavoidable that some extent of scratching of the surface would take place, making this part of the procedure vital.

8. The electrode is entered into the cell, under potentiostatic control (+ 500 mV *vs.* RHE).

9. If the wire was not dried prior to entry then the electrode is dipped in the electrolyte several times and a meniscus is pulled, If it was dried prior to entry then the electrode is only touched to surface of the electrolyte and a meniscus is then pulled.

10. Finally, with the wet electrode, the potential is held at + 500 mV *vs.* RHE until the current goes to zero (crystal sides are dry) then taken to approx. +70 mV *vs.* RHE and again the current is allowed to go to zero.

11. When using the kimwipe aka "magic hanky" method the electrode is dry immediately and the current should reflect this state.

12. If you've made it this far and things are looking good, then have fun, and I hope your results are interesting.

References

1. A. Hamelin, Modern Aspects of Electrochemistry, Eds. B.E. Conway, J.O'M. Bockris and R.E. White, Plenum Publ. Co., NewYork, 16 (1985) 1.

2. J. Clavilier, K. El Achi, M. Petit, A.Rodes and M.A. Zamakhchari, J. Electroanal. Chem., 295 (1990) 333.

IMAGE EVALUATION
TEST TARGET (QA-3)

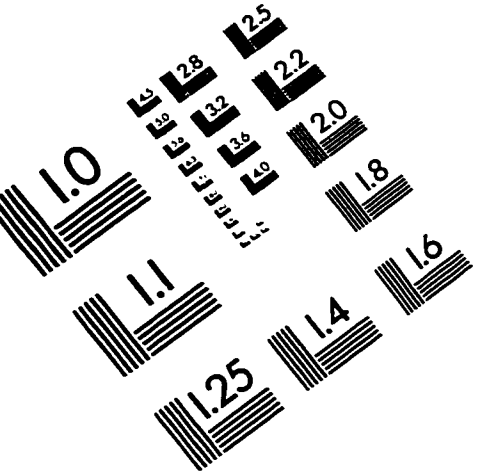

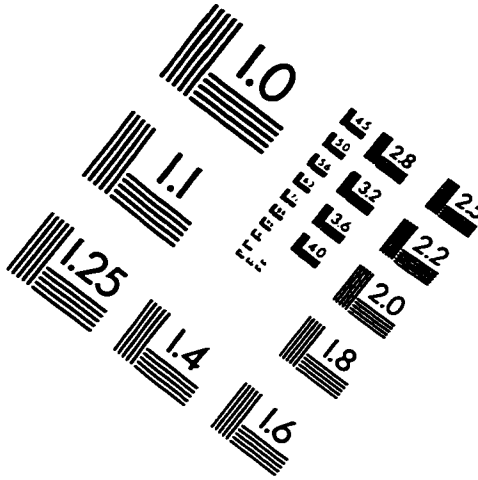

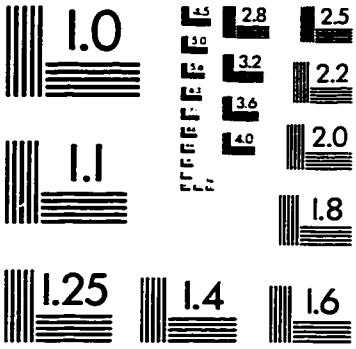

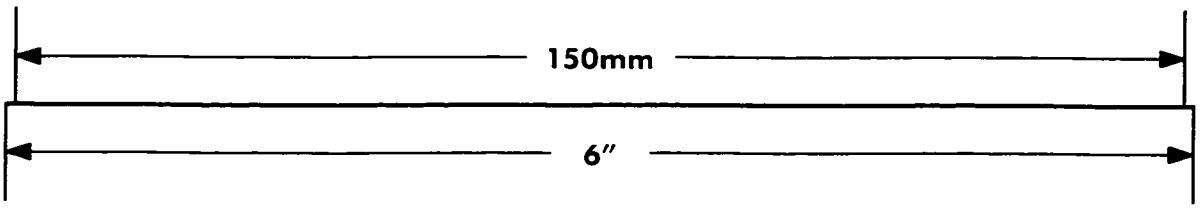

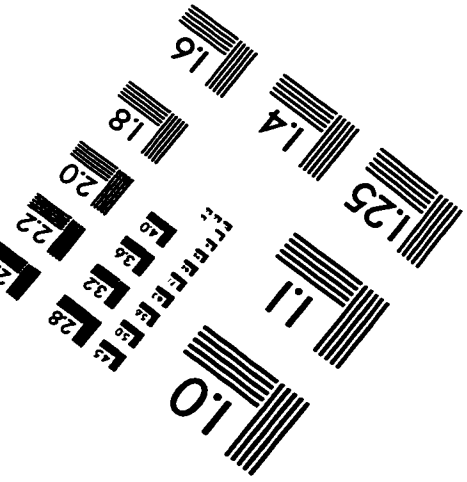

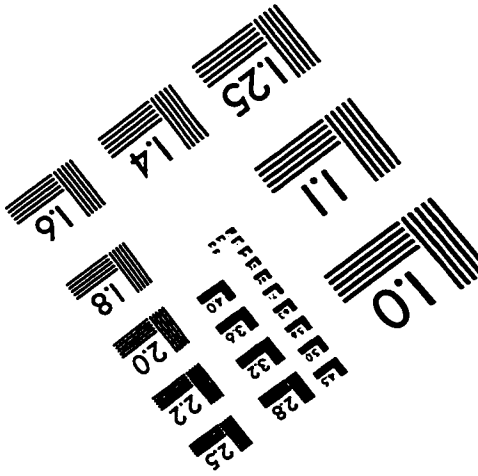

APPLIED IMAGE, Inc
1653 East Main Street
Rochester, NY 14609 USA
Phone: 716/482-0300
Fax: 716/288-5989